THE SPEED OF SOUND IN GASES

WITH APPLICATION TO EQUATIONS OF STATE AND SONIC NOZZLES.

A thesis submitted to the

University of London

for the Degree of Doctor of Philosophy

by

Steven John Boyes.

Department of Chemistry

Christopher Ingold Laboratories

20 Gordon Street

University College London

London WC1H 0AJ

February 1992

ACKNOWLEDGEMENTS.

I would like to thank my supervisor Dr. M. B. Ewing for his patience, particularly during the process of writing this thesis, encouragement and advice. Without him none of this would have been possible. I would also like to thank Dr. J. P. M. Trusler and Dr. A. R. H. Goodwin who showed a continued interest in this work and offered many useful suggestions and advice.

I would like to thank British Gas plc. for the award of a Research Scholarship and in particular Dr. J. G. O'Hair for his interest and enthusiasm in this work.

Thanks are also due to my colleagues in the thermodynamics research group and friends in the department of chemistry. The spherical resonator was expertly fabricated by Mr. D. Morfett whom, along with his colleagues in the mechanical workshop, I would like to thank.

Special thanks are due my parents and family for their unfailing support and encouragement throughout the time spent at University College London.

Last, but by no means least, I would like to thank my fiancée, Anna–Lisa deCastro for all her help, support and encouragement, particularly during the latter stages of this work and the preparation of this thesis.

ABSTRACT.

The speed of sound in a number of gases has been measured. Values were obtained from measurements of the frequencies of the radial modes of a spherical resonator. At low pressures (< 1 MPa) the speed of sound was determined using a 40 mm aluminium spherical resonator which was operable over wide ranges of temperature. Three substances were studied: ethane, tetrafluoromethane and methanol. Perfect–gas heat capacities and, second and third acoustic virial coefficients were determined from an analysis of the results. From the acoustic virial coefficients, estimates of the second and, in some instances, the third (p, V_m, T) virial coefficients were obtained. Results were compared with previous determinations. For measurements at pressures up to 10 MPa a new stainless steel resonator was constructed for which a detailed description is given. Measurements were performed over the temperature range 250 to 350 K and at pressures up to 10 MPa in the pure gases argon, nitrogen, and methane, and in the binary mixture of methane and ethane with mole fraction composition $\{(1-x)CH_4 + xC_2H_6\}$, where $x = 0.15$. Under such conditions the acoustic model was tested severely. The fractional precision of the results was generally better than 10 parts per million in u^2 for the whole temperature and pressure range. Acoustic and volumetric virial coefficients have been calculated from the results and are compared with previous determinations. For the industrially important gases, comparison of the experimental speeds of sound with those predicted from equations of state have been performed.

CONTENTS.

Page

LIST OF TABLES.

Page

LIST OF FIGURES.

Page

CHAPTER 1: INTRODUCTION.

1.1: Introduction.

The speed of sound in a gas is closely related to the thermodynamic properties of that gas[1], and its accurate measurement can therefore be used to gain detailed information about the equation of state[2,3]. Conventionally, this information comes from measurements of the volumes occupied by a given mass of gas at various temperatures and pressures[4–12]. Such measurements are subject to a number of systematic errors; some, but not all, of which may be reduced by use of more elaborate experimental techniques[13]. Speed–of–sound measurements are subject to quite different systematic errors, and these are usually more easily identified and can be greatly reduced. Nevertheless, it is only recently that very accurate measurements have been made in which proper attention has been paid to elimination of sources of uncertainty[14–18,21].

Until a few years ago, most speed–of–sound measurements were performed using an ultrasonic cylindrical interferometer although recently Mehl and Moldover demonstrated that use of a spherical resonator operating at audio frequencies afforded numerous advantages[14,16].

From mechanics the speed of sound, u, in a non–relaxing gas is related to the density and pressure through

$$u^2 = (\partial p/\partial \rho)_S \tag{1.1}$$

which in combination with the virial equation of state

$$pV_{\mathrm{m}}/RT = 1 + B/V_{\mathrm{m}} + C/V_{\mathrm{m}} + \cdots, \tag{1.2}$$

where B, C, $\cdots$ are the second, third, $\cdots$ virial coefficients, leads to the acoustic virial expansion for the speed of sound

$$u^2 = A_0 + A_1 p + A_2 p^2 + \cdots, \tag{1.3}$$

in which

$$A_0 = RT\gamma^{\mathrm{pg}}/M \tag{1.4}$$

and

$$\beta_{\mathrm{a}} = RTA_1/A_0 \tag{1.5}$$

$$\gamma_{\mathrm{a}} = RTA_2/A_1 \tag{1.6}$$

where M is the molar mass and γ^{pg} is the ratio of perfect gas specific heat capacities. β_{a} and γ_{a} are the second and third acoustic virial coefficients and are related to B and C through second–order differential equations[1]. An equivalent density explicit expansion exists.

Speed of sound measurements have many applications and use of sound speed measurements to yield precise equation of state information is most concerned with this work[1–3]. A second application is primary thermometry[18]. Use of the acoustic virial expansion extrapolated to zero pressure yields

$$u^2 = RT\gamma^{\mathrm{pg}}/M; \tag{1.7}$$

if the perfect–gas heat capacity ratio is known along with the molar mass then thermodynamic temperatures may be measured using $T(\mathrm{H_2O}$, s+l+g) = 273.16 K, by definition. Conversely, if the thermodynamic temperature is known exactly, as it is at the triple–point of water, then the zero–pressure intercept of the speed of sound, in a gas where γ^{pg} and M are known with sufficient accuracy, serves to define the gas constant R[21]. More exotic applications are measurement of gas–liquid phase boundaries[19], vibrational relaxation times[17] and zero density thermal conductivities.

(u, T, p) information may be utilised to evaluate a proposed form of the equation of state $V_{\mathrm{m}} = V_{\mathrm{m}}(p, T)$ or assist in the optimisation of an existing (p, V_{m}, T) surface for a particular application[2]. An important industrial application of equations of state lies in calculation of mass flow rates through sonic nozzles[3].

To measure the speed of sound we use the resonance technique. This involves exciting a sound field within a cavity of known geometry and measuring the frequency of the normal modes. The cavity geometry that is most favourable is a spherical enclosure[14,16]. In particular, for the radial modes of a sphere, there is no correction

for the viscous boundary layer and the favourable surface–area to volume ratio ensures that the thermal boundary layer correction is small, and that the energy losses are minimised. Thus, the radial resonances have very high quality factors and consequently, extremely precise determinations of the speed of sound are possible. The relation between the speed of sound and the geometry of the spherical cavity was first established by Rayleigh[20]. This model is very simple and cannot explain the observed finite line–widths. Mehl and Moldover[14] used first–order perturbation theory to make corrections for the presence of the thermal boundary–layer, openings in the wall of the resonator and the effects of shell motion, and explained the observed line–widths of the resonance curves. The model currently used includes some second–order terms and other smaller corrections arising from, for example, slits around the transducer housings[14–18,21]. The simple relation developed by Rayleigh has the form

$$f = u\nu/2\pi a, \tag{1.8}$$

where u is the speed of sound, a is the radius of the cavity, f is the frequency of the normal mode and ν is an eigenvalue which is known exactly. The perturbation model is very similar except that f is now represented by the complex quantity

$$F = f - ig = w\nu/2\pi a + \sum_j (\Delta f - ig)_j. \tag{1.9}$$

in which the sum represents the contributions of the various perturbations to the resonance frequencies and losses observed in the cavity. Thus, the observed frequency of the normal mode is shifted from the perfect–sphere value as given by (1.8).

The radially symmetric modes are non–degenerate, have high quality factors, defined as Q $\{= f/(2g)\}$, and the gas motion is normal to the resonators inner surface. A consequence of this is that there is no viscous damping at the gas–wall interface. The high quality factors permit the use of small inefficient transducers in the resonator wall, thus minimising the perturbation to the resonator–gas boundary. Measurements of the resonance frequency for a particular mode yields the quantity (u/a) where a is the internal radius. To make absolute measurements of the speed of sound, a knowledge of

a as a function of T and p is required. $\{(u/a),\ T,\ p\}$ measurements suffice to determine gas imperfections in the form of an equation of state. However, a knowledge of the radius, $a(T,\ p{=}0)$, allows the evaluation of $C^{\mathrm{pg}}_{p,\mathrm{m}}$, from equation (1.4), for a pure component, or the mole fraction composition for a mixture, given that the $C^{\mathrm{pg}}_{p,\mathrm{m}}$ for each component is known. $(p,\ V_{\mathrm{m}},\ T)$ information, while defining an equation of state, is insufficient to determine many thermodynamic properties. However, when combined with heat capacity information it is possible to calculate the speed of sound in a gas which then provides sufficient information to calculate any thermodynamic quantity for a pure substance or gaseous mixture.

The values of $a(T,\ p{=}0)$ can be obtained from: 1) volume determination by weighing with a fluid of known density[18,21]; 2) dimensional microwave measurements[22–24] and 3) by calibrating with a gas of known A_0 (for example Ar) combined with the pressure dependence determined by auxiliary methods[3,15,17,25].

The measurements presented here were determined using two spherical resonators. The low pressure measurements over wide ranges in temperature were performed in a welded aluminium resonator with an internal radius of 40 mm[17,25]. Measurements are reported for ethane, tetrafluoromethane and methanol. Perfect–gas heat capacities, and second and third acoustic virial coefficients have been determined from the results. Estimates of B, and in some instance C, have been obtained from the acoustic virial coefficients.

A new welded resonator was fabricated from stainless steel and had an internal radius of 45 mm. Measurements at pressures up to 10 MPa are reported for argon, nitrogen, methane and the binary mixture $\{0.85\ CH_4 + 0.15\ C_2H_6\}$, of methane and ethane. The measurements in argon served to characterise the resonator and study the model used to describe acoustic energy losses in the spherical resonator. Second acoustic virial coefficients determined from the results are compared with previous determinations. The measurements on nitrogen yielded second and third acoustic virial coefficients. Estimates of B were obtained from the acoustic results and are compared with previous determinations. Measurements on methane yielded perfect–gas heat

capacities, second and third acoustic virial coefficients and vibrational relaxation times. Comparison with previous determinations is given, as are estimates of B determined from the results. Vibrational relaxation times determined from the results are compared with previous determinations. Measurements on the binary mixture yielded acoustic virial coefficients for the mixture. Cross virial coefficients for methane–ethane have been extracted from the results and are compared with previous determinations.

1.2: References.

1. Van Dael, W. *Experimental Thermodynamics Volume* II, Butterworths: London, 1968.

2. Biswas, S. N.; Seldam, C. A. ten *J. Chem. Thermodynamics* 1991, 23(8), 725.

3. Goodwin, A. R. H. Ph. D. Thesis, University of London, 1988.

4. Pieperbeck, N.; Kleinrahm, R.; Wagner, W.; Jaeschke, M. *J. Chem. Thermodynamics* 1991, 23(2), 175.

5. Kleinrahm, R.; Duschek, W.; Wagner, W.; Jaeschke, M. *J. Chem. Thermodynamics* 1988, 20(5), 621.

6. Douslin, D. R.; Harrison, R. H. *J. Chem. Thermodynamics* 1973, 5, 491.

7. Douslin, D. R.; Harrison, R. H.; Moore, R. T.; McCullough, J. P. *J. Chem. Eng. Data* 1964, 9, 358.

8. Douslin, D. R.; Harrison, R. H.; Moore, R. T.; McCullough, J. P. *J. Chem. Phys.* 1961, 35,1357.

9. Saville, G. *Experimental Thermodynamics Volume* II, Butterworths: London, 1968.

10. Brielles, J.; Dédit, A.; Lallemand, M. Le Neindre, B.; Leroux, Y.; Vermesse, J.; Vidal. D. *Experimental Thermodynamics Volume* II, Butterworths: London, 1968.

11. Malbrunot, P. *Experimental Thermodynamics Volume* II, Butterworths: London, 1968.

12. McCarty, R. D. *Experimental Thermodynamics Volume* II, Butterworths: London, 1968.

13. Ewing, M. B.; Marsh, K. N. *J. Chem. Thermodynamics* 1979, 11, 793.

14. Mehl, J. B.; Moldover, M. R. *J. Chem. Phys.* 1981, 74(7), 4062.

15. Ewing, M. B.; McGlashan, M. L.; Trusler, J. P. M. *Metrologia* 1986, 22, 93.

16. Moldover, M. R.; Mehl, J. B.; Greenspan, M. *J. Acoust. Soc. Am.* 1986, 79(2), 253.

17. Ewing, M. B.; Trusler, J. P. M. *J. Chem. Phys.* 1989, 90(2), 1106.

18. Moldover, M. R.; Trusler, J. P. M. *Metrologia* 1988, 25, 165.

19. Colgate, S. O.; Sivaraman, A.; Dejsupa, C.; McGill, K. *J. Chem. Thermodynamics* 1991, 23(7), 647.

20. Rayleigh, J. W. S. *The Theory of Sound* Dover: New York, 1945.

21. Edwards, T. J.; Davis, R. S.; Mehl, J. B.; Moldover, M. R.; Trusler, J. P. M. *J. Res. Nat. Bur. Standards* **1988**, 93(2), 85.

22. Ewing, M. B.; Mehl, J. B.; Moldover, M. R.; Trusler, J. P. M. *Metrologia* **1988**, 25, 211.

23. Mehl, J. B; Moldover, M. R. *Physical Review A* **1986**, 34(4), 3341.

24. Boyes, S. J.; Ewing, M. B.; Trusler, J. P. M. unpublished results **1989**.

25. Ewing, M. B.; Owusu, A. A.; Trusler, J. P. M. *Physica A* **1989**, 156, 899.

CHAPTER 2: ACOUSTICS.

2.1: Introduction.

The relevant acoustic theory for a spherical resonator is extensively reviewed in the literature[1–13]. For completeness, the theory is considered here, but rather than supplying a strict derivation from first principles only a general overview is given with emphasis placed on the physical significance of the results.

The discussion begins with the Navier–Stokes equation for an unbounded gas. Under most conditions the effects of thermal conductivity and shear viscosity in the bulk of the fluid are small and do not perturb the sound speed. Consideration of molecular relaxation shows that this can severely perturb the speed of sound from the thermodynamic value, in an idealised fluid, and cause severe speed dispersion as well as contributing to the attenuation of the sound wave. Enclosing the fluid in a cavity imposes boundary conditions to the wave equation which must be satisfied. These boundary conditions cannot be satisfied by the propagational mode alone and, near the wall of the cavity, the amplitudes of the corresponding thermal and shear waves are

enhanced. In conditions of steady state excitation the wave motion is one of a standing wave when the frequency of the source is close to a natural frequency of the cavity. The relevant equations can be solved exactly for simple geometries, such as a sphere or cylinder, and consequently equations have been developed which relate the frequencies of the normal modes of the gas–filled cavity to the speed and absorption of sound in a gas. Throughout the discussion we restrict our attention to radial modes.

2.2: Basic Theory[1–3,6].

The dynamics of the gas are described by the Navier–Stokes equation, which consists of Newton's second law and a relation giving the stresses in terms of spatial derivatives of the velocity of the gas. The relevant transport coefficient is the shear viscosity η. Heat flow in the gas is assumed to be governed by Fourier's law with the relevant transport coefficient being the thermal conductivity κ. Two additional equations are statements of the equations of continuity for mass and heat flow. An equation of state for the gas relates changes in the pressure, density and temperature. The second law of thermodynamics is used to relate changes in the entropy of the gas to changes in the pressure and temperature. These are used collectively to construct a linear acoustic theory. By linear it is meant that the squares and products of certain small quantities are neglected. The pressure, temperature and velocity fields are all coupled in this theory.

The fields must satisfy five boundary conditions when the fluid is constrained in a cavity: 1) the radial components of the gas and shell velocities must match; 2) the radial component of the shell velocity is equal to the radial force per unit area exerted on it by the gas multiplied by an effective acoustic admittance; 3) the transverse component of the gas velocity must match the transverse component of the shell velocity (for the radial modes considered in this work this condition is automatically satisfied); 4) a relation between the temperature of the gas and the shell boundary, including the effects of the temperature–jump at the interface; and 5) a statement of continuity of heat flow at the gas–shell interface. These five boundary conditions

constitute a set of equations which can be solved exactly for the spherical geometry. A series expansion of the exact solution shows that the complex eigenfrequencies are given to first order in the frequency perturbation by

$$F_{0n} = f_{0n} - ig_{0n} = \nu_{0n} u/2\pi a + \sum_j (\Delta f - ig)_j \qquad (2.2.1)$$

where $(\Delta f - ig)_j$ is the j–th perturbation term and includes contributions from shell motion, thermal and viscous waves, as well as classical viscothermal losses. Strictly, the eigenfrequencies should have three indices l, m and n. However, since our attention is restricted to radial modes only, the indices l and m are zero and the progression of radial modes is distinguished by the remaining index, n. Conventionally, the $n = 1$ index is reserved for the zero–frequency mode and thus the first non–zero radial mode is the (0,2). Within this formalism account is taken of the volume or bulk (compressional) viscosity. There are additional eigenfrequency perturbations which cannot be calculated within an exact formalism, but inclusion of these is possible using boundary perturbation theory[13]. Such perturbations are due to imperfect spherical geometry and ducts and slits in the shell wall[4,7,12,17]. The important perturbations are considered separately in the following sections.

2.2.1: Thermal Boundary Layer[2,3,6,12,20].

The shift in resonance frequency and contribution to the resonance half–width resulting from the thermal boundary layer is given by

$$\Delta f_h - ig_h = -(1+i)\{(\gamma-1)/2a\}(D_h f/\pi)^{\frac{1}{2}} + i\{(\gamma-1)/2a^2\}(D_h/\pi) + (\gamma-1)f(l_a/a), \qquad (2.2.2)$$

where γ is the ratio of molar heat capacities, D_h is the thermal diffusivity and l_a is the thermal accommodation length. The first term is the classical expression describing the loss at a plane surface, the second term arises from the curvature of the surface and the final term takes account of the temperature–jump effect[3,12]. For a gas of molar mass M and thermal conductivity κ at a mass density ρ the thermal diffusivity and accommodation length are given by

$$D_h = \kappa M/(\rho C_{p,m}) \tag{2.2.3}$$

$$l_a = (\kappa/p)(\pi MT/2R)^{\frac{1}{2}}\{(C_{V,m}/R) + 1/2\}^{-1}\{(2-h)/h\}, \tag{2.2.4}$$

where h is the accommodation coefficient defined as the ratio $\Delta E_1/\Delta E_2$ of the actual net energy ΔE_1 transported across the interface and the energy ΔE_2 that would be transported if all the incident molecules came to thermal equilibrium with the surface before being re–emitted. Experimental results have shown that for the 40 mm aluminium sphere $h = 0.91$, but for the 45 mm stainless steel sphere $h = 1$.

Trusler[17] has considered the effect of propagation of the thermal wave in the shell wall. He concluded that the perturbation due to the thermal boundary layer would be modified by an additional factor

$$(1-i)(\gamma-1)\{\delta_w/(2a)\}(\kappa/\kappa_w) \tag{2.2.5}$$

in which δ_w is the thermal penetration length in the wall and κ_w is the thermal conductivity of the wall material. For common wall materials this contribution is found to be negligible.

2.2.2: Shell Motion[2,5,6].

The response of a spherical isotropic shell to an internal acoustic mode has been calculated from the exact theory of elasticity. Mehl[5], and Moldover, Mehl and Greenspan[6] presented a treatment specific to radial modes and included the effect of radiation from the external surface. The specific acoustic admittance of the shell at $r = a$ is given by

$$y_w = [-i\rho\omega ua/(\rho_w u_{w,l}^2)]S_0(k_w a) \tag{2.2.6}$$

where the subscript 0 refers to radial shell motion and $k_w a = \omega/u_{w,l}$, where $u_{w,l}$ is the longitudinal wave speed in the wall material. The dimensionless function S_0 is given by

$$S_0 = -q\{(G_1 + qRG_2)/(G_3 + qRG_4)\} \tag{2.2.7}$$

where

$$q = \tfrac{1}{2}(1-\sigma)/(1-2\sigma), \tag{2.2.8}$$

$$R = (\rho_g u_g^2/\rho_w u_w^2)\{(k_g b)^2/(1+ik_g b)\}. \tag{2.2.9}$$

In addition

$$G_1 = (1 + AB - qB^2)\tan(B - A) - (B - A) - qAB^2 \qquad (2.2.10a)$$

$$G_2 = (1 + AB)\tan(B - A) - (B - A) \qquad (2.2.10b)$$

$$G_3 = \{(qA^2 - 1)(qB^2 - 1) + AB\}\tan(B - A) - (1 + qAB)(B - A) \qquad (2.2.10c)$$

$$G_4 = (1 + AB - qA^2)\tan(B - A) - (B - A) + qA^2B, \qquad (2.2.10d)$$

where $A = k_w a$ and $B = k_w b$. At zero frequency, the radiation terms vanish and the admittance function S_0 is the limiting value of $-qG_1/G_3$. The shell resonances occur at frequencies for which the denominator in equation (2.2.7) vanishes. If the radiation terms are neglected, the frequencies are given by the zeroes of $G_3(k_w a)$. The lowest root corresponds to the breathing mode of the shell. The higher frequency modes occur when $\tan(k_w a)$ is close to zero. These modes clearly occur at much higher frequencies provided $u_w/(b - a)$ is much larger than u_g/a. This suggests that to a good approximation the zero frequency limit can be scaled by a resonance term $[1 - (f/f_{br})^2]^{-1}$, where f_{br} is the breathing resonance frequency. In this "isolated mode" approximation f_{br} may be calculated from G_3 or from experiment.

To determine the breathing frequency experimentally, we monitor the perturbation and excess half–width of a radial acoustic resonance frequency as it traverses the shell breathing resonance[9]. A convenient determination is possible using helium in which the speed of sound is very large. Consequently, the (0,3) mode is at a frequency close to f_{br} and perturbations are monitored by comparison with the speed of sound determined from the unperturbed (0,2) mode. Frequencies are varied by changing the temperature of the cavity. A typical perturbation and excess half–width trace is shown in Figure 2.1 which was determined from measurements in the 40 mm aluminium resonator. The breathing frequency is at the frequency where the excess half–width is a maximum and the frequency perturbation has a point of inflexion. Also shown are measurements carried out in the stainless steel resonator. A comparison of the two shows that the frequency perturbation is a factor of three less for stainless steel when compared with aluminium; hence the choice of material for construction of the high–pressure resonator. Purely qualitative measurements of shell resonances can be

a)

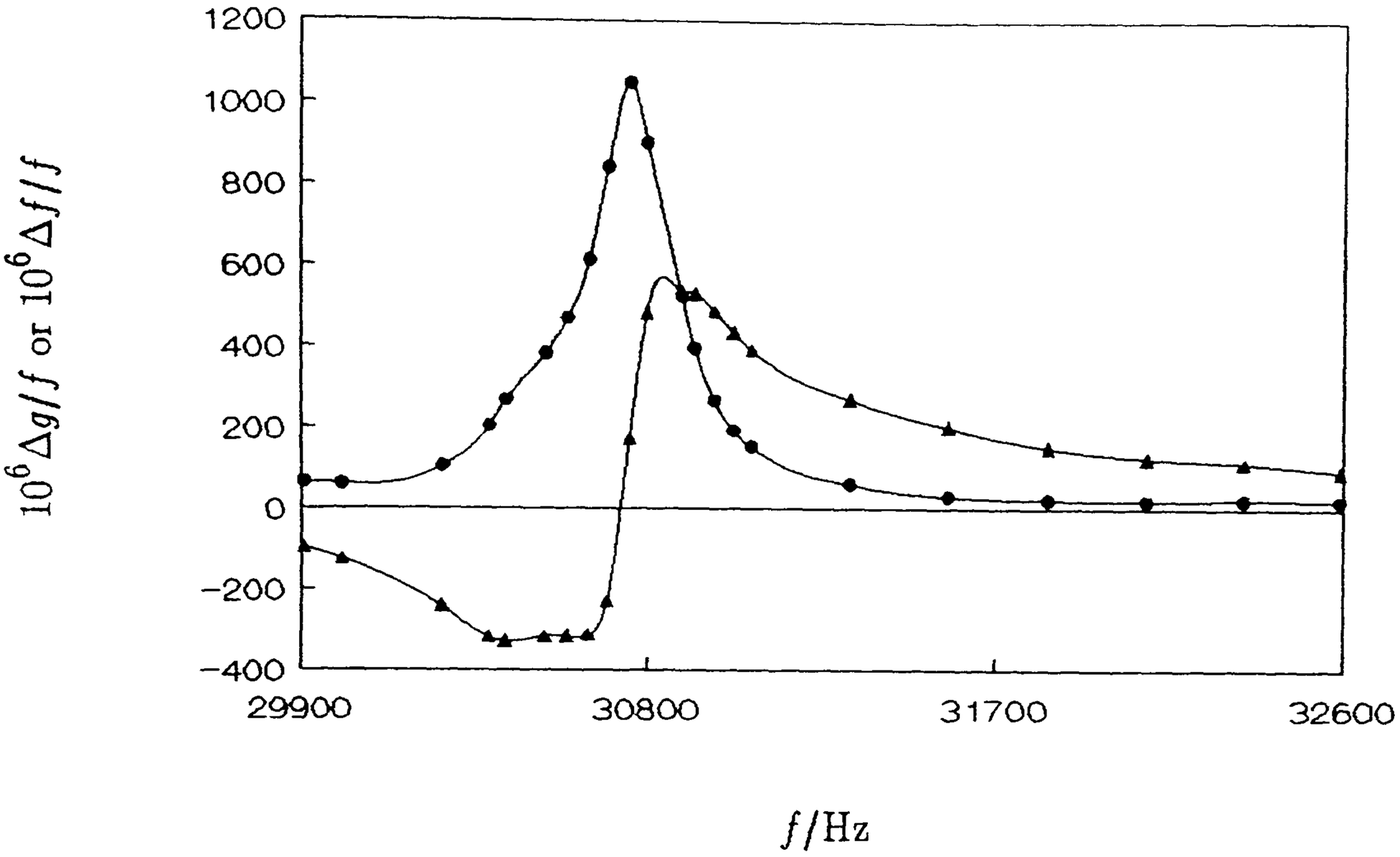

b)

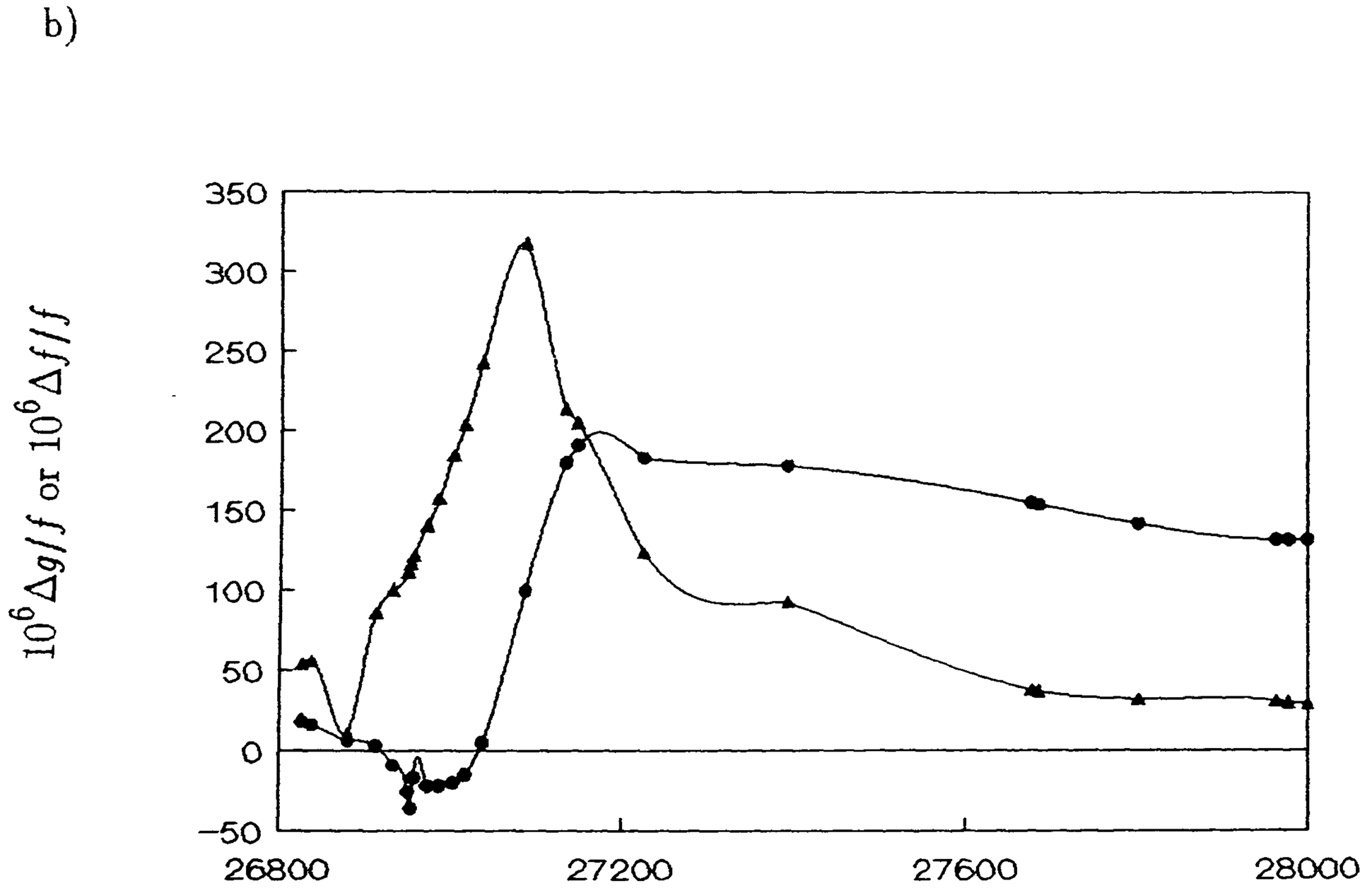

Figure 2.1: Frequency perturbation $\Delta f/f$, ▲ , and excess half–width $\Delta g/f$, • , measured for the (0,3) mode in helium at a pressure of 500 kPa a) in the 40 mm aluminium resonator and b) in the 45 mm stainless steel resonator.

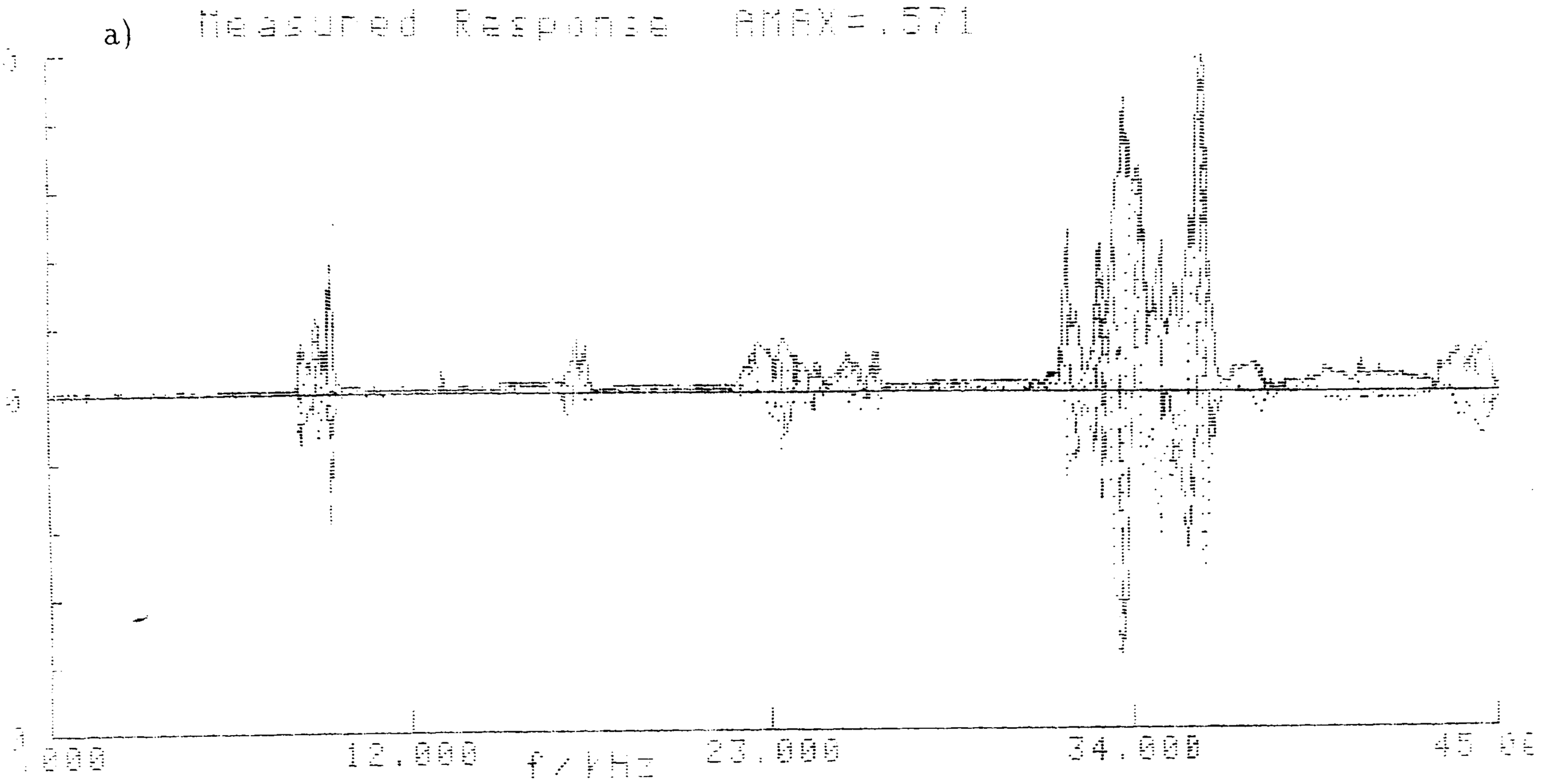

Figure 2.2: Spectrum of shell resonances obtained by exciting the transducers under vacuum; a) 40 mm aluminium resonator and b) 45 mm stainless steel resonator.

made by conducting a frequency scan under vacuum. Under these conditions, vibrations in the source transducer excite shell resonances which are conducted through the wall material to the detector. A typical plot of the output of the detector is shown in figure 2.2 for the 45 mm stainless steel resonator. Important features are indicated and comparison with a similar plot for the 40 mm aluminium sphere recorded by Goodwin shows that the salient features are essentially the same.

For the high pressure measurements, where the shell correction dominates[11], the exact expression is used (including radiation from the external surface). Direct coupling between the gas and shell resonances should only occur when the modes have the same symmetry; however, higher–order coupling between the $l = 0$ acoustic modes and the $l = 1, 2, 3, \cdots$ shell modes might occur when the resonance frequencies are similar and the gas densities are high. Additional coupling between modes of differing symmetry may be possible in the stainless steel resonator due to the imperfect spherical geometry, especially if the geometry is pressure dependent as is suggested by the experimental results. The presence of holes in the shell wall, such as transducer ports, allows for non–volume preserving deformations of the cavity, and consequently additional perturbations, which are difficult to model, may arise. Although the use of radial modes in the gas should minimise these additional perturbations, problems might arise at the highest densities. Under the conditions of the high–pressure measurements, care was taken when finally selecting the modes used in the analysis.

2.2.3: Bulk Absorption and Molecular Relaxation[2,10–12,17–22].

Sound absorption throughout the bulk of the gas increases the half width by

$$g_{\mathrm{b}} = \pi(f/u)^2\{4D_s/3 + (\gamma - 1)D_h + \eta_{\mathrm{b}}/\rho\}, \qquad (2.2.11)$$

in which D_h is the thermal diffusivity, $D_s = \eta/\rho$ is the viscous diffusivity and η_{b} is the bulk viscosity. For monatomic species $\eta_{\mathrm{b}} = 0$. In polyatomic gases, however, there is irreversible energy transfer from the collective motion of the sound wave to other degrees of freedom of the molecules. During the compressional part of the acoustic cycle there is a transfer of energy to the internal degrees of freedom of the molecules,

some of which, due to the finite time–constants associated with the reverse process, is lost and attenuates the sound wave. The bulk viscosity of polyatomics arises mainly from vibrational relaxation. If it is assumed that there is a single relaxation time, τ, arising from either one vibrational state or from a number of states coupling in series, then the effective heat capacity is reduced such that, at angular frequency ω, the ratio of heat capacities becomes

$$\gamma(\omega)/\gamma = 1 + [\omega\tau(\gamma-1)\Delta\{\omega\tau(1-\gamma\Delta) - i\}]/[1 + \{\omega\tau(1-\gamma\Delta)\}^2] \qquad (2.2.12)$$

where $\Delta = C_{\text{vib}}/C_p$ and C_{vib} is the vibrational contribution to the heat capacity. It is sufficient to employ a series expansion of equation (2.2.12) in powers of $\omega\tau$ which gives

$$\{\gamma(\omega)/\gamma\}^{\frac{1}{2}} = 1 - (i/2)(\gamma-1)\Delta\omega\tau + \tfrac{1}{2}(\gamma-1)\Delta(\omega\tau)^2\{1 - \tfrac{1}{4}\Delta(1+3\gamma)\} + O(\omega\tau)^3. \qquad (2.2.13)$$

In terms of this expansion vibrational relaxation makes a contribution to the half width given by

$$g_{\text{rel}}/f = (u/2\pi)\alpha_{\text{rel}} \approx (\gamma-1)\Delta\pi f\tau \qquad (2.2.14)$$

in which α_{rel} is the contribution of vibrational relaxation to the coefficient of absorption. The contribution of vibrational relaxation to the bulk viscosity is given by

$$\eta_{\text{b}} = u^2\rho\Delta(\gamma-1)\tau \qquad (2.2.15)$$

provided that $(\omega\tau)^2 << 1$.

The contribution of vibrational relaxation to the resonance frequencies is given by

$$\Delta f_{\text{rel}}/f \approx 2(\gamma-1)\Delta(\pi f\tau)^2\{1 - \Delta(1+3\gamma)/4\}. \qquad (2.2.16)$$

2.2.4: Ducts and Slits in the Shell Wall[2,6,11,17,20].

The openings in the resonator wall which are relevant to the work carried out are 1) a gas inlet tube with circular cross–section, and 2) annular slots formed between the wall and the transducer housings.

The perturbation to the radial modes for each opening is given by

$$(\Delta f_{\text{o}} - ig_{\text{o}}) = -iy_{\text{o}}S_{\text{o}}\{u/(2\pi a)\}/(4\pi a^2), \qquad (2.2.17)$$

where it is assumed that the specific acoustic admittance, y_{o}, of the opening is uniform

over its surface area S_o. In order to calculate the perturbation, y_o must be known.

For a tube of radius c and length $z = L$ from the opening into the cavity, the specific acoustic impedance at $z = L$ is

$$Z(z = L) = i\rho u \tanh(\delta_L - i\gamma_L) \tag{2.2.18}$$

where the ratio of reflected to incident wave amplitudes is $\exp(-2\gamma_L)$ and the phase shift is $(2\delta_L + \pi)$. It is assumed that only plane waves propagate and bulk absorption is ignored. The corresponding specific acoustic admittance at $z = 0$ on the inner surface of the cavity is

$$y_o = \rho u / Z(z = 0) = i \cot(\delta_L + i\gamma_L + k_{KH}L), \tag{2.2.19}$$

where

$$k_{KH} = k + (1 + i)\alpha_{KH}, \tag{2.2.20}$$

is the tube propagation constant,

$$k = 2\pi f / u \tag{2.2.21}$$

and

$$\alpha_{KH} = \{\pi f/(uc)\}\{\delta_s + (\gamma - 1)\delta_h\} \tag{2.2.22}$$

is the Kirchoff–Helmholtz tube attenuation constant; here $\delta_h = [D_h/(\pi f)]^{\frac{1}{2}}$ and $\delta_s = [D_s/(\pi f)]^{\frac{1}{2}}$ are the thermal and viscous penetration lengths, respectively. The parameters γ_L and δ_L depend on the conditions at $z = L$ and have been considered in some detail in the literature[11].

The tube resonances occur when y_o is a maximum which, for an open tube gives

$$f_m = \{u/(2\pi L)\}(m\pi + \alpha_{KH}L - \delta_L); \qquad m = 0, 1, 2, \cdots. \tag{2.2.23}$$

The perturbation to the radial modes is given by equation (2.2.17) with values of γ_L and δ_L appropriate to the tubes termination. Goodwin[11] noted for an open tube of length $1.023a$, where a is the radius of the cavity, that the radial acoustic resonances lie between resonances of the tube thus minimising the perturbation.

An annular slot can be modeled using parallel semi–infinite plates separated by a distance d and extending to a depth $x = L$[17]. The specific acoustic admittance of the resonator surface at $z = 0$ is given by

$$y_0 = [\{(1+i)(3\gamma)^{\frac{1}{2}}\}/(6\delta_s/d)]\ \tanh[(1+i)(\delta_s/d)kL(3\gamma)^{\frac{1}{2}}]. \qquad (2.2.24)$$

This expression can be used to estimate the effects of the annular slots surrounding plugs and/or transducers fitted closely in holes through the cavity wall. It can also be used to estimate the effect of a small opening at the junction of the two hemispheres.

2.2.5: Geometric Imperfections.[4,7,23,24]

Mehl[4,7] presents an extensive treatment of the effect of geometric imperfections on the acoustic resonances within a spherical cavity. Boundary–shape perturbation theory is used to calculate corrections to both radial and non–radial acoustic modes and also microwave resonances. The formalism has been generalised to enable corrections to be found for arbitrary shape changes but we restrict our attention here to axisymmetric volume–preserving deformations only. The surface of the cavity is described by

$$r = a[1 - \epsilon f(\theta)], \qquad (2.2.25)$$

where $f(\theta) \geqslant 0$ and ϵ is a small parameter. Provided the sphere is distorted at constant volume then corrections only appear in the second order of perturbation theory and the shift in eigenfrequencies is given by

$$\Delta k_{0n}/k_{0n} = -\epsilon^2 \sum_{p=2}^{\infty} (p + \tfrac{1}{2}) F_p^2 S_{np}, \qquad (2.2.26)$$

in which $k_{0n} = \nu_{0n}/a$ and the F_p are proportional to the coefficients in an expansion of $f(\theta)$ in a series of Legendre polynomials. The S_{np} are infinite sums of eigenvalues, numerical values of which are given in reference 4. Specific examples of deformations are treated by Mehl[4,7] and the results are quoted here.

2.2.5a: Spheroids.

Prolate and oblate spheroids are described by the equations $f(\theta) = \sin^2\theta$ and $f(\theta) = \cos^2\theta$, respectively. The resulting perturbation is given by

$$\Delta k_{0n}/k_{0n} = (4/135)\epsilon^2 \nu_{0n}^2, \qquad (2.2.27)$$

and is monotonic in mode number.

2.2.5b: Hemispheres with Unequal Radii.

For this case

$$f(\theta) = \begin{cases} 1, & 0 \leqslant \theta \leqslant \pi/2 \\ 0, & \pi/2 < \theta \leqslant \pi \end{cases}. \tag{2.2.28}$$

Values of the coefficient of ϵ^2 in equation (2.2.26) have been calculated by Mehl, for the radial modes with n extending from 2 to 8, and can be found in reference 4 . It is of note that the perturbation to the (0,2) radial mode is largest; this results from the near degeneracy with the (3,1) non–radial mode.

2.2.5c: Hemisphere with Minor Spherical Segment.

For this shape

$$f(\theta) = \begin{cases} \cos\theta, & 0 \leqslant \theta \leqslant \pi/2 \\ 0, & \pi/2 < \theta < \pi \end{cases}. \tag{2.2.29}$$

Numerical values of the coefficient of ϵ^2 are given in reference 4 and are again monotonic in mode number. The frequency shifts resemble those due to spheroids but, for a given ϵ, are about twice as large.

To apply corrections for any geometric imperfections, determination of ϵ is necessary. The correction for any geometric imperfection can be calculated once the geometric imperfection parameter ϵ is known, and non–radial acoustic resonance or dimensional microwave measurements can provide experimental estimates of ϵ.

For a surface defined by

$$r = a[1 - \epsilon \sum_{l=0}^{\infty} c_{l0} Y_{l0}(\theta)], \tag{2.2.30}$$

we get upon expansion

$$(r-a)/a = -\epsilon(c_{20}Y_{20} + \cdots) - \epsilon[c_{21}(Y_{21} - Y_{2-1}) + \cdots]. \tag{2.2.31}$$

For modes with $l = 1$ the expansion terminates at c_{2i}. For a sphere four cases are particularly simple: 1) when $\theta = 0$ or π; 2) when $\theta = \pi/2$; 3) when $\theta = \pi/4$.and 4) when $\theta = 3\pi/4$. From 1) and 2) we find that,

$$(r_{\mathrm{EW}} - r_{\mathrm{NS}})/a = -\epsilon c_{20}(5/4\pi)^{\frac{1}{2}} \tag{2.2.32}$$

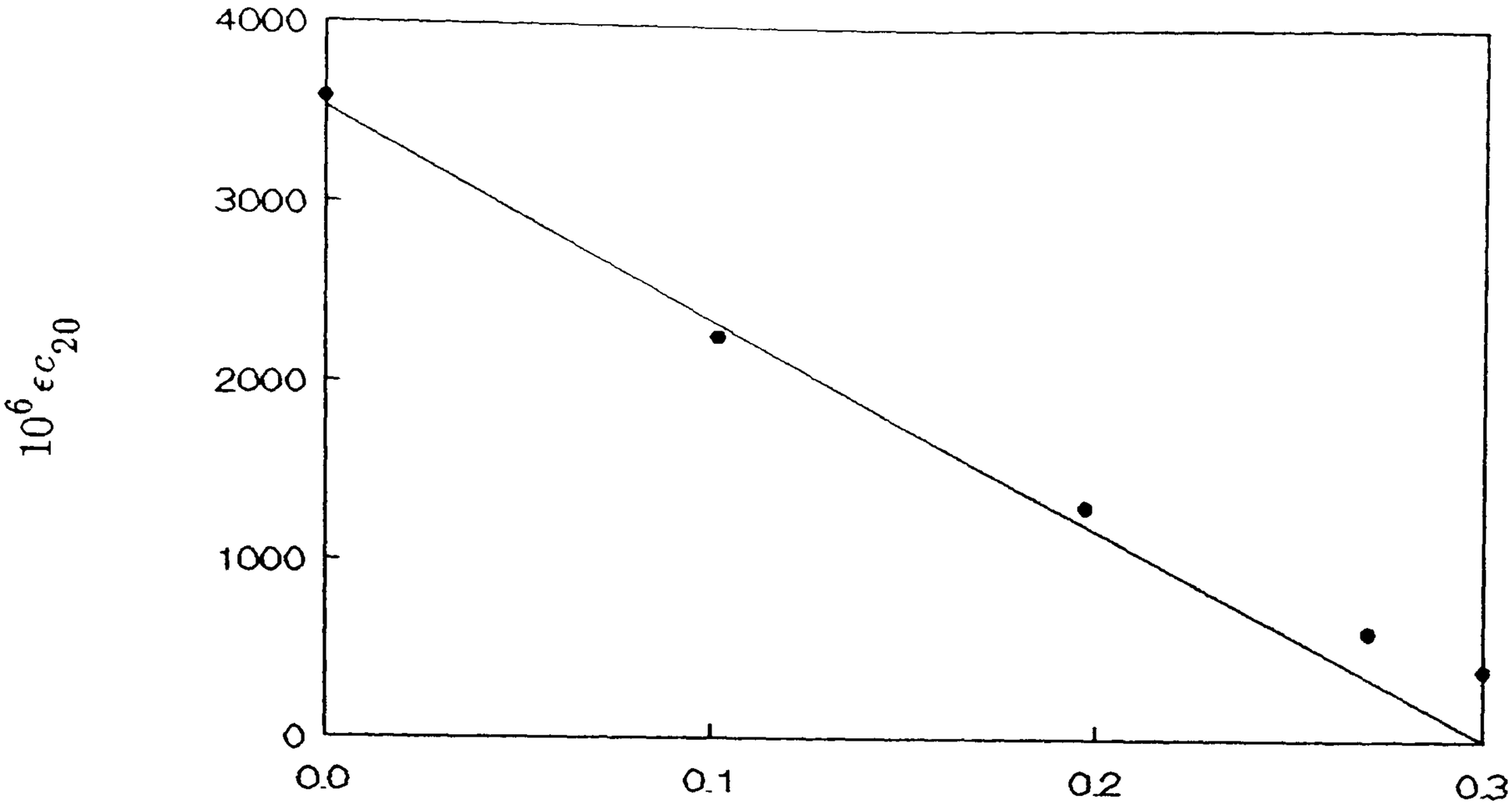

Figure 2.3: Geometric imperfection factor, ϵc_{20}, as a function of the length h removed from the cylindrical extension under the guidance of microwave measurements.

---

where r_{EW} is the equatorial radius and r_{NS} is the polar radius. Equatorial displacements are determined from cases 3) and 4). The frequency shifts relative to perfect sphere frequencies, f_{ps}, are given by

$$(20\pi)^{\frac{1}{2}}\Delta f/f_{\mathrm{ps}} = \epsilon c_{20}\lambda_n Z_x \qquad (2.2.33)$$

in which $\Delta f = f - f_{\mathrm{ps}}$, λ_n is an eigenvalue for a particular mode within a multiplet and Z_x depends on eigenvalues which are particular to the type of resonances studied. From this ϵc_{20} can be determined from any splitting given that to order ϵ^2 the mean of the observed frequencies is f_{ps}.

2.3: Microwave Measurements on the 45 mm Stainless Steel Resonator[14–16].

Microwave measurements were used to guide the fabrication of the resonator. Mechanical measurements, after polishing was complete, indicated a cylindrical extension of 0.3 mm and the removal of this was guided by measurements on the triply degenerate TM(1,1) mode. Symmetry arguments indicate that this mode should be split into a singlet and an unresolved doublet. Analysis was therefore in terms of a "doublet". The imperfection parameter ϵc_{20}, so determined, is shown in Figure 2.3 as a

function of the length h removed from the cylindrical extension on the equator. From this we determine that the radii in the polar and equatorial directions differ by no more than 16 μm.

After welding however, microwave measurements indicated that severe distortion had occurred. The appearance of the TM(1,1) mode is shown in Figure 2.4. Superficially the resonance appears to be a doublet, and the expectation is that the geometric distortion is axisymmetric. However, phase information is not available in the frequency range studied and hence additional infromation is required to unambiguously assign the status of doublet or triplet to the resonance. This information can be obtained from measurements on non–radial acoustic resonances. Geometric imperfections on the order indicated by the microwave measurements will have a significant effect on the radial acoustic resonances. This is confirmed in figure 2.5a. Thus, an alternative method is to compare the experimentally observed perturbations to the radial modes with those predicted from the Mehl models. Values of ϵ required in the models are determined from analyses of the microwave measurements as either a doublet or triplet. A satisfactory analysis of the microwave data is assumed to be found if it can correct the discrepancies in the first four or five radial modes. Analysis of the microwave resonance as a doublet indicated a geometric imperfection parameter of –1434.9 ppm which corresponds to a cylindrical extension of 61 μm. Analysis of the microwave mode as a triplet led to two possible solutions of equal quality. The quality of the solutions was assessed on the basis of the reduced χ^2in the regression analyses; both solutions had a reduced $\chi^2$of less than unity. The first solution indicated that ϵc_{20} = –392.3 ppm and ϵc_{21} = 857.6 ppm (arbitrary sign). These propagate into a cylindrical extension of 16.7 μm and an equatorial displacement of 41.7 μm. The second solution yielded ϵc_{20} = 905.0 ppm and ϵc_{21} = 1075.7 ppm (arbitrary sign). These propagate into a cylindrical contraction of 38.6 μm and an equatorial displacement of 52.9 μm.

From Figure 2.5a it is apparent that the (0,2) mode is the most severely perturbed and shifted to a significantly lower value of u than the remaining modes.

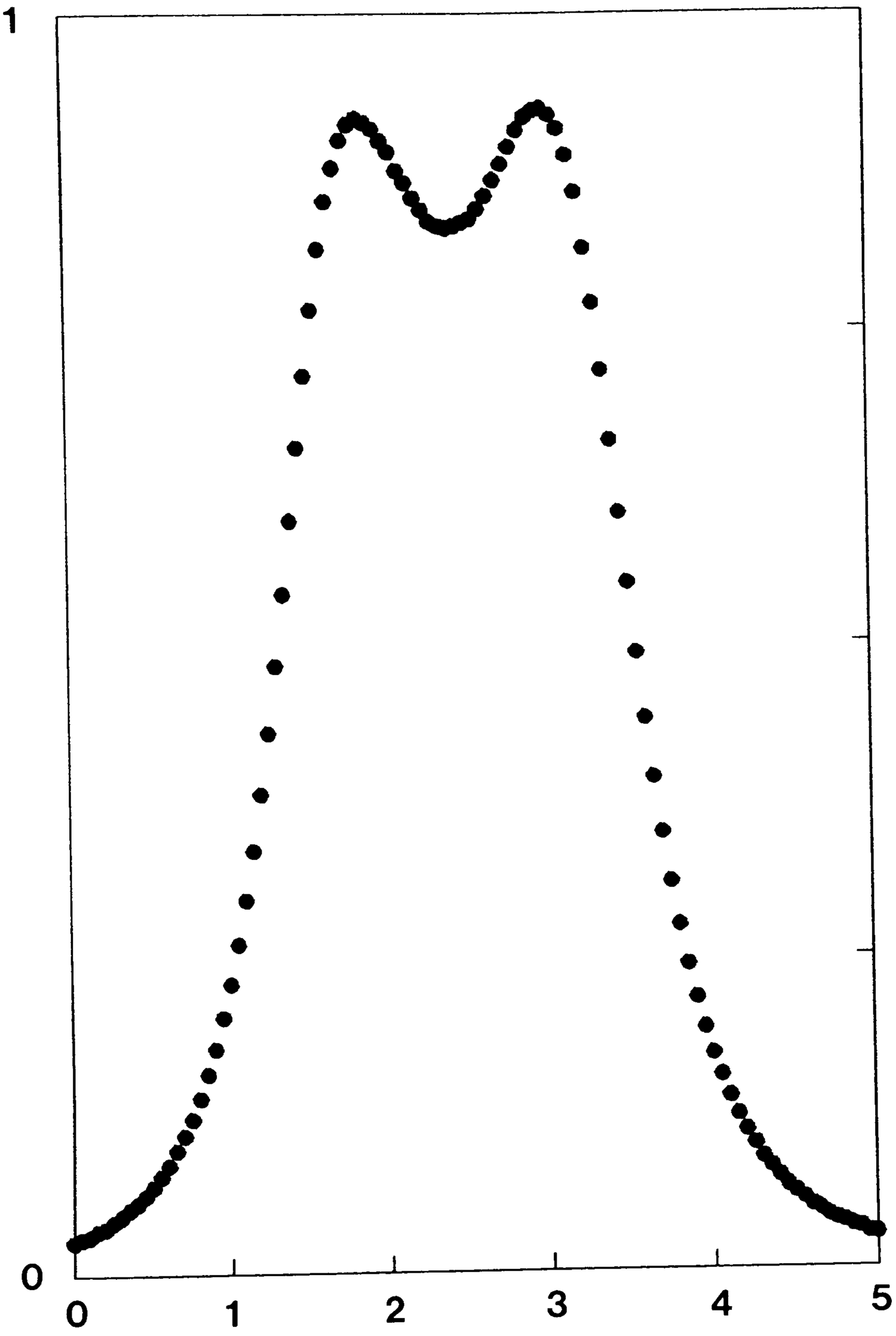

Figure 2.4: TM(1,1) microwave resonance at a temperature near 300 K.

a)

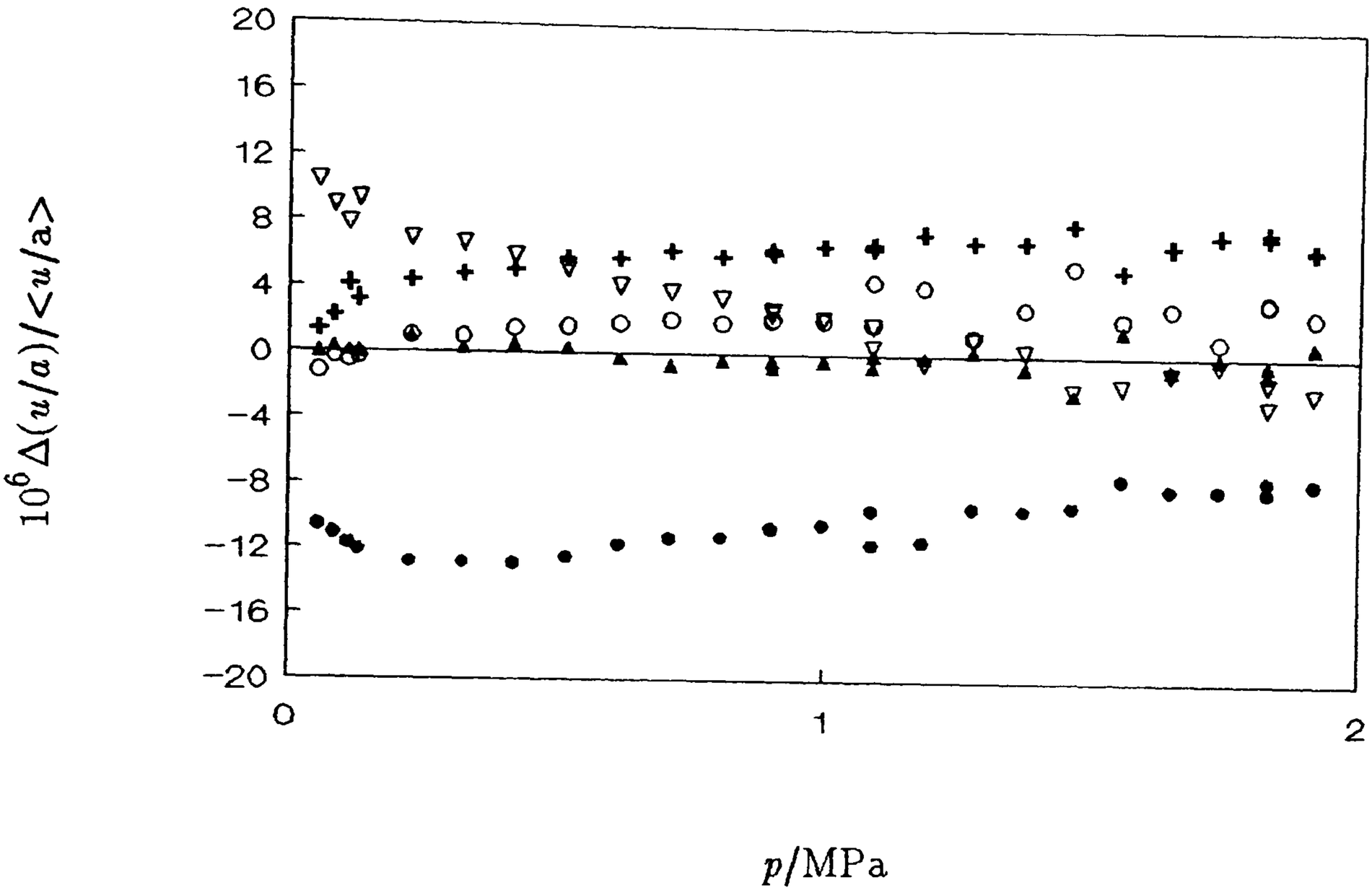

b)

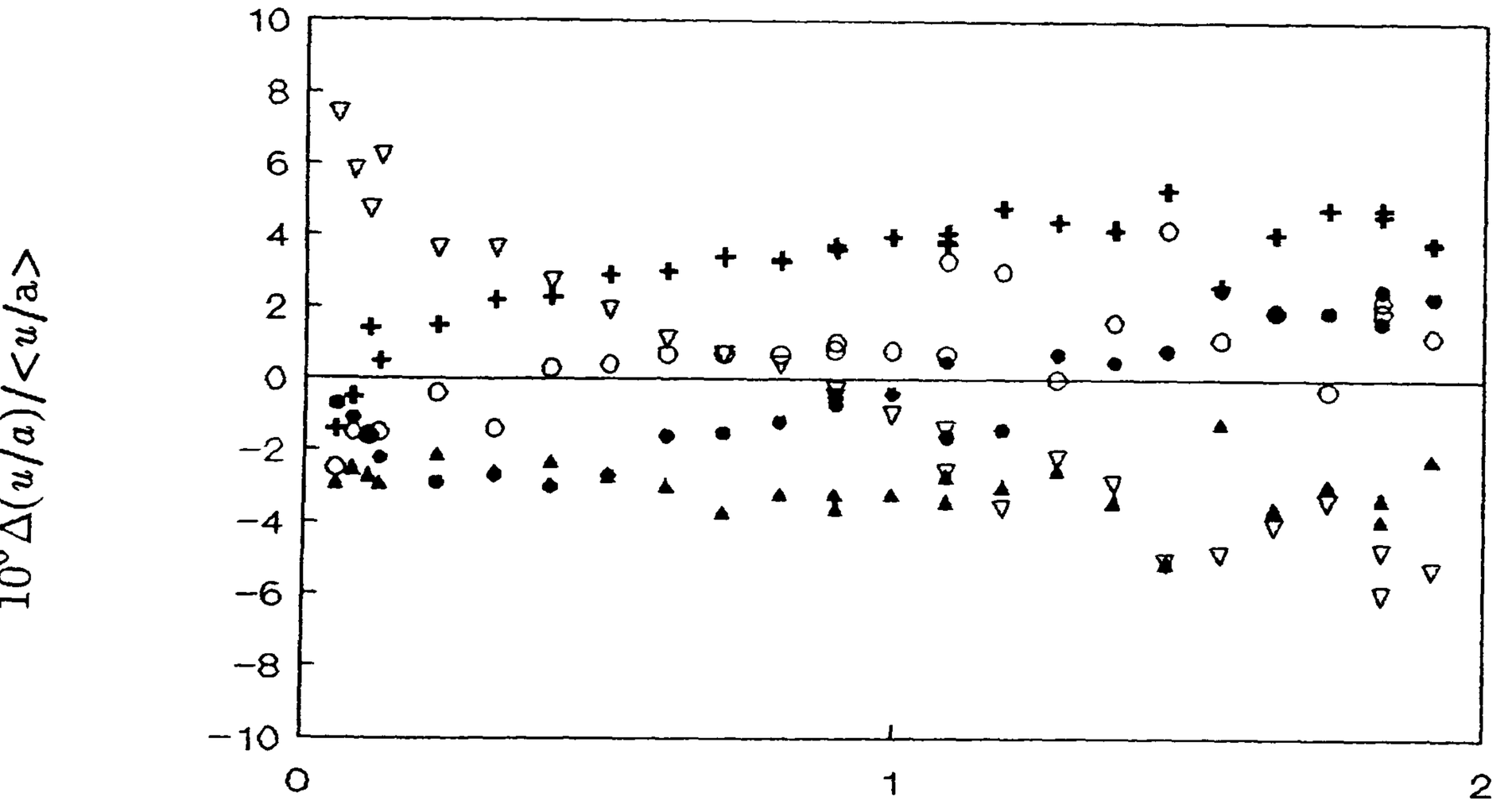

Figure 2.5: Deviation of individual modes from the mean at a given state; a) uncorrected for the geometric imperfection and b) corrected for the imperfection.

• , (0,2); ▲ , (0,3); ∘ , (0,4); + , (0,5), ∇ , (0,6).

The value of ϵc_{20} determined from the doublet analysis of the microwave measurements, combined with the possible corrections given by the Mehl models, does not resolve the discrepancies between the first four radial modes in the acoustic measurements. Given the possible values for ϵc_{20} and ϵc_{21} determined from the microwave measurements analysed as a triplet, the acoustic data is best explained using the second solution to the microwave resonance in combination with the model geometric imperfection of unequal hemispheres discussed by Mehl. This model deformation is seen to influence the (0,2) mode most severely, and in a manner consistent with these experimental observations, with the influence on the remaining modes being relatively slight. The equatorial displacement will have no influence on the radial modes studied in this case. Application of the appropriate correction yields values of the speed of sound determined from individual modes which are far more consistent (Figure 2.5b). We note, however, that there is still a systematic discrepancy apparent. This presumably results from the fact that the actual distortion is not as pure as the model requires and that some spheroidal character is present. However, the model is adequate for present purposes.

Preliminary high–pressure acoustic measurements in nitrogen indicated that the geometry of the sphere was to some extent pressure dependent. This can be seen in figure 2.6. At low pressures, agreement between the individual modes is as expected and independent of pressure. However, as the pressure is increased, a transition is observed whereby the (0,2) mode is shifted relative to the other modes. After this transition the ordering becomes independent of pressure.

Although the geometry may change with the static pressure of the gas, thus influencing the ordering of the modes relative to one another, these discrepancies, which are on the order of 10 ppm, are small compared with the inadequacies in the elastic theory of a thick shell. Inadequacies in the theory may be on the order of 10–20 ppm given losses of 10 or 20 ppm. At any rate the measurements were not conclusive and insufficient time was available to conduct microwave measurements at a series of pressures.

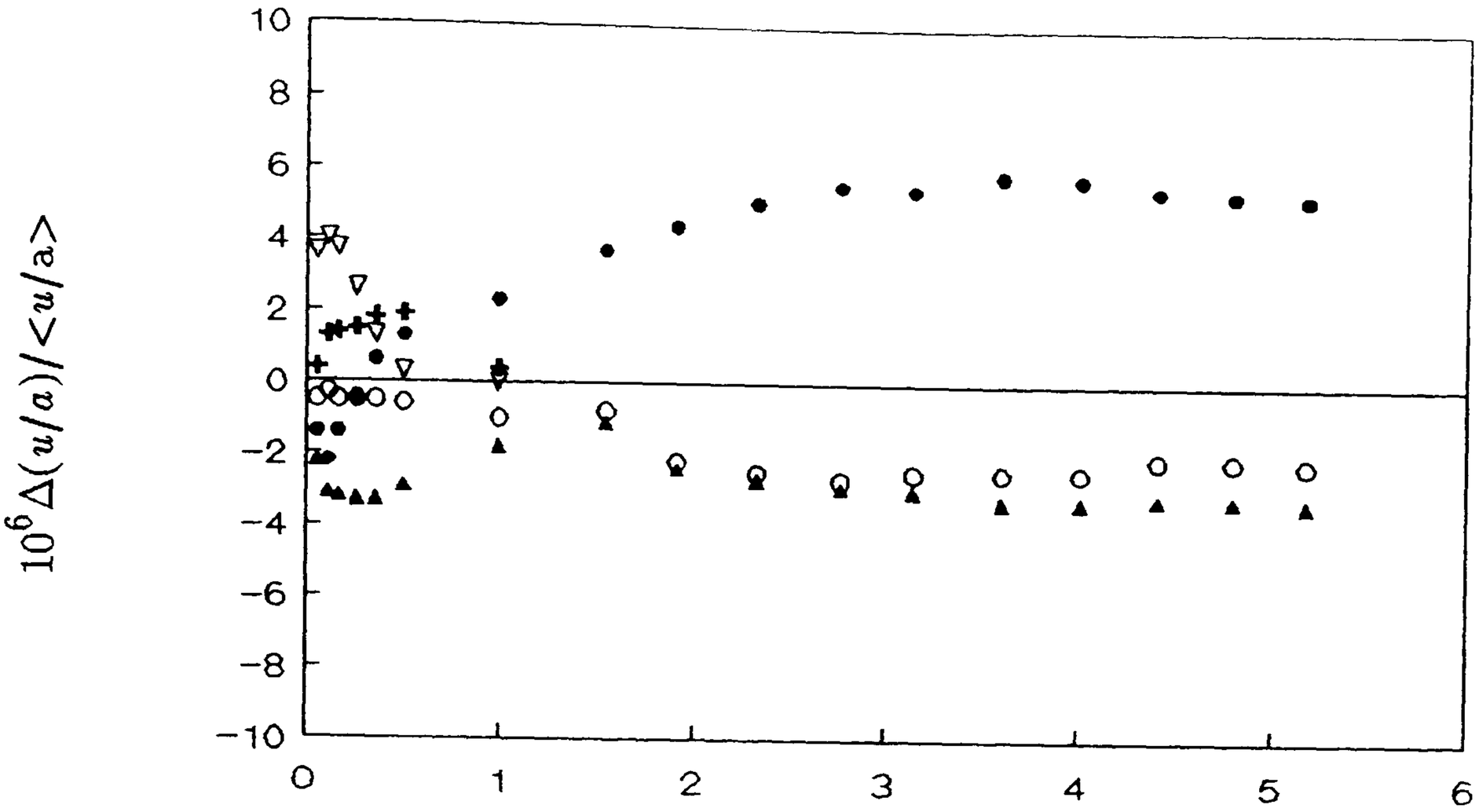

Figure 2.6: Experimental evidence for apparent pressure dependence of the geometry (see text). • , (0,2); ▲ , (0,3); ∘ , (0,4); + , (0,5); ∇ , (0,6).

2.4: Steady State Response of an Acoustic Cavity[2,6].

For a simple–harmonic source {with time dependence $\exp(-i\omega t)$}, excited from a small surface S_s on the boundary of the cavity, at a real frequency $f = \omega/(2\pi)$ with strength sufficiently constant for a steady state to be achieved, the steady–state response can be calculated using a Green's function. To lowest order, the acoustic pressure $p(\boldsymbol{r})$ is a solution of the Helmholtz equation and satisfies a boundary condition given in terms of a specific acoustic admittance. For any point r on the surface the acoustic pressure is given by

$$p(r,r_s) = -if\rho u^2/(2\pi V)\sum_N \phi_N(r)/[\Lambda_N\{F_N^2(f) - f^2\}]\int_{S_s} \phi_N(r_s)U_S(r_s)\mathrm{d}S, \quad (2.4.1)$$

where $U_S(r_s)$ is the radial surface velocity of the source relative to the rest of the shell, ϕ_N are the eigenfunctions of the normal modes, with corresponding complex natural frequencies $F_N(f) = \omega_N(\omega)/(2\pi)$. Λ_N is the average value of ϕ_N over the resonator volume, V, and N indicates the indices (l,m,n). The frequency dependence of the normal modes is slight and F_N is effectively constant for source f close to $\mathbb{R}(F_N)$.

The detector is generally a pressure transducer whose complex output voltage $(u - iv)$ is proportional to the acoustic pressure. In normal experimental practice only one or a small number of modes are excited and the contribution of the excited modes can be described in detail by including one or a small number of terms in the summation. The remaining terms are approximated by using a complex Taylor series in frequency. The detector output can then be written

$$u - iv = -iA_N f/(F_N^2 - f^2) + B + C(f - f_N) + \cdots \quad (2.4.2)$$

where A_N, B, C, $\cdots$ are complex constants with B and C representing the background. In this equation, $F_N = f_N - ig_N$ and the remaining constants are determined from measurements of u and v over a range of f near f_N.

2.5: References.

1. Morse, P. M.; Ingard, K. U. *Theoretical Acoustics*, McGraw–Hill, New York, 1968.

2. Mehl, J. B.; Moldover, M. R. *Topics in Current Physics, Volume 46*, Springer–Verlag, 1989.

3. Ewing, M. B.; McGlashan, M. L.; Trusler, J. P. M. *Metrologia* 1986, 22, 93.

4. Mehl, J. B. *J. Acoust. Soc. Am.* 1982, 71(5), 1109.

5. Mehl, J. B. *J. Acoust. Soc. Am.* 1985, 78(2), 783.

6. Moldover, M. R.; Mehl, J. B.; Greenspan, M. *J. Acoust. Soc. Am.* 1986, 79(2), 253.

7. Mehl, J. B. *J. Acoust. Soc. Am.* 1986, 79(2), 278.

8. Mehl, J. B.; Moldover, M. R. *J. Chem. Phys.* 1982, 77(1), 455.

9. Edwards, T. J.; Davis, R. S.; Mehl, J. B.; Moldover, M. R.; Trusler, J. P. M. *J. Res. Nat. Bur. Standards* 1988, 93(2), 85.

10. Ewing, M. B.; Goodwin, A. R. H.; McGlashan, M. L.; Trusler, J. P. M. *J. Chem. Thermodynamics* 1987, 19, 721.

11. Goodwin, A. R. H. Ph.D. Thesis, University of London 1988.

12. Trusler, J. P. M. Ph.D. Thesis, University of London 1984.

13. Morse, P. M.; Feshbach, H. *Methods of Theoretical Physics*, McGraw–Hill, New York, 1953.

14. Ewing, M. B.; Mehl, J. B.; Moldover, M. R.; Trusler, J. P. M. *Metrologia* 1988, 25, 211.

15. Mehl, J. B.; Moldover, M. R. *Physical Review A* 1986, 34(4), 3341.

16. Boyes, S. J.; Ewing, M. B.; Trusler, J. P. M. unpublished results 1989.

17. Trusler, J. P. M. unpublished results.

18. Herzfeld, K. F.; Litovitz, T. A. *Pure and Applied Physics Volume 7: Absorption and Dispersion of Ultrasonic Waves.* Massey, H. S. W.: Editor. Academic Press: London, 1959.

19. Lambert, J. D. *Vibrational and Rotational Relaxation in Gases.* Clarendon Press: Oxford, 1977.

20. Mehl, J. B.; Moldover, M. R. *J. Chem. Phys.* 1981, 74(7), 4062.

21. Ewing, M. B.; Trusler, J. P. M. *J. Chem. Phys.* **1989**, 90(2), 1106.

22. Boyes, S. J.; Ewing, M. B.; Trusler, J. P. M. *Proceedings of the Meeting of Commission B1 of the International Institute of Refrigeration*, Tel Aviv, Israel, **1990**.

23. Chang, C. T. M. *J. Acoust. Soc. Am.* **1971**, 49(3), 611.

24. Chang, C. T. M. *J. Acoust. Soc. Am.* **1972**, 51(1), 1.

CHAPTER 3: EQUATIONS OF STATE.

3.1: Introduction.

According to the phase rule, a phase of fixed composition has two degrees of freedom and so a chosen third intensive property, X_3, may be described in terms of two independent intensive properties X_1 and X_2 by an equation of state,

$$X_3 = X_3(X_1, X_2), \tag{3.1.1}$$

from which any intensive property can be expressed, using the appropriate thermodynamic relations, in terms of X_1 and X_2.

3.2: Equations of State.

Classical equations of state for a gaseous substance generally relate the intensive properties pressure p, molar volume V_{m}, and temperature T as either:

1) an infinite power series in one intensive property p or V_{m}; or

2) closed empirical equations.

Closed empirical equations can be of two types: a) simple cubic equations in V_{m} which are closely related to the van der Waals equation of state and b) empirical equations which have a variety of functional forms.

3.2.1: The Virial Equation.

The virial equation of state[1],

$$Z_{\mathrm{m}} = pV_{\mathrm{m}}/RT = 1 + B/V_{\mathrm{m}} + C/V_{\mathrm{m}}^2 + \cdots \qquad (3.2.1)$$

or its equivalent pressure–explicit expansion,

$$Z_{\mathrm{m}} = pV_{\mathrm{m}}/RT = 1 + (B'/RT)p + (C'/RT)p^2 + \cdots \qquad (3.2.2)$$

may be derived rigorously from statistical mechanics[2]. Here R is the gas constant, B, C, $\cdots$ are the second, third, $\cdots$ virial coefficients and

$$B' = B \qquad (3.2.3)$$

$$C' = (C - B^2)/(RT). \qquad (3.2.4)$$

In both expansions the series of coefficients are, for a given substance, functions of the temperature, T, only. A statistical mechanical derivation of equation (3.2.1) relates B, C, $\cdots$, to the intermolecular energies of clusters of two, three $\cdots$, molecules. In particular, the second virial coefficient is given by

$$B(T) = 2\pi L \int_0^\infty [1 - \exp\{-U(r)/kT\}] r^2 dr \qquad (3.2.5)$$

where $U(r)$ is the pair–wise intermolecular potential energy function and r is the intermolecular separation[3]. Expressions for the higher virial coefficients are complicated by the non–pairwise additivity of intermolecular potential energies.

For a multicomponent gas mixture, the second virial coefficients are given by

$$B(T, x_{\mathrm{A}}, x_{\mathrm{B}}, \cdots) = \sum_i \sum_j x_i x_j B(T)_{ij} \qquad (i, j = \mathrm{A}, \mathrm{B}, \cdots) \qquad (3.2.6)$$

where, in particular, for the binary gas mixture $\{(1-x)\mathrm{A} + x\mathrm{B}\}$

$$B(T, x) = (1-x)^2 B_{\mathrm{AA}} + 2(1-x)x B_{\mathrm{AB}} + x^2 B_{\mathrm{BB}} \qquad (3.2.7)$$

where B_{AA} and B_{BB} are the virial coefficients arising from interactions of pure A and pure B, respectively and B_{AB} arises from interaction of A and B and is known as the cross, or unlike, virial coefficient.

Both equations suffer the disadvantage that they must be truncated to represent a given set of measurements. Criteria for determining the number of coefficients that can be justified for a set of measurements have been discussed[4–6]. Determination of "true" values for the coefficients from a given set of measurements is more subtle. Determination of reliable estimates of B depends on its definition

$$B = \lim_{p \to 0} \{pV_{\mathrm{m}}/(RT) - 1\} V_{\mathrm{m}}, \qquad (3.2.8)$$

and the experimental realisation of this definition is very important, especially if large systematic errors in the higher coefficients are to be avoided[7,8].

As an alternative to (p, V_{m}, T) relations, equations of state can be written in the form

$$u^2 = u^2(T, p). \tag{3.2.9}$$

u is formally independent of the amount of substance and consequently should be immune from the effects of adsorption. However, an anomaly is known to exist, and has been observed experimentally at pressures greater than about 0.6 of the vapour pressure of the substance under study, when precondensation occurs[9].

For a non–relaxing gas the speed of sound is given by

$$u^2 = (\partial p/\partial \rho)_S = 1/(\rho \kappa_S) \tag{3.2.10}$$

in which ρ is the mass density and κ_S is the isentropic compressibility. Equation (3.2.10) can be written as an expansion

$$u^2 = A_0 + A_1 p + A_2 p^2 + \cdots \tag{3.2.11}$$

where

$$A_0 = RT\gamma^{\mathrm{pg}}/M = RT/\{M(1 - R/C^{\mathrm{pg}}_{p,\mathrm{m}})\}, \tag{3.2.12}$$

in which M is the molar mass, from which can be determined the perfect–gas heat capacities, and the second, β_{a}, and third, γ_{a}, acoustic virial coefficients

$$\beta_{\mathrm{a}} = RTA_1/A_0 \tag{3.2.13}$$

$$\gamma_{\mathrm{a}} = RTA_2/A_0. \tag{3.2.14}$$

The (p, V_{m}, T) virial coefficients B and C (or C') are related to the acoustic virial coefficients through[10]

$$\beta_{\mathrm{a}}(T) = 2B + 2(\gamma^{\mathrm{pg}} - 1)TdB/dT + (\gamma^{\mathrm{pg}} - 1)^2/\gamma^{\mathrm{pg}} T^2 d^2B/dT^2 \tag{3.2.15}$$

and

$$\begin{aligned}\gamma_{\mathrm{a}}(T) = [&\{(1 + 2\gamma^{\mathrm{pg}})/\gamma^{\mathrm{pg}}\}C + \{(\gamma^{\mathrm{pg}^2} - 1)/\gamma^{\mathrm{pg}}\}TdC/dT \\ &+ \{(\gamma^{\mathrm{pg}} - 1)^2/2\gamma^{\mathrm{pg}}\}T^2 d^2C/dT^2 - B\beta_{\mathrm{a}} \\ &+ \{(\gamma^{\mathrm{pg}} - 1)/\gamma^{\mathrm{pg}}\}\{B + (2\gamma^{\mathrm{pg}} - 1)TdB/dT + (\gamma^{\mathrm{pg}} - 1)T^2 d^2B/dT^2\}^2] \\ &\times \{1/(RT)\}.\end{aligned} \tag{3.2.16}$$

$$= (\gamma^{\mathrm{pg}} + 2)C' + 2(\gamma^{\mathrm{pg}} - 1)TdC'/dT$$
$$+ \{(\gamma^{\mathrm{pg}} - 1)^2/2\gamma^{\mathrm{pg}}\}T^2d^2C'/dT^2 + \Gamma(T). \qquad (3.2.17)$$

In equation (3.2.17) the quantity $\Gamma(T)$ is given by

$$\Gamma(T) = \{1/(RT)\}[B^2 + \{(\gamma^{\mathrm{pg}} - 1) + 4(\gamma^{\mathrm{pg}} - 1)^2\}(TdB/dT)^2$$
$$+ \{(\gamma^{\mathrm{pg}} - 1)^3/\gamma^{\mathrm{pg}}\}(T^2d^2B/dT^2)^2 + 4(\gamma^{\mathrm{pg}} - 1)TBdB/dT$$
$$+ 2\{(\gamma^{\mathrm{pg}} - 1)^2/\gamma^{\mathrm{pg}}\}T^2Bd^2B/dT^2 + 2\{(\gamma^{\mathrm{pg}} - 1)^2(2\gamma^{\mathrm{pg}} - 1)/\gamma^{\mathrm{pg}}\}$$
$$\times T^3dB/dTd^2B/dT^2] \qquad (3.2.18)$$

and is independent of C' and its derivatives.

The method of solution of these equations to determine B and C (or C') from the acoustic virial coefficients is discussed in Chapter 5.

For a binary gaseous mixture $u(T, p)$ measurements contain sufficient information to determine the mole fraction, provided that $C^{\mathrm{pg}}_{p,\mathrm{m}}$ and M are known for the pure components.

3.2.2: Empirical Equations.

The simple cubic equations derive from the van der Waals equation and modifications concentrate on the attractive and repulsive terms independently. The non–cubic equations are based on the van der Waals equation but lose the simple cubic form since modifications to both terms are considered simultaneously: hence, these equations have a variety of functional forms and rapidly become complicated.

3.2.2a: Simple Cubic Equations.

The van der Waals equation of state[11] has the following form

$$p = (RT/V_{\mathrm{m}})/(1 - 4y) - a/V^2_{\mathrm{m}} \qquad (3.2.19)$$

where the fraction of the volume actually occupied by the molecules is

$$y = b/(4V_{\mathrm{m}}) \qquad (3.2.20)$$

and b is the volume excluded by the molecules. The first term approximates the pressure of a hard–sphere fluid and the second term represents the effect of attractive interactions.

This equation only gives qualitative agreement with experiment and breaks down at the critical point, along with all analytic equations of state, where it lacks the appropriate singularity.

A pure fluid is said to obey the principle of corresponding states when

$$Z_{\mathrm{m}} = pV_{\mathrm{m}}/(RT) = \phi(p/p^{\mathrm{c}}, T/T^{\mathrm{c}}), \tag{3.2.21}$$

in which p^{c} is the critical pressure and T^{c} is the critical temperature. Extending equation (3.2.21) to three independent variables allows the formulation of a more general expression such that substances which do not obey this equation can be included. Pitzer's equation[12],

$$Z = \phi_{\omega}(p/p^{\mathrm{c}}, T/T^{\mathrm{c}}, \omega), \tag{3.2.22}$$

in which the accentric factor

$$\omega = \log_{10}\{p^{\mathrm{c}}/p^{\mathrm{l+g}}(T/T^{\mathrm{c}} = 0.7)\} - 1 \tag{3.2.23}$$

was chosen such that $\omega = 0$ for argon, krypton and xenon, is an important example. Further examples can be found in the literature[13–15].

The generalised cubic equation of state for a pure substance is

$$p = RT/(V_{\mathrm{m}} - b) - a(T)/\{V_{\mathrm{m}}^2 + V_{\mathrm{m}}cb - (c-1)b^2\} \tag{3.2.24}$$

where $a(T)$ and b are parameters that have been adjusted using p^{c}, T^{c}, and ω. The choice of c is empirical.

The Redlich–Kwong (RK) equation[16] has $c = 1$ and $a(T)$ given by

$$a(T) = a(T^{\mathrm{c}})/T^{\frac{1}{2}}, \tag{3.2.25}$$

and $Z^{\mathrm{c}} = 1/3$. Soave[17] extended the temperature dependence (RKS) by writing

$$a(T) = a(T^{\mathrm{c}})\alpha(T/T^{\mathrm{c}}, \omega) = a(T^{\mathrm{c}})[1 + m(\omega)\{1 - (T/T^{\mathrm{c}})^{\frac{1}{2}}\}]^2 \tag{3.2.26}$$

in which

$$m = e + f\omega + g\omega^2. \tag{3.2.27}$$

Values of e, f, and g are given in reference 17. Gibbons and Laughton[18] (GL) modified $\alpha(T/T^{\mathrm{c}})$ such that

$$a(T) = a(T^{\mathrm{c}})\alpha(T/T^{\mathrm{c}}) = a(T^{\mathrm{c}})[1 + X(T/T^{\mathrm{c}} - 1) + Y(T/T^{\mathrm{c}})^{\frac{1}{2}} - 1\}] \tag{3.2.28}$$

where X and Y are substance dependent constants. Values are given in reference 18.

The Peng–Robinson equation[19] (PR) has $c = 2$ with $a(T)$ having the form proposed by Soave. Peng and Robinson's values for e, f and g can be found in reference 19. Harmens *et al*[20,21] have developed equations with $c = 3$ and with c as a parameter.

The equations discussed above elaborate the attractice term in the van der Waals equation while retaining the repulsive term. An alternative is to elaborate the hard–sphere term.

3.2.2b: Non–Cubic Empirical Equations.

Extensive modifications to both the attractive and repulsive terms leads to equations which are no longer cubic in V_m. Beattie and Bridgeman[22] developed the following equation

$$p = RT/V_m + (B_0RT - A_0 - Rc/T^2)/V_m^2 + (aA_0 - B_0bRT - RB_0c/T^2)/V_m^3 + RB_0bc/(V_m^4T^2) \quad (3.2.29)$$

in which a, b, c, A_0 and B_0 are adjustable parameters. This only provides a representation of fluid surfaces at densities below the critical. Benedict, Webb and Rubin[23] (BWR) modified equation (3.2.29) to obtain

$$p = RT/V_m + (B_0RT - A_0 - C_0/T^2)/V_m^2 + (bRT - a)/V_m^3 + a\alpha/V_m^6 + \{c(1 + \gamma)/V_m^2)\exp(-\gamma/V_m^2)\}/(V_m^3T^2), \quad (3.2.30)$$

where a, b, c, A_0, B_0, α and γ are parameters, and is applicable at densities up to twice the critical. Values of the parameters can be found in the literature[36].

Further modifications to provide more precise representations of volumetric results, and more recently to provide other properties[24,25], have a variety of functional forms, for example Strobridge's equation for nitrogen[26].

Application of these equations to mixtures requires generalisation of the parameters. In the van der Waals one–fluid approximation the molecular parameters for a multicomponent mixture are defined by[27]

$$a(x_A, x_B, \cdots) = \sum_i\sum_j x_i x_j a_{ij} \qquad (i, j = A, B, \cdots) \quad (3.2.31)$$

Table 3.1: Mole fractions x_B of allowed components B in the GERG equation.

B	x_B
CH_4	$\geqslant 0.5$
N_2	$\leqslant 0.5$
CO_2	$\leqslant 0.3$
C_2H_6	$\leqslant 0.2$
C_3H_8	$\leqslant 0.05$
C_4H_{10}	$\leqslant 0.015$
C_4H_{12}	$\leqslant 0.005$
H_2	$\leqslant 0.1$
CO	$\leqslant 0.03$
He	$\leqslant 0.005$

Table 3.2: Components allowed in the GRI equation of state.

Component			
N_2	CO	nC_4H_{10}	nC_7H_{16}
CO_2	H_2	iC_4H_{10}	nC_8H_{18}
H_2S	CH_4	nC_5H_{12}	nC_9H_{20}
He	C_2H_6	iC_5H_{12}	$nC_{10}H_{22}$
O_2	C_3H_8	nC_6H_{14}	

$$b(x_A, x_B, \cdots) = \sum_i \sum_j x_i x_j b_{ij} \qquad (i, j = A, B, \cdots) \tag{3.2.32}$$

where

$$b_{AB}^{\frac{1}{3}} = \tfrac{1}{2}(b_{AA}^{\frac{1}{3}} + b_{BB}^{\frac{1}{3}}) \tag{3.2.33}$$

and

$$a_{AB} = \zeta b_{AB}\{a_{AA}a_{BB}/(b_{AA}b_{BB})\}^{\frac{1}{2}} \tag{3.2.34}$$

are the modified Lorentz–Berthelot combining rules. For the modified van der Waals equations, the adjustable parameters are given by

$$b(x_A, x_B, \cdots) = \sum_i \sum_j x_i b_i \qquad (i = A, B, \cdots) \tag{3.2.35}$$

with $a(x_A, x_B, \cdots)$ being given by equation (3.2.32) with

$$a_{ij} = (1 - \xi_{ij})(a_{ii}a_{jj})^{\frac{1}{2}}. \tag{3.2.36}$$

ζ and ξ are constants close to unity.

For the modified Beattie and Bridgeman (BWR) equation the generalisation of the parameters is given in references 28 and 29.

Equations of state derived solely from experimental results allow modification of the functional forms and revision of the constants to give better representations for the fluids considered. Two equations which have been particularly successful when applied to mixtures are due to Schouten *et al* and Starling *et al.* Schouten *et al*[30–34] developed a virial equation truncated at the third virial coefficient valid for the components and composition ranges given in Table 3.1: this is the GERG equation. Starling *et al*[35], following the approach of Strobridge, developed two modified Benedicts, Webb and Rubin equations: the GRI equations. One was an equation for CH_4 and the other for mixtures containing components given in Table 3.2. Both sets of equations have been validated against the same sets of experimental results.

3.3: Sonic Nozzles.[37–39]

Before considering the flow of a fluid through a nozzle, it is necessary to develop some equations. These are best developed by considering initially the flow of an

unbounded fluid. A fundamental equation of fluid dynamics, which shall be considered axiomatic in this discussion, is Euler's equation. This equation of motion for the fluid is given by

$$\partial \boldsymbol{v}/\partial t + (\boldsymbol{v}\cdot\mathbf{grad})\boldsymbol{v} = -1/\rho \mathbf{grad} p \tag{3.3.1}$$

in which v is the velocity of a unit volume of fluid, p is the pressure exerted on the volume element and ρ is the mass per unit volume. If the flow of the fluid is isentropic (adiabatic + reversible) then the equation of motion can be recast in the following form

$$\partial \boldsymbol{v}/\partial t - \boldsymbol{v}\times\mathbf{curl}\boldsymbol{v} = -\mathbf{grad}(w + \tfrac{1}{2}v^2) \tag{3.3.2}$$

in which w is the heat function per unit mass of fluid (enthalpy). These equations are simplified if the fluid flow is steady. By steady flow it is meant the velocity is constant in time at any point occupied by fluid, that is, $\boldsymbol{v}$ depends only on the coordinates. Equation (3.3.2) then reduces to

$$\tfrac{1}{2}\mathbf{grad}v^2 - \boldsymbol{v}\times\mathbf{curl}\boldsymbol{v} = -\mathbf{grad}w. \tag{3.3.3}$$

Introduction of the concept of streamlines, which are defined such that the tangent to a streamline at any point gives the direction of the velocity at that point, leads to

$$\tfrac{1}{2}v^2 + w = a \tag{3.3.4}$$

which is Bernoulli's equation. In general the constant a takes different values for different streamlines. If there is a point on some streamline at which the gas velocity is zero, then we can write Bernoulli's equation as

$$\tfrac{1}{2}v^2 + w = w_0 \tag{3.3.5}$$

where w_0 is the value of the heat function at the point where $v = 0$. We can deduce from this equation that the greatest possible value of the velocity (for given values of the thermodynamic quantities at the point where $v = 0$) is $v_{\max}^2 = 2w_0$, when $w = 0$. Application of thermodynamics leads to

$$v_{\max} = c_0[2/(\gamma - 1)]^{\frac{1}{2}}, \tag{3.3.6}$$

where γ is the ratio of specific heat capacities. From Euler's equation we find that

$$vdv = -dp/\rho \tag{3.3.7}$$

holds along a streamline. From mechanics we have $dp = u^2 d\rho$, hence

$$d\rho/dv = -\rho v/u^2 \tag{3.3.8}$$

from which we obtain

$$d(\rho v)/dv = \rho\{1 - (v^2/u^2)\}. \tag{3.3.9}$$

From this we can see that as the velocity increases the mass flux density, $j = \rho v$, increases as long as the flow remains subsonic, $v < u$. In the supersonic range, however, the mass flux density diminishes with increasing velocity, and vanishes together with ρ when $v = v_{max}$. This important difference between subsonic and supersonic steady flows can be interpreted as follows. In subsonic flow the streamlines converge in the direction of increasing velocity, whereas in supersonic flow they diverge in that direction. The flux, j, has its maximum value at the point where the gas velocity is equal to the local velocity of sound, $j_* = \rho_* u_*$.

It is now possible to consider the steady flow of a gas out of a large vessel through a tube with variable cross–section (a nozzle). The mass of gas passing through a cross–section of the tube in unit time (the discharge) is $Q = \rho v S$, where S is the cross–sectional area of the tube at the point under consideration, and is constant along the length of the tube. The linear dimensions of the tube are assumed very large in comparison with the diameter of the tube. The velocity of the gas in the vessel may therefore taken to be zero. It has been shown that the flux density, j, cannot exceed a certain limiting value. It is therefore clear that, for a given tube and a given state of the gas, the discharge has an upper limit Q_{max}. The maximum value of j can only be attained at the narrowest point of the tube (the throat), where the cross–sectional area is S_0 and therefore the upper limit to the total discharge is

$$Q_{max} = \rho_* u_* S_0. \tag{3.3.10}$$

Consideration of a nozzle which narrows continually towards its outer end, Figure 3.1a, leads to the flux density increasing monotonically along the tube. The same is true of the gas velocity v and the pressure accordingly falls monotonically. The greatest value of j is reached if v attains the value of u just at the outer end of the tube. At this point $p_e = p_*$. Consideration of the hydrostatics of the system shows that the pressure drop occurring across the nozzle can never exceed $p - p_e = p - p_*$, where p is the

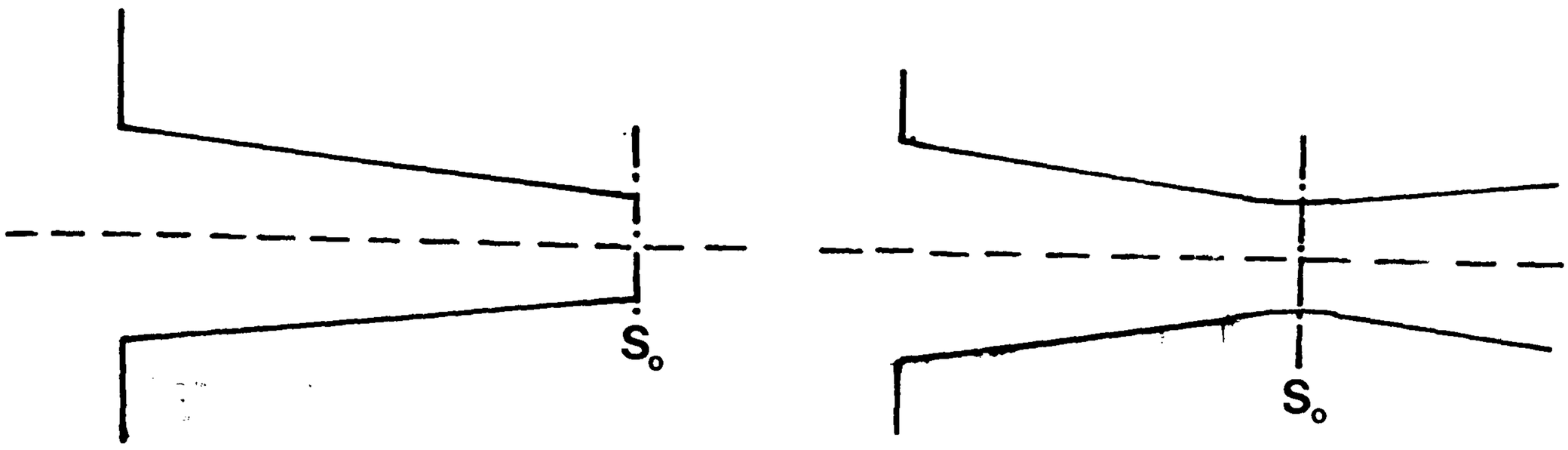

Figure 3.1: a) a sonic nozzle and b) a de Laval nozzle.

---

pressure in the vessel. Thus, the gas cannot acquire a supersonic velocity in flowing through a nozzle of this kind. From this it is clear that supersonic velocities can only be attained by means of a nozzle which first narrows and then widens again. This sort of device is called a de Laval nozzle and is shown in Figure 3.1b.

The interest in sonic nozzles stems from their simplicity and lack of moving parts. Therefore, they are easily maintained and may well become the flow metering standard for the gas industry. Calculation of mass flow rates through nozzles invariably requires the use of an equation of state combined with a method of predicting the perfect–gas heat capacity. These are required to obtain estimates of the speed of sound at the steady state conditions of the throat of the nozzle. Experimentally it has been determined that the nozzles are not perfect and it is necessary to determine a discharge coefficient from auxiliary experiments.[38,39] This is usually a gravimetric analysis using air as the calibration fluid. It has been shown that determinations with one gas are adequate for flow rate measurements with other gases[39].

Evaluation of equations of state is of utmost importance if reliable estimates of flow rates are required. Consequently, comparison of speed of sound predictions with values determined experimentally are invaluable. The experimental results for the industrially important gases reported here are compared with predictions from various equations of state in a later chapter.

3.4: References.

1. Mason, E. A.; Spurling, T. H. *Encyclopedia of Physical Chemistry and Chemical Physics*: *Volume 10.2*; *The Virial Equation of State.* Rowlinson, J. S.: Editor Pergamon: Oxford 1969.

2. Mayer, J. E.; Mayer, M. G. *Statistical Mechanics* Wiley: New York. Second Edition 1977.

3. Maitland, G. C.; Rigby, M.; Smith, E. B.; Wakeham, W. A. *Intermolecular Forces. Their Origin and Determination.* Clarendon: Oxford, 1981.

4. Hall, K. R.; Canfield, F. B. *Physica* 1967, 33, 481.

5. Holleran, E. M. *J. Chem. Thermodynamics* 1970, 2, 779.

6. Ewing, M. B.; Marsh, K. N. *J. Chem. Thermodynamics* 1979, 11, 793.

7. Scott, R. L.; Dunlop, R. D. *J. Phys. Chem.* 1962, 66, 639.

8. Knobler, C. M. *Pure and Appl. Chem.* 1983, 55, 455.

9. Mehl, J. B.; Moldover, M. R. *J. Chem. Phys.* 1982, 77(1), 455.

10. Van Dael, W. *Experimental Thermodynamics Volume* II, Butterworths: London, 1968.

11. van der Waals, J. D. Thesis: Leydon 1873.

12. Pitzer, K. S.; Lipman, R. F.; Curl, R. F.; Huggins, C. M.; Peterson, D. E. *J. Am. Chem. Soc.* 1955, 77, 3433.

13. Leland, T. W.; Chappelear, P. S. *Ind. Eng. Chem.* 1968, 60, 15.

14. Leach, J. W.; Chappelear, P. S.; Leland, T. W. *A. I. Ch. E. J.* 1968, 14, 568.

15. Fisher, G. D.; Leland, T. W. *Ind. Eng. Chem. Fundamentals* 1970, 9, 537.

16. Redlich, O.; Kwong, J. N. S. *Chem. Rev.* 1949, 44, 223.

17. Soave, G. *Chem. Eng. Sci.* 1972, 27, 1197.

18. Gibbons, R. M.; Laughton, A. P. *J. Chem. Soc. Faraday Trans. 2*, 1984, 80, 1019.

19. Peng, D. Y.; Robinson, D. B. *Ind. Eng. Chem. Fundam.* 1976, 15, 59.

20. Harmens, A. *Cryogenics* 1977, 17, 519.

21. Harmens, A.; Knapp, H. *Ind. Eng. Chem. Fundam.* 1980, 19, 291.

22. Beattie, J. A.; Bridgeman, O. C. *Proc. Amer. Acad. Arts Sci.* 1929, 63, 229.

23. Benedict, M.; Webb, G. B.; Rubin, L. C. *J. Chem. Phys.* **1940**, 8, 334.

24. McCarty, R. D. *Experimental Thermodynamics Volume* II, Butterworths: London, **1968**.

25. Younglove, B. A.; McCarty, R. D. *J. Chem. Thermodynamics* **1980**, 12, 1121.

26. Strobridge, T. R. *The Thermodynamic Properties of Nitrogen from 64 to 300 K between 0.1 and 200 Atmospheres.* Tech. Note U. S. Nat. Bur. Stand. 129, **1962**.

27. Leland, T. W.; Rowlinson, J. S.; Sather, G. A. *Trans. Faraday Soc.* **1968**, 64, 1447.

28. Benedict, M.; Webb, G. B.; Rubin, L. C. *J. Chem. Phys.* **1942**, 10, 747.

29. Benedict, M.; Webb, G. B.; Rubin, L. C. *Chem. Eng. Prog.* **1951**, 47, 419.

30. Schouten, J. A.; Michels, J. P. J.; Prins, C.; van der Gulik, P. S.; Trappeniers, N. J. Report No 8410–1, van der Waals Laboratory, Netherlands, **1984**.

31. Schouten, J. A.; ten Seldam, G. A.; Biswas, S. N.; Michels, J. P. J.; Trappeniers, N. J. Report No 8410–2, van der Waals Laboratory, Netherlands, **1984**.

32. Schouten, J. A.; Michels, J. P. J.; ten Seldam, G. A.; Trappeniers, N. J. Report No 8410–3, van der Waals Laboratory, Netherlands, **1984**.

33. Schouten, J. A.; Michels, J. P. J. Report No 8410–4, van der Waals Laboratory, Netherlands, **1984**.

34. Schouten, J. A.; Michels, J. P. J.; ten Seldam, G. A. Report No 8410–5, van der Waals Laboratory, Netherlands, **1984**.

35. Starling, K. E.; Klein, M.; Little, F. G. *Proc. Congress Gas Quality – Specification and Measurement of Physical and Chemical Properties of Natural Gas.* van Rossum, G. J.: Editor, Elsevier: Oxford, **1986**.

36. Reid, R. C.; Sherwood, T. K. *The Properties of Gases and Liquids*, McGraw–Hill: New York. Second Edition **1966**.

37. Landau, L. D.; Lifshitz, E. M. *Course of Theoretical Physics: Volume 6. Fluid Mechanics*, Pergamon Press. Second Edition **1987**.

38. Johnson, R. C. *J. Basic Eng. Trans. A. S. M. E. series D* **1964**, 86, 519.

39. Johnson, R. C. *J. Basic Eng. Trans. A. S. M. E. series D* **1970**, 92, 580.

CHAPTER 4: EXPERIMENTAL TECHNIQUES.

4.1: Introduction.

The resonance frequencies and half–widths of the radial modes were calculated using comparative measurements of the amplitude and phase of the received to reference signals.

Temperatures of the samples in the spherical cavities were determined on the International Practical Temperature Scale of 1968 from measurements of the resistances of several platinum resistance thermometers using an a.c. resistance bridge.

Pressures required in the determination of low–pressure $u(T, p)$ results were measured using either a direct reading differential capacitance manometer, or a differential capacitance manometer, used as an approximately null reading indicator, and a quartz spiral gauge. Measurement of the pressure in the high–pressure apparatus was relative to that of the ballast gas measured using a differential pressure transducer and either an oil–lubricated pressure balance, with atmospheric pressure measured using a Fortin barometer, or directly from the change in resonance frequency of a quartz crystal gauge.

4.2: Measurement of Resonance Frequencies.

The sine–wave signals used for acoustic measurements were synthesized by an impedance analyzer (Hewlett–Packard, model number HP4192A, serial number 820031)

which was controlled by a microcomputer over an IEEE interface, and was phase–locked to the 10 MHz time–base of a counter (Hewlett–Packard 5315B option 004) ensuring that the fractional accuracy of the signals was better than 10^{-7}. The output from the impedance analyzer, which was variable between 0.005 and 1.1 V r.m.s. and 5 to 13 × 10^6 Hz in increments of 0.001 V r.m.s. and 0.001 to 1 Hz, was amplified to 60 V r.m.s. and mixed with a d.c. bias of 300 V before being passed to the source transducer. A reference signal was supplied to the analyzer from a resistive–potential divider placed in parallel with the output of the power amplifier. The detector output was fed to a low noise differential amplifier, based on three operational amplifiers[1], which had a forward potential difference gain of 1000. The signal was further amplified and filtered to remove low– and high–frequency noise by a bandpass amplifier with a potential difference gain variable between 10 and 30, and then fed to the test input channel of the impedance analyzer. Under typical conditions the signal at the input of the analyzer was between 0.1 and 1 V r.m.s. and its amplitude, $\bar{a}$, and phase, ϕ, could be measured with a resolution of 0.01 % and 0.0002 rad, with a time constant of 1 s.

The procedure by which $F_{0n} = f_{0n} - ig_{0n}$ is determined from equation (2.4.2) is well documented in the literature[2–5]. Briefly, estimates of f_{0n} and g_{0n} were obtained from manual scans in the appropriate frequency ranges. The network analyzer was then stepped from a frequency near $f_{0n} - g_{0n}$ in ten equal increments of $g_{0n}/5$ to a frequency near $f_{0n} + g_{0n}$; the sign of the increment was then reversed and the frequency stepped down to its original value. At each discrete frequency a time t was allowed for the acoustic pressure to stabilise, such that the fractional systematic error in the response of the cavity was less than 10^{-7}, before $\bar{a}$ and ϕ were recorded. Measurements of the amplitude and phase at each frequency were then expressed in terms of the real and imaginary parts of the complex potential difference ratio,

$$w = \bar{a}\cos\phi - i\bar{a}\sin\phi = u - iv, \tag{4.2.1}$$

of the received and reference signals. The 11 frequencies and 22 complex potential differences were used to evaluate F_{0n}, A_{0n}, B and, if significant, C in the theoretical form of the resonance

Table 4.1: Coefficients for the measurement of temperature on IPTS–68 from the resistances of various platinum thermometers.

	B145	B225	LN780308
R_0/Ω	24.88165	25.31496	25.56008
$10^3\alpha/^0C^{-1}$	3.925708	3.925129	3.92593
$\delta/^0C$	1.4967	1.4967	1.49665
$10^6 e_4/K$	0.4846525	2.824283	–21.2
$10^6 b_4/K$	–25.88	–83.78	–18.1

$$w = A_{0n} f/(F_{0n}^2 - f^2) + B + Cf, \qquad (4.2.2)$$

using a non–linear fitting procedure similar to the one developed by Mehl[4,5]. As noted in Chapter 2, A_{0n} is a complex amplitude proportional to the source strength (and any phase differences between source and detector), and B and C are the first two terms in a complex Taylor series expansion that accounts for any background arising from, for example, the "tails" of other modes. A precision of $10^{-6} f_{0n}$ or better is possible using the instrumentation and analysis discussed above.

4.3: Temperature Measurement.

Temperatures were measured using platinum resistance thermometers (PRT's) calibrated on the International Practical Temperature Scale of 1968 (IPTS–68)[6,7].

The temperature of the low–pressure resonator was measured using two capsule–type thermometers (Tinsley type, identification numbers B145 and B225). The required constants for the temperature range 13.81 to 373.15 K are given in Table 4.1.

A long–stem platinum resistance thermometer was used to measure the temperature of the high–pressure cavity (Leeds and Northrup, serial number 780308). This was calibrated in the range 90.188 to 903.89 K, the required constants for which are given in Table 4.1.

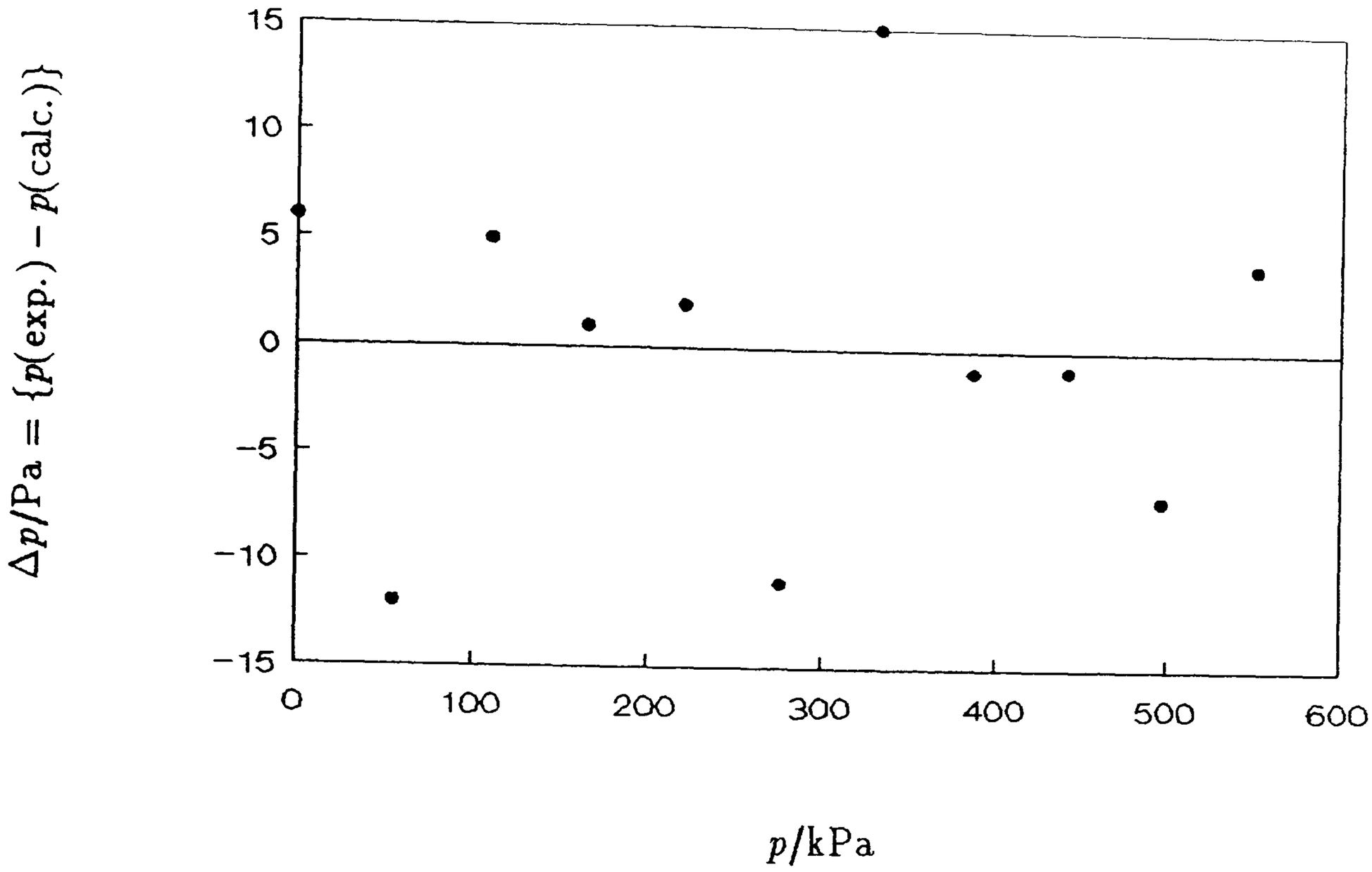

Figure 4.1: Deviation of calibration points from equation (4.4.1).

Resistances were measured using an a. c. bridge (Tinsley type 5840, serial number 830037) operating at 375 Hz and a current of 1 mA , with a precision and resolution of 10 $\mu\Omega$. Drifts in the bridge were monitored using a standard Wilkins Resistor (Wilkins type 5685A, serial number 236201) and PRT resistances were checked frequently in a triple–point of water cell[8].

4.4: Pressure Measurement.

4.4.1: Low Pressure Measurement.

The pressure of the sample gas was generally measured with a differential capacitance manometer (MKS type 310CD, 1.3 MPa full scale) connected in the external pipework, the reference port of which was continually evacuated by a mechanical pump. Calibration of the instrument was by comparison with an air–lubricated pressure balance (Ruska, type 2465–751–00, serial number 18510). The

results could be represented using

$$P(\mathrm{DCM})/\mathrm{mV} = 300.00 + 7.664p - 2.492 \times 10^{-8}p^3, \qquad (4.4.1)$$

with a standard deviation of 0.07 mV (equivalent to 9 Pa). Deviation of calibration points from this equation are shown in Figure 4.1.

For the measurements in methanol, where A_1/A_0 is large and the vapour pressure is low, the sample in the resonator was isolated from a quartz–spiral gauge (Ruska DDR 6000) using a differential capacitance manometer (MKS Baratron, model number 221AH–A–10) which was operated as an approximately null–reading instrument. The span of the manometer was 1.73 kPa and the manufacturer's calibration showed no deviations greater than 0.1 % of reading from linearity. Calibration of the quartz–spiral gauge against a precise mercury manometer, which has a precision and accuracy of 1 Pa, gave

$$p/\mathrm{kPa} = 9.988526_5(\phi_r/\mathrm{V}) \qquad (4.4.2)$$

where p is the pressure indicated by the manometer and quartz–spiral gauge and ϕ_r is the corresponding d.c. potential difference from the gauge.

4.4.2: High Pressure Measurement.

The pressure of the sample gas was measured relative to the pressure–compensating fluid (nitrogen, in this work), the two being isolated by a digital pressure transducer (DPT), by means of a quartz gauge in the pressure range 0–7000 kPa, and an oil–lubricated pressure balance[10,11] for pressures above 7 MPa.

The DPT was supplied by Schaevitz (model number P642–0001, serial number 83911) details of which have been reported previously[13]. The calibration results are reported here for convenience. The positive span could be represented up to 100 kPa by

$$\Delta_+p/\mathrm{kPa} = 19.699(\phi/\mathrm{V}) + 6.27 \times 10^{-3}(\phi/\mathrm{V})^3, \qquad (4.4.3)$$

where ϕ is the d.c. voltage output from the DPT, with a standard deviation of 9 Pa. The negative span functioned only up to $\Delta\_p \approx 31$ kPa and could be represented by

$$\Delta\_p/\mathrm{kPa} = 19.696(\phi/\mathrm{V}) \qquad (4.4.4)$$

with a standard deviation of 4 Pa. The shift in the zero pressure differential reading,

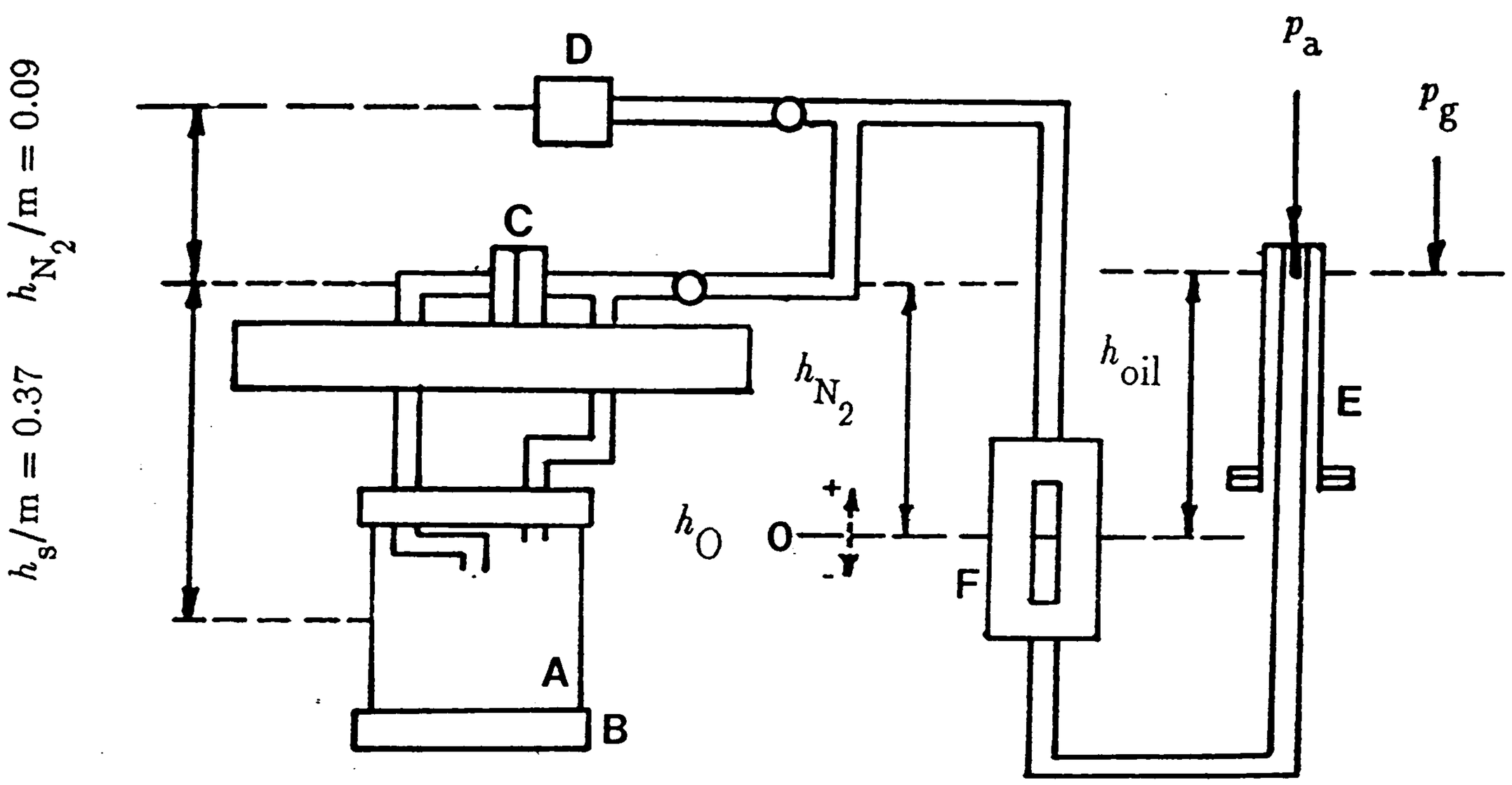

$$h_{N_2}/\mathrm{m} = 0.168 - h_O$$

$$h_{oil}/\mathrm{m} = 0.150 - h_O$$

Figure 4.2: Schematic representation of sample pressure measurement for the high–pressure resonator, A, contained within the pressure vessel, B, using a differential pressure transducer, C, and either 1) the "digiquartz" for direct measurements at pressures up to 7 MPa or 2) an oil lubricated pressure balance, E, with nitrogen connecting A and F, the oil–nitrogen interface. O is a sight gauge allowing observation of the interface.

Table 4.2: Coefficients for determination of pressure from measurements of the pressure and temperature periods of the quartz oscillator in the digiquartz.

Coefficient	Numerical Value
C_1/kPa	33876.052
C_2/kPaμs^{-1}	2432.6106
C_3/kPaμs^{-2}	107466.83
D_1	0.0267322
D_2	–0.3599045
T_1/μs	24.94856
T_2	0.1861965
$T_3\mu$s	14.93324
U_0/μs	5.877146

ϕ_z, as a function of line pressure p could be represented to 0.2 mV by

$$\phi_z/\mathrm{V} = -7.89 \times 10^{-6}(p/\mathrm{kPa}). \tag{4.4.5}$$

The quartz gauge ("digiquartz") was supplied by Paroscientific inc.(model number 2900 AT, serial number 31285) and is temperature compensated. The period of the quartz crystals (one for pressure and one for temperature measurement) were measured with a universal counter (Hewlett Packard 5315B option 004). Pressures were computed from the two frequencies and a set of calibration coefficients determined by the manufacturer. The coefficients appear in the equations

$$p/\mathrm{kPa} = C(1 - T_0^2/\tau_p^2)[1 - D(1 - T_0^2/\tau_p^2)] \tag{4.4.6}$$

where τ_p is the pressure sensor period in microseconds, and

$$C = C_1 + C_2U + C_3U^2 \tag{4.4.7}$$

$$D = D_1 + D_2U^2 \tag{4.4.8}$$

$$T_0 = T_1 + T_2U + T_3U^2 \tag{4.4.9}$$

where

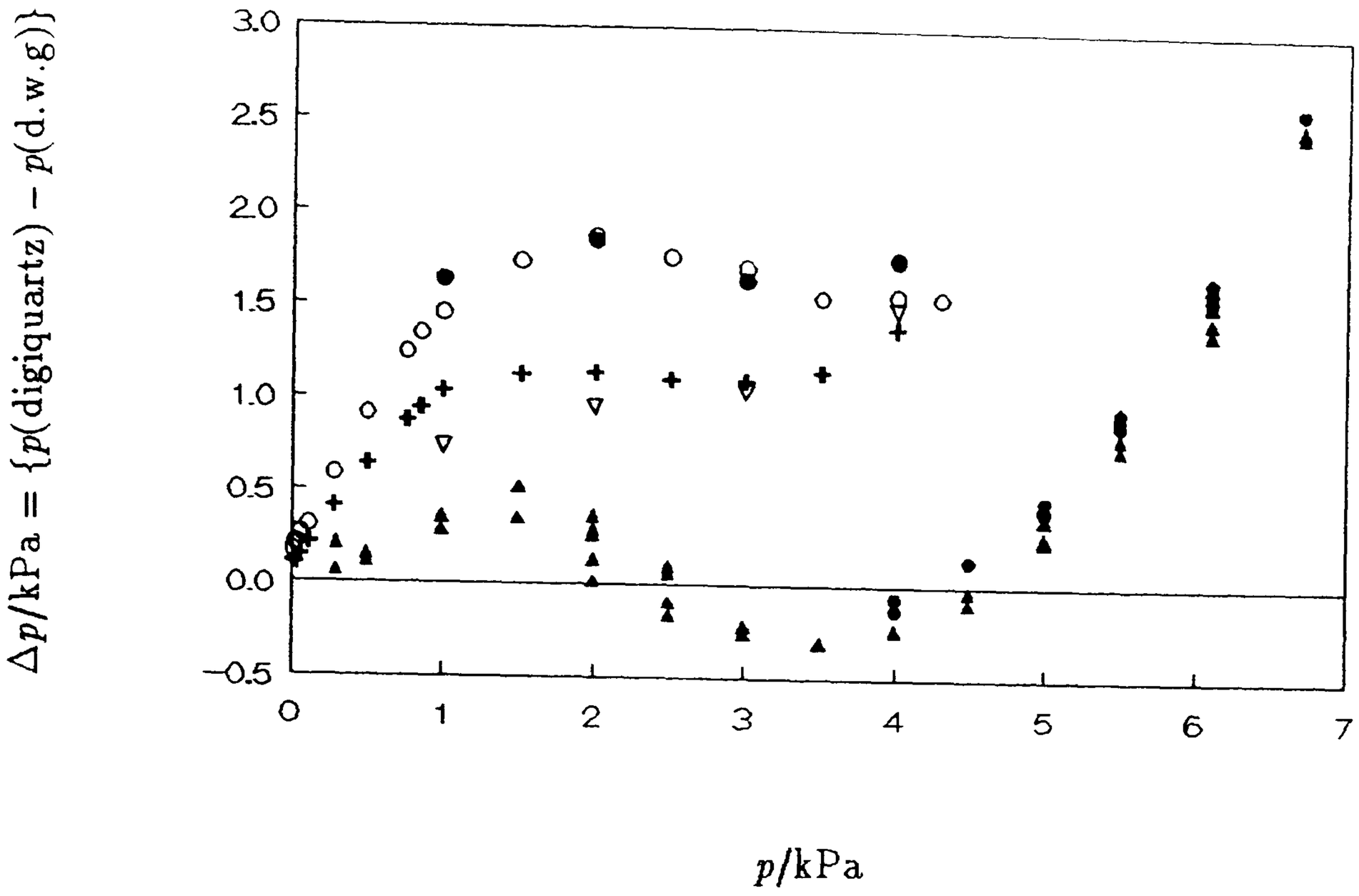

Figure 4.3: Deviation of digiquartz pressure from the true pressure, as measured by a pressure balance, showing hysteresis, which depends on the highest experimental pressure.

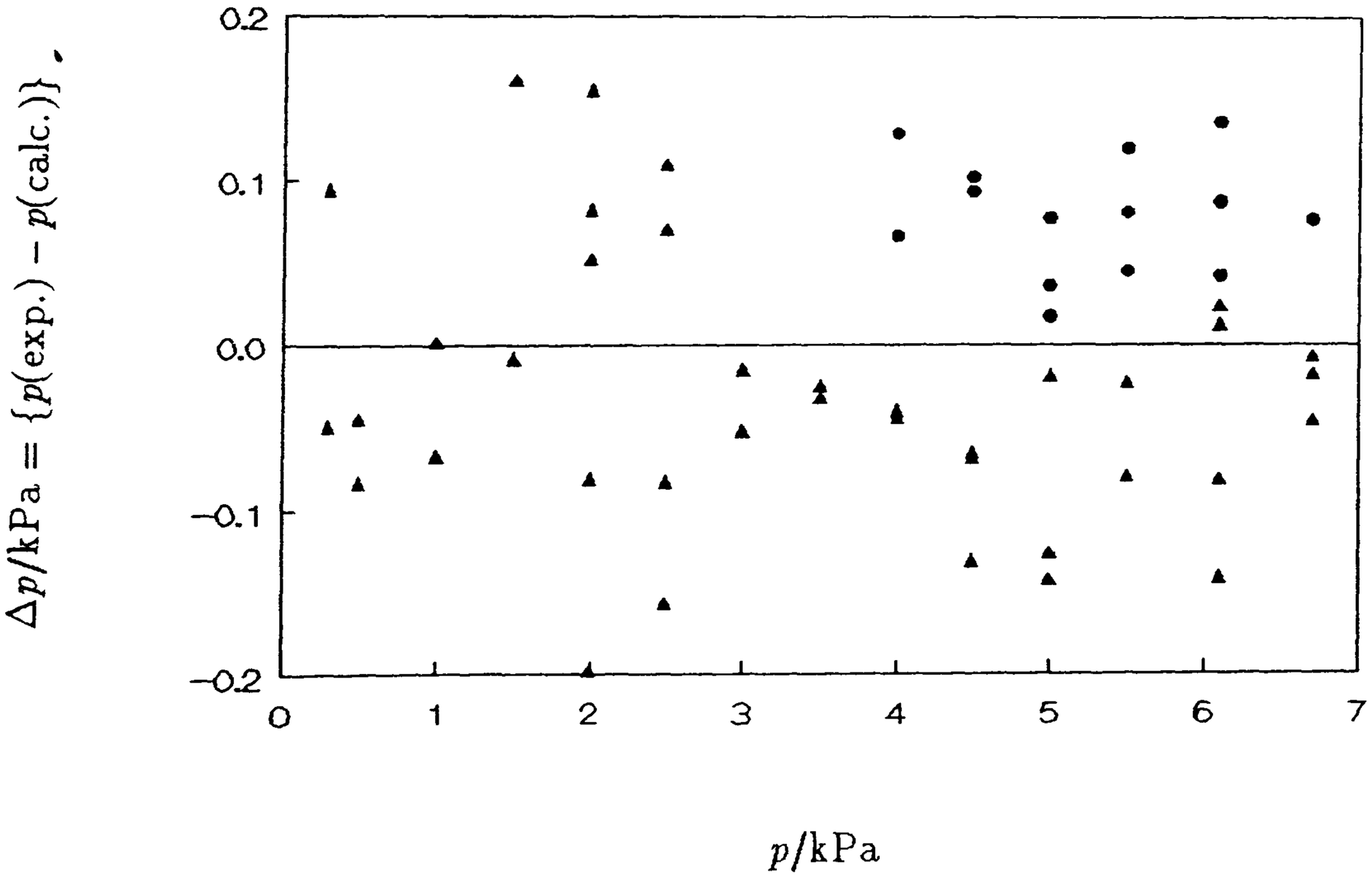

Figure 4.4: Deviation of calibration points from equation (4.4.11).

$$U = \tau_t - U_0 \tag{4.4.10}$$

in which τ_t is the temperature sensor period in microseconds. The coefficients are given in Table 4.2.

Prior to the commencement of any measurements, calibration of the digiquartz was performed by comparison with an oil lubricated pressure balance (Budenberg Ltd., model 280L, serial number 7967/280L). The comparison indicated large deviations from the manufacturers calibration and that, over a closed loop in pressure, hysteresis occurred. This hysteresis was larger than the manufacturers estimated uncertainty and the magnitude was dependent on the highest experimental pressure attained. This is shown in Figure 4.3. Accordingly, the calibration was performed in the way measurements would be carried out throughout the course of an experiment. To eliminate sources of uncertainty that might result from possible drifts in the frequency of the pressure sensor, the measurements were repeated for most pressures over a period of hours as well as repeating points after a period of 24 h. Deviations of the pressure indicated by the digiquartz from that of the pressure balance are given to 100 Pa by

$$\begin{aligned}\delta P = {} & 0.14188p - 0.1515 \times 10^{-1}p^4 + 0.4244 \times 10^{-2}p^5 \\ & - 0.2771 \times 10^{-3}p^6 + 0.25024 \sin(2\pi p/p^*),\end{aligned} \tag{4.4.11}$$

where $p^* = 4228.51$ kPa and p is the pressure obtained from the digiquartz using equation (4.4.6). Deviations of the calibration points from this equation are shown in Figure 4.4 which shows that possible drifts in the pressure sensor are minimal over a time period of up to 24 h. Corrections arising from the hydrostatic head of a given fluid column were calculated correct to the second virial coefficient. Relevant column heights are given in Figure 4.2.

The total sample pressure at the equator of the resonator, when measured using a pressure balance[10,11], is given by

$$p = p_{\mathrm{g}} + p_{\mathrm{a}} + h_{\mathrm{O}}\rho_{\mathrm{O}}g + h_{\mathrm{N_2}}\rho_{\mathrm{N_2}}g + h_{\mathrm{s}}\rho_{\mathrm{s}}g \tag{4.4.12}$$

where p_{g} is the pressure exerted by the oil lubricated pressure balance, p_{a} is atmospheric pressure and each term $h\rho g$ represents the pressure due to a fluid column of

height h and mean density ρ; g is the local acceleration of free fall and the various relevant column heights for the pressure balance are defined in Figure 4.2. The densities ρ required for nitrogen and the sample s were calculated correct to the second virial coefficient and for oil (Shell, Tellus 27) ρ_o was taken to be 878 $kg \cdot m^{-3}$.

The pressure p_g is given by

$$p_g = p_g'(g/g')[1 - (\rho_a - \rho_a')/\rho_w]/[(1 + a_1 p_g)\{1 + a_2(T - T')\}] \qquad (4.4.13)$$

where p_g' is the nominal gauge pressure determined from the calibrated masses constructed from steel with $\rho_w = 8000\ kg \cdot m^{-3}$ and the remaining terms account for the local acceleration of free fall, the buoyancy correction for an air density of ρ_a [9] with ρ_a' $= 1.2\ mg \cdot m^{-3}$ and the effects of temperature and pressure on the piston. The pressure balance was supplied by Budenberg Ltd. The gauge was of the overhang type and could be used with a number of piston and cylinder assemblies. These assemblies all had Class I NPL calibrations. Information for the piston and cylinder assembly used (identification number K287) are the effective piston area given by

$$A_p = A_0(1 + a_1 p) \qquad (4.4.14)$$

where A_p is the area at pressure p and $A_0(293.15\ K) = (1.29035_9 \pm 0.00003_2) \times 10^{-5}\ m^2$ and $a_1 = (25.3 \pm 0.9_4) \times 10^{-16}\ m^2 \cdot Pa^{-1}$, and the fractional variation of piston area with temperature, a_2, taken as $23 \times 10^{-6}\ K^{-1}$. The sensitivity of the instrument, using the above piston/cylinder assembly, is about 625 mg (about 500 Pa); this represents the limit of the imprecision of a given pressure measurement and, at the lowest pressure at which it was used, propagates into an uncertainty of about 6.3 parts in 10^5.

4.5: Samples.

In table 4.3 the samples, suppliers and the stated purities of the materials used, are given. The samples of argon, nitrogen, methane and ethane were used without further purification. The tetrafluoromethane was degassed by repeated freezing with liquid nitrogen, pumping on the solid under vacuum and thawing to room temperature. The sample was admitted to the resonator by allowing the frozen sample to warm to room temperature. Once the required pressure was reached the remaining sample was

Table 4.3: Substance, supplier and stated mole fraction purity.

Sample	Supplier	Purity	Comments
Ethane	Matheson Gases	0.9996	Research Grade
Tetrafluoromethane	BOC plc	0.9999	Electronics Grade
Methanol	BDH Chemicals plc	0.9995	Hygroscopic $x_{H_2O} \leqslant 5 \times 10^{-4}$
Argon	BOC plc	0.99999	Zero Grade
Nitrogen	BOC plc	0.99999	Zero Grade
Methane	Union Carbide	0.99995	Ultra High Purity
Methane	Argo International	0.999995	Research Grade
Methane+Ethane	Electrochem Ltd.	N/A	Certified $x_{C_2H_6} = 0.1500$.

isolated. In this way any air or water contaminating the sample was eliminated. The sample of methanol was from the same lot as that prepared and used by Goodwin in his work. The purity of the sample was assumed to be unchanged and was used after extensive drying. The method of drying was that of Lund and Bjerrum[12]. The sample was degassed extensively in the same manner as the tetrafluoromethane sample and admitted to the resonator to the required pressure by allowing the temperature of the sample to rise. To produce the required pressure at the highest temperatures additional heating of the sample was necessary. The binary mixture of methane and ethane was supplied by Electrochem Ltd and prepared gravimetrically. They certified that the ethane content in the mixture had a mole fraction of 0.1500, with the remainder being pure methane[14]. Masses used in the sample preparation were traceable to NPL.

4.6: References.

1. Horowitz, P.; Winfield, H. *The Art of Electronics*, Cambridge University Press: Cambridge, 1980.

2. Mehl, J. B.; Moldover, M. R. *J. Chem. Phys.* 1981, 74, 4062.

3. Moldover, M. R.; Mehl, J. B.; Greenspan, M. *J. Acoust. Soc. Am.* 1986, 79, 253.

4. Mehl, J. B. *J. Acoust. Soc. Am.* 1978, 64, 1523.

5. Ewing, M. B.; Trusler, J. P. M. *J. Acoust. Soc. Am.* 1989, 85(4), 1780.

6. Preston–Thomas, H.; Quinn, T. J.; Hudson, R. P. *Metrologia* 1985, 21, 75.

7. The International Practical Temperature of 1968 Amended Edition *Metrologia* 1976, 12, 7.

8. Quinn, T. J. *Temperature. Monographs in Physical Measurement.* Editor: Cook, A. H. Academic Press: London, 1983.

9. Kaye, G. W. C.; Laby, T. H. *Tables of Physical and Chemical Constants* Longman: London. Fourteenth Edition 1973.

10. Cross, J. L. *Reduction of Data for Piston Gauge Pressure Measurements.* Nat. Bur. Standards Monograph 65, 1963.

11. Lewis, S.; Peggs, G. N. *The Pressure Balance. A Practical Guide to its use.* National Physical Laboratory 1979.

12. Vogel, A. I. *Textbook of Practical Organic Chemistry* longman: London 1978.

13. Goodwin, A. R. H. Ph.D. Thesis, University of London 1988.

14. Electrochem Ltd., Certificate of Composition 504208 1991.

CHAPTER 5: EXPERIMENTAL RESULTS.

5.1: Introduction.

Low–pressure measurements are reported for the pure substances ethane, tetrafluoromethane and methanol. Analysis of the measurements enabled determinations of the perfect–gas heat capacities, and second and third acoustic virial coefficients. Second and, in some instances, the third (p, V_m, T) virial coefficients have been extracted from the acoustic results.

Measurements at pressures up to 10 MPa are reported for the pure substances

argon, nitrogen and methane and for the mixture (methane + ethane). The measurements in argon and nitrogen characterised the resonator over the experimental range and the results in argon yielded values of the radius of the resonator at zero pressure. For each of the gases studied, second acoustic virial coefficients have been obtained from an analysis of the results. The corresponding (p, V_{m}, T) virial coefficients have been extraccted from the acoustic results and have been compared with values from the literature. Where molecular relaxation is important estimates of the vibrational relaxation times have been obtained.

5.2: Analysis of Acoustic Measurements.

The resonance frequencies f and half–widths g were measured for the lowest four or five radial modes. The correction due to the presence of the thermal boundary layer was calculated using literature values of the transport and equilibrium properties. These are discussed in more detail below. Corrections for imperfect thermal accommodation between the gas and the wall of the resonator were not important under the conditions of these measurements. Accordingly, the thermal accommodation coefficient was taken as unity. The correction due to shell motion was calculated using either literature values of the elastic constants and the isolated–mode approximation or the exact expression derived from classical elasticity; both equations were discussed in Chapter 2. The molar heat capacity $C_{p,\mathrm{m}}$ and the density ρ were estimated from virial coefficients determined in a preliminary analysis of the results. For the low–pressure measurements, the virial equation was truncated at the second virial coefficient while, for the high–pressure measurements, the third virial coefficient was also included. In the analysis the resonance frequencies were weighted by the lesser of $(2 \times 10^{-6} f/\delta f)^2$ and unity, where δf is the estimated standard deviation of f. A check on the completeness of the acoustic model is possible by comparing the experimental and calculated half–widths. If the model were complete and the transport properties exact then the excess half–width

$$\Delta g = g_{\mathrm{exp}} - \sum_j g_j, \tag{5.2.1}$$

where g_j represents the j–th contribution to the known loss mechanisms, would be zero. The summation of equation (5.2.1) includes a term, g_{b}, for the bulk loss contribution to the resonance half–width which depends on the bulk viscosity η_{b}. In general, the bulk viscosity is not known for polyatomic species, but the different dependence of the various terms in equation (5.2.1) may be used to estimate η_{b} and to isolate unknown loss mechanisms by analysis of the excess half–widths. Regression analysis was performed using the equation

$$\Delta g = b_h(f/\rho)^{\frac{1}{2}} + \{(b_{\mathrm{b}}/\rho) + b'_{\mathrm{b}}\}(f/u^2) + b_{\mathrm{r}} f + \sum b_n f_{0n} \tag{5.2.2}$$

and the adaptive regression algorithm which selects the most significant terms from a "bank" of terms. In equation (5.2.2), b_h^2 is proportional to any error in the thermal conductivity, $b_{\mathrm{b}} = \pi\eta_{\mathrm{b}}$ with b'_{b} representing any density dependence in η_{b}, and b_{r} denotes a constant $\Delta g/f$ for the resonator; the b_n are constants similar to b_{r} but for a particular mode.

The experimental quantity is (u/a) and so the results were fitted using either

$$(u/a)^2 = A_0/a^2 + (A_1/a^2)p + (A_2/a^2)p^2 + \cdots, \tag{5.2.3}$$

or its density–explicit equivalent. In equation (5.2.3)

$$A_0 = RT\gamma^{\mathrm{pg}}/M, \tag{5.2.4}$$

$$\beta_{\mathrm{a}} = RTA_1/A_0, \tag{5.2.5}$$

and

$$\gamma_{\mathrm{a}} = RTA_2/A_0 \tag{5.2.6}$$

where

$$\gamma^{\mathrm{pg}} = 1/(1 - R/C^{\mathrm{pg}}_{p,\mathrm{m}}), \tag{5.2.7}$$

and M is the molar mass. β_{a} and γ_{a} are the second and third acoustic virial coefficients, respectively. The (p, V_{m}, T) virial coefficients B and C are related to the acoustic virial coefficients through second–order differential equations. These equations were given in Chapter 3.

For absolute measurements of u the radius, a, of the cavity is required. The radii

of both resonators were determined from calibration measurements in argon for which A_0 is known with sufficiently high accuracy. For the high–pressure resonator the results in argon are discussed in detail; for the low–pressure cavity the reader is referred to the literature[6]. Once the radius has been determined, perfect–gas heat capacities can be determined from A_0. From the second and third acoustic virial coefficients, estimates of the second and third (p, V_m, T) virial coefficients can be made.

In order to determine the second virial coefficient B from the experimental information it is necessary to solve equation (3.2.15). Numerical integration with specified boundary conditions has been used, but this method favours the use of at least one initial condition at the lowest experimental temperature[1–3]. It is at the lowest temperatures that conventional methods are least reliable and the requirement of virial coefficients at these temperatures defeats the purpose of exploiting acoustic measurements independently of other experimental methods. Reliable estimates of virial coefficients can be obtained using semi–empirical methods based on assumptions of the functional form of the intermolecular potential[5,6,8]. Since B is related to the intermolecular pair potential, $U(r)$, by the integral equation

$$B(T) = 2\pi L \int_0^\infty [1 - \exp\{-U(r)/kT\}] r^2 dr, \qquad (5.2.8)$$

where r is the intermolecular separation, the assumption of a functional form for $U(r)$ implicitly imposes a functional form on B and provides a route to the solution of the differential equation. In this approach, no explicit account is taken of the integration constants required for the general solution of the equation although Boyd and Mountain argue that the method implicitly accounts for the homogeneous solution[4]. Thus, if one fits the parameters of a model pair potential to the experimental values of the second acoustic virial coefficient using equations (5.2.8) and (3.2.15), then a self–consistent solution may be obtained. Various model potentials are used and the differences between the values of B so obtained are used to assess the systematic uncertainty introduced by imposing a particular functional form.

A similar approach has been used to obtain C from equations (3.2.16) or (3.2.17)

and the experimental third acoustic virial coefficient. Additional uncertainties are inherent since the reliability of representing third virial coefficients by this method is less well understood and truncation of the infinite series in the analysis of the experimental data often means that only apparent third virial coefficients are obtained.

All the regression analyses used to obtain smoothing equations for $C^{pg}_{p,m}$, B and C were weighted by the normalised inverse variance of the experimental quantity.

5.3: Low Pressure Measurements.

Measurements over wide ranges of temperature at pressures below 1 MPa have been performed in the pure substances ethane, tetrafluoromethane and methanol. The measurements were performed in a 40 mm aluminium spherical resonator.

5.3.1: Apparatus.

The apparatus is based on the 40 mm aluminium sphere used by Ewing and Goodwin in their measurements on gases up to 7 MPa and is described in detail elsewhere[5,7,8]. The thermal environment of the resonator is shown in figure 5.1. The resonator was thermally linked by a copper post to the control block where the temperature was controlled. The block was bolted to the lid of a copper radiation shield and the sides and bottom of this shield were wound with a wire heater and the entire outer surface was covered by superinsulation. The temperature of the shield was also controlled but, since the thermal coupling between it and the resonator was much less than between the resonator and the control block, only crude control was required. An outer stainless–steel can, sealed with indium wire, served as a vacuum enclosure; with continual pumping, the pressure inside the enclosure was less than 1 mPa. The apparatus was immersed in a Dewar which was filled with liquid nitrogen for operation at temperatures below ambient. The apparatus is suitable for measurements in gases up to 1.3 MPa in the temperature range 80 to 375 K. A more detailed account of the apparatus is given in the literature[7,8].

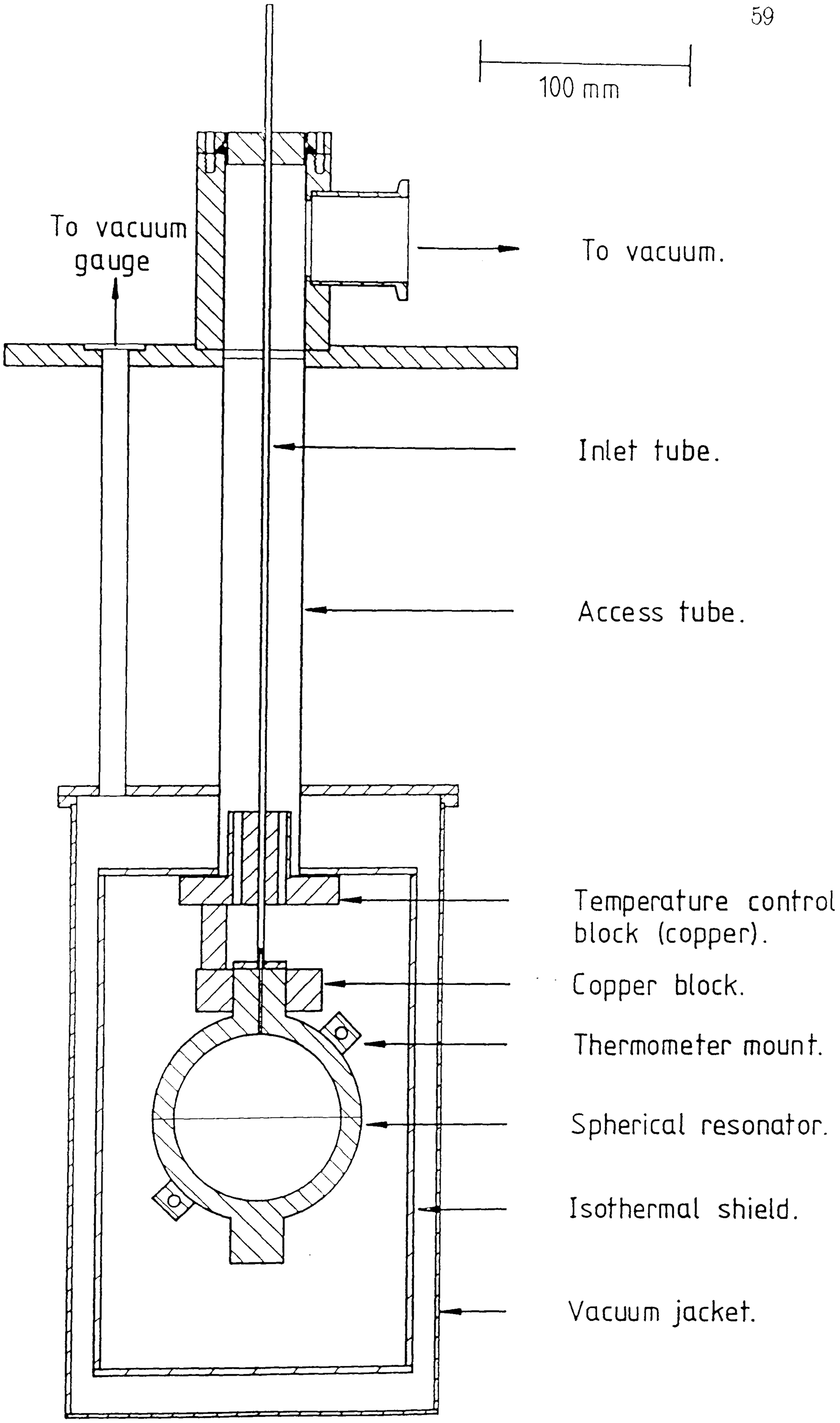

Figure 5.1: The thermal environment of the low–pressure resonator.

5.3.2: Ethane.

Measurements were conducted along seven isotherms between 210 and 360 K, and an isochore at an amount density of $\rho_n = 95$ mol·m^{-3}. The greatest pressure on each isotherm was limited to the lesser of 1 MPa and 0.6 of the vapour pressure to avoid the known effects of precondensation[9].

The correction for the thermal boundary layer requires values of the thermal conductivity of the gas at the experimental temperatures. The values used were taken from the correlation of Hanley, Gubbins and Murad[10]. The estimated uncertainty of the values is ± 8 % at worst which means the thermal boundary–layer correction is known to about 5 ppm of the resonance frequency at worst. To assess the internal consistency of the required data values of the thermal conductivity were calculated from the viscosity using the Eucken and the modified Eucken equations. From previous work it has been found that the "true value" of the thermal conductivity lies between the values calculated using the two equations. Since this was the case with the correlation values they were taken to be self–consistent and sufficiently accurate for the purposes of this experiment. Corrections for imperfect thermal accommodation between the gas and the wall of the resonator are not important under the conditions of our measurements. Accordingly, the thermal accommodation coefficient was taken to be unity. Thermodynamic properties required in this and other corrections were calculated correct to the second virial coefficient which was itself obtained from a preliminary analysis of the results as described previously. The thermal boundary layer also makes an important contribution to the resonance half–widths.

The corrections for coupling of gas and shell motion and for the presence of the gas inlet tube were calculated as described in Chapter 2. The tube corrections require the gas viscosity and values were taken from the correlation of Hanley, Gubbins and Murad. The estimated uncertainty associated with the coefficients of viscosity is ± 5 %.

The radius, a, of the resonator at zero pressure as a function of temperature was determined from calibration measurements in argon, the results of which have been reported elsewhere. Since the resonator was not pressure compensated, corrections to

Table 5.1: Mean values of u^2 with standard deviations σ from N modes, and deviations δ from equation (5.2.3) at temperatures T and pressures p.

$\frac{T}{\mathrm{K}}$	$\frac{p}{\mathrm{kPa}}$	$\frac{u^2}{\mathrm{m}^2\cdot\mathrm{s}^{-2}}$	$\frac{10^6\sigma(u^2)}{u^2}$	N	$\frac{10^6\delta(u^2)}{u^2}$	$\frac{p}{\mathrm{kPa}}$	$\frac{u^2}{\mathrm{m}^2\cdot\mathrm{s}^{-2}}$	$\frac{10^6\sigma(u^2)}{u^2}$	N	$\frac{10^6\delta(u^2)}{u^2}$
210.000	200.88	67597.95	3.4	4	0.6	100.38	69799.62	1.0	4	0.2
	179.41	68076.80	3.6	4	–1.2	80.09	70232.62	0.9	4	–0.1
	159.22	68522.40	2.6	4	(a)	59.91	70659.77	1.0	4	–1.8
	139.42	68956.18	1.9	4	0.7	40.02	71078.02	1.2	4	1.8
	119.45	69389.37	1.1	4	0.3	19.97	71496.21	1.3	4	–0.5
230.000	419.75	70352.05	4.6	4	1.6	167.96	75054.77	1.9	4	–0.4
	376.11	71194.81	2.8	4	–1.5	126.29	75799.24	2.0	4	0.5
	336.04	71957.62	3.3	4	–4.1	83.65	76551.77	1.7	4	(a)
	293.94	72749.10	2.5	4	4.4	41.93	77280.82	1.3	4	–2.5
	251.83	73529.45	2.7	4	1.5	21.26	77639.39	4.0	4	2.1
	209.17	74309.84	2.5	4	–1.5					
250.000	460.94	76978.10	3.7	4	0.9	208.60	80884.49	1.6	4	–0.5
	407.24	77826.47	3.4	4	–1.0	159.17	81627.25	0.8	4	–0.4
	357.36	78605.86	2.9	4	–2.2	97.45	82545.18	1.6	4	–1.6
	307.79	79372.94	2.0	4	2.2	58.71	83116.51	2.1	4	1.2
	258.39	80129.43	1.9	4	1.4					
273.160	815.23	80362.35	17.7	5	(a)	364.32	86251.05	5.9	5	0.2
	726.77	81547.37	6.8	5	–0.1	274.54	87382.03	3.5	5	2.7
	636.05	82747.46	4.8	5	1.1	183.99	88509.92	3.6	5	–1.3
	546.11	83921.29	7.3	5	–1.9	93.39	89627.03	2.7	5	–3.0
	454.87	85096.93	6.5	5	(a)	46.85	90197.14	3.4	5	2.3
300.000	999.51	88208.09	5.6	4	0.3	399.23	94492.18	2.1	4	–2.6
	900.51	89263.58	5.1	4	–1.6	299.77	95508.65	2.4	4	4.2
	798.36	90344.83	5.0	4	1.9	199.50	96525.57	1.6	4	–0.3
	699.02	91388.09	4.8	4	0.2	99.72	97531.15	1.1	4	–2.2
	600.02	92421.06	3.6	4	(a)	49.51	98035.14	3.4	4	1.1
	499.83	93457.83	2.9	4	–1.1					
330.000	613.56	101995.03	6.3	4	3.5	306.55	104520.23	1.8	4	1.8
	552.30	102499.33	4.0	4	–3.5	244.93	105025.34	1.7	4	2.1
	490.94	103004.80	3.4	4	–1.9	131.13	105955.99	2.0	4	–1.6
	429.14	103513.27	2.9	4	–0.9	61.24	106526.68	3.0	4	–1.1
	367.78	104017.62	2.2	4	0.8	30.64	106776.44	3.6	4	0.8
360.000	664.13	111041.62	5.1	4	–0.5	337.93	113213.07	1.8	4	–1.8
	598.30	111478.61	3.6	4	(a)	271.74	113654.42	2.2	4	–0.9
	532.93	111914.33	2.7	4	–0.3	206.29	114091.01	2.3	4	–0.4
	467.49	112350.19	2.6	4	1.0	140.88	114527.36	2.6	4	–0.6
	402.17	112785.43	2.4	4	2.5	75.62	114963.07	2.5	4	1.1

(a), Pressure omitted from analysis

Table 5.2: Perfect–gas heat capacities, second and third acoustic virial coefficients, and standard deviations s obtained by analysis of N modes for ethane. Here, and elsewhere uncertainties are one standard deviation only.

T/K	N	$C_{p,\mathrm{m}}^{\mathrm{pg}}/\mathrm{R}$	$\beta_{\mathrm{a}}/(\mathrm{cm}^3\cdot\mathrm{mol}^{-1})$	$\gamma_{\mathrm{a}}/(\mathrm{dm}^6\cdot\mathrm{mol}^{-2})$	$10^6 s(u^2)/u^2$
210.000	36	5.1943 ± 0.0001	–501.62 ± 0.13	0.0474 ± 0.0022	2.0
230.000	40	5.4135 ± 0.0001	–421.56 ± 0.08	0.0354 ± 0.0008	3.4
250.000	36	5.6555 ± 0.0002	–360.08 ± 0.09	0.0330 ± 0.0008	2.5
273.160	40	5.9569 ± 0.0002	–303.98 ± 0.08	0.0315 ± 0.0005	4.8
300.000	40	6.3247 ± 0.0001	–252.74 ± 0.04	0.0262 ± 0.0002	3.7
330.000	40	6.7827 ± 0.0001	–208.86 ± 0.03	0.0243 ± 0.0001	3.5
360.000	36	7.2504 ± 0.0002	–173.06 ± 0.03	0.0219 ± 0.0001	2.8

the zero–pressure radius for dilation of the sphere were significant. The compliance $(1/a)(\partial a/\partial p)$, under the condition where the exterior pressure is constant, was calculated using literature values for the elastic constants. Young's modulus was obtained from reference 10 at each temperature, while Poisson's ratio was taken as 0.355 and was assumed independent of temperature. The compliance of the resonator is estimated to be known to about 5 %.

In table 5.1 we list mean values of u^2 at each temperature and pressure, together with fractional standard deviations and the number of resonant modes from which each mean was determined. Small corrections have been applied to reduce all values to the stated temperature for each isotherm.

Heat capacities and acoustic virial coefficients were determined by regression analysis with equation (5.2.3) using the full set of results. In table 5.2, we list the values of $C_{p,\mathrm{m}}^{\mathrm{pg}}$, β_{a}, and γ_{a} obtained in the analysis along with the fractional standard deviation of u^2 for each isotherm. It appears that 300 K is a transition point in terms of order of fit; isotherms above 300 K require a three term fit whilst those below this temperature apparently require a four term fit to accommodate the data.

We have also analysed the experimental half–widths g_{0n} of the radial modes and obtained estimates of the vibrational relaxation time τ and bulk viscosity η_b for ethane.

The method of analysis first requires subtraction of various known contributions to the half widths: $g_{h,}$ arising from losses in the thermal boundary layer ; g_{b}, arising from classical viscothermal losses in the bulk of the gas; and g_{o}, arising from damping in the gas inlet pipe.

We assumed that the vibrational modes of the molecule are strongly coupled so that the entire vibrational heat capacity relaxes with a single time constant τ so that the effective ratio of heat capacities $\gamma(\omega)$ at angular frequency ω is given by equation (2.2.13) with $\Delta = C_{\text{vib}}/C_{p,\text{m}}$ and $C_{\text{vib}} = (C^{\text{pg}}_{p,\text{m}} - 4R - C_{\text{torsion}})$ is the purely vibrational contribution to the heat capacity. The finite rate of rotational relaxation is neglected because the time constant is much less than that of vibrational relaxation. The torsional mode was excluded from Δ for similar reasons and, in addition, the torsional and vibrational modes are thought to relax independently. Although theoretically possible to distinguish the two vibrational processes, this work does not extend to sufficiently large values of (f/p) along the dispersion curve to enable us to do this reliably. Since the product $\tau\rho$ is expected to be nearly independent of the density along an isotherm, the residual half widths were then fit by

$$\Delta g = \{g_{0n} - \sum_j g_j\} = \{(\gamma - 1)\Delta\pi f^2_{0n}/\rho\} \cdot (b_0 + b_1\rho), \qquad (5.3.1)$$

in which g_{0n} is the observed line–width, g_j is the j–th contribution to the known loss mechanisms, ρ is the mass density , $b_0 = \tau\rho$ and the additional term $b_1 = \partial(\tau\rho)/\partial\rho$ was found to be necessary to accommodate the measured half–widths. Both terms were significant at a probability of 0.999 and no other terms were significant. The transport and equilibrium properties used in this calculation are those described above. The experimentally determined quantity used in the above fit is $\tau\rho\Delta$ from which it is possible to extract a relaxation time by imposing an artificial partition. The density is arbitrarily assigned a value of 1 kg m^{-3} and the remaining partition depends on what value we assign to the relaxing heat capacity. For a molecule with few fundamental vibrations or where we can unambiguously assume series excitation of vibrational modes, the relaxing heat capacity can be calculated extremely accurately and hence

accurate relaxation times can be reported. However, in the case of ethane, the assignment of the relaxing heat capacity is ambiguous; we have parallel excitation of two vibrational series. An accurate partition of relaxing heat capacities is required to determine relaxation times associated with each series. This is difficult because the heat capacity associated with the torsional mode of vibration cannot be calculated with sufficient accuracy from statistical mechanics. Fortunately, the contribution from the remaining modes can be calculated accurately using statistical mechanics and spectroscopic data; experimentally determined heat capacities, in conjunction with the calculated results for the remaining modes, can then be used to calculate the contribution of the torsional mode. At 300 K the contribution is found to be 0.9817 R which agrees with (0.98 ± 0.11) R determined by Holmes, Jones and Pusat[11]. For a parallel process involving two series the total or bulk contribution is

$$\Delta_t \tau_t \rho = \Delta_1 \tau_1 \rho + \Delta_2 \tau_2 \rho, \tag{5.3.2}$$

where the subscripts 1 and 2 refer to the two parallel processes; Δ is the ratio of the relevant vibrational contribution(s) to the heat capacity and the total heat capacity. The above expression enables us to calculate a value for the relaxation time associated with the "true" vibrations from our experimentally determined bulk relaxation assuming a reasonable value for the relaxation time of the torsional mode. The value of the time constant for the torsional mode was taken as 0.59 ns·kg·m^{-3} from the paper by Holmes, Jones and Pusat[11]. The time constant of the second process calculated using the above expression is 11.83 ns·kg·m^{-3} at 300 K. This value is in good agreement with the value of 12.3 ns·kg·m^{-3}, at 296.6 K, reported by Valley and Legvold[13], but disagrees with the value of 9.3 ns·kg·m^{-3} at 303.15 K reported by Holmes, Jones and Pusat, and the value of 14.6 ns·kg·m^{-3} at 298 K reported by Lambert and Salter[12]. The experimentally determined quantity $\Delta\tau\rho$ represents a bulk relaxation and unambiguous analysis of this is possible in terms of bulk viscosity. For polyatomic gases the bulk viscosity η_b arises (mainly) from vibrational relaxation which reduces the effective heat capacity. If it is assumed that there is a single relaxation time τ arising either from one vibrational state or from a number of states

Table 5.3: Bulk viscosities in ethane.

T/K	η_b/μPa·s·kg·m^{-3}	$(\partial\eta_b/\partial\rho)/\mu$Pa·s
210.000	28.96 ± 0.32	5.62 ± 0.36
230.000	37.73 ± 0.32	7.39 ± 0.32
250.000	48.78 ± 0.73	7.27 ± 0.37
273.160	60.05 ± 0.76	7.20 ± 0.36
300.000	71.86 ± 0.90	8.57 ± 0.51
330.000	79.84 ± 0.34	10.39 ± 0.34
360.000	86.91 ± 0.97	11.96 ± 0.51

coupling in series then, at angular frequency ω, the ratio of heat capacities is as given in Chapter 2. The bulk viscosities η_b obtained from an analysis of the excess half–widths are given in table 5.3; also tabulated is $\partial\eta_b/\partial\rho$ at the experimental temperatures. In figure 5.2 they are shown as a function of temperature.

The two sets of perfect–gas heat capacities determined represent those obtained from the isotherms and those obtained from the isotherms as modified by the isochore. The effect of non–uniformity of sample on the heat capacities is a first–order effect, and thus any variation in sample purity should be manifest in the scatter associated with the experimentally determined values.

The heat capacities of table 5.2 may be represented by

$$C^{\mathrm{pg}}_{p,\mathrm{m}}/R = 1.729 \times 10^{-2}(T/\mathrm{K}) + 7.354 \times 10^{-12}(T/\mathrm{K})^4 + 3.258 \times 10^{2}(\mathrm{K}/T) \tag{5.3.3}$$

with a standard deviation of 0.002 R; we note however that the results are not a smooth function of temperature to within a reasonable multiple of the (very small) individual standard deviations. The observed scatter could be due to systematic errors arising from variations in sample purity. In an attempt to reduce these likely systematic errors, the isotherms were coupled by means of an isochore which, by necessity, ensures that the coupled results represent a uniform sample. These results are shown in table 5.4 and may be represented by

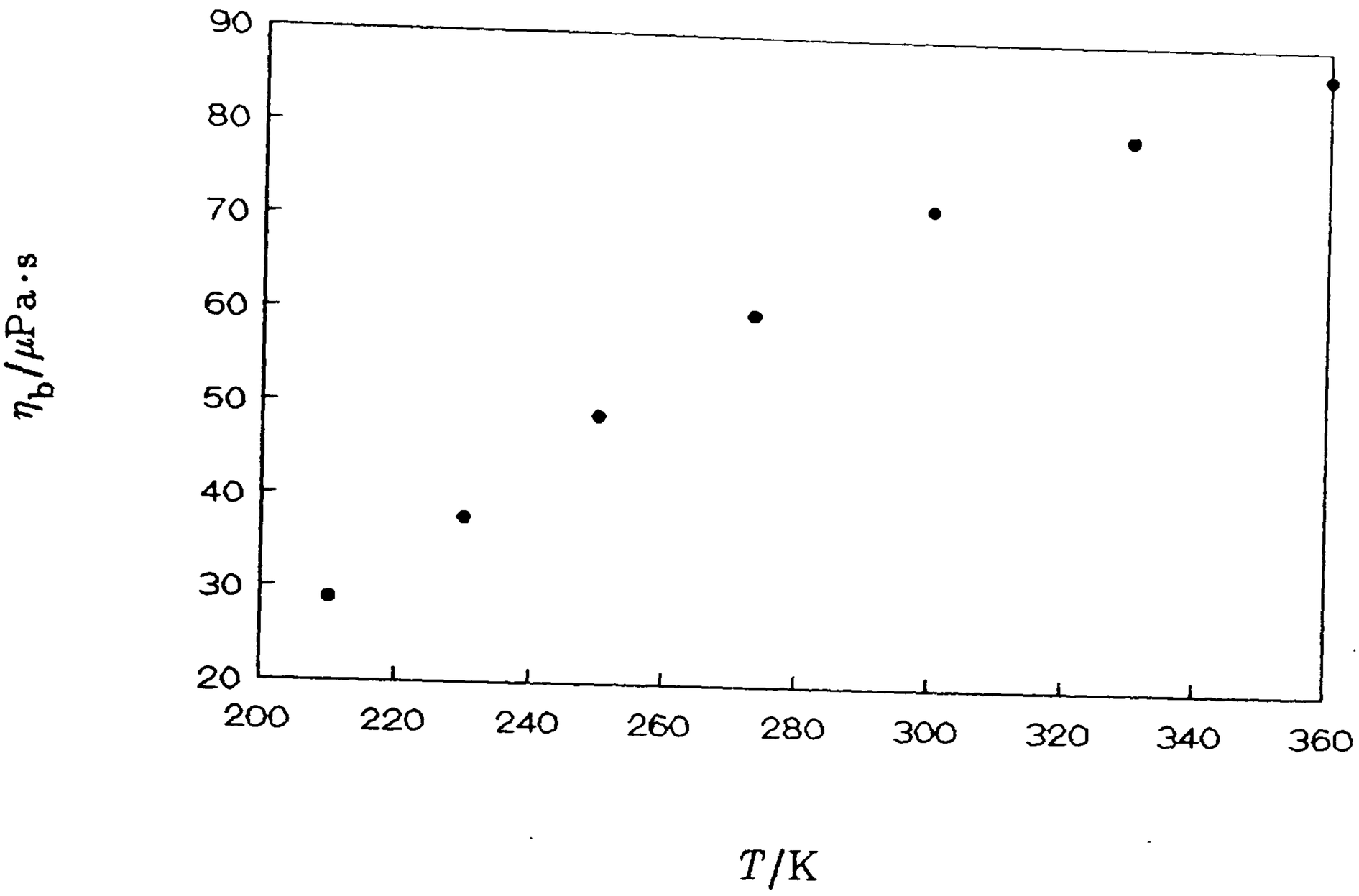

Figure 5.2: Bulk viscosities in ethane.

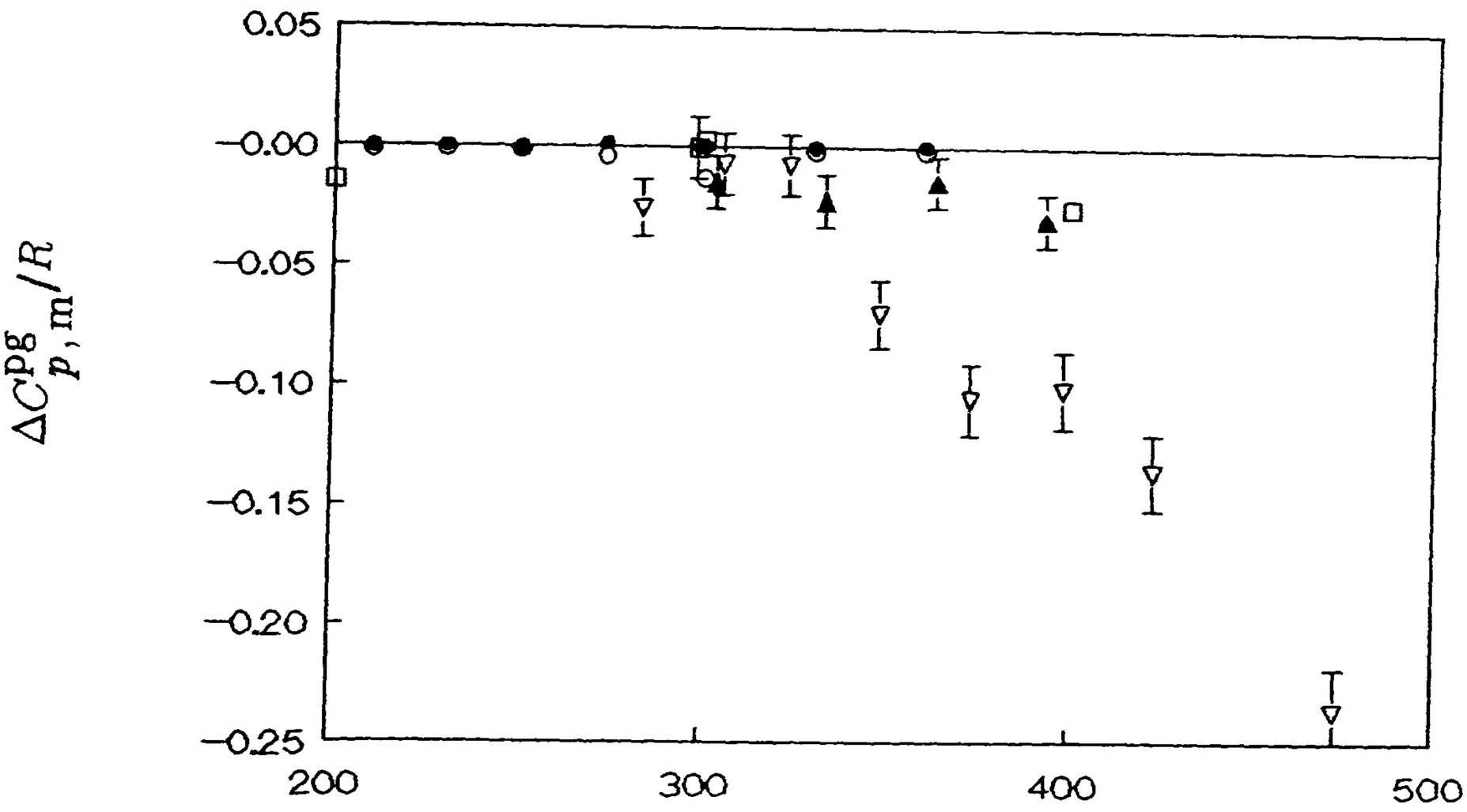

Figure 5.3: Deviations $\Delta C^{pg}_{p,m} = \{C^{pg}_{p,m}(\text{exp.}) - C^{pg}_{p,m}(\text{calc.})\}$ of experimental heat capacities at constant pressure from equation (5.3.4). ● , ○ , this work; ▲ , reference 14; □ , reference 15; ▽ , reference 16.

$$C^{\mathrm{pg}}_{p,\mathrm{m}}/R = 1.675 \times 10^{-2}(T/\mathrm{K}) + 2.349 \times 10^{-6}(T/\mathrm{K})^2 + 3.309 \times 10^{2}(\mathrm{K}/T) \quad (5.3.4)$$

with a standard deviation of 0.0007 R; clearly a significantly better fit which demonstrates the advantage of isochoric coupling to ensure sample uniformity. The results are shown as deviations from (5.3.4) in figure 5.3. In this figure the scale is extremely sensitive showing that the scatter associated with systematic errors has been reduced; however the results are still not smooth to within a reasonable multiple of the individual standard deviations. This remaining scatter is presumably due to some small impurity present in the sample (as supplied) condensing out at low reduced temperatures, whilst being present at higher reduced temperatures. (This hypothesis was tested by conducting an isotherm both in and out of the cryostat ensuring that in at least one state the gas was subjected to liquid nitrogen temperatures; although this represents an extreme case it did suggest that it was a plausible explanation). In figure 5.3 the experimental results of other workers are also shown as deviations from (5.3.4). The agreement with Ernst and Hochberg[14] is excellent as is the agreement with the calculated values given in the TRC Thermodynamic Tables for Hydrocarbons[15]. The (p, V_{m}, T) determination of Michels, van Straaten and Dawson[17] agrees with our results to within their estimated error although their results appear to be systematically low. The flow–calorimetric results of Bier, Kunze and Maurer[16] show agreement at moderate temperatures but begin to diverge with a significant change of gradient at higher temperatures. This is in contrast to the more recent flow–calorimetric determination of Ernst and Hochberg. This observation was noted by Bier, Kunze and Maurer but their insistence that the change is correct, in the light of these results, must be considered erronous. The rationalisation of the observation is questionable since it should lead to a smoothly varying function of temperature and not the step function they observe. Thus we can conclude that the results of Bier *et al* are systematically low, at least at higher temperatures.

In the absence of reliable initial conditions for a numerical integration of equation (3.2.15) the second virial coefficient of the gas has been obtained from the second acoustic virial coefficient using semi–empirical methods. Elsewhere[5,6,8,27,] it has

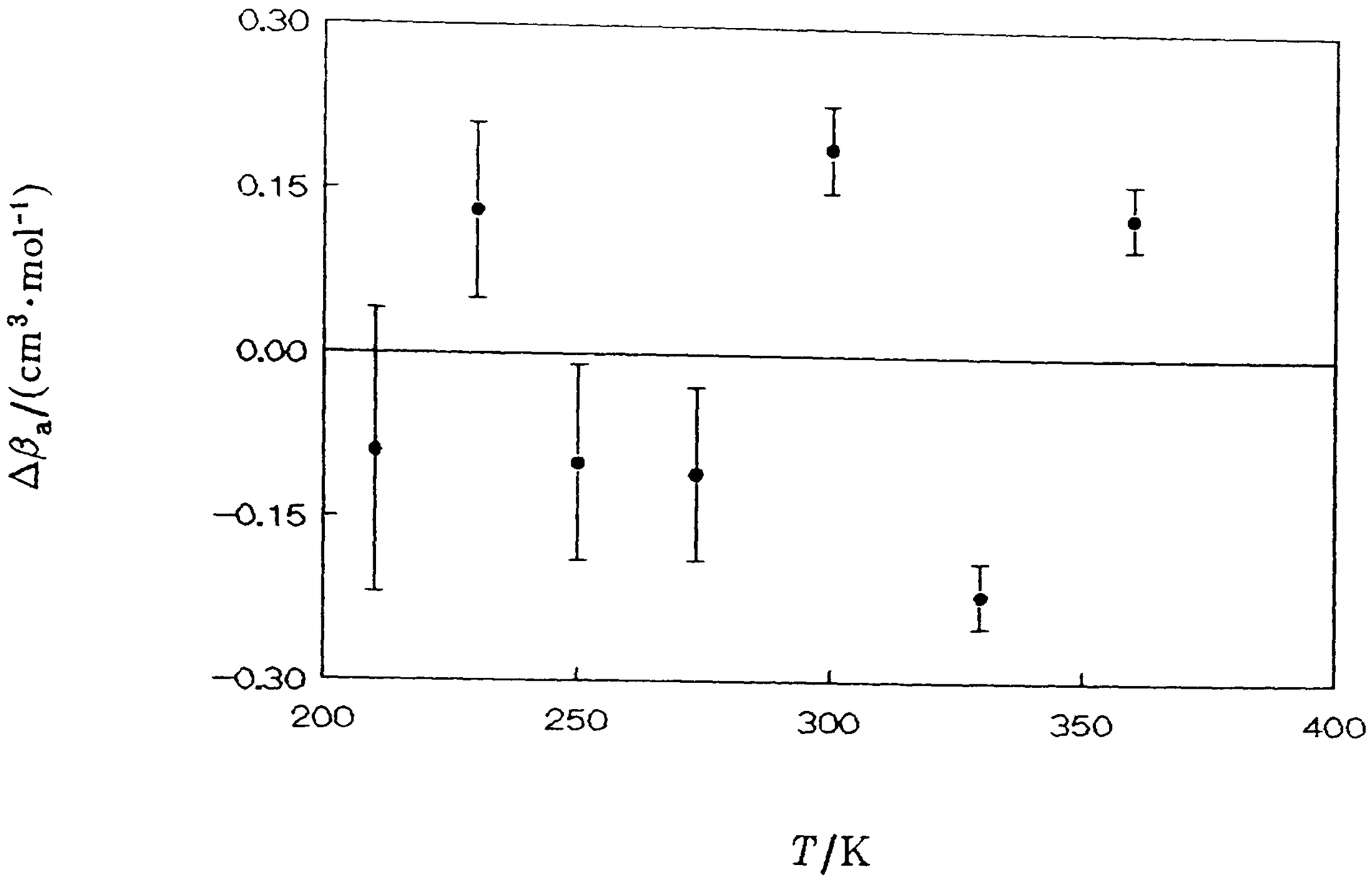

Figure 5.4: Deviations $\Delta\beta_a = \{\beta_a(\text{exp.}) - \beta_a(\text{calc.})\}$ of the experimental β_a given in table 5.2 from equation (5.3.5) and (3.2.15) with $C^{pg}_{p,m}/R$ taken from table 5.2.

---

been shown that these less formal methods produce results of high accuracy. Further justification of this assertion is provided by this work where four different assumptions about the functional form of B yield results which are essentially the same.

The first method assumes that B may be represented by the expression derived from the square–well potential. Weighted non–linear regression using the experimental β_a and γ^{pg} then gave

$$B/(\text{cm}^3 \cdot \text{mol}^{-1}) = 267.28 - 191.504 \exp(256\ \text{K/T}) \qquad (5.3.5)$$

and fit β_a with a standard deviation of 0.23 $\text{cm}^3 \cdot \text{mol}^{-1}$; or about 0.07 % of the average value. Figure 5.4 shows the experimental second acoustic virial coefficients as deviations of β_a from the smoothing equation. This figure illustrates well the high level of internal consistency. The isochoric coupling discussed in the analysis of the perfect gas heat capacities is largely a second–order effect with respect to the acoustic virial coefficients and we do not attribute a significant part of the small experimental scatter

to variations in sample purity. The square–well functional form of B provides a simple and convenient path to extrapolation of second virial coefficients, with little or no loss of precision. The success of this approach has been shown in previous publications. Further evidence of its success is provided here, but this should be taken as an indication of the general insensitivity of second virial coefficients to the detailed form of the potential energy function, rather than as evidence of the square–well potential being the correct solution to equation (3.2.15).

In the second solution to equation (3.2.15) we assumed that B may be represented by the family of Lennard–Jones (n,6) functions in which we varied the well depth ϵ, collision diameter σ, and the repulsive exponent n. Weighted non–linear analysis of β_a finally gave $\epsilon/k = 428$ K, $2\pi L\sigma^3/3 = 88.095$ cm$^3\cdot$mol^{-1}, and $n = 42$, with a standard deviation of 0.22 cm$^3\cdot$mol^{-1} in β_a. This is, to say the least, an unusual potential, but not unreasonable. Given that the square–well model yields results of high accuracy, as has been shown in previous publications, then it seems plausible to suggest that the high repulsive exponent in the Lennard–Jones potential seeks to mimic the infinity at values of $r \leqslant \sigma$ in the square–well potential. However, as a consequence of having such a diverse combination of exponents the equation is complicated and ease of extrapolation in B suffers. Indeed, compared with the square–well, the Lennard–Jones solution is far more complicated and the standard deviation of fit only fractionally better. Differences in the values of B calculated from the Lennard–Jones and square–well solutions are no greater than 0.5 % over the temperature range of study.

The third solution assumes that B may be represented by the Kihara spherical core potential which has the form

$$U(r)/\epsilon = 4\{(\sigma - 2a/r - 2a)^{12} - (\sigma - 2a/r - 2a)^{6}\}, \quad r > 2a \tag{5.3.6}$$

where a is the radius of the molecular core at which $U(r)/\epsilon = \infty$, σ is the collision diameter, and ϵ is the well depth. This contains features of both the pseudo–real Lennard–Jones potential and the square–well potential. The method of analysis was by direct integration of the relevant functions. Weighted non–linear analysis in which we varied the well–depth ϵ, the collision diameter σ, and the reduced core diameter a^*

(which is the ratio of the core diameter to the shortest distance between core surfaces at zero potential energy), finally gave ϵ/k = 382 K, $2\pi L\sigma^3/3$ = 91.841 $cm^3 \cdot mol^{-1}$ and a^* = 0.28, with a standard deviation of 0.195 $cm^3 \cdot mol^{-1}$ in β_a. This solution affords the best representation of the data and provides an accurate extrapolation, in B, to high temperatures but, since the potential is complicated, no simple analytic form of B is available and consequently mathematical tractibility is poorer when compared with the square–well potential. Deviations from the square–well solution are small and, over the experimental temperature range, the values of B determined from both solutions agree to better than 0.3 %.

The fourth solution is purely empirical and B is represented by a polynomial in T^n. Using the adaptive analysis, described previously[18], to select the most significant terms, with $-6 \leqslant n \leqslant 6$ the best representation was found to be

$$B/cm^3 \cdot mol^{-1} = -16.99 \times 10^6 (K/T)^2 + 6.489 \times 10^{-5} (T/K)^2 \qquad (5.3.7)$$

which fits β_a with a weighted standard deviation of 0.27 $cm^3 \cdot mol^{-1}$. Again we note that the agreement with the square–well functional form of B is good, the deviation being most pronounced at the lowest reduced temperature where it reaches 0.7 % in B. Extrapolation of B with this function is by necessity poorer than with the others since it is purely empirical and we are constraining the fit over the limited temperature range of study. An extrapolative comparison is still made for completeness.

The (p, V_m, T) virial coefficients calculated from each solution are shown as deviations from the square–well solution in figure 5.5. As can be seen the agreement is excellent. The Lennard–Jones potential agrees extremely well, especially at higher temperatures, even over an extrapolation of 260 K outside the temperature range of study. At lower temperatures the potential encounters difficulties accommodating the data (the worst deviation is about 1.5 $cm^3 \cdot mol^{-1}$); this has been noted before and presumably results from the combination of such diverse exponents. The Kihara spherical core potential shows agreement, over the whole extrapolation, which is significantly better than that of the Lennard–Jones solution but shows the same form of deviation. The deviation is most pronounced at the lowest temperature where it

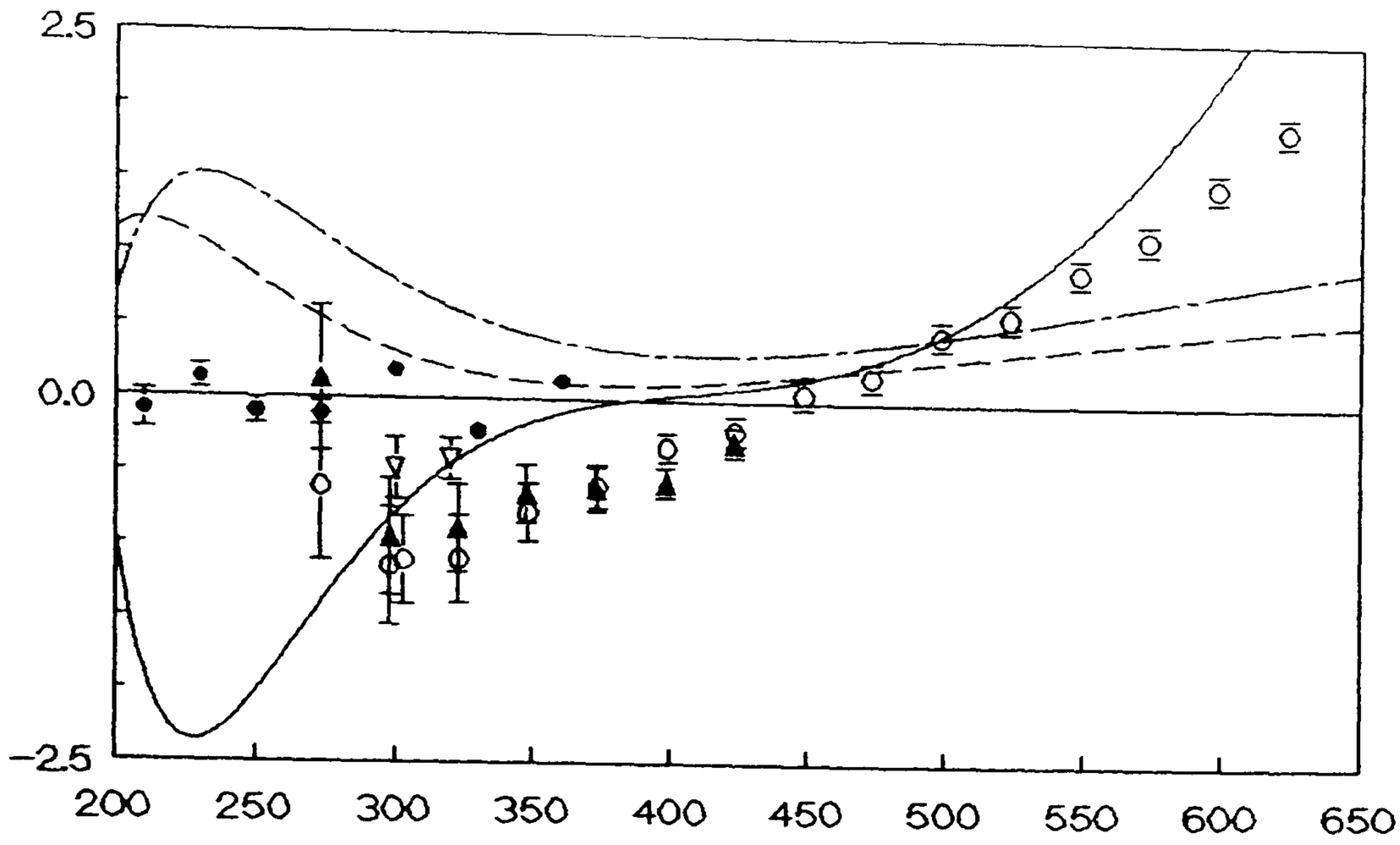

Figure 5.5: Deviations ΔB = {B(alt.) – B(sq.–well)} of the alternative solutions to equation (3.2.15) from the square–well solution given by equation (5.3.5). ——— , polynomial in T; — — — , Kihara spherical core model; —— – —— , Lennard–Jones (42,6) potential. Also shown as deviations from (5.3.5) are the experimental results of other workers. • , this work; ▲ , reference 17; ∘ , reference 19; ▽ , reference 20.

---

reaches about 1 $cm^3 \cdot mol^{-1}$. At higher temperatures the solutions converge giving essentially the same result. The polynomial affords the poorest fit and shows the greatest deviation from the square–well. At the lowest temperatures, negative deviations are observed with a maximum of about 2.2 $cm^3 \cdot mol^{-1}$ (about 0.7 %) and at the highest temperatures of the extrapolation the deviation is positive and diverging. Even so, agreement with the square–well solution to within 0.5 $cm^3 \cdot mol^{-1}$ is observed up to about 500 K which still represents a considerable extrapolation (It is of note that, although the polynomial represents the poorest fit to the experimental data, it extrapolates at higher temperatures very closely with the results of Douslin and Harrison[19]; the deviation remains less than 1 $cm^3 \cdot mol^{-1}$ even when extrapolated more than 250 K outside of the experimentally covered range). Since the differences between the four solutions are small we adopt equation (5.3.5), which is mathematically simple and tractible as the best estimate of B and regard the variations in the solutions

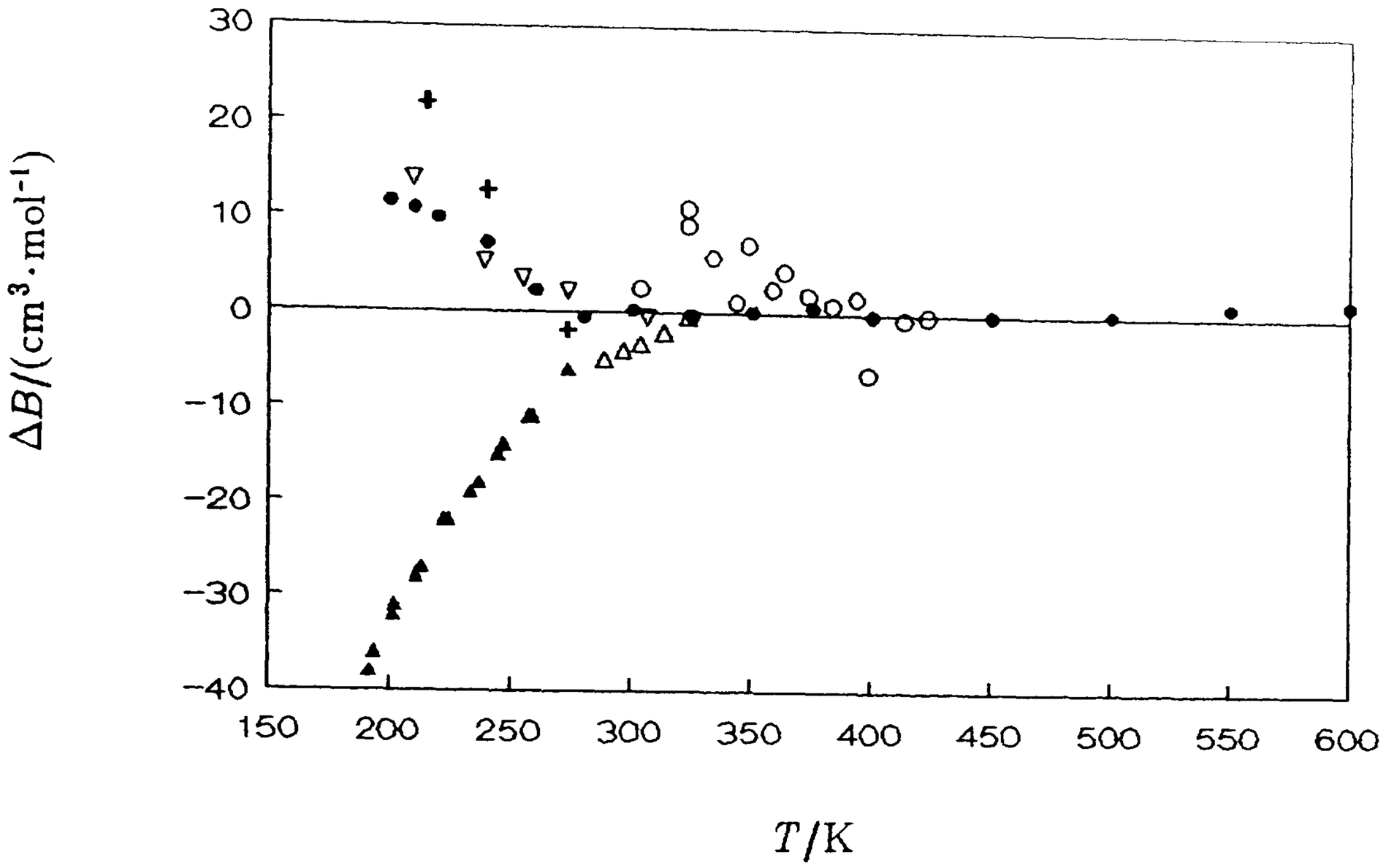

Figure 5.6: Deviations $\Delta B = \{B(\text{exp.}) - B(\text{sq.–well})\}$ of second virial coefficients from equation (5.3.5). , reference, 21; • , reference 22; ∇ , reference 23; + , reference 24; ∘ , reference 25; ▲ , reference 26; Δ , reference 27.

---

as a measure of the likely systematic error arising from the imposition of a functional form. Additional small uncertainties arise from the truncation of the infinite series (5.2.3).

Also shown in this deviation plot are the results of other workers. It is immediately evident that the agreement with our results is excellent. Most notable is the agreement with Douslin and Harrison[19] where the deviation remains less than 2 $cm^3 \cdot mol^{-1}$ over an extrapolation of more than 250 K outside the temperature range of this work. At lower reduced temperatures the reults deviate from ours quite significantly but this is to be expected since (p, V_m, T) measurements are subject to the systematic errors associated with adsorption at these temperatures. Agreement with the recent values of Gammon *et al*[20] is very good, the results deviating by less than 0.5 $cm^3 \cdot mol^{-1}$. Close agreement is observed with Strein, Lichtenthaler, Schramm and Schäfer[21], where their values agree with ours to within their estimated

imprecision, though there is evidence from the plot that their results show a small systematic deviation. Agreement is also observed, to within 1 $cm^3 \cdot mol^{-1}$, with Michels, van Straaten and Dawson[17] although these results show a more scattered deviation from the square–well solution when compared with the results of Douslin and Harrison. This plot employs a sensitive scale and illustrates the remarkably high level of agreement between the results.

Figure 5.6 shows the deviations from the square–well solution of the second virial coefficients reported by other workers, many being at low reduced temperatures, but on a less sensitive scale. From the plot it can be seen that above 300 K the results are consistent with ours, convincing evidence coming from the recommended smoothed values of Dymond and Smith[22]. At temperatures below this the results show very significant deviations. The recommended values of Dymond and Smith are too positive by about 10 $cm^3 \cdot mol^{-1}$, although this is comparable with the estimated error, as are the experimental values of Pope, Chappelear and Kobayashi[23]; Hoover, Leland and Kobayashi[24] are too positive by about 15 $cm^3 \cdot mol^{-1}$, and the results reported by Hamann and McManamey[25] show significant scatter but are consistently too positive by about 5 $cm^3 \cdot mol^{-1}$. The values reported by Eucken and Parts[26] are too negative, at worst by about 40 $cm^3 \cdot mol^{-1}$; the results of Lichtenthaler and Schäfer[27] are initially too negative by about 5 $cm^3 \cdot mol^{-1}$ but converge with ours at higher temperatures. Nevertheless, the level of agreement is remarkable considering that such different techniques have been used.

To solve equation (3.2.16) for C we adopted essentially the same semi–empirical method of solution as used for B and again resorted to the square–well and Lennard–Jones models. If the theory of intermolecular forces holds for third virial coefficients then in zeroth order one would expect the attractive well parameters of the solution for B and C to be the same. In practice, due to the non–additivity of intermolecular potentials, modification of the well paremeters is required. Using these features, it seemed constructive to attempt to find solutions of equation (3.2.16) in which the well parameters were constrained to those found in the solution of the second

virial coefficients, equation (5.3.5) above. Solutions were also obtained in which we had the full complement of adjustable parameters.

Initially, as a first approximation, the well depth and width associated with the third virial coefficient were the same as those obtained for the second virial coefficient with the collision diameter being the only parameter. Needless to say the fit obtained was rather poor. The second solution assumed the depth of the well was the same as that for the second virial coefficient, but the collision diameter and well width were taken as adjustable parameters. Values of the constants in the model were obtained by weighted non–linear adjustment using equation (3.2.16) with the experimental γ_a and γ^{pg}. The resulting expression is

$$C/b_0^2 = 0.625 - 1.057x + 0.979x^2 - 0.220x^3, \tag{5.3.8}$$

where $b_0 = 151.48\ \mathrm{cm}^3\cdot\mathrm{mol}^{-1}$, $x = \{\exp(256\ \mathrm{K}/T) - 1\}$, and the coefficients of x correspond to a well width equal to 0.29 of the core diameter. The standard deviation of the fit was $0.0007\ \mathrm{dm}^6\cdot\mathrm{mol}^{-2}$; a relatively good fit considering that we are constraining the well depth to the value obtained from the second virial coefficients.

The third, and best, solution obtained had all three parameters as variables and, using weighted non–linear adjustment as above, the resulting expression was

$$C/b_0^2 = 0.6250 - 1.7083x + 3.7283x^2 - 1.7136x^3, \tag{5.3.9}$$

where $b_0 = 120.18\ \mathrm{cm}^3\cdot\mathrm{mol}^{-1}$, $x = \{\exp(160\ \mathrm{K}/T) - 1\}$, and the coefficients of powers of x correspond to a well width equal to 0.5222 of the core diameter. The standard deviation of the fit was $0.0005\ \mathrm{dm}^6\cdot\mathrm{mol}^{-2}$. A remarkable feature of this solution is that the well width obtained using regression analysis is the same as that calculated from the square–well solution representing the second virial coefficients.

An alternative solution was found using the Lennard–Jones (12,6) potential in which we varied the well depth ϵ and the collision diameter σ. Weighted non–linear analysis finally gave $2\pi L\sigma^3/3 = 135.16\ \mathrm{cm}^3\cdot\mathrm{mol}^{-1}$ and $\epsilon/k = 170$ K with a standard deviation of $0.001\ \mathrm{dm}^6\cdot\mathrm{mol}^{-2}$. This fit, when compared with the square–well solution, does not seem to accommodate the data particularly well. This inadequacy has been

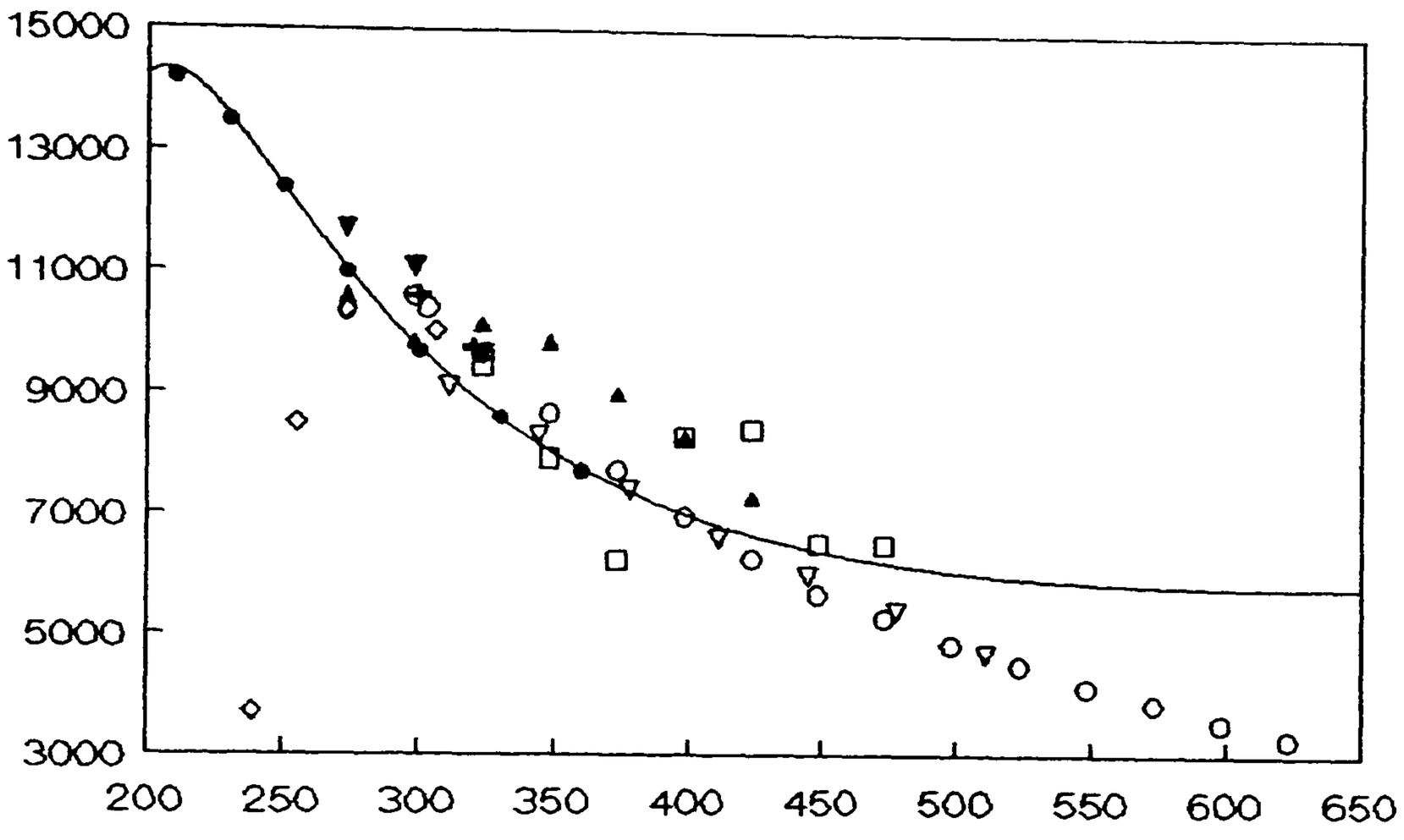

Figure 5.7: Values of the third virial coefficient, C, for ethane.

———— , equation (5.3.9); • , this work; ▲ , reference 17; ○ , reference 19; + , reference 20; ▽ , reference 28; ◇ , reference 29; ▼ , reference 30.

---

noted before where the variations of γ_a and C with temperature are fairly rapid.

Figure 5.7 shows the calculated values of C, using equation (5.3.9), and the experimental results of other workers. Both solutions to equation (3.2.16) fail to produce the observed maximum at about 290 K. The Lennard–Jones solution produces results which are too low between 273 and 360 K and evidence from the slope suggests that it would give values which are too high at temperatures above this. Accordingly, extrapolation with this function was not attempted. The square–well solution, although not showing the required maximum, nevertheless produces results between 273 and 400 K which agree with the experimental results to within the observed scatter. At

Table 5.4: Perfect–gas heat capacities obtained by analysis of N modes coupled by the isochore. Second and third virial coefficients for ethane from equations (5.3.5) and (5.3.9).

T/K	$C^{pg}_{p,m}$/R	B/(cm^3·mol^{-1})	C/(dm^6·mol^{-2})
210.000	5.1958	–380.75 ± 0.52	0.0142
230.000	5.4145	–315.57 ± 0.51	0.0135
250.000	5.6552	–265.92 ± 0.51	0.0124
273.160	5.9623	–221.58 ± 0.51	0.0110
300.000	6.3380	–182.26 ± 0.50	0.0097
330.000	6.7844	–148.70 ± 0.50	0.0086
360.000	7.2522	–122.66 ± 0.50	0.0077

temperatures above this, however, the equation gives results which are too positive, the deviation diverging with increasing temperature. Extrapolation of the same order as that for second virial coefficients seems unreliable in this case, at least with the solutions given; the range of reliable extrapolation is reduced by about a factor of 3. This could simply be some general artifact of the solution since the reliability of the square–well model for representing third virial coefficients is less well established.

Table 5.4 gives values of B an C calculated from equations (5.3.5) and (5.3.9), respectively. The reliability of the square–well model for representing second virial coefficients and the close agreement between the alternative solutions both suggest that extrapolation to higher temperatures is possible with a high degree of accuracy (perhaps with an accuracy comparable with direct measurement); support for this is provided by figures 5.5 and 5.6. Similar claims cannot be made for the third virial coefficients represented by the above solutions.

5.3.3: Tetrafluoromethane.

These measurements have been reported elsewhere[8,28] and a reprint of the latest publication is to be found in Appendix 1. In this section additional analysis not included in the publication is reported.

Table 5.5: Vibrational relaxation times in CF_4 at a density of 1 $kg \cdot m^{-3}$.

T/K	$\tau\rho/\mu s \cdot kg \cdot m^{-3}$	$\partial(\tau\rho)/\partial\rho$ μs^{-1}
174.780	7.129 ± 0.042	0.0168 ± 0.0022
196.960	5.490 ± 0.018	0.0198 ± 0.0007
224.450	4.442 ± 0.010	0.0135 ± 0.0005
249.300	3.649 ± 0.014	0.0085 ± 0.0006
275.000	3.002 ± 0.008	0.0057 ± 0.0004
300.000	2.529 ± 0.009	0.0043 ± 0.0006
325.000	2.145 ± 0.004	0.0034 ± 0.0003
350.090	1.870 ± 0.007	0.0015 ± 0.0006
375.020	1.616 ± 0.004	0.0021 ± 0.0003

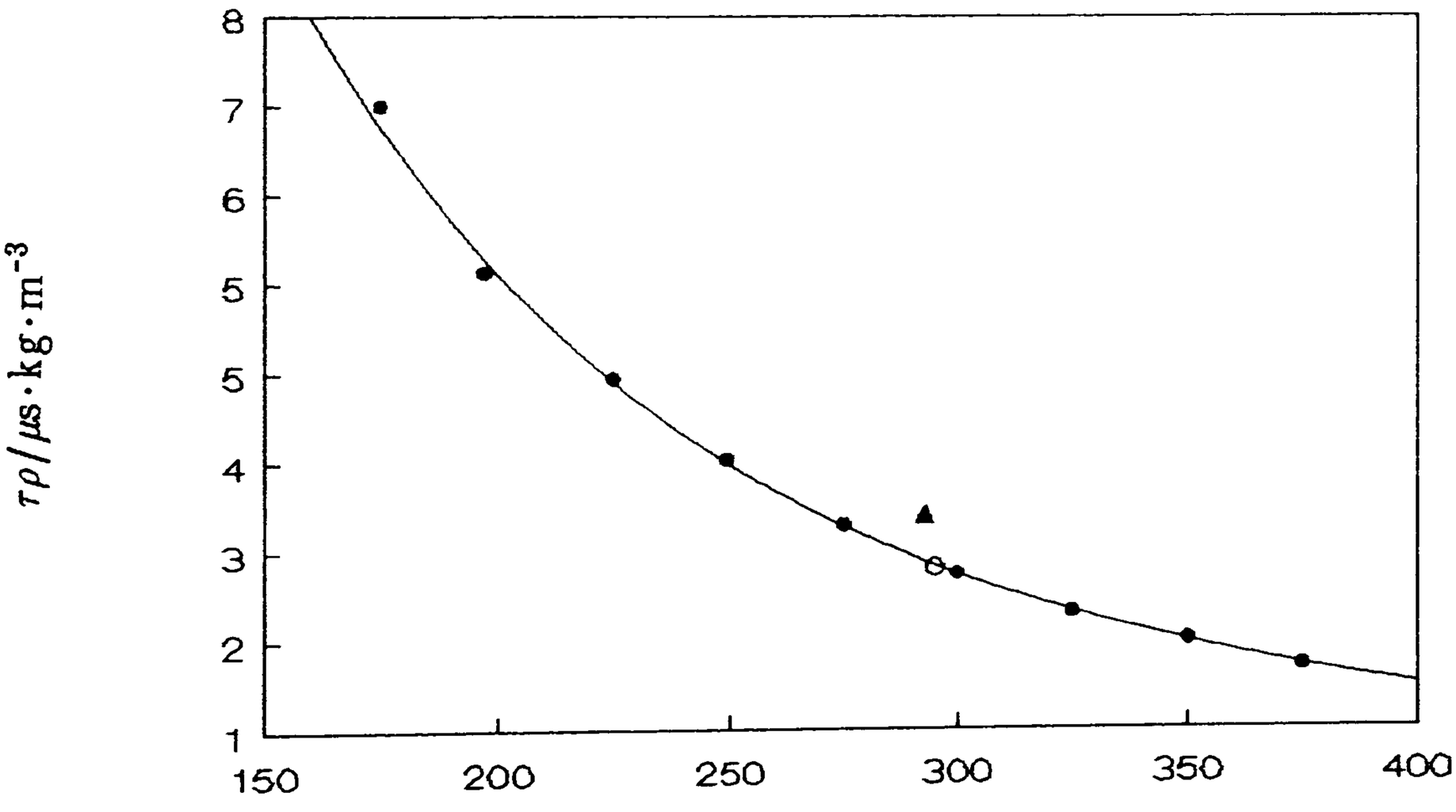

Figure 5.8: Vibrational relaxation times in CF_4. ● , this work; ○ , reference 32; ▲ , reference 33.

Vibrational relaxation is the most important loss mechanism operating in CF_4 under the conditions of these measurements. Analysis of the measured half–widths, after allowance for the other loss mechanisms, allowed determination of the vibrational relaxation time. This was then used to correct the frequencies for the very small dispersion that occurs at audio frequencies.

It is assumed that the entire vibrational specific heat capacity relaxes with a single time constant τ. Since the product $\tau\rho$ is expected to be nearly independent of density along an isotherm, this quantity was obtained by analysis of the residual half–widths in terms of equation (5.3.1).

The results of the vibrational relaxation times, at a density of 1 $kg \cdot m^{-3}$, could be represented by the following equation

$$\tau/\mu s = 228848(K/T)^2 - 0.161297 \times 10^{14}(K/T)^6 \qquad (5.3.10)$$

to 26 ns. Results are listed in table 5.5. These are shown plotted as a function of temperature in figure 5.8. Also shown in figure 5.8 are the results of other workers. From the work of Byers[29] we calculate $\tau = (2.58 \pm 0.06)$ μs at 295.15 K and 1 $kg \cdot m^{-3}$. Agreement with the value of 2.602 μs obtained by interpolation of our measurements is very satisfying and within experimental error. Corran *et al*[30] report a value of $\tau = 3.1$ μs at 1 $kg \cdot m^{-3}$ and 293 K which lies above our results by about 0.46 μs. Insufficient information was given for a re–evaluation of the results.

5.3.4: Methanol.

Methanol has been studied along twelve isotherms between 280 and 360 K. Nine of these isotherms have been reported previously[5], but since a re–analysis of the whole data[31] set was carried out the results are quoted here for clarity. Frequencies were corrected as indicated in Chapter 2. The values of $<u>$ so determined from the N modes are given in table 5.6 along with the standard deviation of the mean, σ. Small corrections have been applied to reduce all values to the stated temperature of the isotherm.

The shear viscosities used in the calculation of corrections were taken from

Craven and Lambert[32] and could be represented by

$$\eta/\mu\text{Pa}\cdot\text{s} = 0.03286(T/\text{K}) \tag{5.3.12}$$

to 0.03 μPa·s.

The thermal conductivities were taken from the measurements of Renner, Kucera and Blander[33] and the zero–density values could be represented to 0.09 $\text{mW}\cdot\text{m}^{-1}\cdot\text{K}^{-1}$ by

$$\kappa(T,\ p=0)/\text{mW}\cdot\text{m}^{-1}\cdot\text{K}^{-1} = 0.1818 \times 10^{-3}(T/\text{K})^2. \tag{5.3.13}$$

For the pressure range covered by the measurements, the pressure dependence of κ is small. Virial coefficients required in the correction terms were estimated from a preliminary analysis of the results.

Analysis of the excess half–widths used equation (5.3.1) and terms in b_0 and b_1 for temperatures above 300 K, but below this temperature the only significant term was b_1. No significance is attached to b_1 for the analysis of the half–widths at temperatures below 300 K. Resulting values for the relaxation times do not compare favourably with literature values[34].

Since methanol is a hydrogen–bonding fluid and the reduced temperatures were very low, the method of analysis of the results differed from that used previously. The curvature of the isotherms was so extreme that conventional regression analysis yielded virial coefficients that depended, at an unacceptable level, on the pressure range studied. The curvature of an isotherm in methanol is compared with that in ethane in figure XXX. The method finally adopted was advocated by Douslin in his precise (p, V_m, T) measurements[19]. Briefly, the mean values of u^2 were fitted using

$$u^2 = A_0 + A_1 p + A_2 p^2 + \cdots \tag{5.3.14}$$

to obtain estimates of A_0, A_1, A_2 $\cdots$. Values of A_0 were then refined non–linearly by fitting the residual expression

$$\{u^2 - A_0\}/p = A_1 + A_2 p + \cdots \tag{5.3.15}$$

to the results and obtaining in the process improved estimates of A_1 and A_2 $\cdots$. The process of fitting further residuals allowed refining of A_1 and A_2. The analysis was usually carried out by a series of regressions, of different orders, over various ranges of

Table 5.6: Mean values of u with standard deviations σ determined from N modes at temperatures T and pressures p.

$\frac{T}{\mathrm{K}}$	$\frac{p}{\mathrm{kPa}}$	$\frac{u}{\mathrm{m \cdot s^{-1}}}$	$\frac{10^6\sigma(u)}{u}$	N	$\frac{p}{\mathrm{kPa}}$	$\frac{u}{\mathrm{m \cdot s^{-1}}}$	$\frac{10^6\sigma(u)}{u}$	N
360.000	80.506	331.2325	1.3	5	71.941	331.8023	1.3	5
	63.909	332.2989	1.3	5	55.950	332.7630	1.3	5
	47.955	333.2017	1.4	5	39.935	333.6171	1.4	5
	31.974	334.0089	1.7	5	23.979	334.3829	2.0	5
	15.980	334.7406	2.6	5	8.013	335.0811	0.8	4
340.000	66.460	320.1513	1.6	5	59.498	321.3672	2.2	5
	53.149	322.3611	2.0	5	46.521	323.2862	1.7	5
	39.861	324.0979	1.6	5	33.195	324.8024	1.7	5
	26.577	325.4079	1.7	5	19.944	325.9367	1.6	5
	13.296	326.4053	1.8	5	6.722	326.8244	0.7	4
330.000	43.880	316.9419	2.8	5	39.556	317.9935	2.0	5
	35.124	318.9397	1.8	5	30.748	319.7666	1.9	5
	26.368	320.4809	2.0	5	21.956	321.0912	1.9	5
	17.565	321.6080	2.1	5	13.174	322.0497	2.2	5
	8.787	322.4326	2.0	5	4.398	322.7778	2.4	5
320.000	22.444	315.0924	1.7	5	20.544	315.6082	1.5	5
	18.184	316.1766	1.3	5	16.521	316.5308	1.3	5
	14.503	316.9130	1.1	5	11.909	317.3359	0.9	5
	10.267	317.5691	1.9	5	8.135	317.8379	1.3	5
	6.166	318.0589	2.3	5	4.313	318.250	3.2	5
	2.733	318.402	4.7	3				
315.000	19.568	312.4681	2.3	5	17.164	313.3265	1.7	5
	15.461	313.8540	1.7	5	13.481	314.3863	1.1	5
	11.192	314.9005	1.1	5	9.517	315.2168	1.7	5
	7.585	315.5283	1.3	5	6.198	315.7234	2.1	5
	4.582	315.926	4.4	4	2.720	316.137	4.6	2
	1.511	316.269	15	2				
310.000	17.157	309.5951	2.5	5	15.740	310.3136	1.4	5
	14.347	310.9502	1.0	5	12.982	311.5039	1.4	5
	11.528	312.0191	0.4	5	9.812	312.5322	1.0	5
	8.325	312.9019	1.2	5	6.755	313.2277	0.8	4
	5.307	313.4797	0.8	4	3.720	313.715	4.8	4
	2.338	313.896	5.9	2				
305.000	13.952	307.2262	1.4	5	13.211	307.6811	1.4	5
	11.962	308.4445	1.4	5	10.807	309.0737	1.2	5

$\frac{T}{\mathrm{K}}$	$\frac{p}{\mathrm{kPa}}$	$\frac{u}{\mathrm{m \cdot s^{-1}}}$	$\frac{10^6\sigma(u)}{u}$	N	$\frac{p}{\mathrm{kPa}}$	$\frac{u}{\mathrm{m \cdot s^{-1}}}$	$\frac{10^6\sigma(u)}{u}$	N
305.000	9.601	309.6399	1.6	5	8.659	310.0257	1.6	5
	7.482	310.4363	1.7	5	6.067	310.8427	1.0	4
	4.580	311.176	3.9	4	3.505	311.376	4.1	4
	2.363	311.557	6.6	3				
300.000	10.180	305.6296	2.2	5	9.327	306.2870	2.9	5
	8.556	306.8185	2.5	5	7.641	307.3712	1.6	5
	6.729	307.8396	2.0	5	5.987	308.1636	2.0	5
	4.960	308.5367	2.0	5	3.877	308.8479	2.9	4
	2.887	309.075	4.1	4	1.910	309.261	8.4	4
295.000	7.745	303.5692	2.6	5	7.075	304.2099	2.2	5
	6.390	304.7929	2.4	5	5.694	305.2993	2.6	5
	4.940	305.7566	2.6	5	4.256	306.1004	2.4	5
	3.506	306.400	4.3	5	2.793	306.632	5.3	4
	2.081	306.816	8.2	3	1.357	306.9715	0.4	2
290.000	5.890	301.501	4.6	5	5.231	302.237	3.4	5
	4.954	302.533	4.4	5	4.478	302.972	4.0	5
	4.001	303.376	4.6	5	3.496	303.734	3.8	5
	2.997	304.001	4.2	5	2.485	304.232	5.7	4
	1.979	304.415	5.7	5	1.512	304.555	7.9	2
	1.028	304.678	9.5	2				
285.000	4.238	299.530	5.8	5	3.882	300.060	5.8	5
	3.605	300.430	6.4	5	3.243	300.858	4.8	5
	2.920	301.163	7.4	5	2.648	301.393	6.8	5
	2.224	301.690	6.4	5	1.898	301.872	8.4	5
	1.592	302.017	13	5	1.253	302.146	12	5
280.000	2.980	297.621	15	5	2.652	298.176	9.1	5
	2.443	298.499	8.7	5	2.173	298.850	9.5	4
	1.980	299.053	9.7	5	1.412	299.510	9.0	5
	1.118	299.675	8.6	4				

pressure. The advantage of this approach is that the limiting values of the coefficients so obtained do indeed correspond to the definition of the virial coefficients. Truncation of the series was determined by monitoring the residuals and when no further information was present the analysis was deemed complete. Arguments have been put forward which indicate that the above virial expansion is not the best representation for methanol. The alternative expansion

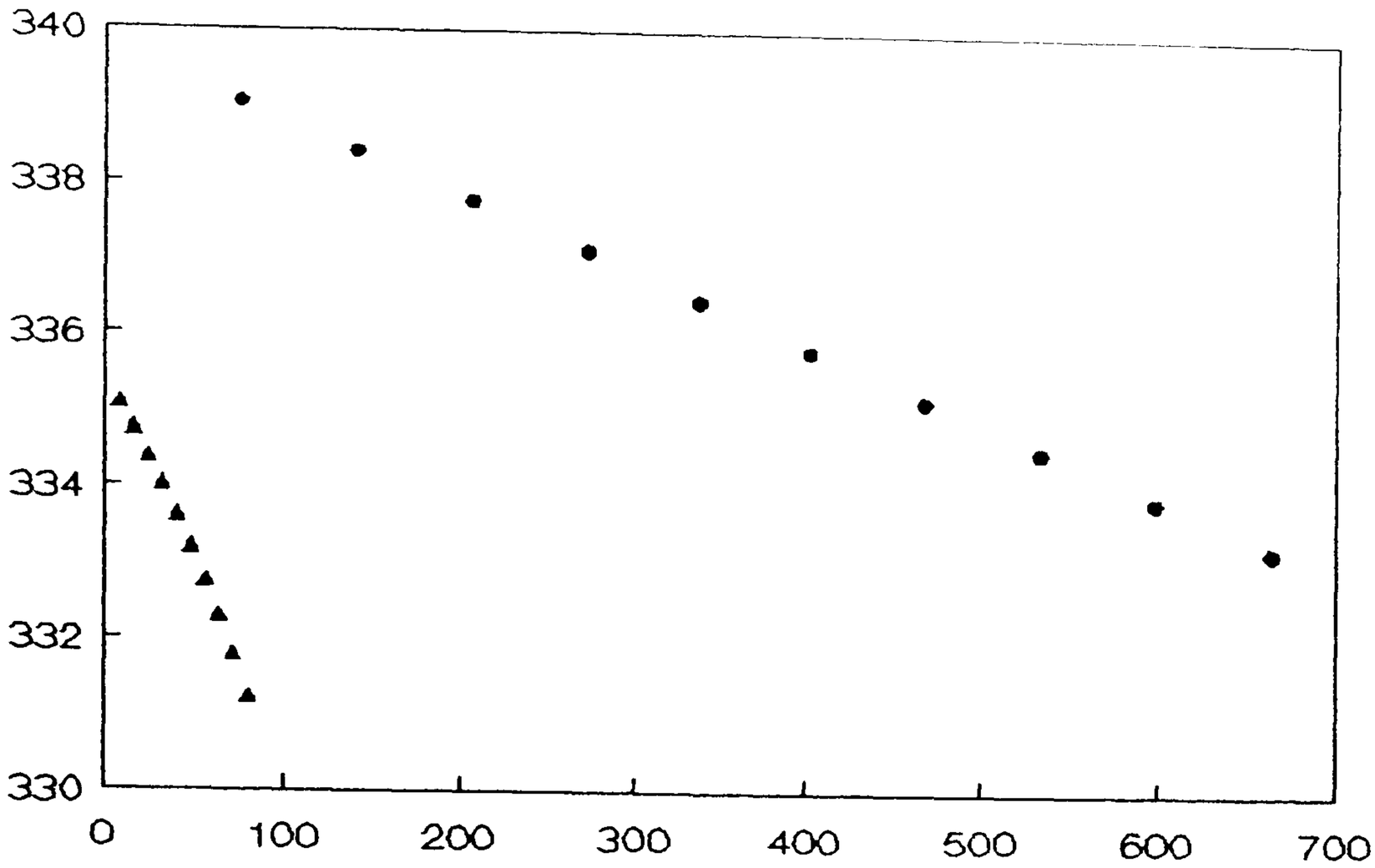

Figure 5.9: Speeds of sound, u, in ethane, • , and methanol, ▲ , as a function of pressure, p, showing the extreme curvature of the measurements in methanol.

$$u^2 = A_0 + A_1 p + A_3 p^3 + \cdots, \qquad (5.3.16)$$

in which only odd powers of p appear, has been suggested[38,39]. Accordingly, the results were also analysed using this series and the method of fitting residuals to refine the coefficients in the expansion. The method, when used in conjunction with regression algorithms, suffers from the disadvantage that all coefficients determined in the analysis are correllated. To try and counter this the pressure range was successively truncated and the variation of the coefficients so determined was used to estimate any likely systematic error associated with the analysis. The output from the regression analyses was such that it returned values of the perfect–gas heat capacity $C^{\mathrm{pg}}_{p,\mathrm{m}}$, the second acoustic virial coefficient β_{a} and the third coefficient of the series which will be either γ_{a} or δ_{a}, depending on the series expansion adopted. Analysis of the results indicated that the odd power series expansion was indeed the best representation and gave the most self–consistent results. Accordingly, results quoted are from analysis with this series expansion.

The values of the perfect–gas heat capacity are listed in table 5.7 and are, on average, about 0.2 % above those of reference 40. The difference at the higher

Table 5.7: Perfect–gas heat capacities $C^{pg}_{p,m}/R$, and second acoustic virial coefficients, β_a, determined in the regression analyses with equation (5.3.16). Second (p, V_m, T) virial coefficients, B, were determined using equation (5.3.17).

T/K	$C^{pg}_{p,m}/R$	β_a/(cm^3·mol^{-1})	B/(cm^3·mol^{-1})
360.000	5.8940	–742 ± 1.3	–643
340.000	5.6795	–1032 ± 1.7	–873
330.000	5.5633	–1246 ± 2.5	–1031
320.000	5.4873	–1526 ± 3.0	–1230
315.000	5.4456	–1701 ± 5.2	–1349
310.000	5.4047	–1888 ± 7	–1483
305.000	5.3660	–2135 ± 10	–1636
300.000	5.3298	–2368 ± 17	–1811
295.000	5.2928	–2710 ± 25	–2011
290.000	5.2494	–3130 ± 35	–2240
285.000	5.2169	–3490 ± 50	–2506
280.000	5.1813	–4100 ± 100	–2814

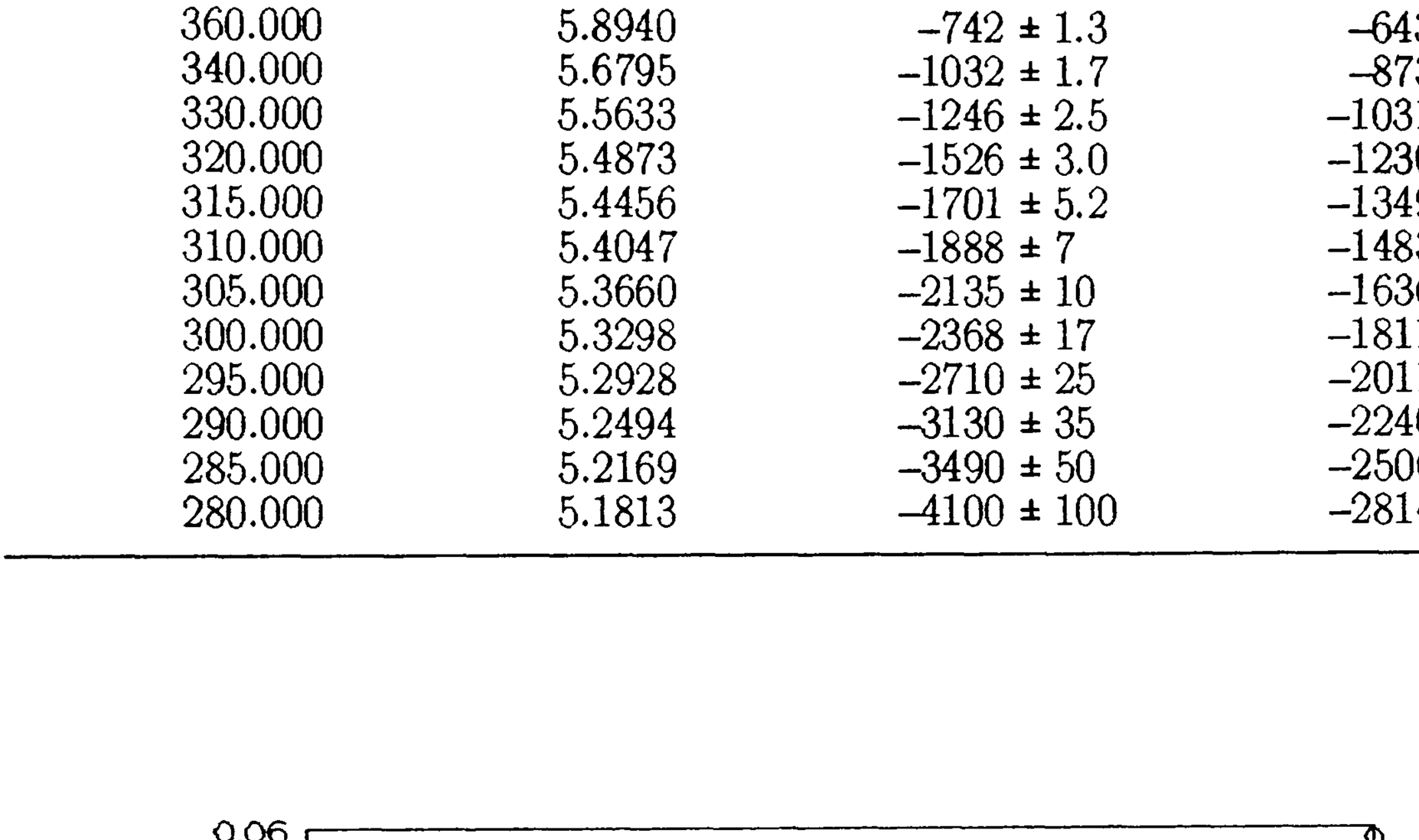

Figure 5.10: Experimental perfect–gas heat capacities at constant pressure shown as deviations from the equation given in reference 40. o , this work, • , reference 5 reanalysed.

temperatures increases to about 1 % and is probably due to contamination of the methanol with water. This is shown in Figure 5.10.

The second acoustic and (p, V_m, T) virial coefficients are given in table 5.7. Estimates of B were extracted from the acoustic coefficients by analysis of the results using the square–well solution. This is obviously inadequate for a fluid such as methanol but is a convenient method of assessing internal consistency. Agreement with the estimates of B obtained from the potential of Opel *et al*[38] is really rather good as is the agreement of the results obtained from a psuedo–Stockmayer potential. The psuedo–Stockmayer potential was derived from the Stockmayer potential[39] using a method developed by Pople[40,41]. Pople considered the angle dependent part of the Stockmayer potential as a perturbation on a spherically symmetric radial potential. Expanding the angle dependent contributions allows inclusion or exclusion of various terms. For the potential considered here the perturbations were truncated after the second term and included the effects of dipole–dipole interactions only. The expression derived from the square–well was

$$B/(\mathrm{cm}^3\cdot\mathrm{mol}^{-1}) = 14 - 3.96\exp(1840\ \mathrm{K}/T) \qquad (5.3.17)$$

which fit the results with a weighted standard deviation of 3.2 $\mathrm{cm}^3\cdot\mathrm{mol}^{-1}$. Deviations of previous experimental determinations from this result are shown in figure 5.11. The (12, 8, 6, 3) potential of Opel *et al*[38] is in good agreement with the square–well potential determined in this work. The maximum deviation is 245 $\mathrm{cm}^3\cdot\mathrm{mol}^{-1}$ at 298 K although on average the agreement is on the order of 40 $\mathrm{cm}^3\cdot\mathrm{mol}^{-1}$. The rapid increase in the deviation at the lowest temperatures is not unexpected since extreme experimental difficulties are expected for conventional (p, V_m, T) measurements in this region. The results of Kell *et al*[47] agree, on average, to better than 40 $\mathrm{cm}^3\cdot\mathrm{mol}^{-1}$ across the whole range as do the results of Kudchadker *et al*[48] with the exclusion of the point at 298 K. The results of Lambert *et al*[42] show a systematic deviation of about 300 $\mathrm{cm}^3\cdot\mathrm{mol}^{-1}$ from (5.3.17) although extrapolation, of their results, suggests that the results may be converging. Fox *et al*[44] differ by about 150 $\mathrm{cm}^3\cdot\mathrm{mol}^{-1}$ as do the results of Bottomley *et al*[45]. Knoebel *et al*[46] show a large systematic deviation

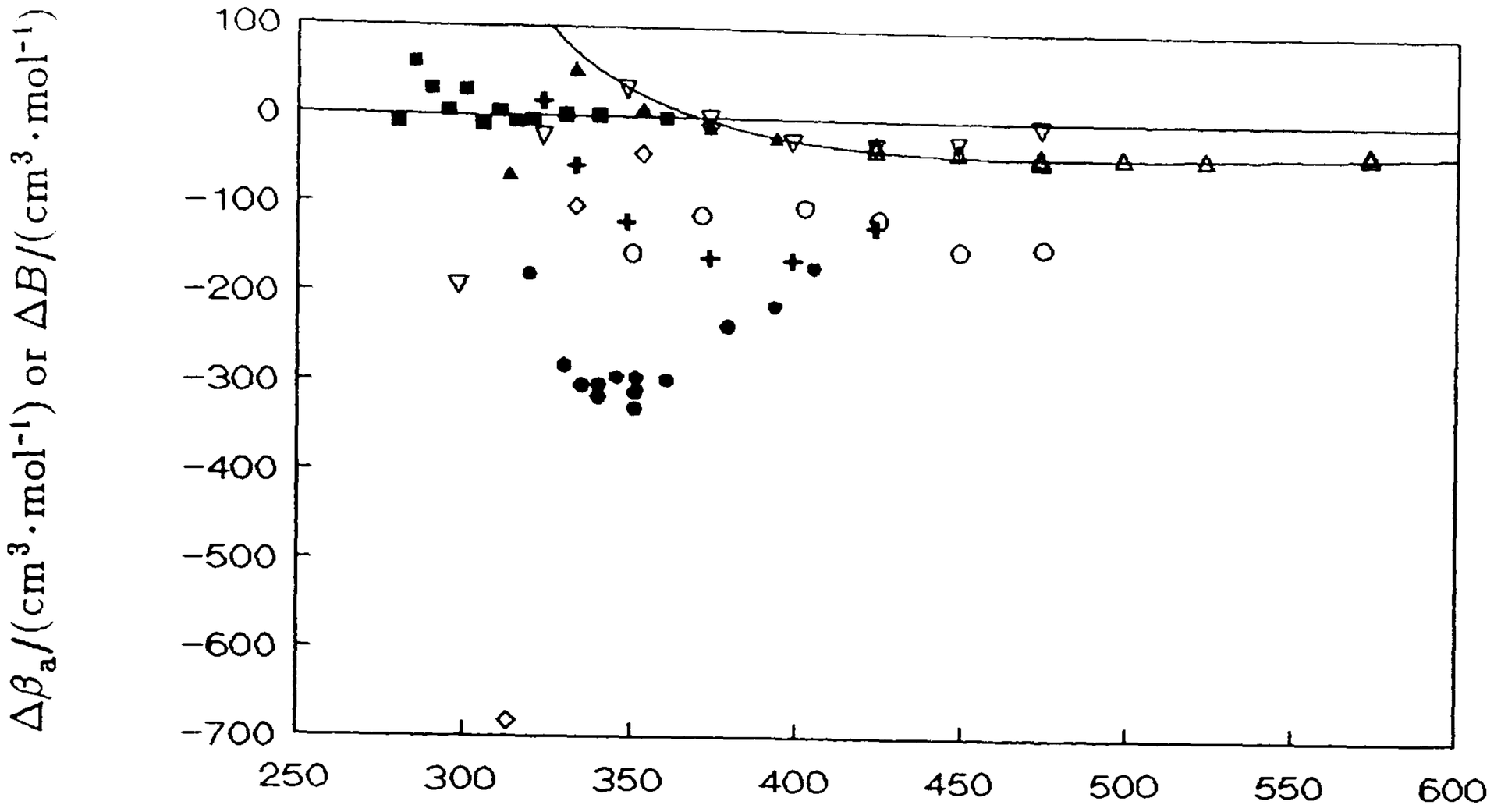

Figure 5.11: Deviations of experimental β_a from (5.3.17) and (3.2.15). Also shown are deviations $\Delta B = \{B(\text{exp.}) - B(\text{sq.–well})\}$ of second virial coefficients from equation (5.3.17). ■ , this work; ——— , reference 41; • , reference 45; ▲ , reference 46; ○ , reference 47; + , reference 48; ◇ , reference 49; △ , reference 50; ▽ , reference 51.

---

from the square–well solution reaching, at worst, nearly 700 $cm^3 \cdot mol^{-1}$ at the lowest temperature studied; the high temperature results converge with (5.3.17). Kretschmer *et al*[46] agree with this work to better than 70 $cm^3 \cdot mol^{-1}$, although if the result at 313 K is excluded the agreement is better than 50 $cm^3 \cdot mol^{-1}$. It is of note that the results of Kell *et al*, Kudchadker *et al* and Kretschmer *et al* agree exteremely well with the potential of Opel *et al*. Although the Opel potential diverges from the square–well solution at the lowest temperatures, the agreement is still very satisfying and is taken as an indication that a satisfactory solution has been obtained. The differences at the lowest temperatures may be due to inadequacies in the square–well solution for representing the results or, the extreme experimental difficulties expected for conventional (p, V_m, T) measurements in this regime; or a combination of both. For a thorough analysis of the results, solutions derived from the complete Stockmayer potential should be found.

5.4: High Pressure Measurements.

High–pressure measurements were performed in a new welded 45 mm stainless steel resonator. Details of its construction are given below. Measurements were performed in the pure substances argon, nitrogen and methane and in the binary mixture of methane and ethane $\{(1 - x)CH_4 + xC_2H_6\}$, with $x = 0.15$. The measurements in argon and nitrogen served to characterise the resonator over the temperature and pressure range of study.

5.4.1: Apparatus.

Two hemispheres with nominal internal radius of 45 mm were machined from a cylindrical bar of type 321 stainless steel. The hemispheres were both machined such that the polar depth was greater than the equatorial radius. In this way any rounding at the equator due to polishing could be removed by machining. Tooling marks were removed by hand–polishing using: 1) coarse emery paper (100) with cutting oil; 2) silicon carbide papers of varying grit sizes extending from 240 to 1200; and 3) aluminium oxide paste of various particle sizes extending from 5 μm down to 0.015 μm. After polishing the surface had a near mirror finish to the eye. Under a microscope residual depressions could be seen and these had a size on the same order as that of the finest aluminium oxide paste. The depressions were "comet–like" in appearance with a core of roughly twice the diameter of the particle size and a tail of perhaps five times the diameter in length but only half to a quarter of the diameter in width. The dimensions of the cavity, after machining to remove rounding due to polishing, showed asymmetry about the polar and equatorial diameters; the polar diameter was greater than the equatorial. This asymmetry was cylindrical in nature and about 0.3 mm in magnitude. This was an intentional feature since it is possible to measure the dimensions of the cavity, to high accuracy, using microwave resonances. Knowing the dimensions accurately allows high precision machining of the sphere to obtain near perfect dimensions. After machining, under the guidance of microwave measurements, the dimensions of the sphere, as determined from mechanical measurements, were

90.083 (= 2 × 45.042) and 45.044 mm for the equatorial diameter and depth of the upper hemisphere and 90.076 (= 2 × 45.038) and 45.038 mm for the lower hemisphere. The two hemispheres met at an interlocking step of nominal dimensions 2 mm × 2 mm on the outer surface. This step ensured that the two hemispheres were aligned coaxially and that they made contact only on the inner surface. After final polishing, but before final machining of the polar diameter, the two transducer ports and the 2 mm diameter gas filling tube were drilled. The transducer ports were machined in the northern hemisphere at a polar angle of $\pi/4$ separated by an azimuthal angle of π and then reamed to have a diameter of 7 mm at the inner surface. Approximately 8 mm from the inner surface a "flat" was machined on which were drilled six bolt holes of 6 BA thread and 20 mm pcd. These were for location of the acoustic transducers and differed from the previous design of the 40 mm aluminium resonator so that the ease with which pressure and vacuum tight seals could be made was improved. The outside surface of the resonator was left cylindrical to enable a large copper block to be in good thermal contact with the sphere surface and the thermometer well. The two hemispheres were joined with a partial penetration (roughly 60 %) weld along the inner mating surface using an electron beam. The experiment involves pressure compensation; hence the weld does not have to support the full pressure differential but only a small fraction thereof. The primary function of the weld is to form a vacuum and gas tight seal. The gas tight seal is essential to prevent mixing of the gas under study and the ballast gas, typically nitrogen. Under a helium leak test the join was found to be vacuum tight. Before the resonator was welded, but after assembly, the geometry of the resonator was determined using microwave resonances. These are very similar to the acoustic resonances, in that the frequency is largely determined by geometric factors, but the TMlm modes studied are $(2l+1)$–fold degenerate. This enables geometric imperfections to be determined since under such conditions the degeneracy of the mode is lifted. The apparatus and the method have been discussed previously[49,50]. Measurements indicate that the polar and equatorial radii differ by no more than 16 μm. Microwave measurements after welding indicate that there was some distortion. The appearance of

a triply degenerate mode (of a perfect sphere) becomes a singlet and a partially resolved doublet. The magnitude of the splitting of these components can be used to calculate the size of the geometric imperfection. Analysis of the TM(1,1) mode as a triplet yields a geometric imperfection of 38.6 μm in the polar direction and an equatorial displacement of 52.9 μm. Imperfections on this order will manifest themselves as discrepencies between the speeds of sound determined from individual modes, see section 2.3, and thus corrections to the resonance frequencies were applied. Finally the 46.0 mm ($1.023a$)[5,8] gas inlet tube was completed with a 1.7 mm internal diameter stainless steel tube pressed into the northern boss.

5.4.2: Pressure Vessel.

The pressure vessel is that used by Ewing and Goodwin in their measurements on gases up to pressures of 7 MPa and is described in detail elsewhere[5]. The vessel was designed to operate up to 673 K and pressures of 20 MPa and is fabricated entirely of austenitic stainless steels. The apparatus was used without modification except to upgrade the leadthroughs. The electrical leadthroughs that bring the electrical connections from inside the apparatus at working pressures to atmospheric pressure were commercial devices supplied by Conax and were suitable for sealing on bare wires up to 34 MPa in the temperature range 250 to 350 K. The sealing material was teflon and the seal was formed by compressing the material around the wires by a screw press. A potential problem was electrical cross–talk between the transducers resulting from the small lengths of unshielded cable. To this end, two leadthroughs were employed; one which carried only the source connections and another which carried the remaining wires. No cross–talk was observed. The apparatus is shown in figure 5.12.

5.4.3: Transducers.

Both electroacoustic transducers were of the capacitance type and were of essentially the same design. Each consisted of a thin dielectric membrane clamped by a ceramic sleeve within a brass housing. The metalized outer surface was in electrical

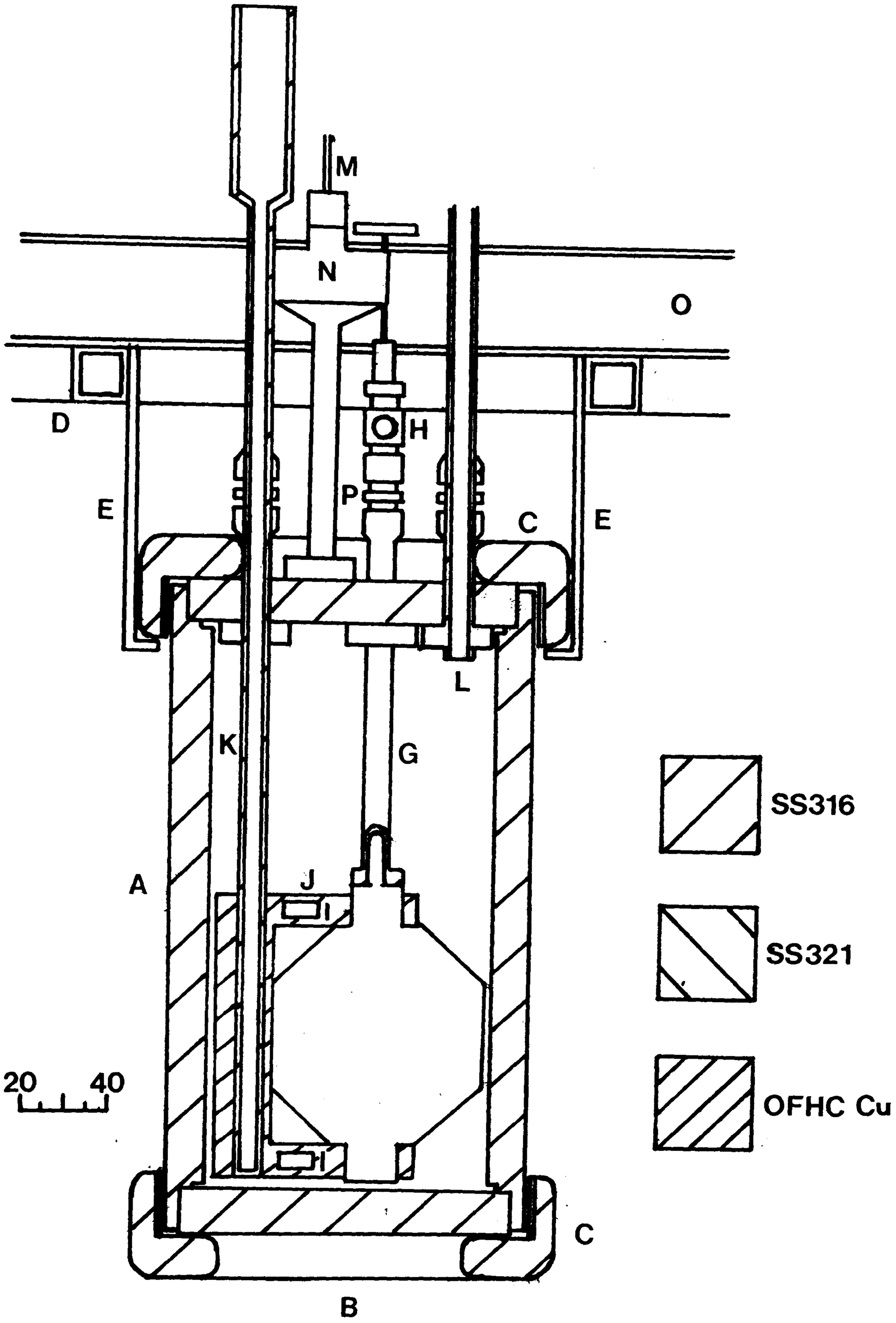

Figure 5.12: See following page for a description.

Figure 5.12: High–pressure apparatus. The pressure vessel consisting of a cylinder, A, end covers, B, and end caps, C, were suspended in a stirred fluid thermostat from a square–sectioned frame, D, using aluminium plates E. The sample passed through G via H, a bellows sealed, all welded, stainless steel valve. The resonator heaters, I, were mounted on copper blocks, J, which connected the sphere to the thermometer well K. This well held a long stem platinum resistance thermometer (LN 780308) which had its sensing element located at the resonator's equator; to improve thermal contact the well was filled with ethanol. The nitrogen gas, required for pressure compensation of the resonator, entered the vessel through tube L. The necessary electrical connections were made using two sealed leadthroughs, M, housed in a smaller end cover and cap arrangement, N. The thermostat was insulated with Kaowool blanket, O, sandwiched between aluminium sheets. The joints, P, were made with stainless steel Swagelock couplings suitable for 12.7 mm diameter tubing.

---

contact with the housing. The front face of this housing was machined with the same radius of curvature as the inner surface of the resonator and was flush with it when the housing was bolted in place with an indium wire seal. A circular area of the membrane was exposed to the interior of the resonator by a hole in the front of the housing. A brass electrode, of same cross–sectional area as the membrane exposed, was held against the centre of the membrane by a spring which also served as an electrical contact. The volume inside each transducer was connected to the interior of the resonator by a small pressure equalization port. Isolation of the sample from the ballast gas was maintained by passing the electrical connections through an hermetically sealed single pin leadthrough.

5.4.3a: Source.

In the source transducer, shown in figure 5.13, a 12 μm thick polyester membrane (Melinex, ICI plc) coated with a 50 nm thick aluminium layer was used, the active element of which had a diameter of 2 mm. The area was purposely kept small for two

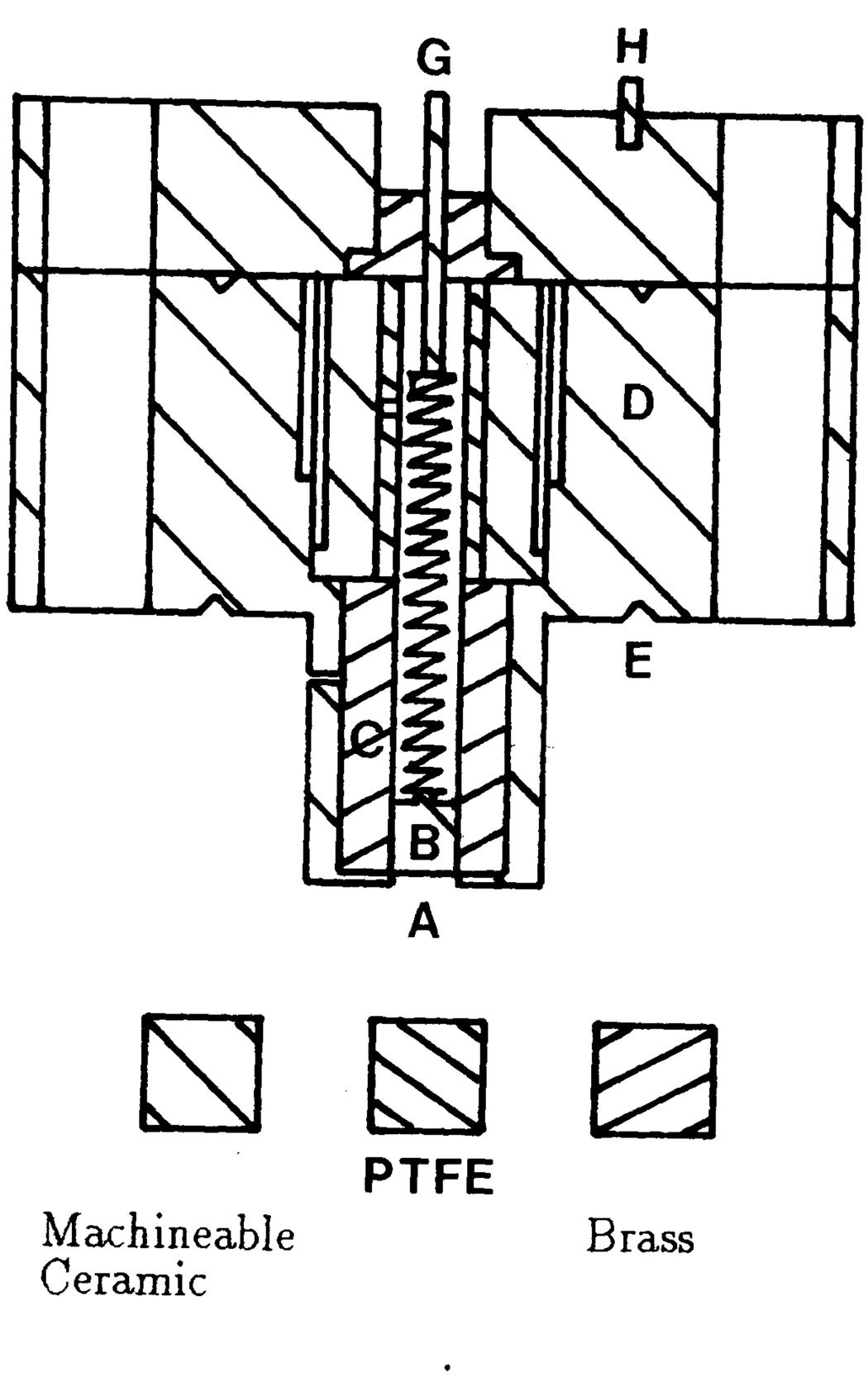

Figure 5.13: Acoustic transducer used in the high–pressure resonator.

A, Metal coated plastic film; B, brass backplate machined on face A with 5 equally spaced holes of diameter 0.3 mm and depth 0.5 mm which was held in contact with the plastic film with a spring; C, machineable ceramic insulating sleeve; D, brass body; E, groove suitable for indium wire seal; F, PTFE insulating sleeve; G, Hermetically sealed ceramic single pin leadthrough; H, earth pin.

reasons; to reduce perturbations on the resonance frequencies of the cavity caused by the transducers and to prevent large mechanical loading of the membrane. The back electrode had an area the same as the active element and the volume of gas trapped behind the membrane was increased by machining holes in the front surface of the backplate. Five equally spaced holes were drilled 0.3 mm in diameter and 1 mm deep. These served to increase the compliance of the element and exert critical damping on the motion of the membrane thus ensuring that no natural resonances of the membrane perturbed the resonance frequencies of the normal modes of the cavity[51]. The housing, and the metalized layer with which it was in contact, were held at ground potential, while the back electrode was excited with an ac signal of up to 60 V rms superimposed on a dc level of about 300 V. Under these conditions, the electrostatic force drives the membrane to produce sound at the excitation frequency.

5.4.3b: Detector.

The membrane of the detector transducer, shown in figure 5.13, was a 6 μm thick polyvinylidene fluoride disc coated with aluminium on the outer surface. This material was obtained with a permanent dielectric polarization "frozen" in so that no dc bias was required. The membrane had a diameter of 3 mm to increase the active element surface area and thus increase the efficiency. This was necessary to ensure useful signals at the highest pressures where the amplitudes of the sound waves are greatly reduced. The back plate had five equally spaced holes of 0.5 mm diameter and 1 mm depth. The larger trapped volume was required to increase the compliance of the membrane at higher frequencies thus ensuring a roughly flat, frequency–independent response. The detector had an active capacitance of only about 5 pF and therefore acts as a very high impedance signal source when the membrane is set in motion by audio frequency sound. A preamplifier is required very close to the transducer to prevent division of this signal by the large ratio of stray–to–active capacitance that would result from even a few cm of coaxial cable. A simple JFET circuit was soldered directly to the electrical feedthrough pin on the back cover plate of the transducer. This device

has low power dissipation, a potential difference gain of ≈0.6, negligible phase shift at audio frequencies, and a low output impedance.

5.4.4: Argon.

Argon has been studied along seven isotherms between 250 and 350 K at pressures up to 10 MPa. Since this work formed part of a laboratory intercomparison, various state points were chosen at which measurements should be performed. The important points were 10, 7.5, 5 and 2.5 MPa at 250, 275, 300 and 350 K. Since recording data at exactly these pressures would have been difficult, generally three points were studied in the required region. This will enable interpolation to the exact pressures to be performed. In some instances extrapolation is required to determine information at 10 MPa but because argon is well behaved this should not represent a problem.

Experimentally determined frequencies were corrected as outlined in Chapter 2. Thermophysical properties required in the various correction terms were obtained from the literature[52–55]; the thermodynamic properties required were calculated correct to the second virial coefficient which was itself obtained from a preliminary analysis of the results. In table 5.8 we list the mean quantity (u/a), measured along the seven isotherms, determined from N modes together with the standard deviation of the mean at a given state, σ, and the deviation of the mean from the equation of best fit, δ. Small corrections have been applied to reduce all values of (u/a) to the stated temperature of each isotherm.

At pressures above 1.5 MPa the dominant correction was that due to shell motion. Corrections varied from 338 ppm for the (0,5) mode at 350 K and 10 MPa to 27 ppm for the (0,2) mode at 252 K and 1.5 MPa. The (0,6) mode, which would normally be measured, was not always recorded along the high–pressure isotherms since previous experience indicated that this mode was always significantly perturbed by shell motion, and the resulting sound speed did not agree with values determined from other modes. Below 1.5 MPa corrections were dominated by the thermal boundary layer. The thermal accommodation coefficient was taken as unity as determined from a

Table 5.8: Mean values of (u/a) and u with standard deviation σ determined from N modes, and deviations δ from equation (5.2.3) at temperatures T and pressures p. The coefficients of equation (5.2.3) are given in Table 5.9.

$\frac{T}{\mathrm{K}}$	$\frac{p}{\mathrm{kPa}}$	N	$\frac{u}{a}\cdot\mathrm{s}$	$\frac{u}{\mathrm{m}\cdot\mathrm{s}^{-1}}$	$\frac{10^6\sigma(u)}{u}$	$\frac{10^6\delta(u)}{u}$
251.989	9859.79	3	6831.7555	307.1299	6.5	(a)
	9780.96	3	6827.0995	306.9206	8.1	1.0
	9706.80	3	6822.6542	306.7207	7.6	–0.9
	7667.65	3	6718.5544	302.0408	2.7	1.4
	7583.62	3	6714.9436	301.8785	1.6	–2.3
	7517.54	3	6712.1191	301.7515	3.4	(a)
	5084.25	3	6631.4576	298.1253	1.3	1.9
	4998.18	3	6629.3273	298.0295	1.9	1.2
	4910.78	3	6627.2030	297.9340	1.5	–0.8
	2588.30	3	6587.6766	296.1570	3.5	–2.7
	2502.19	3	6586.7417	296.1150	1.8	(a)
	2412.47	3	6585.9098	296.0776	3.0	–1.1
	1438.31	3	6578.8813	295.7616	2.3	1.0
	981.86	3	6577.1437	295.6835	1.8	1.3
	478.35	3	6576.3053	295.6458	0.5	–0.1
	384.51	3	6576.2875	295.6450	0.7	2.1
	290.01	3	6576.2900	295.6451	0.9	1.7
	240.94	3	6576.3123	295.6461	1.2	2.4
	190.30	3	6576.3248	295.6467	1.5	–0.1
	142.04	4	6576.3486	295.6478	2.8	–2.2
	99.41	4	6576.3953	295.6499	2.6	–1.4
	51.05	4	6576.4555	295.6526	1.7	–0.8
275.000	10228.27	2	7193.8695	323.5267	5.5	–0.6
	10139.11	2	7188.6921	323.2939	3.9	3.1
	10052.86	2	7183.8266	323.0751	4.5	(a)
	9973.23	2	7179.1051	322.8627	4.6	–0.7
	9956.25	2	7178.2538	322.8244	5.8	(a)
	7672.85	2	7062.6803	317.6268	4.1	–5.2
	7595.89	2	7059.3151	317.4755	4.1	–2.4
	7519.99	2	7055.9576	317.3245	3.9	(a)
	5116.67	3	6966.9913	313.3234	3.1	1.2
	5115.56	3	6966.9594	313.3220	2.2	1.6
	5028.52	3	6964.2993	313.2024	2.2	3.5
	4915.31	3	6960.8668	313.0480	2.5	2.0
	2587.43	3	6903.8408	310.4834	1.4	–1.3
	2494.38	3	6902.0683	310.4037	1.2	–1.4
	2404.69	3	6900.3997	310.3286	0.8	–0.8
	2403.98	3	6900.3702	310.3273	2.6	–3.1
	1439.06	3	6884.5216	309.6146	1.8	–1.1
	984.20	4	6878.3505	309.3370	3.1	–1.6
	484.89	4	6872.5224	309.0749	2.4	0.8
	484.18	4	6872.5273	309.0751	2.4	2.6
	392.09	4	6871.5628	309.0318	2.2	4.0

$\frac{T}{\mathrm{K}}$	$\frac{p}{\mathrm{kPa}}$	N	$\frac{u}{a}\cdot\mathrm{s}$	$\frac{u}{\mathrm{m}\cdot\mathrm{s}^{-1}}$	$\frac{10^6\sigma(u)}{u}$	$\frac{10^6\delta(u)}{u}$
275.000	296.42	4	6870.5672	308.9870	2.5	1.6
	245.65	4	6870.0636	308.9643	1.7	1.9
	198.68	4	6869.5793	308.9426	2.3	–1.8
	150.20	4	6869.1081	308.9214	2.4	–2.6
	101.27	4	6868.6425	308.9004	2.0	–3.2
	51.73	4	6868.2112	308.8810	0.8	0.7
300.030	9795.12	4	7510.7651	337.9108	2.7	–3.1
	9780.29	4	7510.0112	337.8769	2.7	3.1
	9776.95	4	7505.9382	337.6937	1.9	(a)
	7722.10	4	7407.8545	333.2809	1.7	–2.6
	7637.86	4	7404.0950	333.1117	2.1	3.7
	7633.63	4	7403.9656	333.1059	2.3	(a)
	7548.46	4	7400.0864	332.9314	2.3	3.6
	7543.55	4	7399.8064	332.9188	2.5	–4.7
	5121.21	3	7303.3406	328.5788	3.4	–0.3
	5026.25	3	7300.0034	328.4286	2.9	–2.6
	4933.68	3	7296.8377	328.2862	3.2	2.8
	2593.15	3	7226.2827	325.1119	3.3	–0.3
	2492.37	3	7223.6944	324.9955	3.5	0.5
	2395.20	3	7221.2268	324.8844	3.5	0.5
	1499.05	3	7200.0126	323.9300	2.3	–0.7
	1498.62	3	7200.0002	323.9295	2.1	–1.1
	990.32	3	7189.2147	323.4442	0.4	1.0
	489.38	3	7179.4252	323.0038	1.3	1.1
	391.48	3	7177.6001	322.9217	1.7	–0.3
	317.22	4	7176.2474	322.8608	2.7	0.1
	244.52	4	7174.9352	322.8018	2.3	–0.3
	171.75	4	7173.6391	322.7435	2.7	–0.7
	102.04	4	7172.4179	322.6885	1.9	–0.6
	53.08	4	7171.5800	322.6508	1.0	0.9
300.738	6757.54	3	7375.4137	331.8252	4.1	–3.4
	6757.31	3	7375.4174	331.8254	3.8	–1.6
	6757.12	3	7375.3960	331.8244	3.5	–3.4
	6749.71	3	7375.1239	331.8122	4.4	1.6
	6748.66	3	7375.0867	331.8105	4.1	2.5
	6742.81	3	7374.8286	331.7989	4.3	0.5
	6742.15	3	7374.8106	331.7981	5.2	1.8
	6738.22	3	7374.6507	331.7909	4.5	2.3
	6737.10	3	7374.5666	331.7871	4.8	–2.8
	6064.79	3	7347.5206	330.5703	5.3	1.9
	6060.79	3	7347.3626	330.5632	4.6	1.6
	5074.15	3	7310.8365	328.9198	4.8	2.7
	4524.00	3	7292.0518	328.0747	5.4	–1.3
	4013.86	3	7275.6862	327.3384	5.0	0.3
	3521.82	3	7260.7828	326.6679	5.1	–1.9
	3521.75	3	7260.7714	326.6674	4.6	–3.2
	3015.45	3	7246.3786	326.0198	4.5	–2.1
	2477.70	3	7232.1021	325.3775	4.8	0.4
	1972.37	3	7219.5840	324.8143	4.2	–0.8

$\frac{T}{\mathrm{K}}$	$\frac{p}{\mathrm{kPa}}$	N	$\frac{u}{a}\cdot\mathrm{s}$	$\frac{u}{\mathrm{m}\cdot\mathrm{s}^{-1}}$	$\frac{10^6\sigma(u)}{u}$	$\frac{10^6\delta(u)}{u}$
300.738	1971.44	3	7219.6075	324.8154	4.4	5.5
	1488.41	3	7208.4408	324.3130	3.0	1.3
	1007.98	3	7198.1473	323.8499	1.1	1.6
	790.08	3	7193.7172	323.6506	0.3	–0.1
	490.23	3	7187.8873	323.3883	1.4	–0.9
	415.82	3	7186.4742	323.3247	2.3	–2.7
	346.85	3	7185.2008	323.2674	2.6	–1.5
	276.28	3	7183.9082	323.2092	1.9	–1.0
	203.70	3	7182.5983	323.1503	2.2	–0.1
	128.63	3	7181.2588	323.0900	2.1	0.4
	78.08	3	7180.3784	323.0504	1.9	2.4
302.309	786.01	5	7212.4598	324.5018	2.3	0.1
	691.45	5	7210.5560	324.4162	2.3	–0.2
	596.27	5	7208.6661	324.3312	2.7	–0.6
	502.57	5	7206.8485	324.2494	2.8	1.1
	406.36	5	7204.9935	324.1659	2.7	0.5
	311.28	5	7203.1791	324.0843	2.4	–1.4
	155.43	5	7200.3014	323.9548	2.9	0.4
309.136	1912.40	4	7320.2540	329.3872	3.7	0.9
	1826.59	3	7318.0811	329.2894	4.5	0.7
	1826.46	3	7318.0647	329.2887	4.1	–1.1
	1735.80	4	7315.8134	329.1874	3.4	1.4
	1645.96	5	7313.5915	329.0874	3.6	1.7
	1554.10	5	7311.3211	328.9853	3.1	–1.3
	1462.88	5	7309.1184	328.8861	5.0	–0.8
	1372.47	5	7306.9553	328.7888	3.2	–1.0
	1278.40	5	7304.7305	328.6887	2.7	–1.3
	1183.73	5	7302.5171	328.5891	3.8	–1.9
	1090.48	5	7300.3666	328.4923	3.3	–2.2
	1089.39	5	7300.3525	328.4917	2.7	–0.7
	997.21	5	7298.2575	328.3974	2.6	–0.5
	902.63	5	7296.1308	328.3017	2.6	–0.8
	901.23	5	7296.1194	328.3012	2.5	1.9
	807.28	5	7294.0389	328.2076	2.4	2.1
	712.25	5	7291.9586	328.1140	2.7	1.8
	616.98	5	7289.9019	328.0215	2.4	1.5
	519.67	5	7287.8317	327.9283	2.6	1.5
	422.68	5	7285.7973	327.8368	2.6	1.3
	327.09	5	7283.8163	327.7476	2.8	0.5
	228.80	5	7281.8007	327.6569	2.7	–1.4
	130.80	4	7279.8222	327.5679	1.4	–3.2
	112.22	4	7279.4707	327.5521	1.8	–0.8
	84.54	4	7278.9297	327.5277	0.8	0.2
	55.23	4	7278.3567	327.5020	1.0	0.8
350.064	10176.68	2	8146.1173	366.8040	2.3	–3.6
	10091.43	2	8141.6654	366.6036	1.6	1.1
	9999.29	2	8136.8467	366.3866	4.3	2.6

$\frac{T}{\mathrm{K}}$	$\frac{p}{\mathrm{kPa}}$	N	$\frac{u}{a}\cdot\mathrm{s}$	$\frac{u}{\mathrm{m}\cdot\mathrm{s}^{-1}}$	$\frac{10^6\sigma(u)}{u}$	$\frac{10^6\delta(u)}{u}$
350.064	7638.22	2	8020.6837	361.1560	2.7	–1.3
	7549.73	2	8016.7288	360.9779	3.7	(a)
	7478.78	2	8013.3729	360.8268	3.6	0.6
	5082.80	3	7910.8412	356.2100	1.4	3.6
	4999.30	3	7907.4880	356.0590	3.0	–0.2
	4917.33	3	7904.2158	355.9117	3.0	–3.5
	2588.84	4	7818.7197	352.0619	3.1	–1.2
	2508.46	4	7816.0296	351.9408	2.1	2.7
	2425.80	4	7813.2222	351.8144	3.9	–0.6
	988.85	4	7767.5057	349.7559	2.4	–1.6
	477.90	4	7752.4905	349.0798	2.4	0.6
	234.30	4	7745.5522	348.7673	3.9	0.5
	105.16	4	7741.9220	348.6039	2.5	–1.1

(a), Pressure omitted from final analysis.

preliminary analysis of the results.

The fractional excess half–widths for the isotherm at 252 K are shown in figure 5.14. For all modes measured the excess half–widths are less than 25 ppm over the whole pressure range and below 1.5 MPa the average excess half–width is 6.5 ppm. Above 1.5 MPa the half–widths increase with pressure until a maximum is reached at 5 MPa. Beyond this pressure the excesses decrease slightly. The pressure dependence of the increase can be understood since, in the region of increase, corrections are dominated by shell motion. Although the exact expression of classical elasticity is used it cannot be expected to hold in a real resonator, which is not isotropic, and where additional loss mechanisms are possible. Noting that the acoustic resonance frequencies depend strongly on the temperature and pressure, and that the shell resonance frequencies depend only weakly on T and p through the elastic properties of the wall material, the behaviour of the (0,5) mode can be understood if we refer to figure 2.2b. From this it can be seen that a non–radial shell resonance occurs in the experimental frequency range of the (0,5) mode. If, during the course of the experiment, the frequency of the (0,5) mode passes through the frequency of the shell resonance then, due to higher–order coupling between the acoustic and shell resonances, we expect the excess half–width to increase and then decrease. This is the observed pattern and so

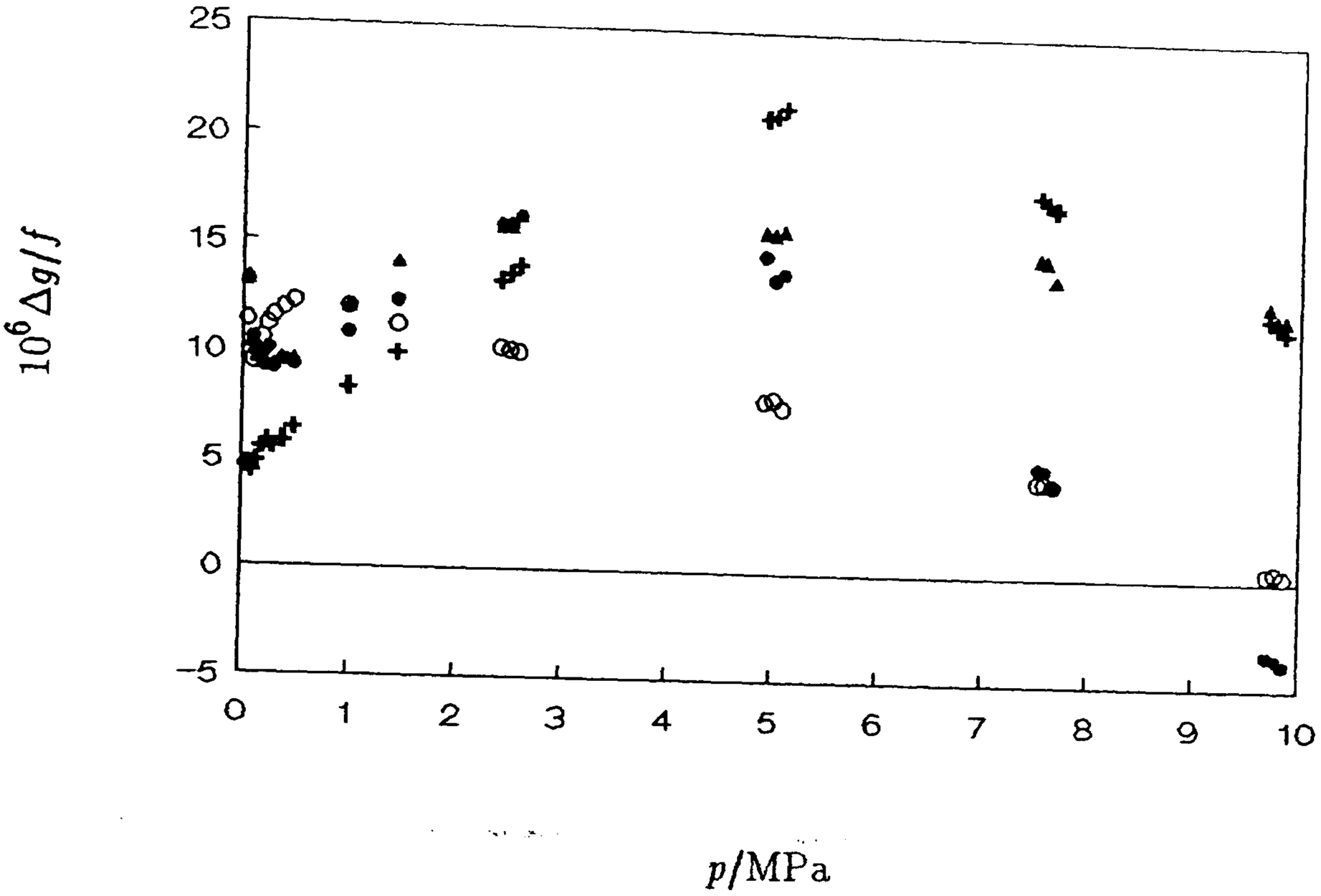

Figure 5.14: $\Delta g/f$ as a function of pressure for argon at 252 K.

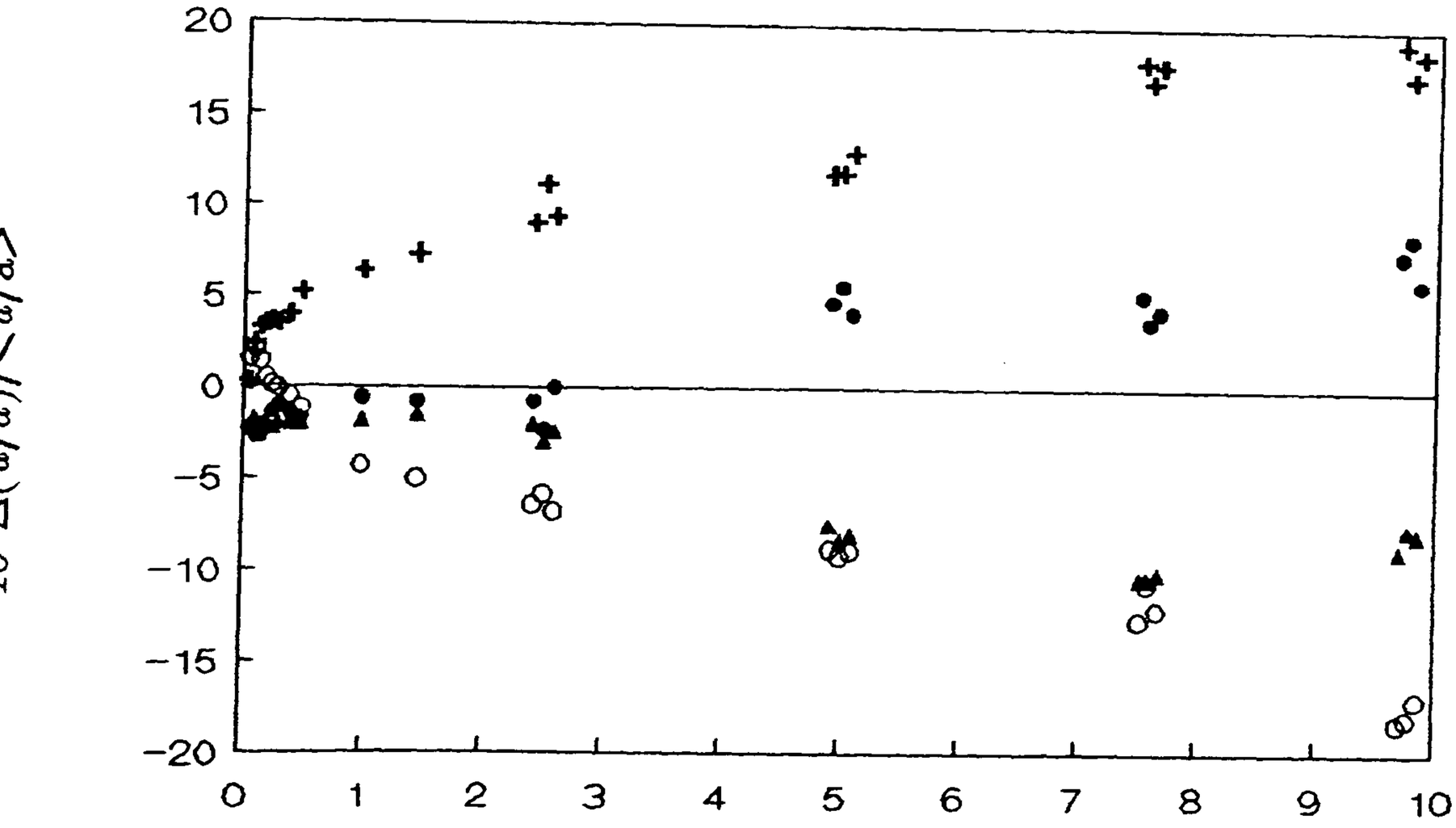

Figure 5.15: Fractional deviations of (u/a) for individual modes in argon at 252 K from $<u/a>$ of the modes finally selected.

• , (0,2); ▲ , (0,3); ∘ , (0,4); + , (0,5); ▽ , (0,6).

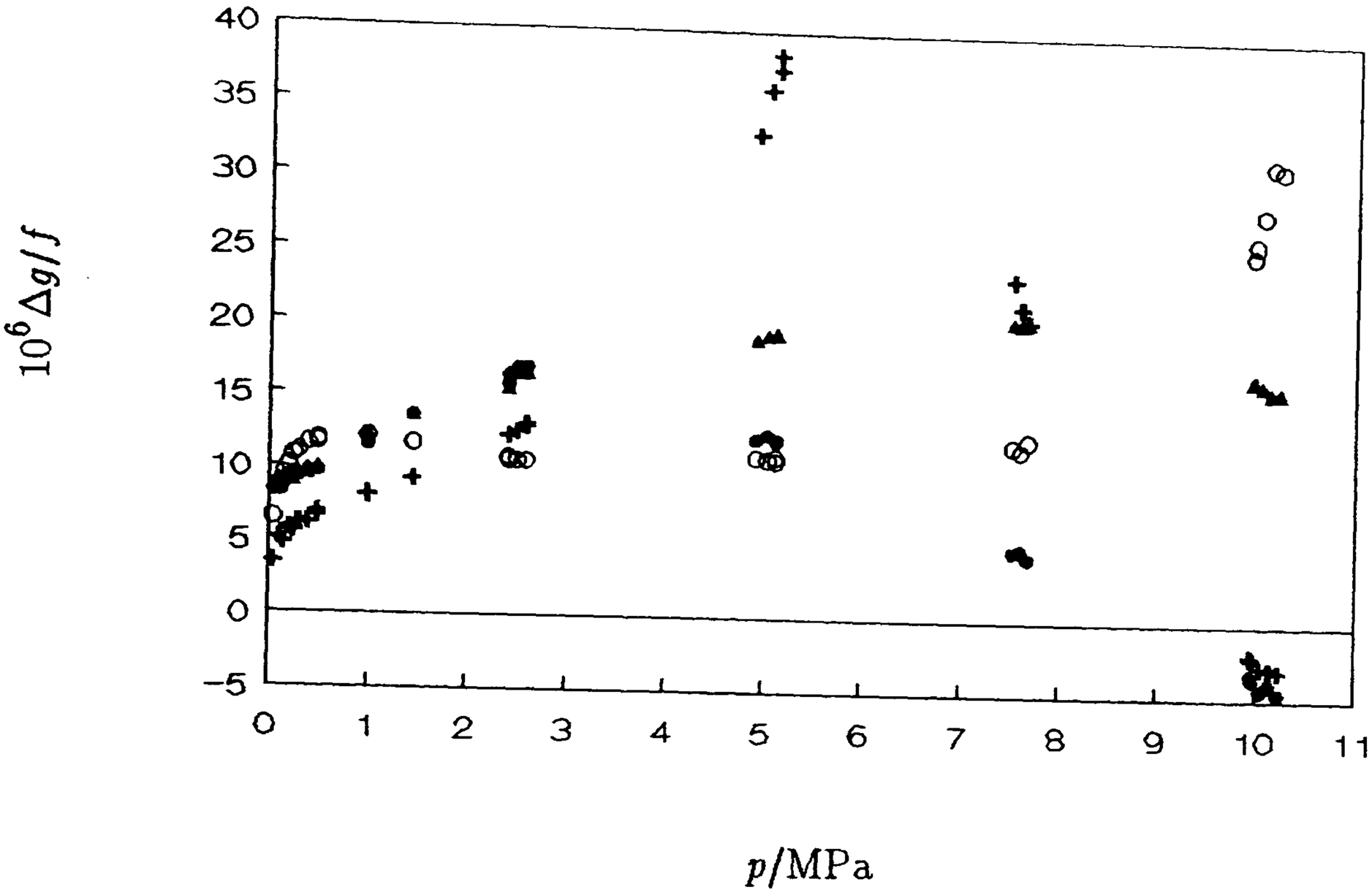

Figure 5.16: $\Delta g/f$ as a function of pressure for argon at 275 K.

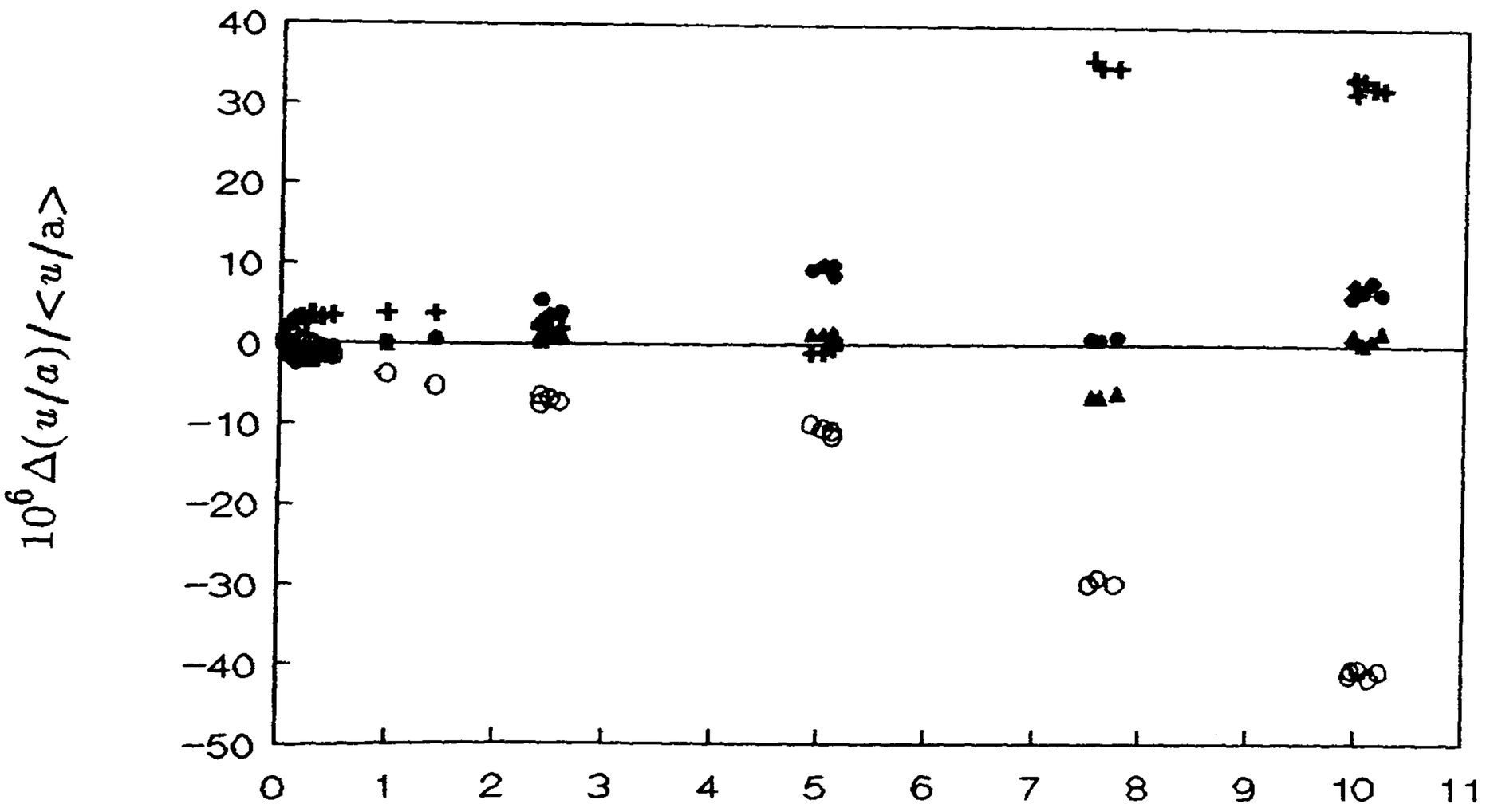

Figure 5.17: Fractional deviations of (u/a) for individual modes in argon at 275 K from $<u/a>$ of the modes finally selected.

• , (0,2); ▲ , (0,3); ∘ , (0,4); + , (0,5); ▽ , (0,6).

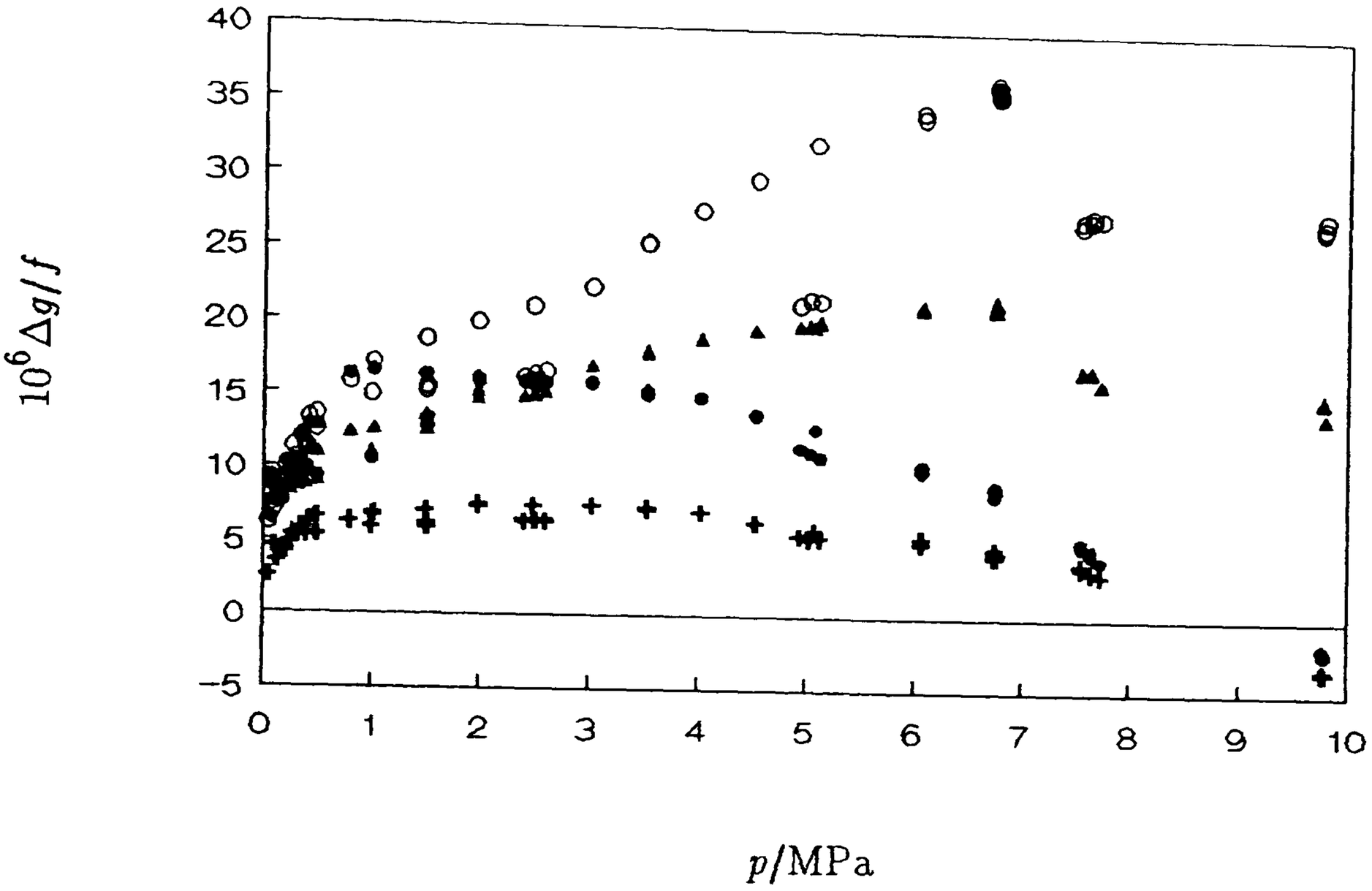

Figure 5.18: $\Delta g/f$ as a function of pressure for argon at 300 and 300.1 K.

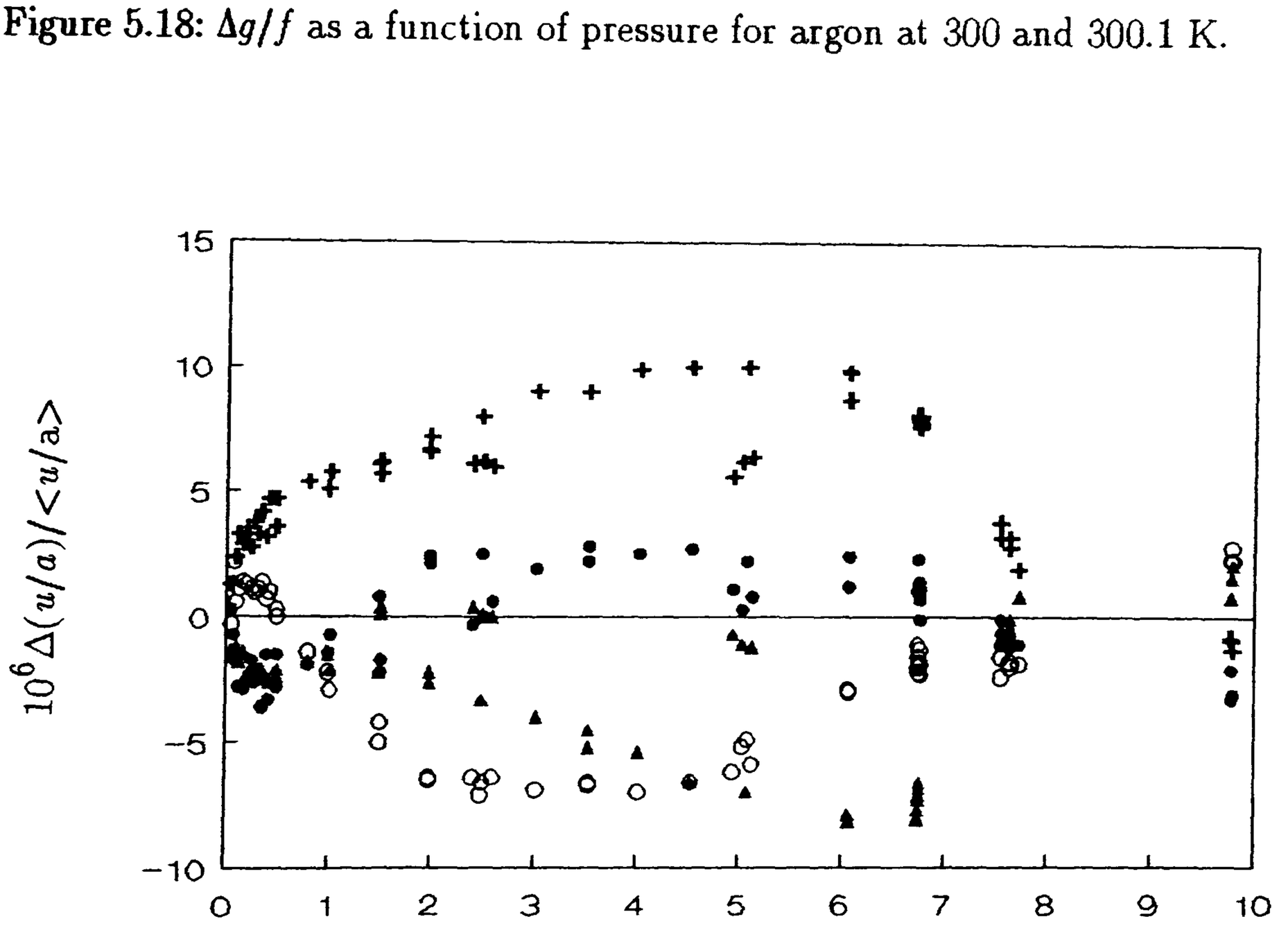

Figure 5.19: Fractional deviations of (u/a) for individual modes in argon at 300 and 300.1 K from $<u/a>$ of the modes finally selected.

• , (0,2); ▲ , (0,3); ∘ , (0,4); + , (0,5); ▽ , (0,6).

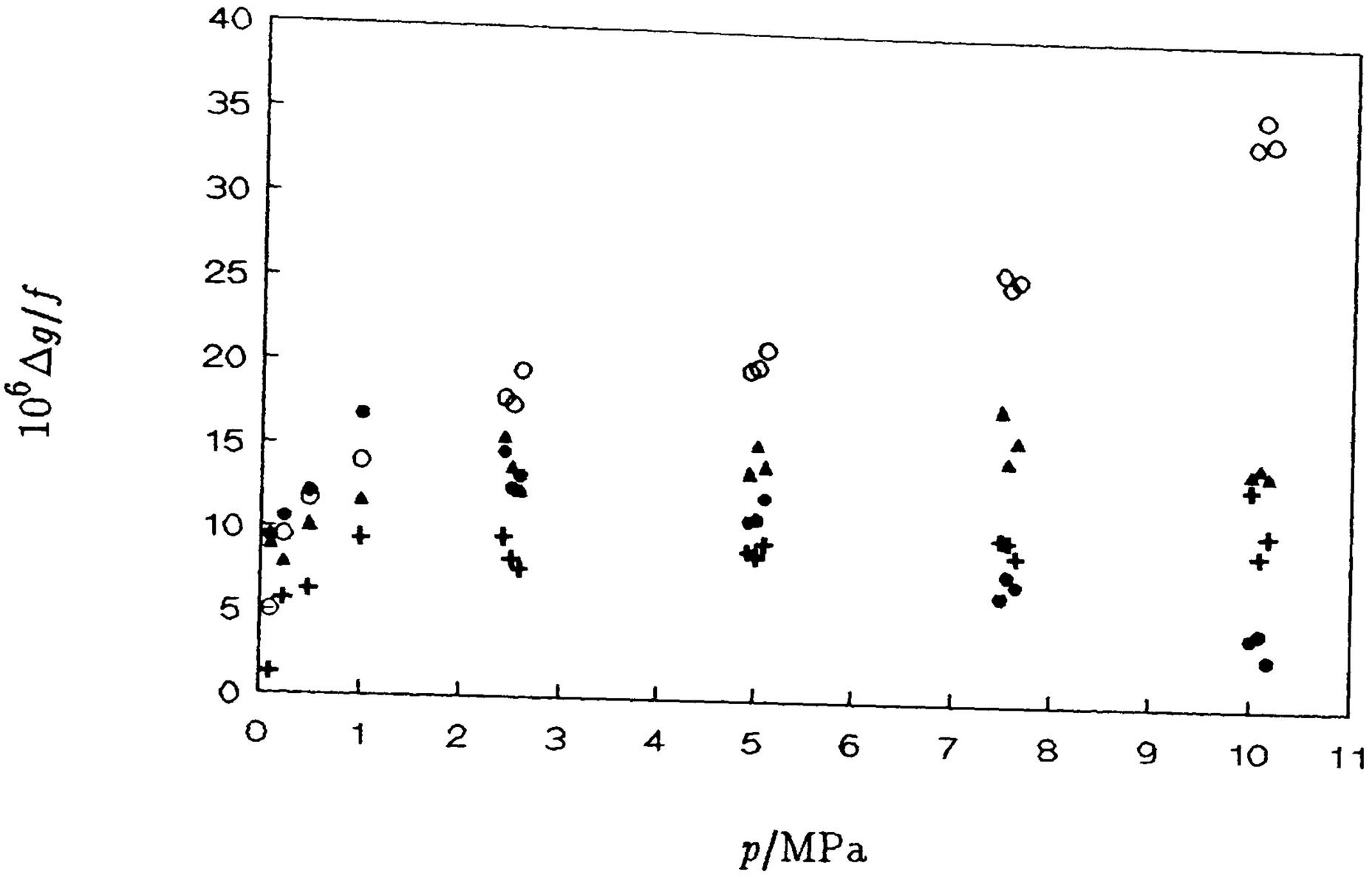

Figure 5.20: $\Delta g/f$ as a function of pressure for argon at 350 K.

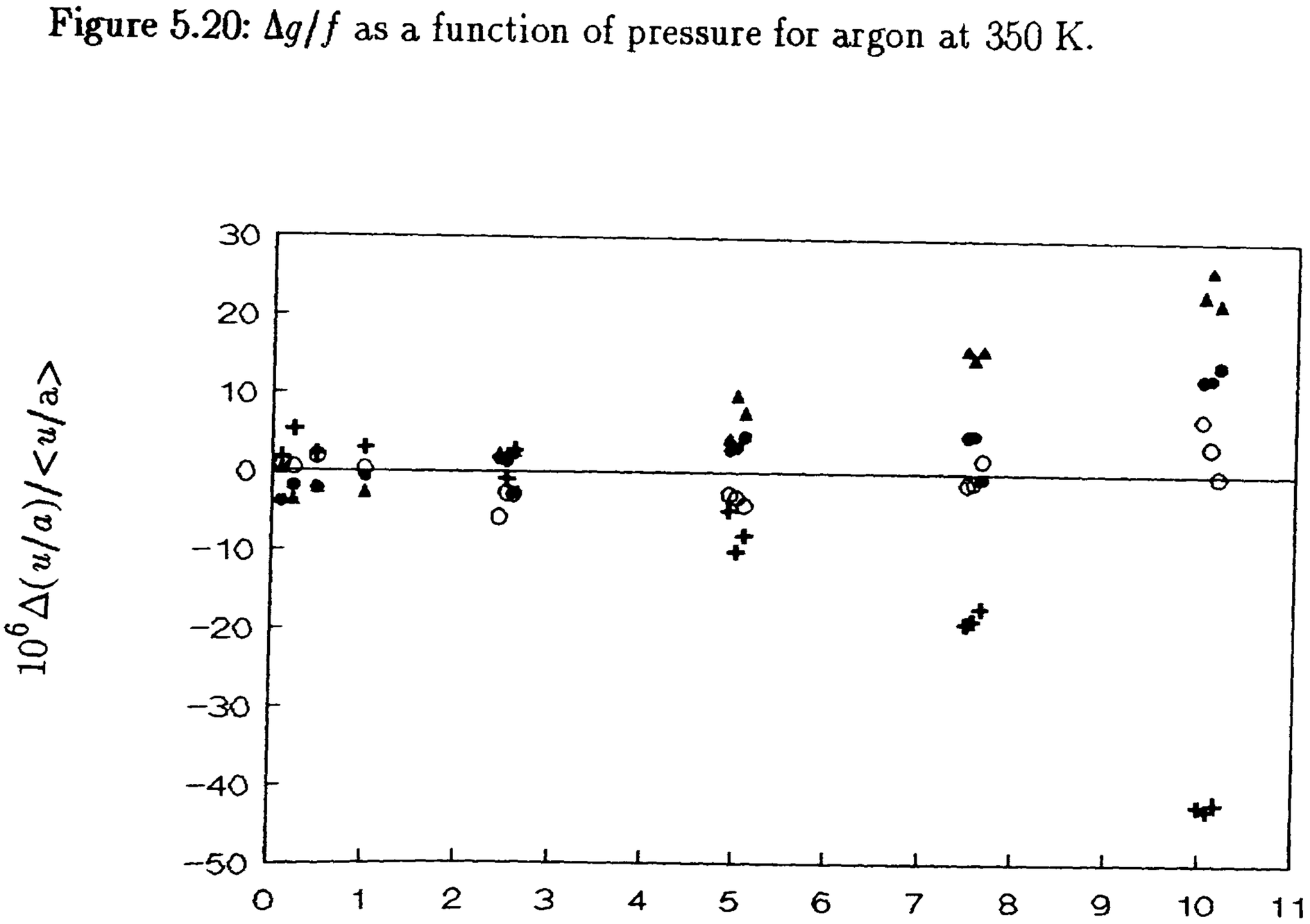

Figure 5.21: Fractional deviations of (u/a) for individual modes in argon at 350 K from $<u/a>$ of the finally selected modes.

• , (0,2); ▲ , (0,3); ∘ , (0,4); + , (0,5); ▽ , (0,6).

the explanation is valid. Deficiencies in the theory of shell motion for real resonators cannot explain the observed decrease in the excess half–widths for the other modes. No observed shell resonances should perturb them since they do not occur in the correct frequency ranges. An explanation for the (0,2) mode exists since there is a close lying non–radial acoustic resonance; the (3,1) mode. Measurements on the (0,2) and (3,1) modes do not show a significant overlap between them, but we can expect them to couple through the shell wall under conditions of high–pressure since the geometry is imperfect. If the geometry is pressure dependent, which may be the case (see Chapter 2), then the coupling between the (0,2) and (3,1) modes may vary and we can expect the (0,2) mode to have an unusual pressure dependent excess half–width. All things considered the excess half–widths are respectably small considering the large pressure range under study.

The quantity (u/a) determined from each mode is shown as deviations from the mean at a given pressure in figure 5.15. Over the whole pressure range the first four radial modes agree to better than 37 ppm. However, it is apparent that the (0,5) mode deviates systematically from the other modes. The deviation is very much density dependent and consistent with a perturbation arising from shell motion, as indicated above. Neglect of this mode in the analysis brings the level of agreement to better than 15 ppm across the whole pressure range. At pressures of 7.5 MPa and below the agreement is better than 7 ppm.

The observed $\Delta g/f$ at 275 K are shown in figure 5.16. The observed trends are much the same as those observed at 252 K with the exception of the sharp peak in the excess observed for the (0,5) mode and the rapid increase with pressure of the Δg for the (0,4) mode at the highest experimental pressure. The average excess half–width below pressures of 1.5 MPa is on the order of 5.5 ppm. The peak in the excess half–widths for the (0,5) mode can be explained if the acoustic mode passes through a minor shell resonance. As indicated above, a minor non–radial shell resonance occurs in the correct frequency range and through higher order coupling would produce the observed increase in the losses. The increase in the $\Delta g/f$ of the (0,4) mode is linear in pressure at the

highest experimental pressures. This is consistent with a perturbation due shell motion. From figure 2.2b it is not clear which shell resonance this might be but, at the highest pressures, coupling will be enhanced, and consequently coupling may be with an unobserved shell resonance or the shell resonance perturbing the (0,5) mode.

Deviations of (u/a) determined from a particular mode from the mean is shown in figure 5.17. As can be seen, the (0,4) and (0,5) modes are perturbed in a manner consistent with shell resonances. The (0,2) and (0,3) modes agree to better than 7 ppm across the whole pressure range. At pressures below 1 MPa agreement of the first four radial modes is on the order of 5 ppm.

The excess half–widths observed for the isotherms at temperatures near 300 K are considered together. The $\Delta g/f$ are shown in figure 5.18. With the exclusion of the (0,4) mode the excess half–widths are less than 20 ppm across the pressure range, and the two isotherms are consistent with each other and similar to those observed in the lower temperature isotherms. Below 1 MPa the average excess half–width is about 5.4 ppm. There is an inconsistency between the two isotherms for the (0,4) mode at pressures above 1 MPa. The density dependence of the excess half–widths is the same but the magnitudes are different. The density dependence is consistent with a perturbation due to shell motion. The difference in magnitude may be due to the fact that the temperatures are different and thus the frequencies in one isotherm consistently higher than in the other. This means that in the higher temperature isotherm the overlap with the shell resonance is greater and the losses correspondingly greater. This is observed experimentally and is consistent with the fact that at the lowest pressures the excesses tend towards the same value.

The individual (u/a) are shown as deviations from the mean in figure 5.19. With the exclusion of the (0,5) mode the agreement is better than 10 ppm across the whole pressure range for both isotherms. The (0,5) mode is consistently higher than the other modes for both isotherms and the deviation is density dependent. This is indicative of a perturbation due to shell motion where the acoustic mode is at a higher frequency than the shell resonance. An inconsistency with this explanation is that the

excess half–widths are never greater than 5 ppm. However, if the shell resonance is particularly sharp then the loss will not increase significantly until the acoustic and shell resonances are virtually coincident, and the perturbation will influence the frequencies more than the excess half–widths.

At 350 K, with the exclusion of the (0,4) mode, the $\Delta g/f$ are less than 20 ppm over the whole pressure range and similar to those observed for the other isotherms. This is shown in figure 5.20. At pressures below 0.5 MPa the average excess is about 6 ppm. The (0,4) mode shows a density dependent excess half–width which is consistent with a perturbation due to shell motion.

Deviations of the (u/a) from the mean are shown in figure 5.21. The (0,5) is severely perturbed by shell motion although the excess half–widths are never greater than 10 ppm. The (0,4) is also perturbed, as expected. Additional problems with temperature stability meant that the agreement between modes was worse than previously, but it was possible to have at least two, and in most cases three, modes agreeing to better than 10 ppm.

The additional isotherms at 303 and 310 K are at pressures below 2 MPa. Excess half–widths are on the order of 10 ppm for the first five radial modes over the whole range. In this pressure region the theory should hold extremely well, and although the excess half–widths are larger than expected they are still satisfyingly small.

Agreement of the individual (u/a) from the first five radial modes is on the order of 5 ppm for the isotherm at 303 K and less than 10 ppm for the one at 310 K.

The experimental (u/a) can be adequately represented by up to five terms in the infinite series (5.2.3). The results of the regression analyses are given in table 5.9 along with the number of modes N and the fractional standard deviation for an isotherm. All coefficients were statistically significant at a probability of 0.999. Individual modes were rejected on the basis of a statistically significant reduction in the standard deviation of the mean at a given state, and state points were rejected on the basis of a significant reduction in the standard deviation for the isotherm. The deviations of the selected mean speeds of sound at a given state from the adopted smoothing equation are

Table 5.9: Coefficients of equation (5.2.3) required to represent the measurements of (u/a) in argon at temperatures T with standard deviations σ.

T/K	i	$\{A_i/a^2\}$/s^{-2}·Pa^{-i}	T/K	i	$\{A_i/a^2\}$/s^{-2}·Pa^{-i}
251.990		$10^6\sigma(u^2)/u^2 = 6.6$	275.000		$10^6\sigma(u^2)/u^2 = 7.6$
	0	$(43.250744 \pm 0.000077)\cdot 10^6$		0	$(47.166025 \pm 0.000087)\cdot 10^6$
	1	-0.01932 ± 0.00019		1	0.12231 ± 0.00021
	2	$(0.27093 \pm 0.00094)\cdot 10^{-7}$		2	$(0.2548 \pm 0.0010)\cdot 10^{-7}$
	3	$(0.847 \pm 0.015)\cdot 10^{-15}$		3	$(0.575 \pm 0.017)\cdot 10^{-15}$
	4	$(0.1780 \pm 0.0080)\cdot 10^{-22}$		4	$(0.0529 \pm 0.0088)\cdot 10^{-22}$
300.030		$10^6\sigma(u^2)/u^2 = 5.6$	300.738		$10^6\sigma(u^2)/u^2 = 8.2$
	0	$(51.418427 \pm 0.000076)\cdot 10^6$		0	$(51.53797 \pm 0.00012)\cdot 10^6$
	1	0.24495 ± 0.00017		1	0.24940 ± 0.00021
	2	$(0.23806 \pm 0.00086)\cdot 10^{-7}$		2	$(0.23016 \pm 0.00077)\cdot 10^{-7}$
	3	$(0.284 \pm 0.014)\cdot 10^{-15}$		3	$(0.3979 \pm 0.0074)\cdot 10^{-15}$
	4	$(0.467 \pm 0.073)\cdot 10^{-23}$			
302.309		$10^6\sigma(u^2)/u^2 = 5.1$	309.136		$10^6\sigma(u^2)/u^2 = 6.3$
	0	$(51.80387 \pm 0.00024)\cdot 10^6$		0	$(52.958652 \pm 0.000083)\cdot 10^6$
	1	0.2565 ± 0.0011		1	0.28367 ± 0.00020
	2	$(0.227 \pm 0.012)\cdot 10^{-7}$		2	$(0.23206 \pm 0.00098)\cdot 10^{-7}$
350.064		$10^6\sigma(u^2)/u^2 = 9.6$			
	0	$(59.89250 \pm 0.00025)\cdot 10^6$			
	1	0.42650 ± 0.00046			
	2	$(0.2054 \pm 0.0021)\cdot 10^{-7}$			
	3	$(-0.137 \pm 0.033)\cdot 10^{-15}$			
	4	$(0.135 \pm 0.017)\cdot 10^{-22}$			

shown in figures 5.22, 5.23 and 5.24. The majority of the $<u/a>$ are within 5 ppm of the regression equation with a typical standard deviation for an isotherm being about 6 ppm. Since A_0 is known with sufficient accuracy for argon, values of the zero–pressure radius of the cavity were determined from the coefficient (A_0/a^2) determined in the regression analyses. Values so obtained are given in table 5.10.

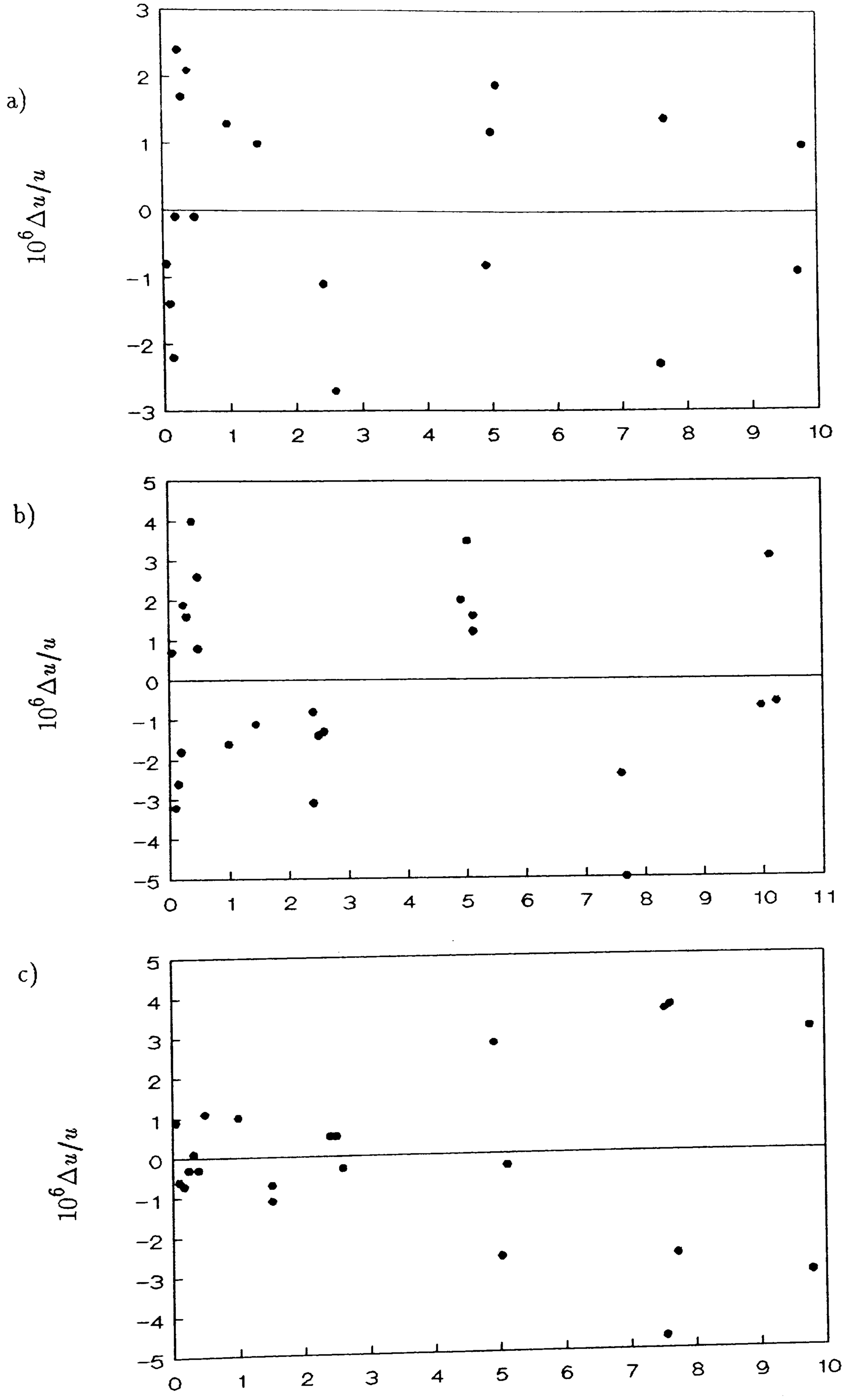

Figure 5.22: Fractional deviations of $<u/a>$ for the selected modes from the adopted smoothing equation; a) 252 K, b) 275 K and c) 300 K.

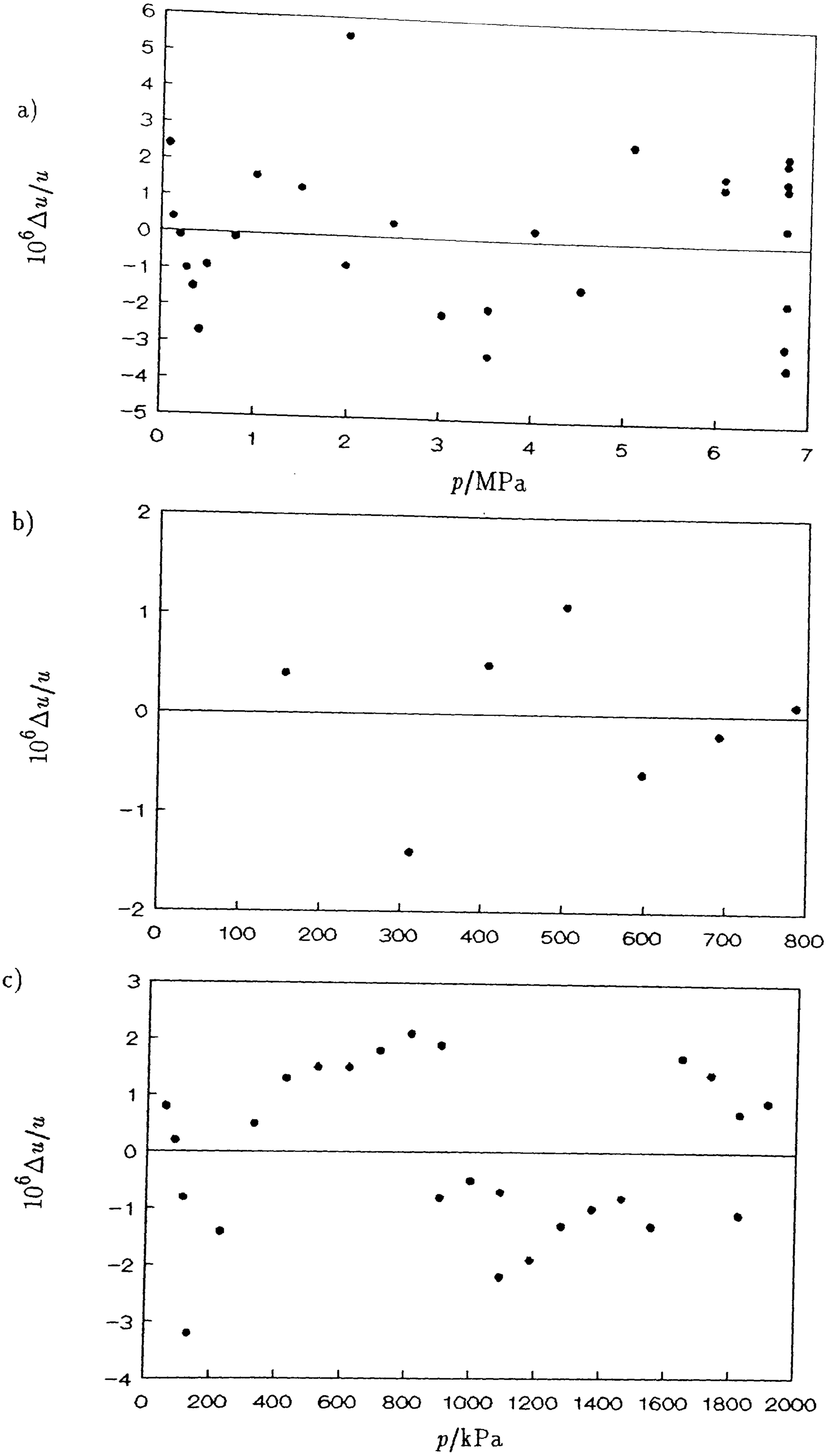

Figure 5.23: Fractional deviations of $<u/a>$ for the selected modes from the adopted smoothing equation; a) 301 K, b) 303 K and c) 310 K.

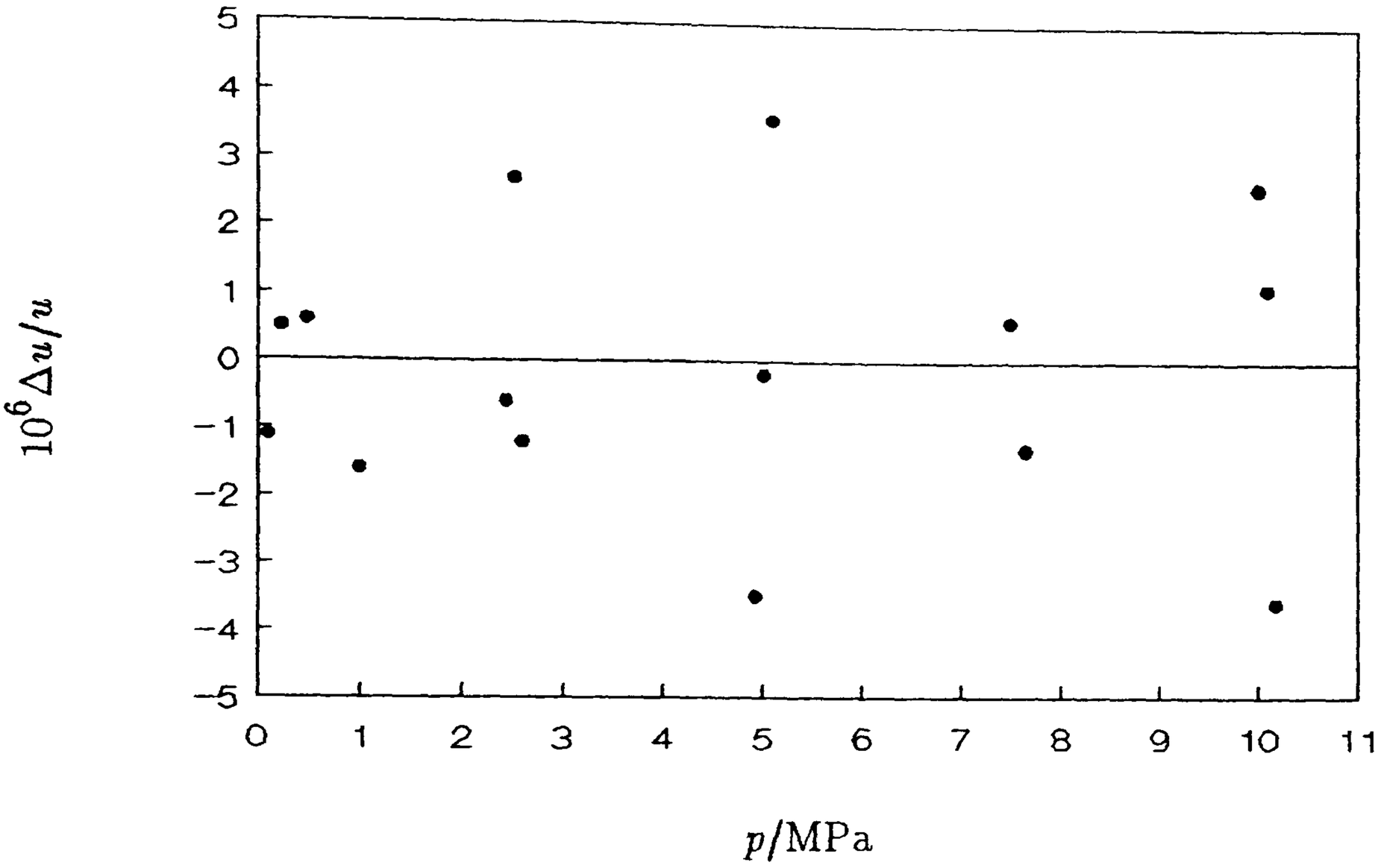

Figure 5.24: Fractional deviations of $<u/a>$ for the selected modes from the adopted smoothing equation at 350 K.

For purposes of short range extrapolation and interpolation the results were analysed using the adaptive regression algorithm. Weighted regression on the full set of results yielded

$$a(T,\ p{\to}0)/\mathrm{mm} = 44.97142 + 0.738 \times 10^{-3}(T/\mathrm{K} - 273.16) \qquad (5.4.1)$$

with a standard deviation of 0.80 μm.

For absolute measurements of the speed of sound, the variation of a with p is required. This was calculated using the $a(T,\ p{\to}0)$ given by equation (5.4.1) and literature values for the elastic properties of stainless steel[59].

Table 5.10: The zero–pressure radius of the resonator, a, and the second acoustic virial coefficient, β_a, of argon at temperatures T.

T/K	a/mm	β_a/cm$^3\cdot$mol^{-1}
251.989	44.95620 ± 0.00004	–0.936 ± 0.009
275.000	44.97258 ± 0.00003	5.972 ± 0.004
300.030	44.99026 ± 0.00004	11.885 ± 0.010
300.738	44.99098 ± 0.00005	12.100 ± 0.010
302.309	44.99242 ± 0.00010	12.448 ± 0.054
309.136	44.99886 ± 0.00003	13.768 ± 0.009
350.064	45.02808 ± 0.00007	20.746 ± 0.016

literature values for the elastic properties of stainless steel[59].

The second acoustic virial coefficients determined from the coefficients of table 5.9 are given in table 5.10. Comparison with previous experimental acoustic determinations[5,7,60–62] is afforded by fitting all results to equations derived from the square–well potential and a power series in T. Weighted linear regression of the results yielded

$$B/\text{cm}^3\cdot\text{mol}^{-1} = 157.29 - 122.581\exp(101.5\ \text{K}/T) \qquad (5.4.3)$$

for the square–well solution with a standard deviation of 0.15 cm$^3\cdot$mol^{-1}. As can be seen from the plot in figure 5.26 deviations from this solution are systematic and the square–well solution appears to have difficulties accommodating the data. This is particularly apparent at the highest temperatures where the deviation becomes as great as 0.75 cm$^3\cdot$mol^{-1}.

The alternative solution derived from a power series in T using the adaptive regression algorithm was

$$B/\text{cm}^3\cdot\text{mol}^{-1} = 31.368 - 9290(\text{K}/T) - 0.13166\times10^7(\text{K}/T)^2 - 0.1615\times10^{13}(\text{K}/T)^6 \qquad (5.4.4)$$

which fit the results with a standard deviation of 0.05 cm$^3\cdot$mol^{-1}. Deviations of the experimental quantities from this equation are shown in figure 5.27. Clearly this is a much better fit and, with the exclusion of the results of reference 7 which show a

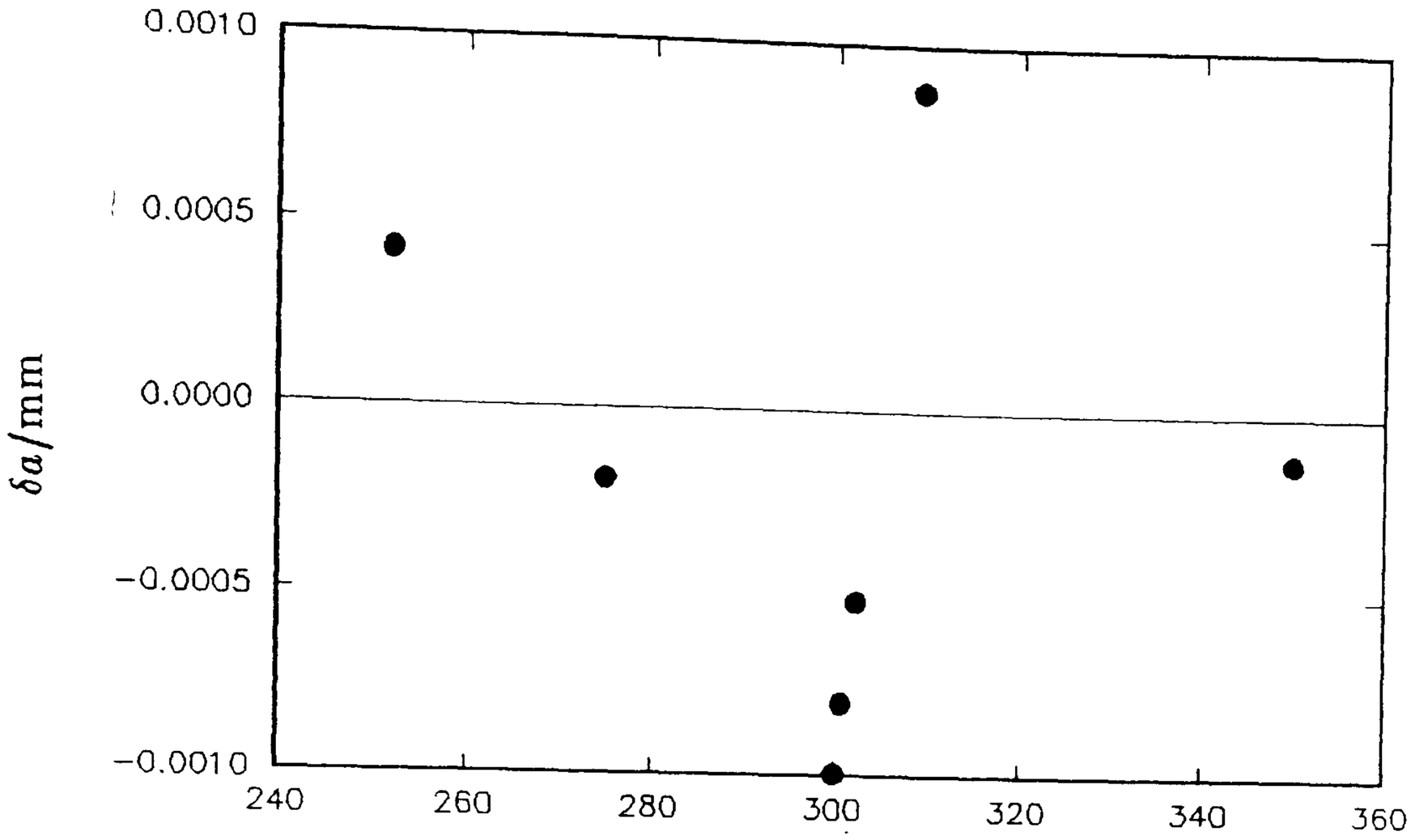

Figure 5.25: Deviations $\delta a = \{a(\text{exp.}) - a(\text{calc.})\}$ of the experimentally determined radii for the high–pressure cavity from equation (5.4.1).

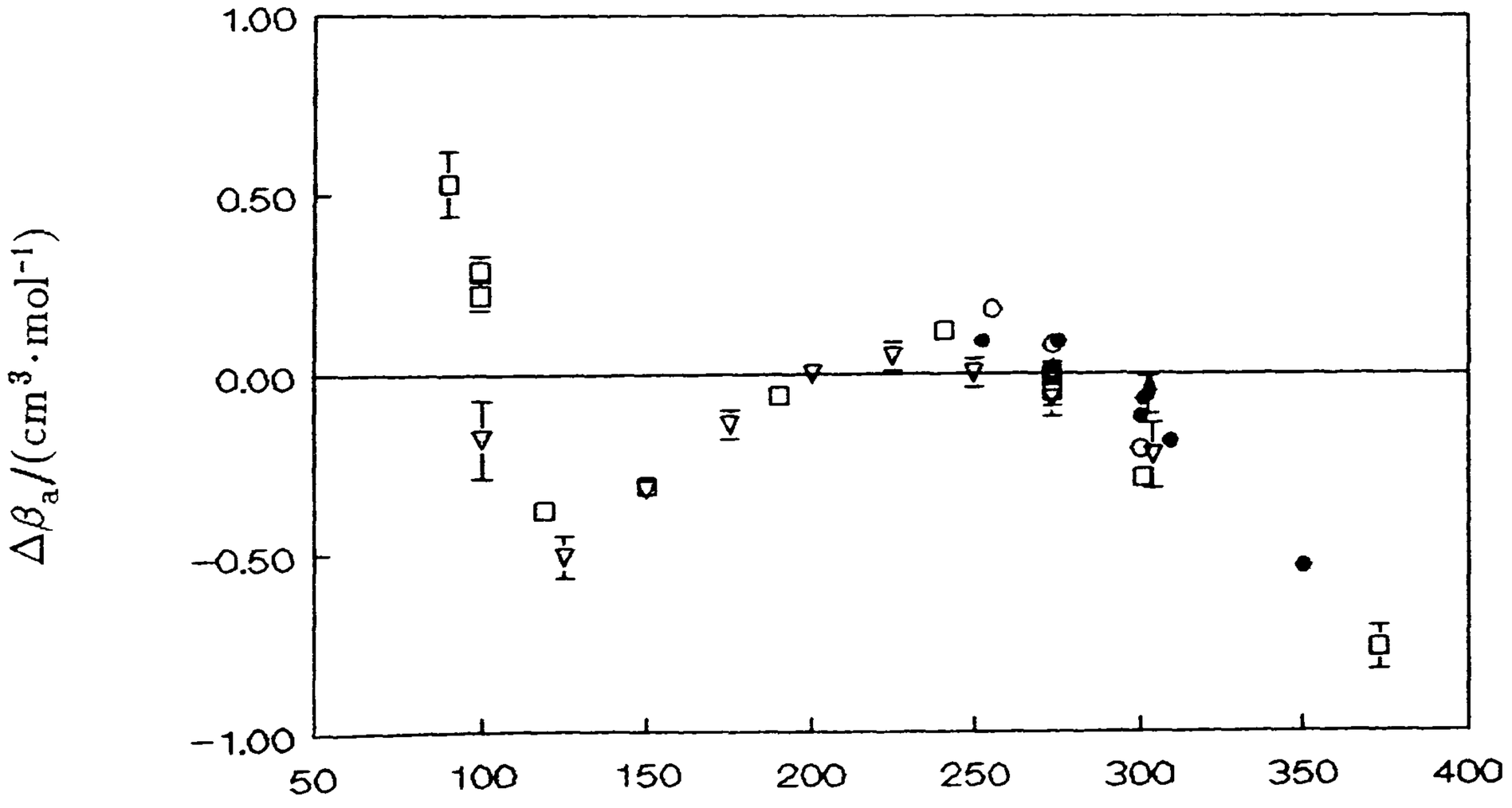

Figure 5.26: Deviations $\Delta\beta_a = \{\beta_a(\text{exp.}) - \beta_a(\text{calc.})\}$ of experimental β_a from equation (5.4.3) and (3.2.15). • , this work, ∘ , reference 5; ▽ , reference 7; ▲ , reference 60 and 61; □ , reference 62.

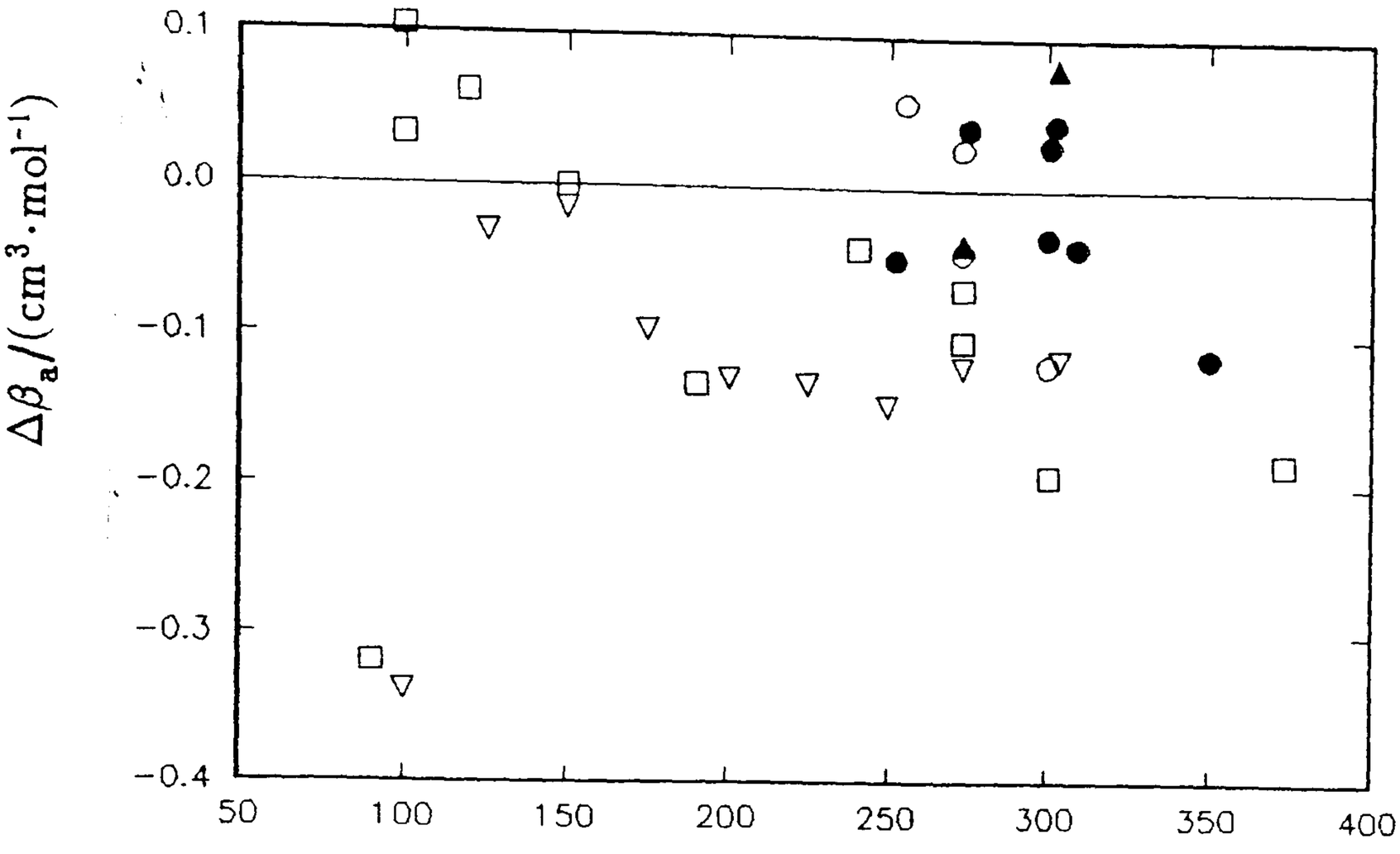

Figure 5.27: Deviations $\Delta\beta_a = \{\beta_a(\text{exp.}) - \beta_a(\text{calc.})\}$ of experimental β_a from equation (5.4.4) and (3.2.15). • , this work, ∘ , reference 5; ∇ , reference 7; ▲ , reference 60 and 61; □ , reference 62.

---

systematic deviation from the equation, the results are very much randomly distributed. This is unexpected since one generally expects the power series solution to be inferior to the square–well solution. However, since the temperature range is extremely large a compromise in the accommodation of data at one end of the temperature range may be expected using the square–well solution. Accommodation of data at both ends of the temperature range can be effected using the power series solution by inclusion of terms of high–order in T. At temperatures near the triple–point of water the results are extremely consistent, the span of the results being no more than 0.15 $cm^3 \cdot mol^{-1}$.

An equation has also been determined which represents the acoustic virial coefficient in argon as a function of temperature. This has been included since this quantity is very important in acoustic measurements and an equation enabling precise and simple estimation of β_a is of value. It is possible to determine the acoustic virial

coefficient from equation (5.4.4) in combination with (3.2.15) but this is not so straight forward. The best representation of the acoustic virial coefficients was found to be

$$\beta_a/(\mathrm{cm}^3\cdot\mathrm{mol}^{-1}) = 92.684 - 0.0352(T/\mathrm{K}) - 20386(\mathrm{K}/T) - 0.6108 \times 10^8(\mathrm{K}/T)^3 - 0.4245 \times 10^{13}(\mathrm{K}/T)^6 \quad (5.4.5)$$

which fit the results to 0.05 $\mathrm{cm}^3\cdot\mathrm{mol}^{-1}$.

5.4.5: Nitrogen.

Nitrogen has been studied along six isotherms between 250 and 325 K at pressures up to 7 MPa. Experimentally determined frequencies were corrected as outlined in Chapter 2. Thermophysical properties required in the various correction terms were obtained from the literature[55,57,63]; the thermodynamic properties required were calculated correct to the second virial coefficient which was itself obtained from a preliminary analysis of the results. In table 5.11 we list the mean quantity (u/a) and u, measured along the seven isotherms, determined from N modes together with the standard deviation of the mean at a given state and the deviation of the mean from the equation of best fit. Small corrections have been applied to reduce all values of (u/a) to the stated temperature of each isotherm.

At pressures above 1.5 MPa the dominant correction was that due to shell motion which varied from 133 ppm for the (0,5) mode at 325 K and 7 MPa to 23 ppm for the (0,2) mode at 250 K and 1.5 MPa. The (0,6) mode, which would normally be measured, was not always recorded along the high–pressure isotherms for reasons mentioned previously. Below 1.5 MPa corrections were dominated by the thermal boundary layer. The thermal accommodation coefficient was taken as unity as determined previously.

Analysis of the excess line–widths using equation XXX and the adaptive regression algorithm indicated that the term in $\Delta g/f$ for all modes was the most significant term. The term in $\tau\rho$ was insignificant. Although nitrogen should display

Table 5.11: Mean values of (u/a) and u with standard deviations σ determined from N modes, and deviations δ from equation (5.2.3) at temperatures T and pressures p. The coefficients of equation (5.2.3) are given in table 5.12.

$\frac{T}{\mathrm{K}}$	$\frac{p}{\mathrm{kPa}}$	N	$\frac{u}{a}\cdot\mathrm{s}$	$\frac{u}{\mathrm{m}\cdot\mathrm{s}^{-1}}$	$\frac{10^6\sigma(u)}{u}$	$\frac{10^6\delta(u)}{u}$
250.064	6476.73	2	7406.7984	332.9715	2.8	–3.3
	6041.56	2	7379.4850	331.7436	2.0	2.7
	5617.17	2	7354.4847	330.6198	2.4	2.0
	5040.47	2	7323.1397	329.2106	2.8	0.0
	4542.35	2	7298.4974	328.1029	2.6	1.2
	3987.92	2	7273.6292	326.9849	2.7	–0.7
	3538.31	2	7255.4457	326.1675	3.1	0.1
	3003.31	3	7236.0264	325.2945	5.3	–3.5
	2446.40	3	7218.4103	324.5026	5.2	–0.1
	1929.61	3	7204.3173	323.8690	5.4	0.7
	1927.71	3	7204.2608	323.8665	5.9	–0.5
	1454.54	3	7193.2975	323.3736	4.7	(a)
	1003.24	3	7184.3775	322.9726	3.0	4.0
	785.51	3	7180.6367	322.8044	2.2	2.5
	606.01	3	7177.8031	322.6771	1.1	–1.3
	399.60	3	7174.8754	322.5454	0.1	–1.1
	192.70	2	7172.2334	322.4267	5.3	–4.0
	192.48	2	7172.2320	322.4266	1.0	–3.9
	100.77	3	7171.1892	322.3797	0.4	–1.3
	50.96	3	7170.6658	322.3562	0.9	2.6
273.160	6602.55	3	7784.2896	350.0692	2.5	–0.4
	6012.14	3	7746.2143	348.3569	2.1	0.7
	5999.47	3	7745.4122	348.3208	2.1	–0.7
	5562.90	3	7718.8245	347.1251	2.3	1.0
	5015.56	3	7687.2979	345.7073	2.5	0.3
	4529.07	3	7660.9900	344.5242	3.1	0.6
	3989.92	3	7633.6942	343.2967	2.9	–0.4
	3542.70	3	7612.5404	342.3454	2.6	–0.9
	3539.55	3	7612.3883	342.3385	2.9	–1.9
	3006.05	3	7588.9194	341.2831	2.8	–1.6
	2453.36	3	7566.6246	340.2805	3.5	2.9
	1947.75	3	7547.9412	339.4403	3.4	2.2
	1466.15	3	7531.6743	338.7087	2.8	1.1
	1008.24	3	7517.5645	338.0742	1.8	–1.1
	795.63	3	7511.4684	337.8000	1.5	–0.9
	608.11	3	7506.3196	337.5685	1.0	–1.3
	418.61	3	7501.3351	337.3443	0.9	–1.7
	196.96	3	7495.7943	337.0952	1.3	–0.6
	100.38	3	7493.4758	336.9909	1.7	0.3
	48.33	3	7492.2626	336.9363	0.7	2.5
295.504	1911.97	4	7859.4504	353.5733	2.6	1.1

$\frac{T}{\mathrm{K}}$	$\frac{p}{\mathrm{kPa}}$	N	$\frac{u}{a}\cdot\mathrm{s}$	$\frac{u}{\mathrm{m\cdot s^{-1}}}$	$\frac{10^6\sigma(u)}{u}$	$\frac{10^6\delta(u)}{u}$
295.504	1732.54	4	7851.9809	353.2372	1.4	–0.5
	1547.52	4	7844.4618	352.8990	0.6	–1.0
	1364.72	4	7837.2103	352.5727	0.4	–1.1
	1364.10	4	7837.1972	352.5721	1.2	0.4
	1178.26	4	7830.0044	352.2486	1.0	0.5
	1178.01	4	7829.9963	352.2482	1.1	0.6
	990.24	5	7822.9022	351.9291	2.3	–0.5
	796.68	5	7815.7963	351.6094	1.6	0.2
	602.51	5	7808.8619	351.2974	1.8	0.5
	409.90	5	7802.1762	350.9967	2.1	0.5
	215.89	5	7795.6330	350.7023	2.8	–0.4
	117.57	5	7792.3996	350.5568	2.9	0.1
	58.51	5	7790.4765	350.4703	2.9	–0.3
297.277	5176.63	4	8050.6888	362.1825	4.8	–0.3
	4795.30	3	8028.3328	361.1768	2.3	0.3
	4406.11	3	8006.2932	360.1853	2.2	0.3
	4009.52	3	7984.6459	359.2114	2.0	0.1
	3605.21	3	7963.4318	358.2570	1.9	0.9
	3145.68	4	7940.3357	357.2180	3.2	–1.1
	3144.18	4	7940.2730	357.2152	3.4	0.3
	2762.63	4	7921.9435	356.3906	2.8	–0.9
	2326.84	4	7901.9580	355.4915	2.5	0.0
	1909.91	4	7883.7683	354.6732	2.6	0.8
	1544.82	4	7868.5727	353.9895	3.7	–0.3
	990.39	5	7846.8597	353.0127	3.1	1.7
	502.58	5	7829.0536	352.2117	1.9	–0.4
	357.73	5	7824.0168	351.9851	2.1	0.4
	357.43	5	7823.9887	351.9838	2.3	–1.8
	261.46	5	7820.7147	351.8365	2.3	–0.9
	164.09	5	7817.4348	351.6890	2.7	–0.9
	114.04	5	7815.7688	351.6140	2.8	–0.8
	55.81	5	7813.8756	351.5288	2.2	3.0
302.924	6639.47	2	8223.4654	369.9924	1.9	(a)
	6016.19	2	8182.4324	368.1462	2.4	–1.4
	5583.44	2	8155.0184	366.9128	1.7	2.0
	5575.10	2	8154.4643	366.8879	1.8	–2.3
	5031.85	2	8121.4341	365.4017	3.3	5.5
	4519.38	3	8091.5273	364.0562	3.3	–0.2
	3996.42	3	8062.4169	362.7464	2.8	0.0
	3544.23	3	8038.3328	361.6628	2.7	–1.9
	3539.12	3	8011.0420	361.6497	2.6	–5.0
	3007.01	3	8011.0861	360.4369	3.1	0.5
	2452.94	4	7984.4969	359.2406	4.1	3.5
	1934.18	4	7960.9464	358.1810	3.8	1.6
	1461.82	4	7940.6583	357.2682	3.3	–0.5
	1001.40	4	7921.9557	356.4268	3.0	–0.9
	790.10	4	7913.5792	356.0499	2.9	(a)
	602.30	4	7906.5978	355.7358	2.4	0.3
	415.80	4	7899.6701	355.4241	2.4	–1.4

$\frac{T}{\mathrm{K}}$	$\frac{p}{\mathrm{kPa}}$	N	$\frac{u}{a}\cdot\mathrm{s}$	$\frac{u}{\mathrm{m}\cdot\mathrm{s}^{-1}}$	$\frac{10^6\sigma(u)}{u}$	$\frac{10^6\delta(u)}{u}$
302.924	189.90	4	7891.4962	355.0563	2.9	–4.8
	100.03	4	7888.3701	354.9157	1.9	1.1
	99.75	4	7888.3565	354.9151	2.1	0.6
	49.61	4	7886.6273	354.8373	1.6	3.6
324.608	6025.11	3	8478.8512	381.6190	0.8	(a)
	5602.81	3	8451.9695	380.4091	2.0	2.5
	4982.06	3	8413.2877	378.6681	3.5	–0.4
	4555.46	3	8387.5728	377.5107	0.4	–3.7
	3999.56	3	8355.2211	376.0546	1.6	0.5
	3510.65	3	8327.7794	374.8195	2.2	2.3
	3011.01	4	8300.6451	373.5983	3.1	–7.1
	2439.99	4	8271.0466	372.2661	2.5	1.2
	2414.61	4	8269.7090	372.2059	3.2	–4.8
	1920.70	4	8245.2813	371.1064	1.4	6.2
	1454.92	4	8223.0883	370.1076	2.1	5.6
	1005.49	4	8202.5325	369.1824	2.4	3.7
	788.52	4	8192.9090	368.7492	2.1	2.1
	610.24	4	8185.1276	368.3990	2.9	–2.3
	402.83	4	8176.2629	368.0000	2.9	–5.3
	185.45	4	8167.1931	367.5918	2.7	–5.7
	102.39	4	8163.8175	367.4399	1.7	–1.4
	51.62	4	8161.8064	367.3494	1.2	5.9

(a), Pressure removed from final analysis.

vibrational relaxation no speed dispersion is observed and the excess line–widths are on the same order as those observed in argon.

At 250 K the excess half–widths are shown in figure 5.28 and less than 40 ppm across the whole range for the first four radial modes. The (0,4) mode is perturbed in a manner consistent with shell motion. A non–radial shell resonance is in the correct frequency range and we can expect this to couple with the acoustic mode and increase the losses. Exclusion of this mode brings the $\Delta g/f$ to less than 20 ppm across the whole range. At pressures below 1 MPa the average $\Delta g/f$ for the modes is on the order of 10 ppm.

Deviations of the individual (u/a) from the mean are shown in figure 5.29. The (0,4) mode shows a deviation consistent with a perturbation arising from shell motion. Exclusion of this mode brings the agreement of the remaining modes on the order of 20 ppm across the whole range. The (0,5) mode also appears to be perturbed by shell

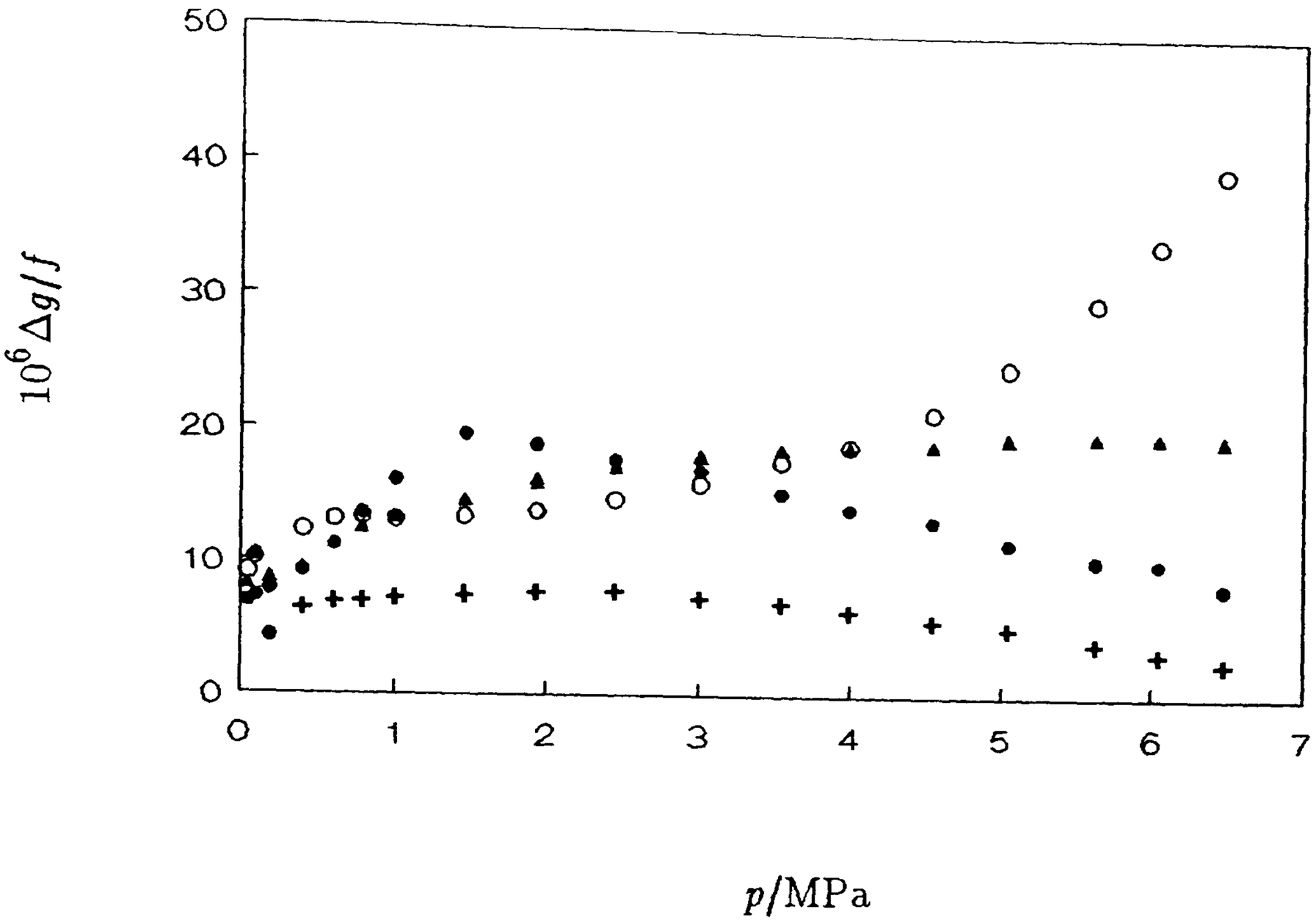

Figure 5.28: $\Delta g/f$ as a function of pressure for nitrogen at 250 K.

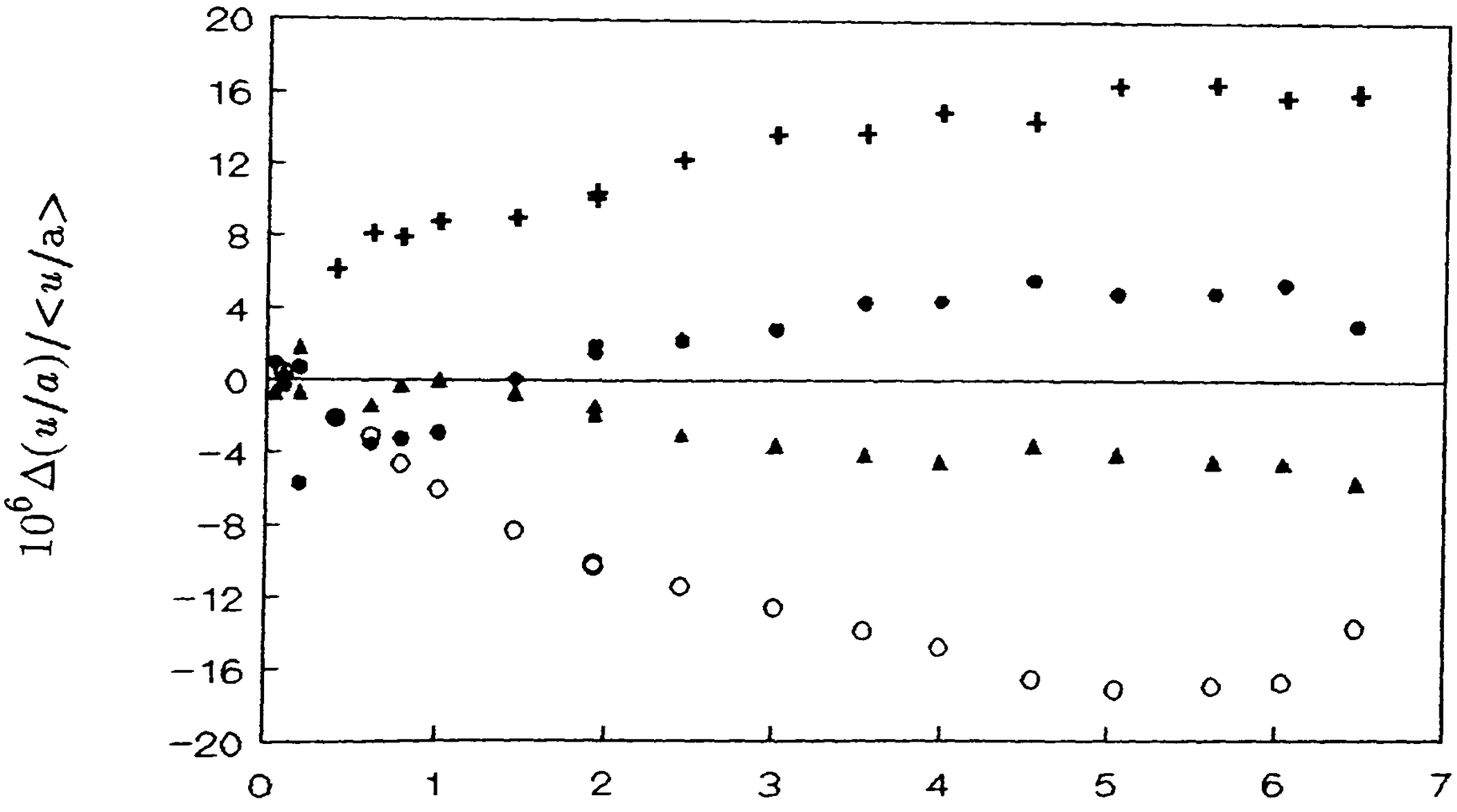

Figure 5.29: Fractional deviations of (u/a) for individual modes in nitrogen at 250 K from $<u/a>$ of the finally selected modes.

• , (0,2); ▲ , (0,3); ∘ , (0,4); + , (0,5); ▽ , (0,6).

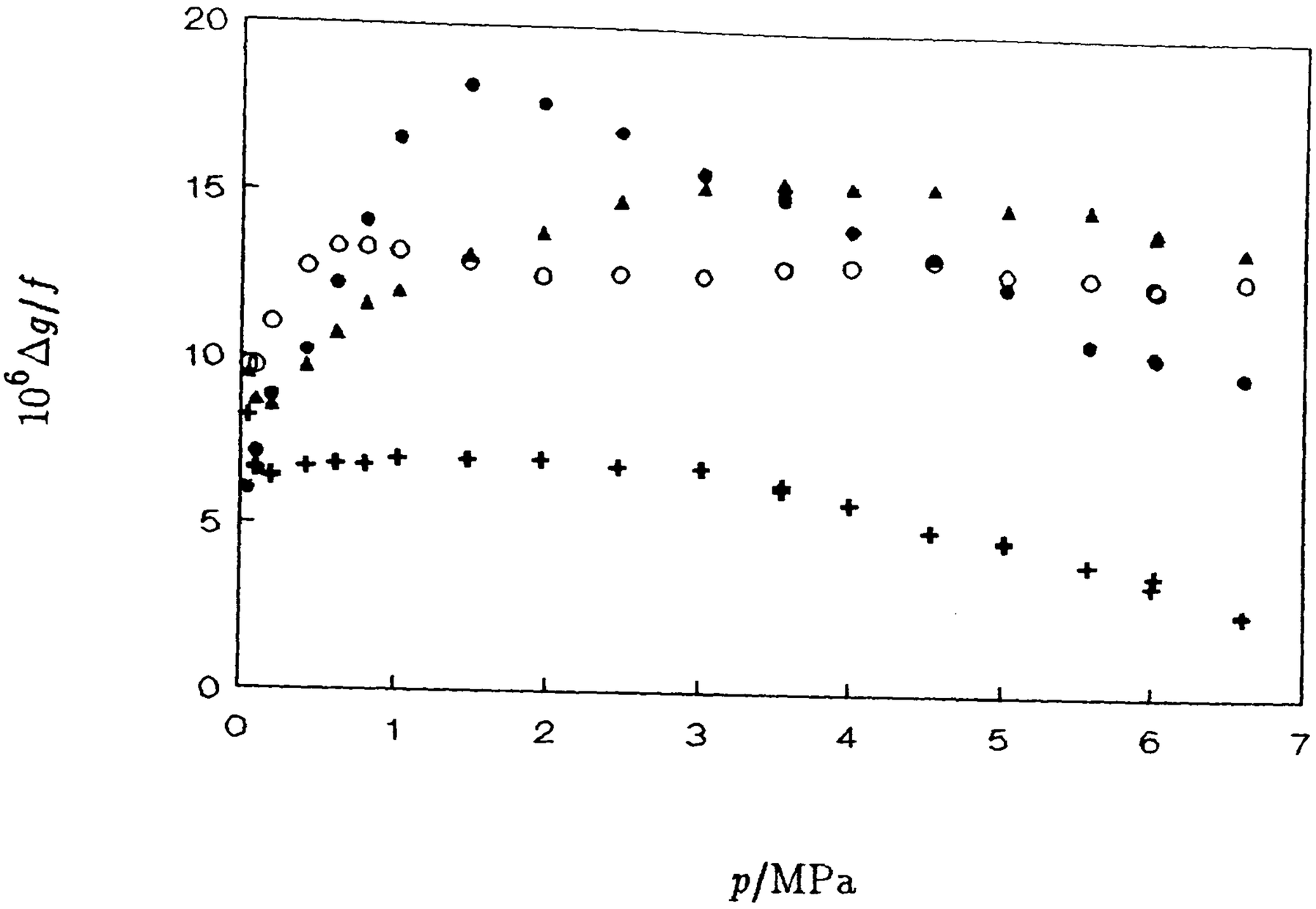

Figure 5.30: $\Delta g/f$ as a function of pressure for nitrogen at 273.16 K.

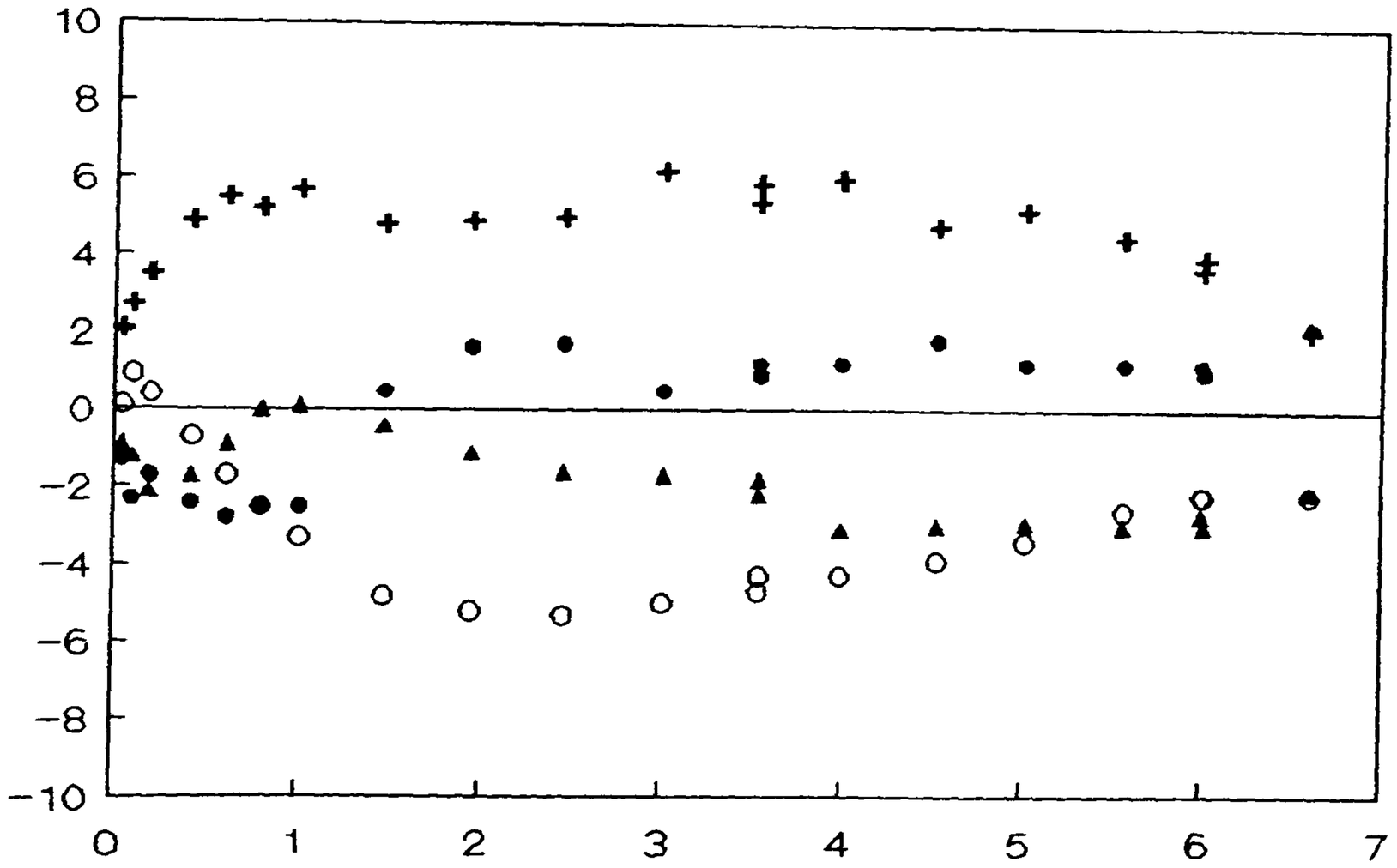

Figure 5.31: Fractional deviations of (u/a) for individual modes in nitrogen at 273.16 K from $<u/a>$ of the finally selected modes.

• , (0,2); ▲ , (0,3); ∘ , (0,4); + , (0,5); ∇ , (0,6).

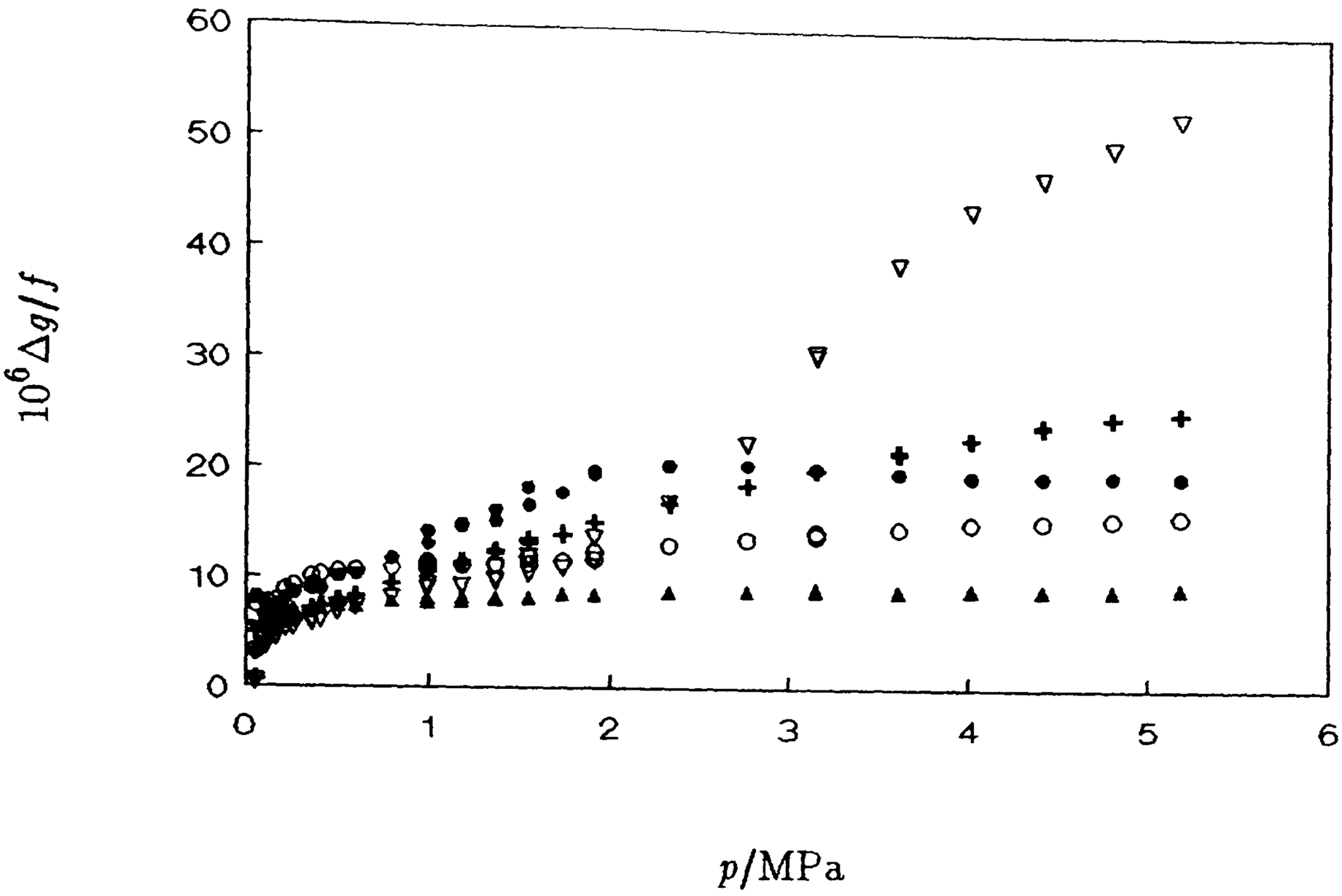

Figure 5.32: $\Delta g/f$ as a function of pressure in nitrogen at 295 and 297 K.

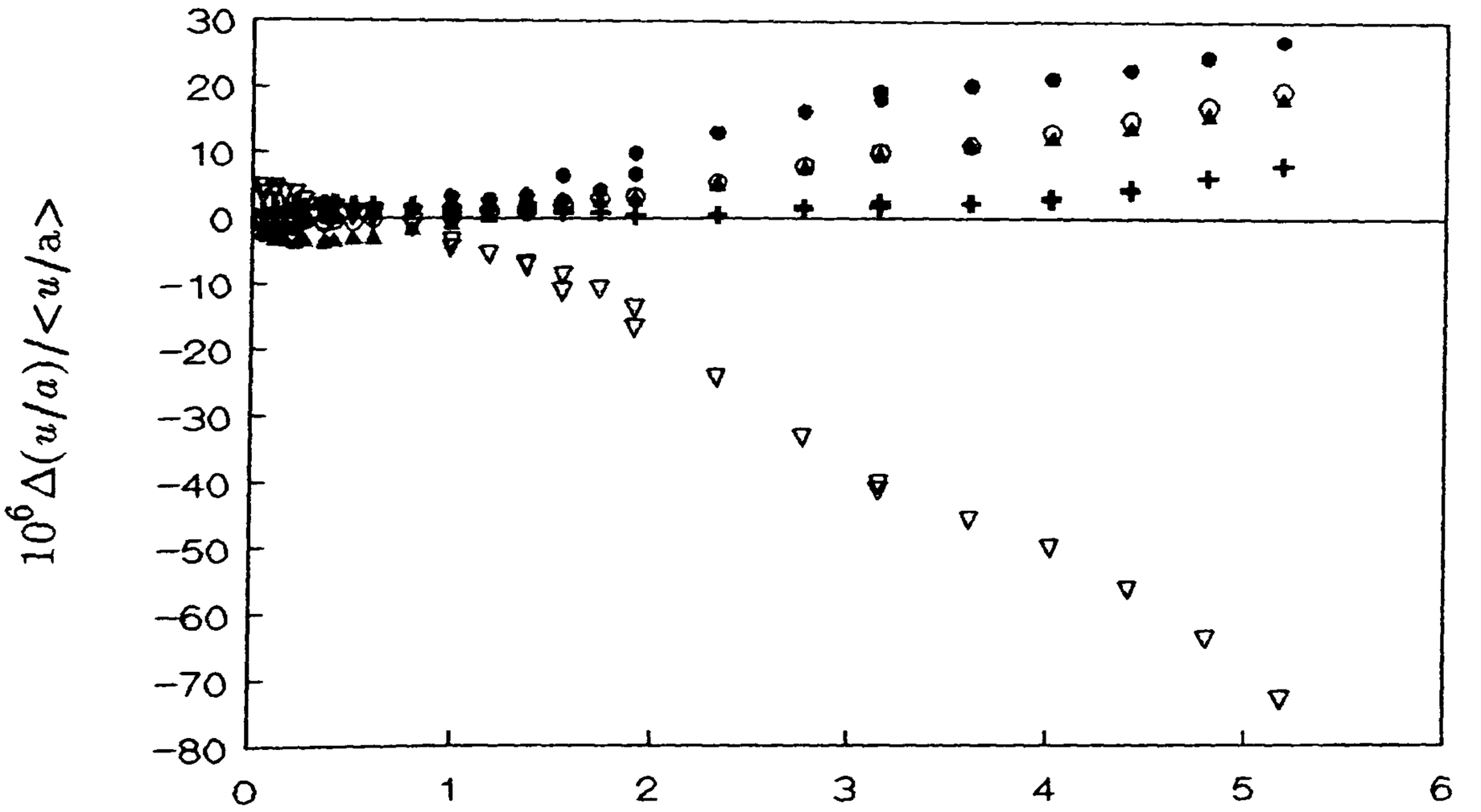

Figure 5.33: Fractional deviations of (u/a) for individual modes in nitrogen at 295 and 297 K from $<u/a>$ of the finally selected modes.

• , (0,2); ▲ , (0,3); ∘ , (0,4); + , (0,5); ∇ , (0,6).

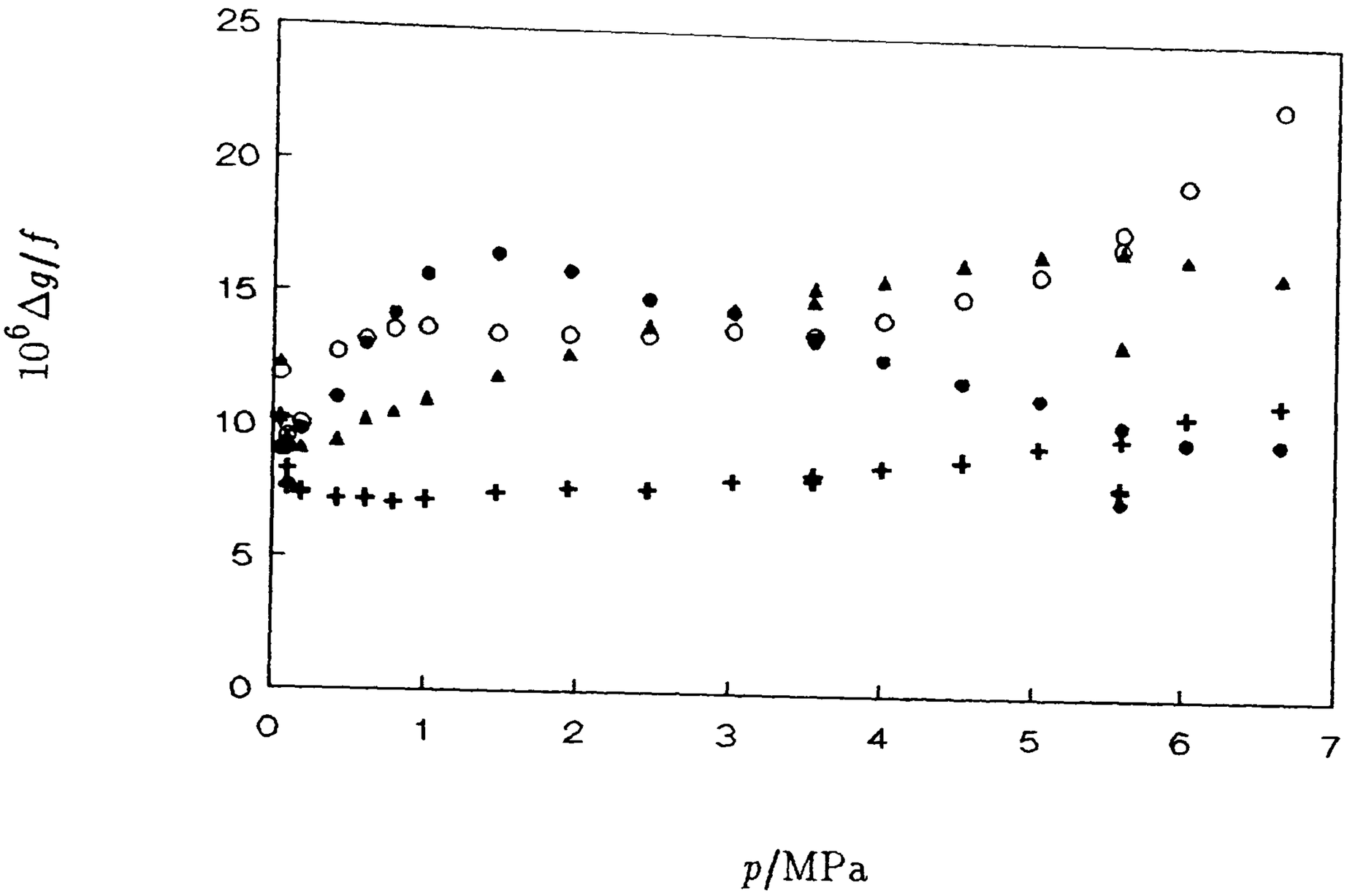

Figure 5.34: $\Delta g/f$ as a function of pressure in nitrogen at 303 K.

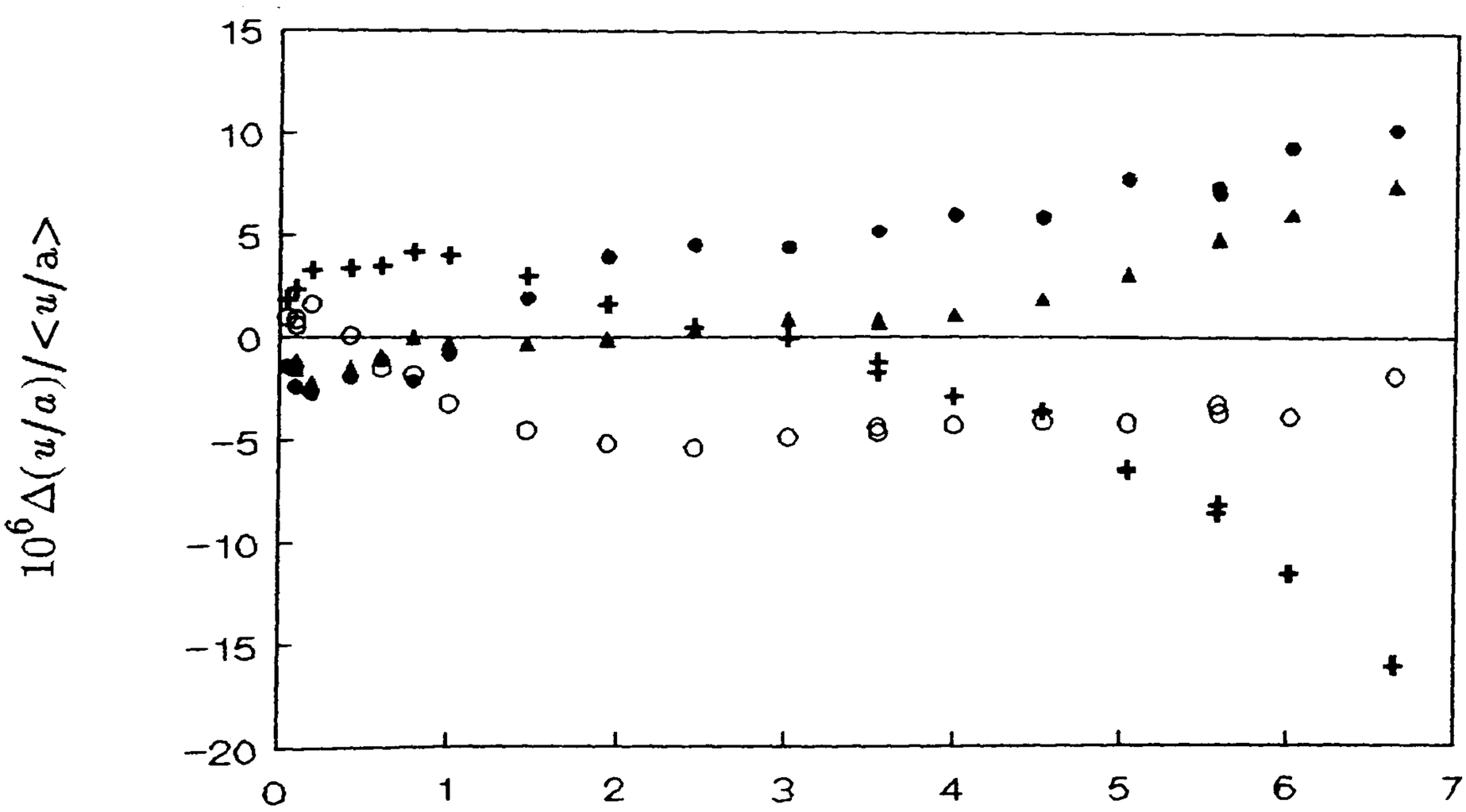

Figure 5.35: Fractional deviations of (u/a) for individual modes in nitrogen at 303 K from $<u/a>$ of the finally selected modes.

• , (0,2); ▲ , (0,3); ∘ , (0,4); + , (0,5); ▽ , (0,6).

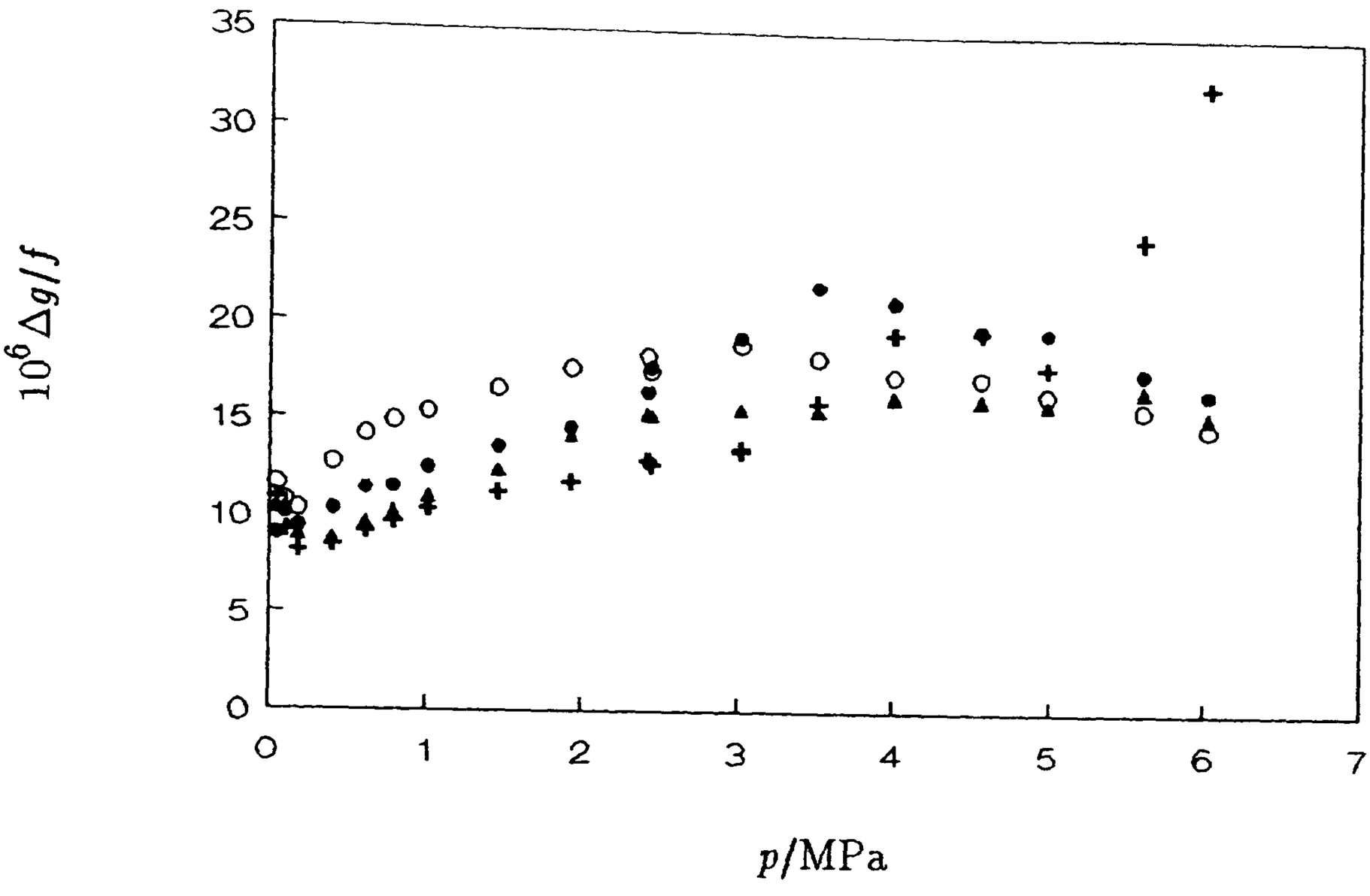

Figure 5.36: $\Delta g/f$ as a function of pressure in nitrogen at 325 K.

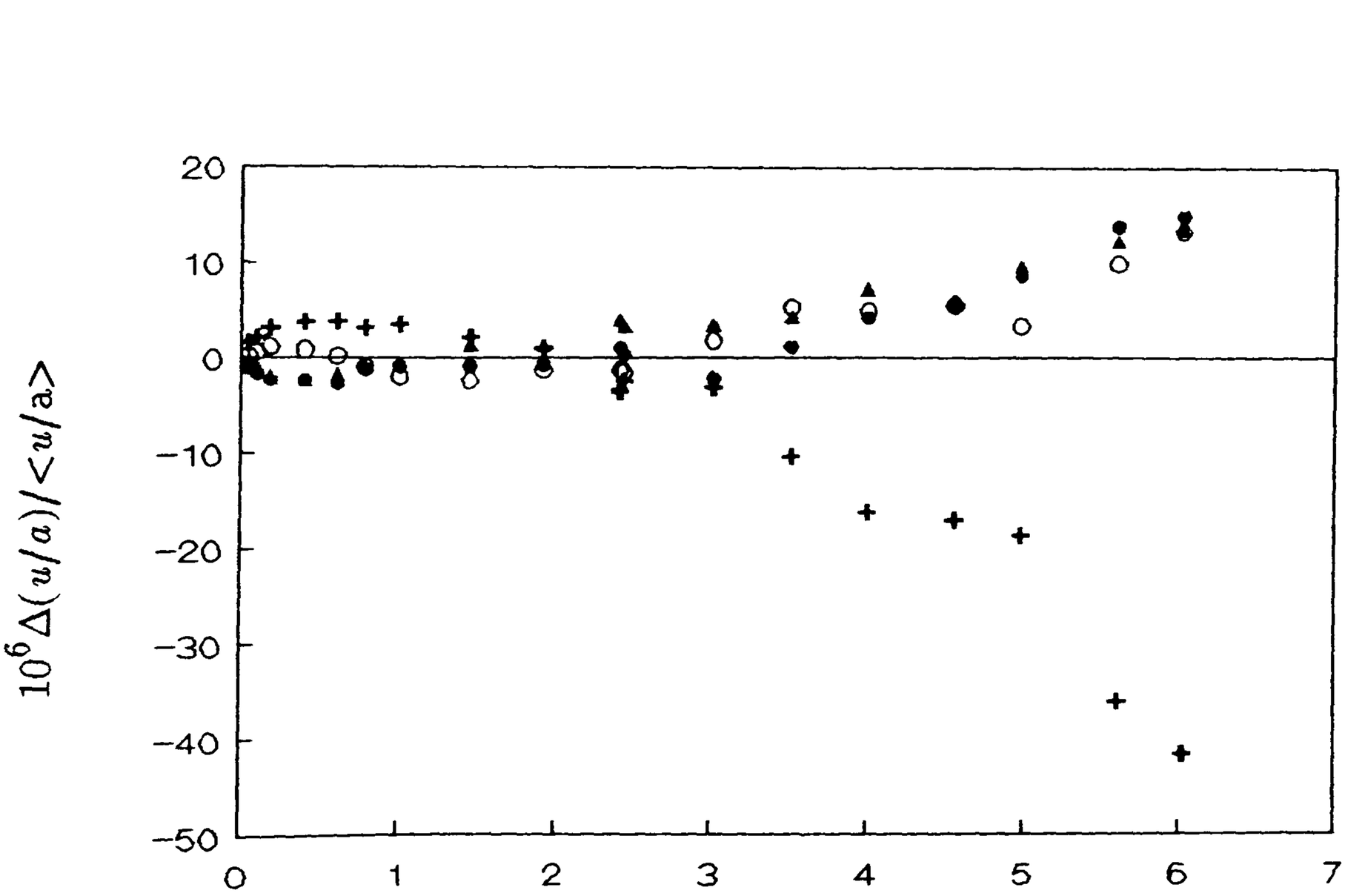

Figure 5.37: Fractional deviations of (u/a) for individual modes in nitrogen at 325 K from $<u/a>$ of the modes finally selected.

• , (0,2); ▲ , (0,3); ∘ , (0,4); + , (0,5); ∇ , (0,6).

motion. However, this is inconsistent with the observations of the $\Delta g/f$ unless the shell resonance is extremely sharp in which case frequency perturbations exceed the increased losses.

At 273.16 K the excess half–widths are shown in figure 5.30 and are below 20 ppm across the whole range with trends in accord with those expected from the measurements in argon. No modes appear to be adversely affected by shell motion.

Deviations of the individual (u/a) are shown in figure 5.31. The agreement of the first four modes is on the order of 10 ppm across the whole range.

The isotherms at temperatures near 296 K are considered together. The $\Delta g/f$ are shown in figure 5.32. The excess half–widths are similar to those observed in argon with the (0,5) mode being perturbed by a shell resonance. The excess half–widths are below 30 ppm across the whole range.

Deviations of the individual (u/a) are shown in figure 5.33. In both cases the (0,6) mode is perturbed by a shell resonance with the remaining modes showing good agreement.

At the triple point of gallium the excess half–widths are below 25 ppm across the whole range and shown in figure 5.34. The (0,4) mode shows a density dependence consistent with a perturbation due to shell motion. The remaining modes show excess half–widths similar to those in argon.

Deviations of the individual (u/a) are shown in figure 5.35. The (0,5) mode is seriously perturbed by a shell resonance. Exclusion of this mode brings the agreement of the remaining modes to better than 15 ppm across the whole range. The (0,4) mode appears to be perturbed by a minor shell resonance but the magnitude of the affect is less than that which perturbs the (0,5) mode. The (0,2) and (0,3) modes agree to better than 5 ppm across the whole range.

At 325 K the excess half–widths are shown in figure 5.36 and are below 35 ppm across the whole range. The (0,5) mode shows a density dependence consistent with coupling to a shell resonance.

Deviations of the individual (u/a) are shown in figure 5.37. The (0,5) mode is

Table 5.12: Coefficients of equation (5.2.3) required to represent the measurements of (u/a) in nitrogen with standard deviation σ at temperatures T.

T/K	i	$\{A_i/a^2\}$/s^{-2}·Pa^{-i}	T/K	i	$\{A_i/a^2\}$/s^{-2}·Pa^{-i}
250.064		$10^6\sigma(u^2)/u^2 = 7.4$	273.160		$10^6\sigma(u^2)/u^2 = 6.6$
	0	$(51.41013 \pm 0.00013)\cdot 10^6$		0	$(56.11718 \pm 0.00012)\cdot 10^6$
	1	0.15158 ± 0.00024		1	0.34584 ± 0.00021
	2	$(0.51571 \pm 0.00095)\cdot 10^{-7}$		2	$(0.46356 \pm 0.00080)\cdot 10^{-7}$
	3	$(0.11247 \pm 0.00098)\cdot 10^{-14}$		3	$(0.6053 \pm 0.0082)\cdot 10^{-15}$
295.504		$10^6\sigma(u^2)/u^2 = 3.3$	297.277		$10^6\sigma(u^2)/u^2 = 5.3$
	0	$(60.662106 \pm 0.000068)\cdot 10^6$		0	$(61.028639 \pm 0.000016)\cdot 10^6$
	1	0.49937 ± 0.00017		1	0.50941 ± 0.00022
	2	$(0.42102 \pm 0.00088)\cdot 10^{-7}$		2	$(0.4149 \pm 0.0011)\cdot 10^{-7}$
				3	$(0.268 \pm 0.014)\cdot 10^{-15}$
302.924		$10^6\sigma(u^2)/u^2 = 7.3$	324.608		$10^6\sigma(u^2)/u^2 = 9.8$
	0	$(62.17128 \pm 0.00012)\cdot 10^6$		0	$(66.58014 \pm 0.00016)\cdot 10^6$
	1	0.54553 ± 0.00026		1	0.66000 ± 0.00017
	2	$(0.3948 \pm 0.0011)\cdot 10^{-7}$		2	$(0.36871 \pm 0.00032)\cdot 10^{-7}$
	3	$(0.322 \pm 0.013)\cdot 10^{-15}$			

perturbed in a manner consistent with shell motion and exclusion of this in the analysis brings the agreement of the remaining modes to better than 5 ppm across the whole range.

The (u/a) finally selected for inclusion in the analysis can be adequately represented by up to four terms in the infinite series (5.2.3). All coefficients were significant at a probability of 0.999. The (A_i/a^2) determined in the regression analysis are given in table 5.12 along with the number of modes N included in the analysis and the fractional standard deviation for the isotherm. Deviation of state points from the regression equations are shown in figures 5.38 and 5.39. Clearly the majority of points

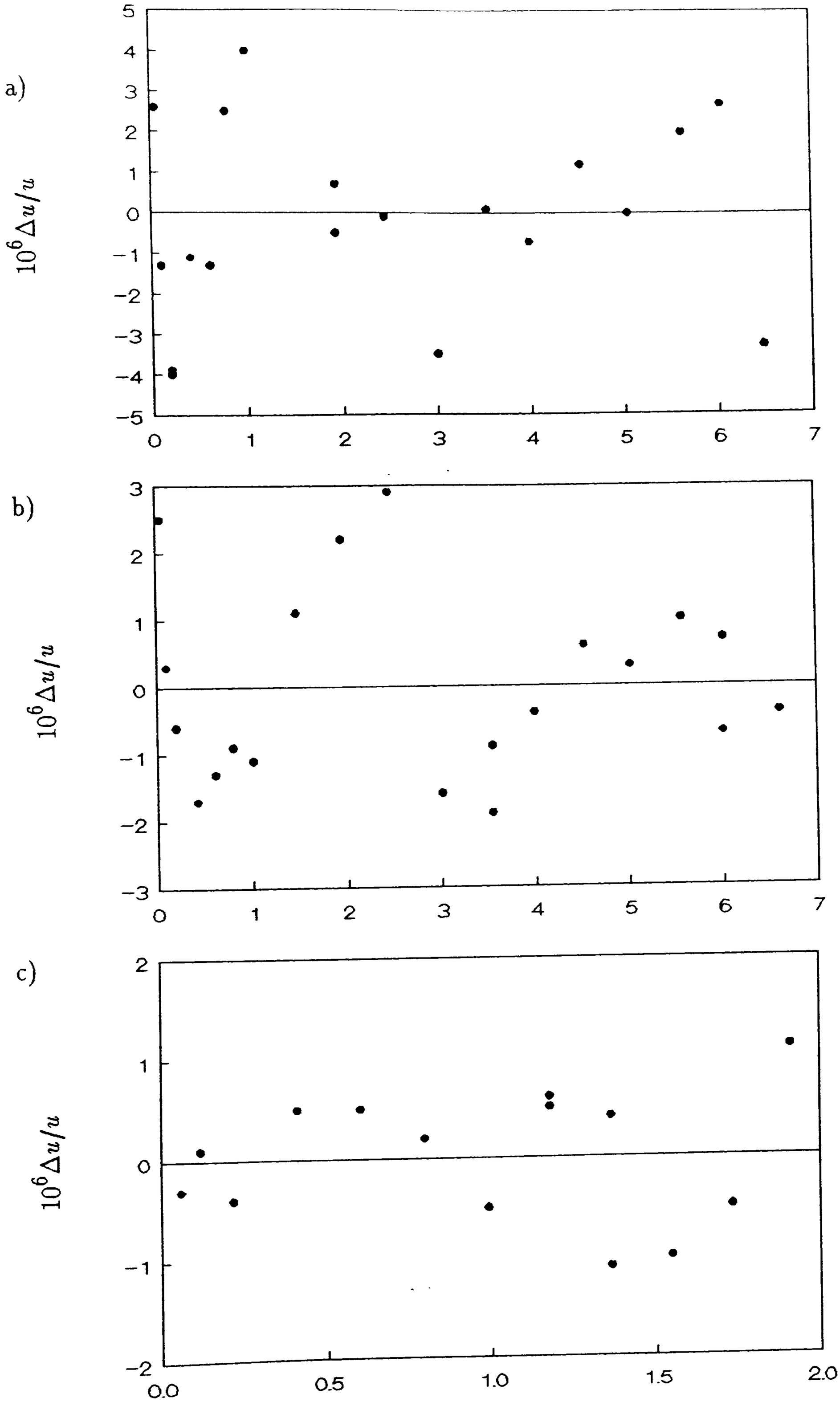

Figure 5.38: Fractional deviations of $<u/a>$ for the selected modes from the adopted smoothing equation; a) 250 K, b) 273.16 K and c) 295 K.

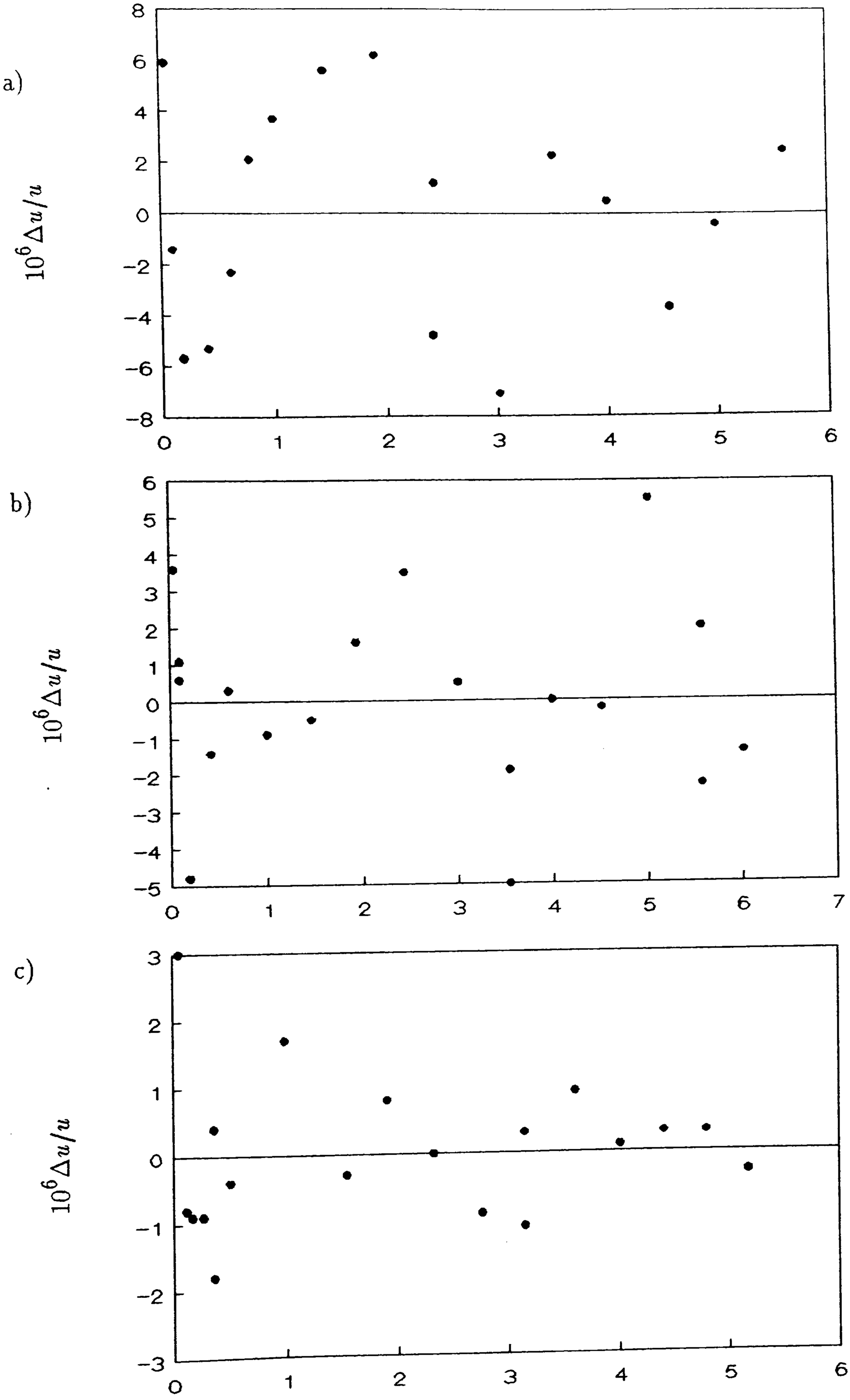

Figure 5.39: Fractional deviations of $<u/a>$ for the selected modes from the adopted smoothing equation; a) 297 K, b) 303 K and c) 325 K.

Table 5.13: Second acoustic virial coefficient, β_a, and second virial coefficient B, represented by equation (5.4.6), for nitrogen at temperatures T.

T/K	β_a/cm^3·mol^{-1}	B/cm^3·mol^{-1}
250.064	6.130 ± 0.010	–16.254
273.160	13.997 ± 0.008	–10.197
295.504	20.226 ± 0.007	–5.378
297.277	20.632 ± 0.009	–5.032
302.924	22.100 ± 0.010	–3.960
324.608	26.754 ± 0.007	–0.247

lie within 5 ppm of the regression equation with a typical standard deviation for an isotherm being about 6 ppm.

Absolute measurements and determination of perfect–gas heat capacities from the (A_i/a^2) require values of $a(T, p\to 0)$. Values of a required in the analysis were taken from the calibration measurements in argon and use of equation (5.4.2) for short–range extrapolation and interpolation. A check on the values of a used is possible; from A_0 values of $C^{pg}_{p,m}$ are returned. For a diatomic molecule under the conditions of the experiment $C^{pg}_{p,m}$ should be 3.5 R. As expected these were the values returned within experimental error and possible contamination with impurities. Deviations of the experimentally determined heat capacities from those expected from statistical mechanics and further discussion is given in the next section.

The β_a determined from the results are given in table 5.13 and compared with previous determinations in this laboratory[64,74] by means of the square–well and power series in T solutions to equation (3.2.15). The square–well solution yielded

$$B/\text{cm}^3\cdot\text{mol}^{-1} = 172.38 - 128.735\exp(95\text{ K}/T) \qquad (5.4.5)$$

which fit the results with a weighted standard deviation of 0.17 cm^3·mol^{-1}. Deviations from this equation are again, as in argon, systematic and we conclude that the square–well solution has difficulties in representing the data. This is especially true at the lowest temperatures where the deviation approaches 3.5 cm^3·mol^{-1} in β_a. Deviations of this solution to (3.2.15) from the alternative are shown in figure 5.41.

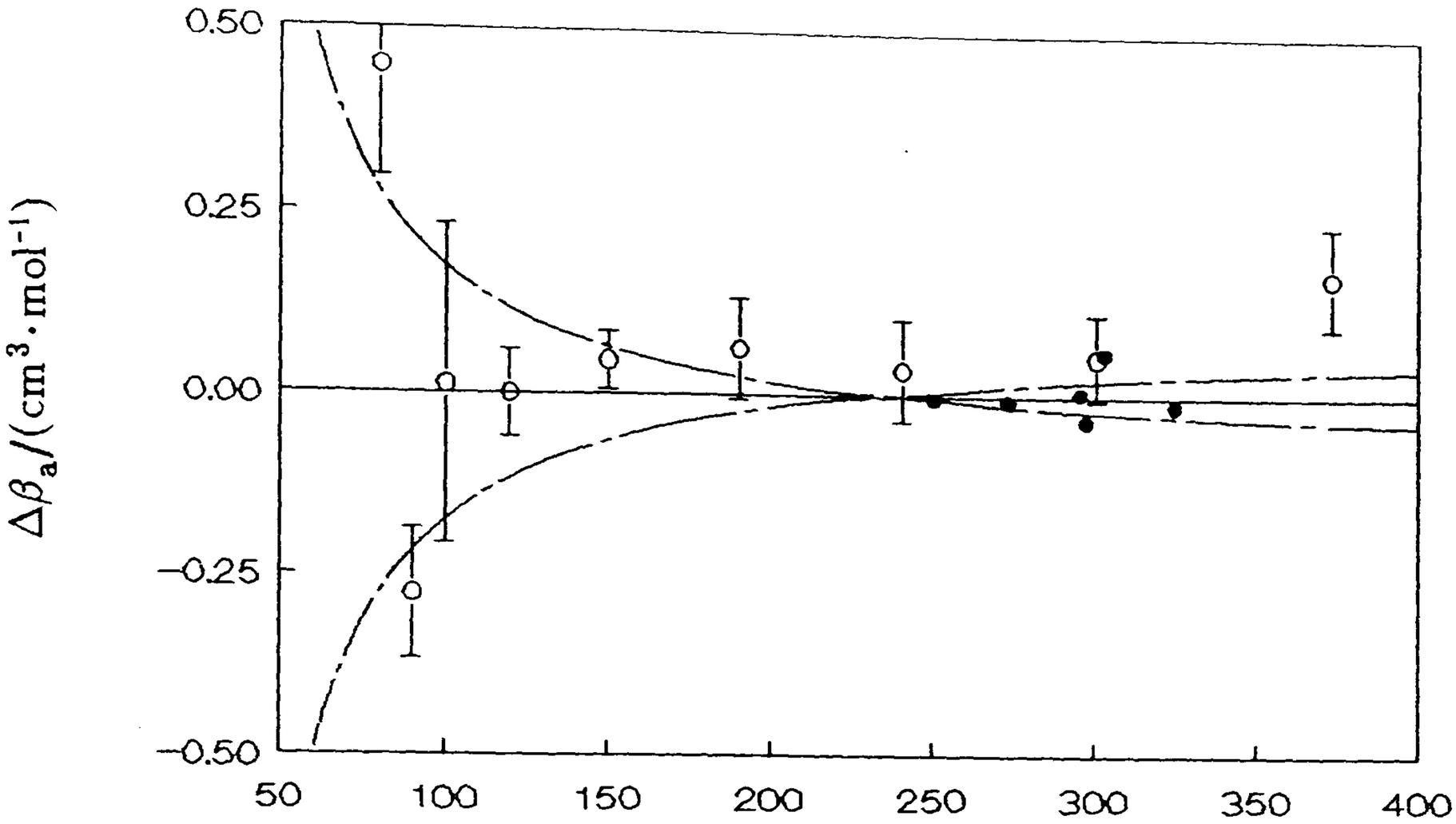

Figure 5.40: Deviations $\Delta\beta_a = \{\beta_a(\text{exp.}) - \beta_a(\text{calc.})\}$ of experimental β_a from equation (5.4.6) and (3.2.15). • , this work; ∘ , reference 64 and 74, ——–——, 0.1 %.

The alternative solution, determined using the adaptive regression algorithm was

$$B/\text{cm}^3\cdot\text{mol}^{-1} = 57.634 - 0.0145(T/\text{K}) - 0.168 \times 10^5(\text{K}/T) - 0.474 \times 10^8(\text{K}/T)^3 \qquad (5.4.6)$$

and fit the results with a weighted standard deviation of 0.035 $\text{cm}^3\cdot\text{mol}^{-1}$.† Again this is a surprising result but, considered in the light of the argon results, not unexpected. Deviations of the experimental results from this equation are shown in figure 5.40. With the exception of the result at 373 K and the highly precise value at 303 K, the values of β_a are seen to lie within 0.1 % of equation (5.4.6). The level with which this highly empirical equation represents the results is extraordinary. The standard deviation of the fit to the combined acoustic data set is comparable with experimental error and is even more remarkable when we consider that two entirely independent determinations are included.

In figure 5.41 the deviation of the square–well solution from equation (5.4.6) is

† An alternative, and perhaps better polynomial expansion is

$$B/\text{cm}^3\cdot\text{mol}^{-1} = 40.804 - 9978(\text{K}/T) - 0.10597 \times 10^7(\text{K}/T)^2 \qquad (5.4.6a)$$

shown. As can be seen, at low temperatures the two solutions do not agree very well, and the deviation reaches 2 $cm^3 \cdot mol^{-1}$ (about 0.8 %) at 90 K. However, at higher temperatures the solutions converge and, in the range 110 to 600 K the differences are less than 1 $cm^3 \cdot mol^{-1}$, while at temperatures above this the difference reaches about 2 $cm^3 \cdot mol^{-1}$. At temperatures near 350 K the differences are on the order of 0.1 $cm^3 \cdot mol^{-1}$. Also shown in this figure as deviations from (5.4.6), are values of B determined by other workers. The recent measurements of Pieperbeck, Kleinrahm, Wagner and Jaeschke[65] agree extremely well with (5.4.6), to better than 0.15 $cm^3 \cdot mol^{-1}$, and are within experimental error. The measurements of Roe and Saville[66], and Crain *et al*[72] are initially too negative and deviate from the present results by, at worst, 1 $cm^3 \cdot mol^{-1}$; however, the results converge, to within experimental error, with these results at temperatures above 250 K. The values quoted by Gunn[69] agree to better than 0.5 $cm^3 \cdot mol^{-1}$ across the whole range. The recommended values of Dymond and Smith[22] are initially too positive and show significant deviations from (5.4.6), particularly at the lowest temperatures where the deviation reaches 5 $cm^3 \cdot mol^{-1}$. At temperatures above 200 K the values converge with (5.4.6) to better than 0.8 $cm^3 \cdot mol^{-1}$. Even so, the recommended values agree with (5.4.6) over the whole range to within the error estimates given by Dymond and Smith. The results of Michels, Lunbeck and Wolkers[67] are also shown and deviate from the present results by about 0.25 $cm^3 \cdot mol^{-1}$; this is just outside the combined estimates of the experimental error. Although the results of Michels *et al* are not particularly recent, the measurements were performed at pressures up to 300 MPa and the coefficients determined should not be subject to any large systematic errors associated with correlation of terms. The values of Holborn and Otto[68] deviate by as much as 2 $cm^3 \cdot mol^{-1}$ at temperatures below 200 K but above this temperature agree to better than 1 $cm^3 \cdot mol^{-1}$. The values of B quoted by Hoover *et al*[71] show a systematic oscillition around (5.4.6) the maximum aplitude being about 1.5 $cm^3 \cdot mol^{-1}$. The values derived recently by Pocock and Wormald[73] also show a systematic deviation from (5.4.6); at temperatures below 200 K the values are too negative, and deviate by more

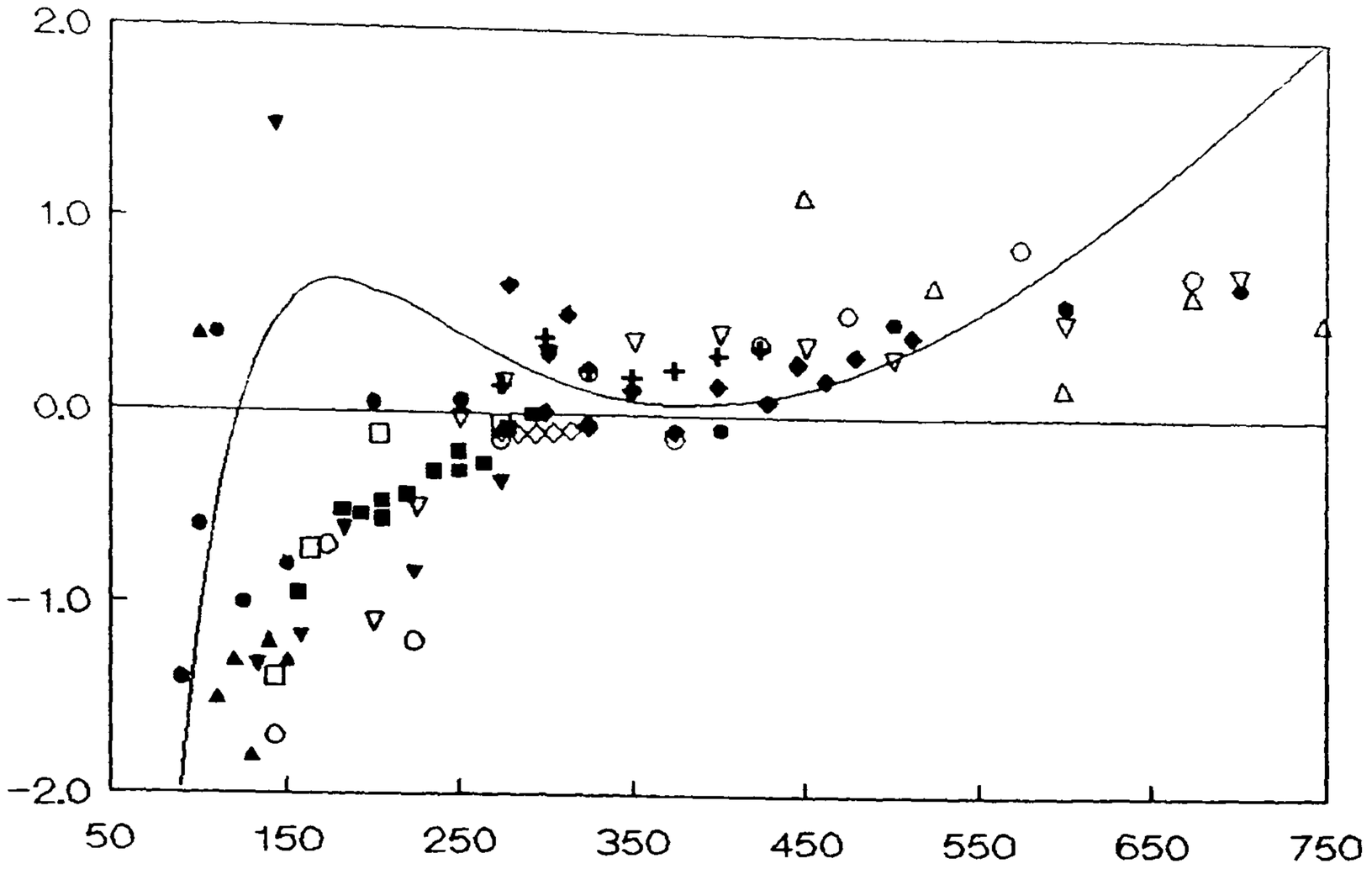

Figure 5.41: Deviations $\Delta B = \{B(\text{exp.}) - B(\text{calc.})\}$ of previous determinations of B from (5.4.6). ———— , square–well; • , reference 22; ◇ , reference 65; ■ , reference 66; + , reference 67; ○ , reference 68; ♦ , reference 69; △ , reference 70; ▼ , reference 71; □ , reference 72; ▽ , reference 73; ▲ , reference 75.

---

than 5 $cm^3 \cdot mol^{-1}$, but at temperatures above this they are too positive, although they agree to within the estimated precision of 1 $cm^3 \cdot mol^{-1}$. The values of Witonsky and Miller[70] are too positive by, on average, 0.7 $cm^3 \cdot mol^{-1}$. The values of B derived by van Itterbeek *et al*[75], also from speed of sound measurements, show a systematic deviation from (5.4.6); at temperatures below 100 K they are too positive, by as much as 16 $cm^3 \cdot mol^{-1}$, but at temperatures above this they are too negative by about 1.5 $cm^3 \cdot mol^{-1}$. However, all things considered, if the differences between the two solutions to (3.2.15) reported here are taken as an indication of the systematic error associated with the imposition of a functional form on B, then most results are seen to be in agreement with (5.4.6).

5.4.6: General Comments on the Characterisation of the Resonator.

The zero–pressure limit of the raduis of the resonator has been determined from the measurements in argon between 252 and 350 K. The equation finally adopted should provide estimates of the radius at intermediate temperatures, and short

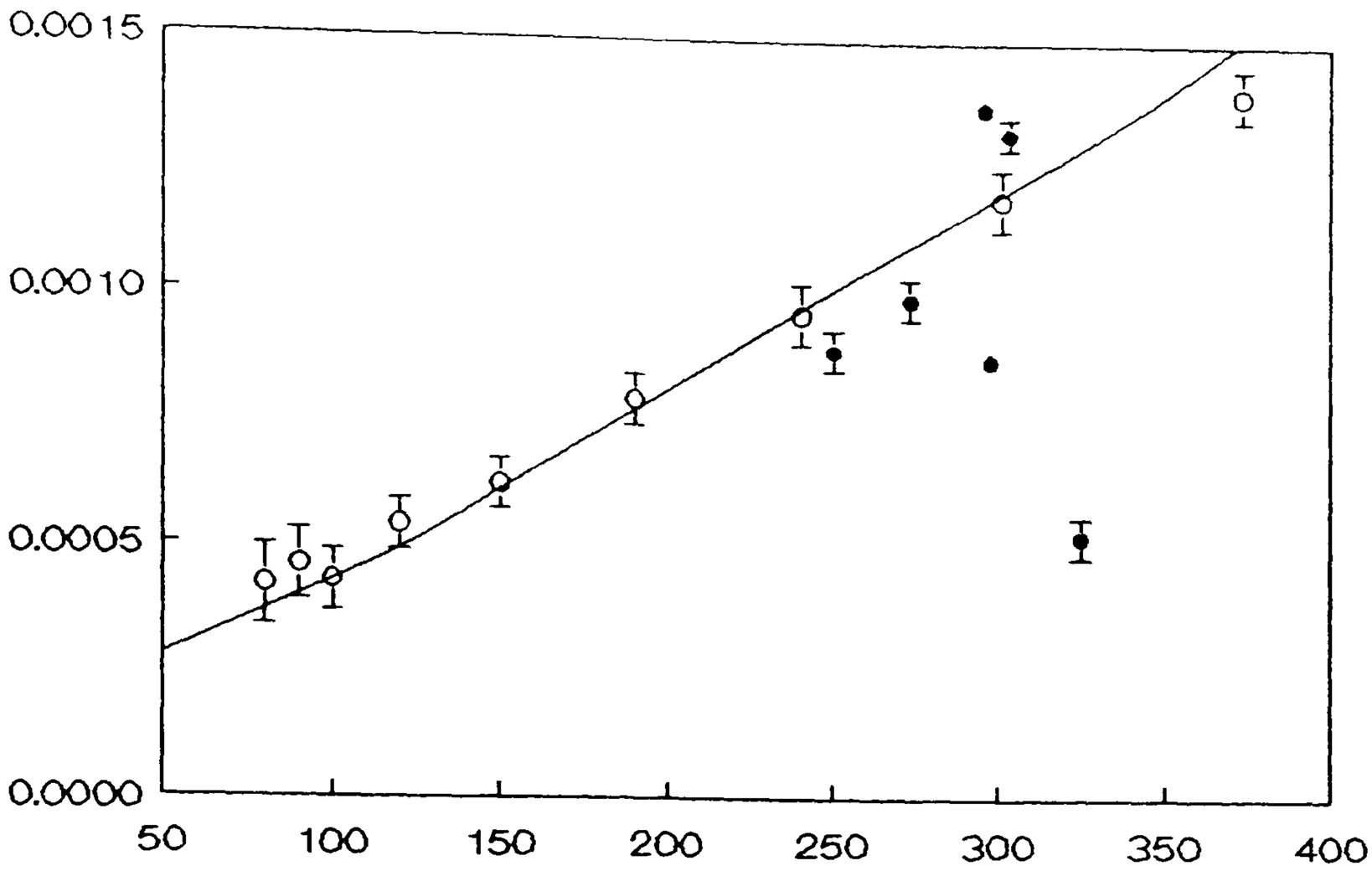

Figure 5.42: Dynamic values of the constant–pressure perfect–gas heat capacity of nitrogen plotted as $\Delta C^{pg}_{p,m}/R = \{C^{pg}_{p,m}(\text{exp.})/R - 3.5\}$.

• , this work, ∘ , reference 74, ———— , centrifugal distortion.

---

extrapolations outside the temperature range of study, to better than 0.1 μm.

Once the zero–pressure radius has been determined, absolute measurements of the speed of sound and determination of perfect–gas heat capacities are possible. Therefore, using the experimental results obtained for nitrogen, a check on the internal consistency of the argon results is provided. This is by comparison of experimental and calculated perfect–gas heat capacities. Since the vibrational relaxation time for nitrogen is very long compared with the period of the sound waves under the conditions of the experiments, the small vibrational contribution to the heat capacity is not observed. However, the measurements are of sufficient precision to resolve the small effects of centrifugal distortion on the rotational contribution to the heat capacity. The results are compared with values calculated from statistical mechanics and are shown in Figure 5.42. The results of Ewing and Trusler[74] are seen to agree with the calculated values (indicated by the solid line) to within experimental error, except at the highest temperature.

The present values, although not agreeing within experimental error, are seen to deviate from the spectroscopic values by an amount which is in agreement with the systematic error associated with the use of equation (5.4.1) to determine the radius.

Calculation of the radius from the zero–pressure speed of sound in nitrogen indicates, in general, that the two sets of radii agree to about 1 μm.

However, if we consider the alternative equation (where the standard deviation is about 1 μm), which was determined from the whole set of argon measurements, then the results are seen to agree at a level comparable with the standard deviation associated with the smoothing equation. The nitrogen data is therefore considered to be consistent with the combined argon data set.

The measurements in argon also served to demonstrate that the application of the geometric perturbation was correct. Convincing evidence for this assertion is provided by the measurements at pressures below 1 MPa. The measurements in nitrogen again provided a check on these results and the geometric corrections are seen to accommodate the data extremely well. However, the high pressure measurements in nitrogen indicated that there was some apparent pressure dependence of the geometry. This is discussed in some detail in Chapter 2. All things considered, the resonator is suitably well characterised to determine speeds of sound in the required pressure range to better than 10 ppm.

Comparison of the similarity between the excess half–widths observed in argon and nitrogen can be performed by considering all the observed $\Delta g/f$ in one figure. This is shown in figure 5.43. As can be seen, the bulk of the excesses show similar trends. Individual modes which are affected by various shell resonances show discrepancies but on average the $\Delta g/f$ are below 30 ppm for both substances across the whole range. At pressures below 1 MPa the average excess half–width is less than 10 ppm.

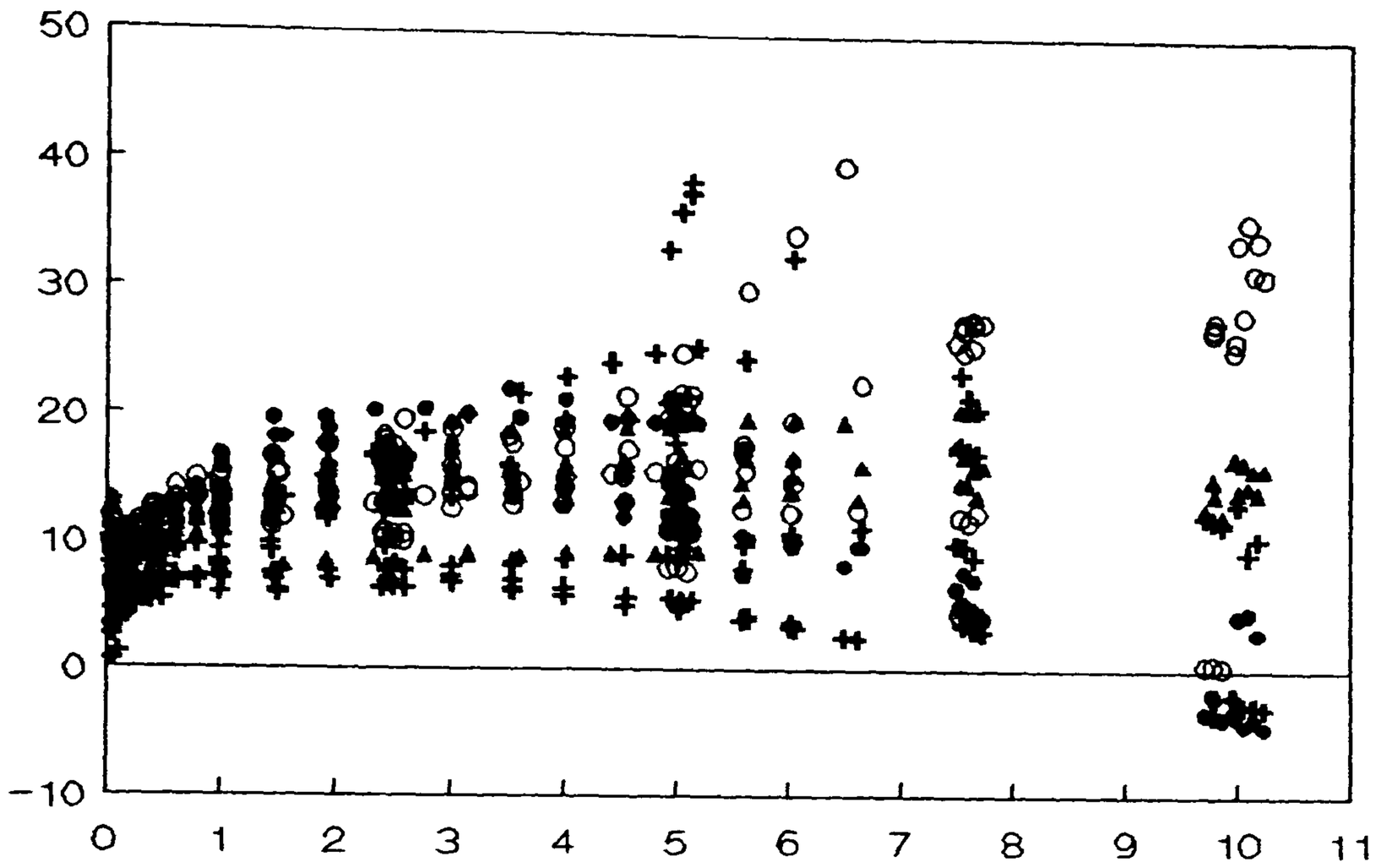

Figure 5.43: Fractional excess half–widths for argon and nitrogen, at all temperatures, as a function of pressure.

• , (0,2); ▲ , (0,3); ∘ , (0,4); + , (0,5).

5.4.7: Methane.

Methane has been studied along six isotherms between 250 and 350 K at pressures below 10 MPa. The minimum pressure at which measurements were conducted was about 200 kPa since the signal intensity was too small at pressures below this due to line–broadening. However, this pressure is sufficiently low to facilitate precise extrapolation to zero pressure to obtain estimates of the perfect–gas heat capacity at constant pressure. The resonance frequencies of the first four radial modes were corrected as outlined in Chapter 2. Table 5.14 lists the mean (u/a) and u at a given state along with the number of modes, N, used in determining the mean, the standard deviation of the mean, and the deviation of the mean from the equation of best fit. The

Table 5.14: Mean values of (u/a) and u with standard deviations σ determined from N modes, with deviations δ from equation (5.2.3). The coefficients of equation (5.2.3) are given in table 5.17.

$\frac{T}{\mathrm{K}}$	$\frac{p}{\mathrm{kPa}}$	N	$\frac{u}{a}\cdot\mathrm{s}$	$\frac{u}{\mathrm{m}\cdot\mathrm{s}^{-1}}$	$\frac{10^6\sigma(u)}{u}$	$\frac{10^6\delta(u)}{u}$
249.977	10042.67	2	8736.5038	392.7477	15.7	(a)
	10001.37	2	8728.6233	392.3934	13.5	–9.1
	9940.90	2	8717.3161	391.8851	10.6	9.4
	8740.45	2	8552.2925	384.4665	3.4	(a)
	7687.10	3	8490.7399	381.6994	3.9	3.1
	7605.87	3	8488.7995	381.6122	3.2	–1.6
	7547.03	3	8487.8286	381.5686	4.7	(a)
	6681.33	3	8491.1056	381.7159	4.4	–5.6
	6673.70	3	8491.3515	381.7269	3.4	1.3
	5159.32	3	8572.5333	385.3764	3.1	6.8
	5087.96	3	8578.1547	385.6291	2.8	1.3
	5017.64	3	8583.8129	385.8835	3.9	–6.1
	3583.28	3	8725.6244	392.2586	2.8	5.7
	2581.59	3	8845.8320	397.6625	3.6	–4.7
	2504.70	3	8855.7632	398.1090	3.9	(a)
	2422.70	3	8866.0553	398.5717	4.2	–7.4
	2418.63	3	8866.6696	398.5993	3.4	3.0
	1517.95	4	8986.1145	403.9689	3.8	1.3
	1004.06	3	9057.2233	407.1656	1.1	4.7
	778.95	3	9088.8607	408.5878	3.1	–0.4
	578.04	3	9117.3907	409.8704	1.5	–0.3
	386.21	2	9144.9299	411.1084	20.8	9.6
	386.18	2	9144.7961	411.1024	0.4	–5.5
	247.02	2	9164.8774	412.0051	3.8	–0.2
274.974	10307.04	2	9353.8992	420.6684	4.8	–3.5
	10225.37	2	9345.0582	420.2708	1.3	1.5
	10154.26	2	9337.5385	419.9326	3.5	2.3
	8609.21	2	9220.3812	414.6638	2.4	(a)
	7654.84	2	9187.6275	413.1908	1.9	5.2
	7579.20	2	9186.1358	413.1237	2.3	–4.8
	7518.29	2	9185.1615	413.0799	2.2	–1.2
	6173.48	2	9188.2101	413.2170	4.1	–0.5
	5088.75	2	9221.6929	414.7228	3.8	–0.6
	5007.19	2	9225.1821	414.8797	4.3	–0.5
	4930.30	2	9228.6137	415.0340	3.7	2.4
	2587.67	3	9378.2216	421.7623	3.2	3.7
	2504.11	3	9384.9161	422.0633	3.0	1.3
	2425.13	3	9391.2659	422.3489	3.7	–6.4
	996.67	3	9518.1975	428.0573	2.4	–1.0
	786.24	3	9538.3771	428.9649	1.1	–1.9
	596.19	3	9556.9583	429.8005	2.5	5.0
	410.54	2	9575.2683	430.6240	0.6	2.6
	246.18	2	9591.6020	431.3585	2.6	–6.8

$\frac{T}{\mathrm{K}}$	$\frac{p}{\mathrm{kPa}}$	N	$\frac{u}{a}\cdot\mathrm{s}$	$\frac{u}{\mathrm{m}\cdot\mathrm{s}^{-1}}$	$\frac{10^6\sigma(u)}{u}$	$\frac{10^6\delta(u)}{u}$
275.098	9223.75	2	9247.1938	415.8704	4.2	(a)
	9145.46	2	9241.9626	415.6352	1.0	1.0
	9067.17	2	9236.9626	415.4016	2.3	−1.8
	7626.49	2	9177.6124	412.7412	0.6	1.6
	7560.61	2	9176.3888	412.6862	0.6	−2.5
	7553.89	2	9176.3269	412.6834	0.4	3.1
	7466.40	2	9174.9936	412.6234	0.1	(a)
	6570.94	2	9172.8895	412.5288	0.5	3.5
	6000.87	2	9181.9303	412.9354	1.7	(a)
	5993.08	2	9182.1285	413.9443	1.3	−3.9
	5597.02	2	9192.8632	413.4271	2.1	−4.2
	5070.82	2	9212.1718	414.2954	2.3	−3.2
	4997.61	2	9215.2895	414.4356	2.4	−2.8
	4993.81	2	9215.5239	414.4462	2.9	4.8
	4915.82	2	9218.9263	414.5992	2.4	1.5
	3983.98	2	9268.2078	416.8155	2.8	3.5
	3009.13	3	9334.0235	419.7754	4.0	−0.1
	2580.41	3	9366.9101	421.2544	3.3	−1.2
	2497.16	3	9373.5747	421.5541	2.6	1.6
	2417.33	3	9380.0853	421.8469	3.1	(a)
	2013.12	3	9413.6859	423.3580	2.8	3.3
	2001.04	3	9414.6698	423.4023	3.0	−1.8
	1466.67	4	9461.7337	425.5189	3.7	−0.9
	996.33	4	9505.2601	427.4764	3.5	−0.8
	783.07	4	9525.5722	428.3898	3.5	−2.4
	606.49	4	9542.6977	429.1600	3.7	1.2
	422.18	3	9560.7694	429.9728	1.4	0.3
	326.95	3	9570.2181	430.3977	1.2	1.7
	200.32	3	9582.8439	430.9655	1.4	0.1
298.885	2127.69	3	9851.9160	443.2319	2.3	−0.2
	1934.70	3	9862.5956	443.7124	2.6	0.4
	1744.40	3	9873.4780	444.2019	3.5	0.4
	1551.90	3	9884.8253	444.7125	4.1	−0.5
	1548.45	3	9885.0282	444.7216	4.1	−0.9
	1356.20	3	9896.7413	445.2486	2.7	2.2
	1162.36	3	9908.8010	445.7911	4.1	−2.1
	966.14	3	9921.3596	446.3561	2.0	−3.1
	968.36	3	9921.2833	446.3527	1.8	3.8
	767.04	3	9934.4542	446.9452	1.7	0.2
	779.06	3	9933.6615	446.9096	2.0	0.6
	584.24	3	9946.6953	447.4960	2.5	−1.2
	389.07	4	9960.0605	448.0972	1.6	0.6
	190.95	2	9973.8614	448.7181	0.6	−0.4
300.000	10230.67	3	9898.8111	445.3506	6.9	(a)
	10226.75	3	9898.5475	445.3387	6.6	(a)
	10154.63	3	9893.1164	445.0944	6.4	0.7
	10076.54	3	9887.2008	444.8282	5.7	1.1
	9999.83	3	9881.5002	444.5717	5.9	−1.0
	9914.46	3	9875.3162	444.2935	5.4	−2.7

$\frac{T}{\mathrm{K}}$	$\frac{p}{\mathrm{kPa}}$	N	$\frac{u}{a}\cdot\mathrm{s}$	$\frac{u}{\mathrm{m}\cdot\mathrm{s}^{-1}}$	$\frac{10^6\sigma(u)}{u}$	$\frac{10^6\delta(u)}{u}$
300.000	9066.96	3	9822.8427	441.9327	3.3	4.1
	9055.02	3	9822.1601	441.9020	3.8	–1.2
	8572.57	3	9799.2693	440.8722	3.1	8.0
	8013.86	3	9778.5041	439.9379	2.0	5.1
	7646.99	3	9768.0894	439.4694	2.8	–5.2
	7593.85	3	9766.8463	439.4134	2.5	–1.1
	7559.81	3	9766.0293	439.3767	2.4	–3.4
	7505.55	3	9764.8796	439.3250	2.1	3.9
	7447.99	3	9763.4716	439.2616	2.0	(a)
	7371.55	3	9761.9869	439.1948	2.1	(a)
	6548.06	3	9751.9947	438.7453	1.8	–1.3
	5576.40	3	9754.7979	438.8714	1.9	–0.8
	5089.34	3	9761.7406	439.1837	2.4	1.9
	4998.65	3	9763.3796	439.2575	2.1	–1.5
	4914.06	3	9765.0284	439.3316	2.3	–3.1
	4909.04	3	9765.1985	439.3393	2.3	3.9
	3539.75	3	9805.6347	441.1585	3.1	(a)
	2587.98	3	9847.0440	443.0216	3.1	2.7
	2497.83	3	9851.4613	443.2203	3.3	0.9
	2405.49	3	9856.0956	443.4288	3.2	1.5
	1986.68	3	9878.1073	444.4191	3.2	–3.1
	1454.16	3	9908.5579	445.7891	4.7	–0.9
	997.53	3	9936.6169	447.0515	3.1	–1.1
	793.50	3	9949.7069	447.6404	1.1	–0.9
	609.72	3	9961.7749	448.1833	1.3	–0.6
	424.68	3	9974.1956	448.7421	0.1	1.1
	205.86	3	9989.2061	449.4175	0.4	3.4
348.762	8600.78	2	10726.2925	482.9731	5.9	–0.6
	7533.77	2	10684.5279	481.0926	4.8	4.5
	7447.92	2	10681.5827	480.9600	8.1	–3.4
	5017.30	2	10630.5956	478.6642	0.3	0.1
	4930.88	2	10629.7908	478.6280	2.0	–1.7
	2545.40	2	10633.7969	478.8083	0.4	–1.7
	2405.59	2	10635.5593	478.8877	0.4	5.2
	990.22	3	10660.7823	480.0234	2.8	–5.5
	517.48	3	10672.5132	480.5516	4.3	6.2
	241.10	2	10679.9095	480.8846	1.6	–0.2

transport properties used to account for losses at the surface, the effects of the gas–inlet tube and classical bulk absorption were taken from reference 55; the original measurements were made by Kestin *et al*[63,76,77]. In this work the density dependence of the transport properties is important and appropriate account of this has been taken. Second and third virial coefficients required in the estimation of the various correction terms were taken from the work of Douslin *et al*[84]. Representation

Table 5.15: Vibrational relaxation times, τ, for methane at a density of 1 $kg \cdot m^{-3}$ and density dependence of the product $\tau\rho$ at temperatures T.

T/K	$\tau\rho/(\mu s \cdot kg \cdot m^{-3})$	$\{\partial(\tau\rho)/\partial\rho\}_T/\mu s$
249.977	2.201 ± 0.027	0.0340 ± 0.0033
274.974	1.744 ± 0.024	0.0162 ± 0.0017
275.098	1.746 ± 0.009	0.0152 ± 0.0019
298.885	1.372 ± 0.006	0.0114 ± 0.0014
300.000	1.383 ± 0.008	0.0110 ± 0.0014
348.762	0.907 ± 0.006	0.0106 ± 0.0005

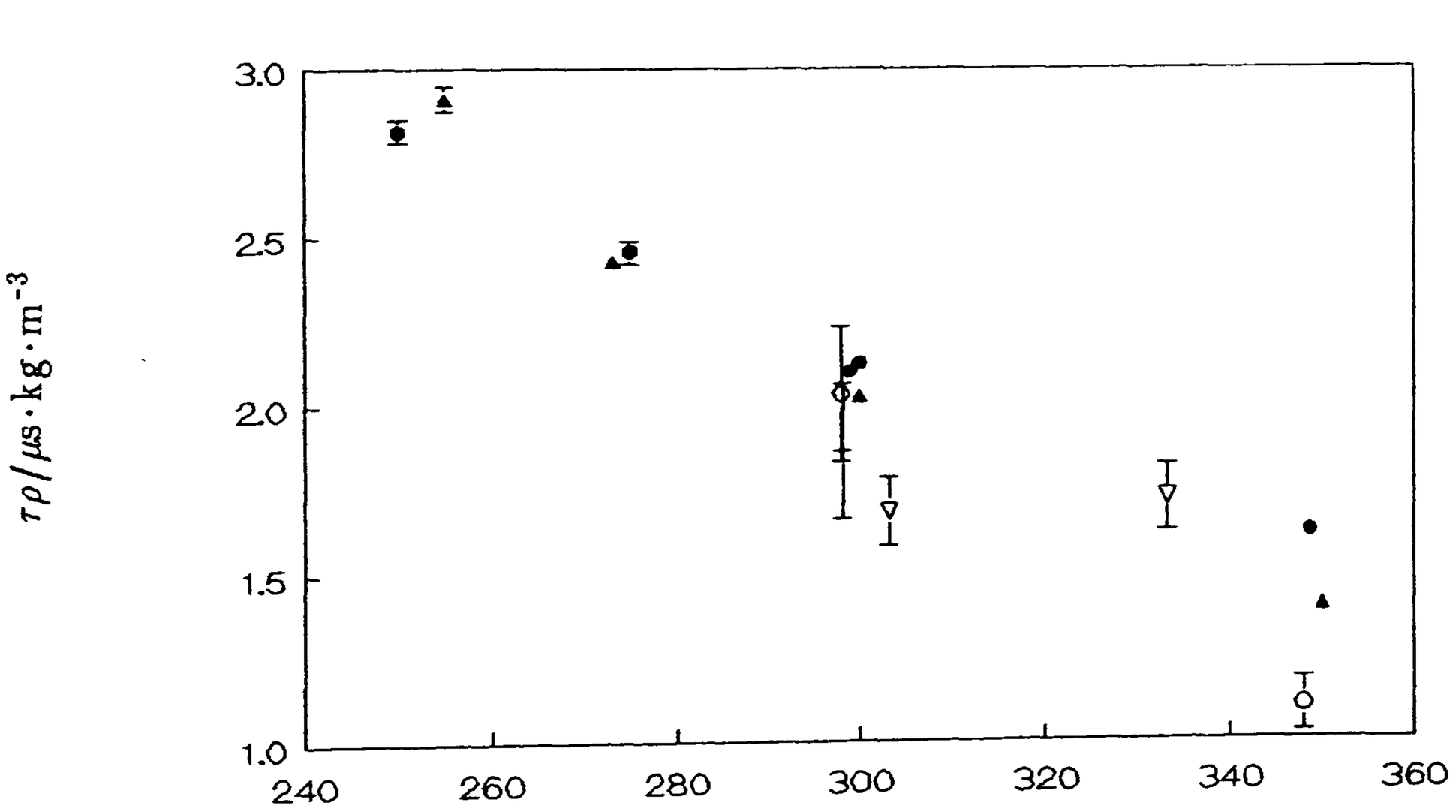

Figure 5.44: Vibrational relaxation times in methane at a density of 1 $kg \cdot m^{-3}$.
• , this work, ▲ , reference 5; ○ , reference 79; + , reference 80; ▽ , reference 81.

of their results was by means of square–well equations which were reported in reference 5.

Vibrational relaxation makes an important contribution to the losses in methane. In order to account for this and to correct the observed frequencies for dispersion an estimate of the vibrational relaxation time is required. Estimates can be obtained by subtracting from the observed line–widths contributions from known loss mechanisms and analysing the residual experimental half–widths using equation (5.3.1). Estimates of the relaxing heat capacity were calculated from the vibrational frequencies of Shimanouchi[78] assuming that the vibrations could be represented as pure harmonic oscillators. Terms in $\tau\rho$ and $\partial(\tau\rho)/\partial\rho$ were required. Values of $\tau\rho$ at a density of 1 $kg \cdot m^{-3}$ are given in table 5.15 along with $\partial(\tau\rho)/\partial\rho$. Comparison of the values so obtained with previous determinations is by means of figure 5.44 where the vibrational relaxation time at a density of 1 $kg \cdot m^{-3}$ is plotted as a function of temperature. At 275 K the two determinations in this work agree to well within experimental error. At temperatures near 300 K the agreement between these estimates, which agree within experimental error, and those of Ewing and Goodwin[5] and Cottrell and Matheson[79] is excellent. The two independent audio–frequency determinations agree to 100 ns which is about five times the combined standard deviation. The variation of τ with temperature is different from that observed by Ewing and Goodwin, as is that determined by Cottrell and Matheson. The difference is small and in the worst case the difference between the two determinations of this laboratory is about 0.2 μs; this occurs at 350 K where Goodwin notes that transducer instabilities compromised the precision of the measurements of g and so some of the discrepency may be attributable to this. The two samples are likely to be of similar purity. The values derived by Cottrell and Martin[81], and Edmonds and Lamb[80] were obtained from samples which were likely to be severely contaminated although it should be noted that the value at 333.15 K quoted by Cottrell and Martin is in agreement with the results of this work.

The excess half–widths, after allowance for vibrational relaxation, are shown in figure 5.45 and 5.46. As can be seen, they are much the same as those observed in

a)

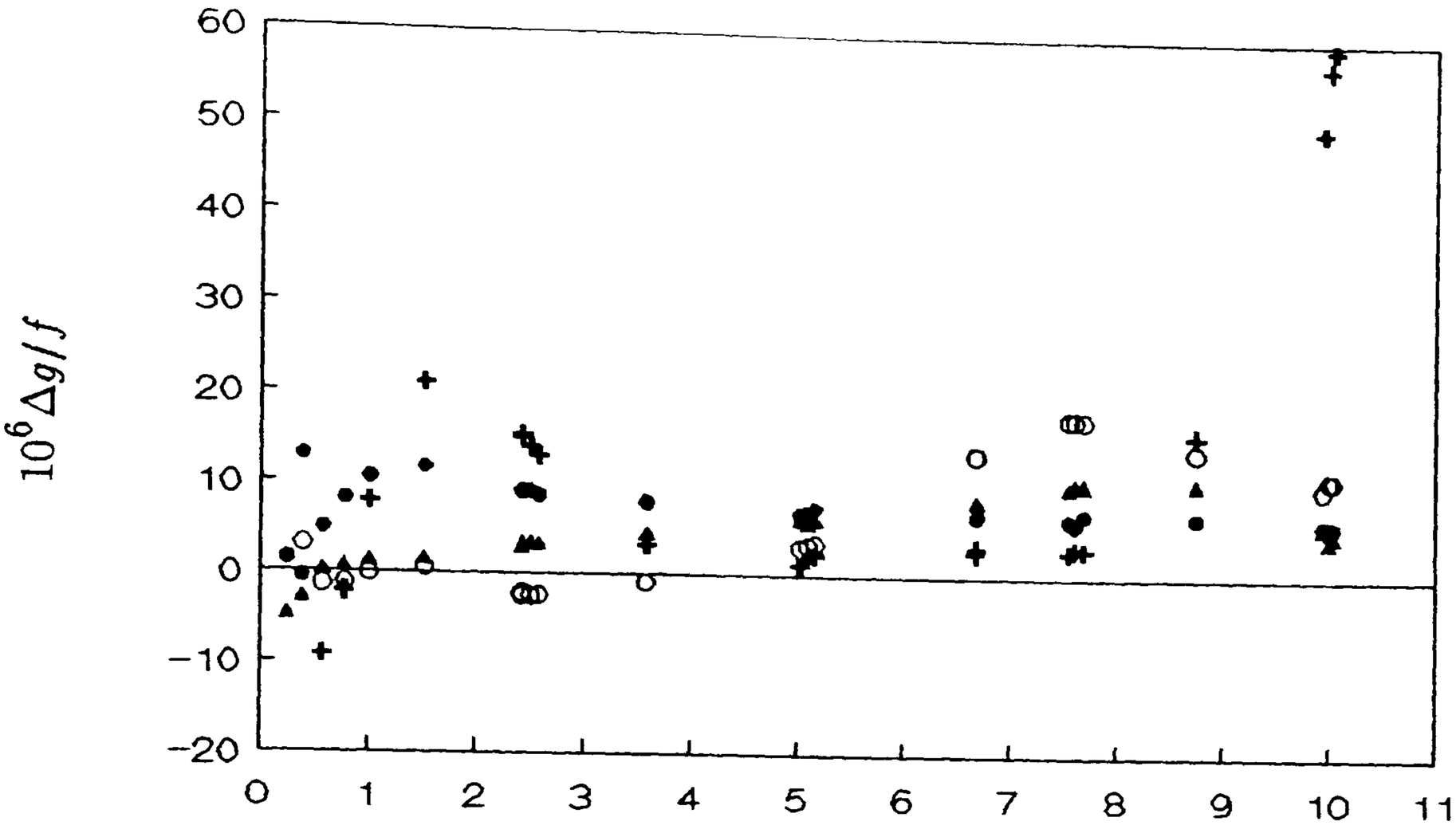

b)

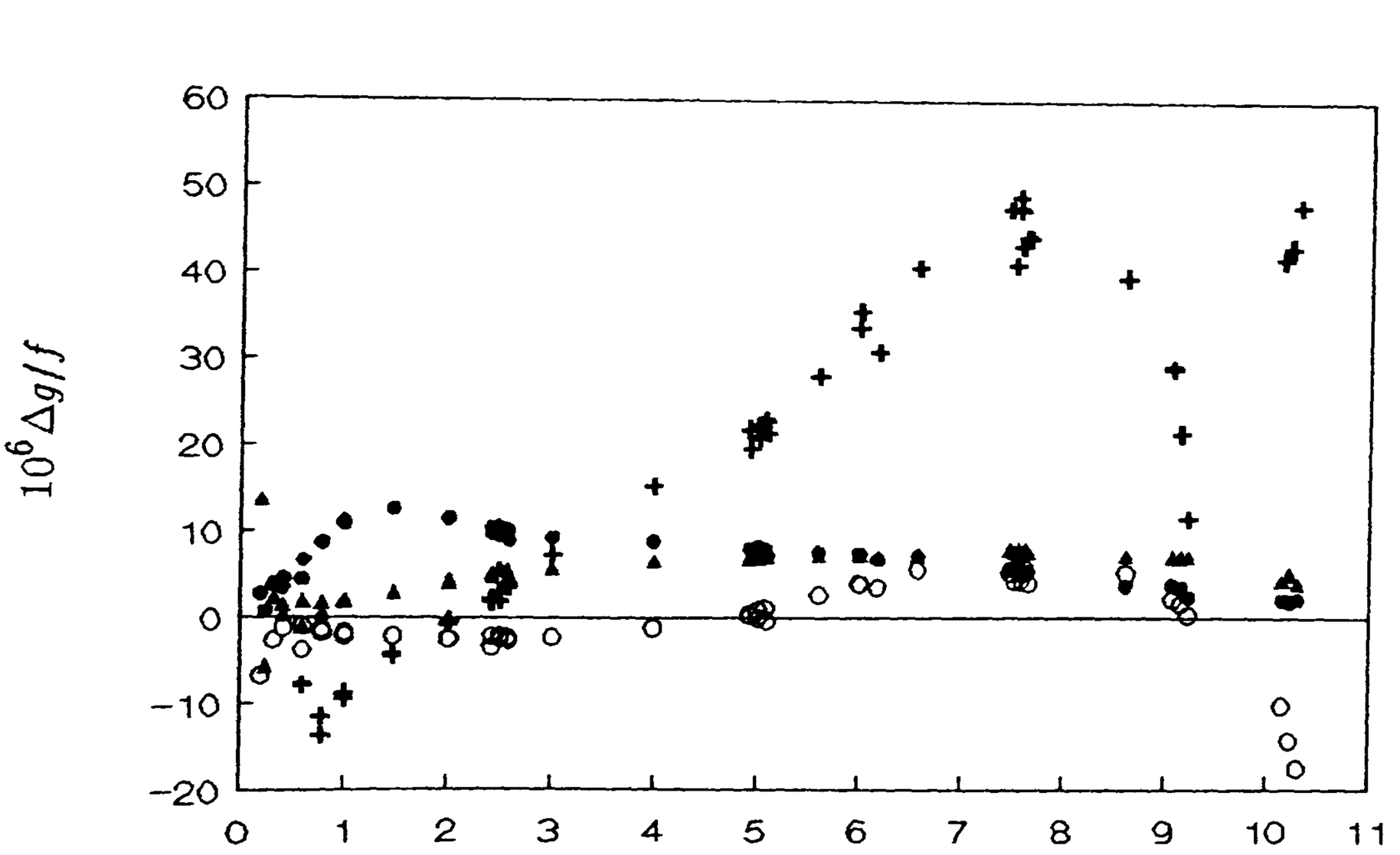

Figure 5.45: $\Delta g/f$, after allowance for vibrational relaxation, as a function of pressure for methane at: a) 250 K, and b) 275 and 275.1 K.

• , (0,2); ▲ , (0,3); ∘ , (0,4); + , (0,5).

a)

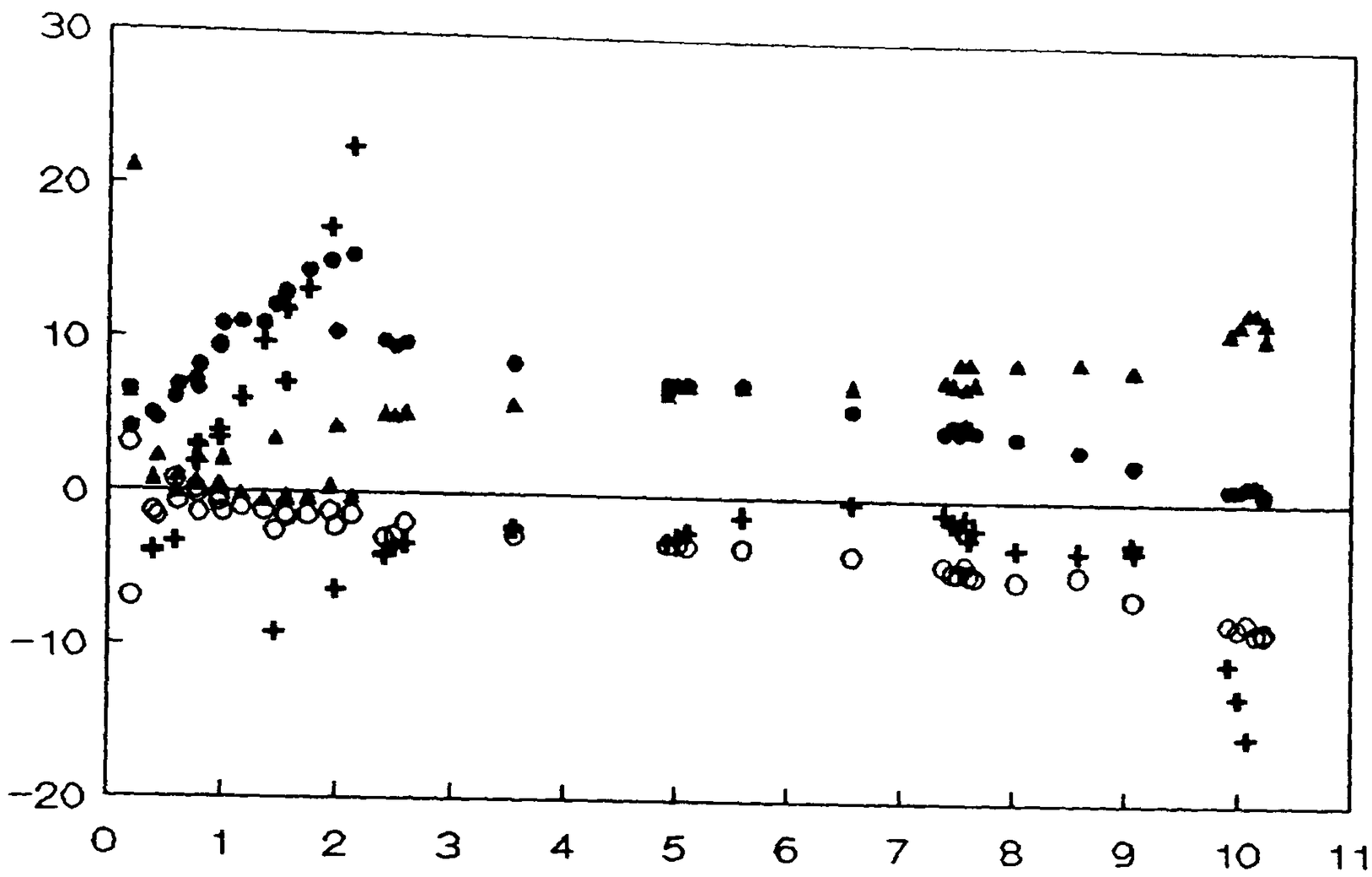

b)

Figure 5.46: $\Delta g/f$, after allowance for vibrational relaxation, as a function of pressure for methane at: a) 299 and 300 K, and b) 349 K.

• , (0,2); ▲ , (0,3); ∘ , (0,4); + , (0,5).

argon and nitrogen and are typically less than 20 ppm across the whole range. The excess half–width of the (0,5) mode is extremely large and density–dependent in some instances. This is to be expected since the frequency of this mode (generally > 20 kHz) brings it in close proximity with the shell resonances shown in figure 2.2. This means that the perturbation to the (0,5) mode due to shell motion will be extremely large and consequently the losses will be increased. Losses due to shell motion are difficult to model for real resonators and consequently, the observed losses are expected to exceed the calculated losses. Since the perturbation is proportional to the product of the density and the square of the speed of sound the perturbation should tend to zero as the pressure is reduced. This is the observed trend. If we exclude the (0,5) mode we see that, for all isotherms, the excess half–widths are very similar with each other and to those observed in argon. The two isotherms studied at 275 K are considered together as are the two isotherms at temperatures near 300 K. It is interesting to note that the $\Delta g/f$ of the (0,2) mode has a maximum at about 2 MPa for all temperatures. This reflects the conflicting trends of increased overlap, due to line–broadening, with the (3,1) mode and decrease in signal strength of the (3,1) mode relative to the (0,2) mode as the pressure is reduced. Consequently, we expect the excess half–width of the (0,2) mode to increase to a maximum, at a moderate pressure, as the overlap with the (3,1) mode becomes more significant due to line broadening, as the pressure is reduced, with the excess tending towards zero as the pressure is reduced further since the signal intensity of the (3,1) mode falls off with pressure more rapidly than that of the (0,2). All things considered, the half–widths are satisfyingly small and the absence of significant residual trends after analysis for $\tau\rho$ indicates that the estimates should be reliable and the resulting correction to the frequencies, due to dispersion, extremely good.

Deviations of the individual modes from the mean at a given state are shown in figure 5.47 for the isotherm at 250 K. As expected from the $\Delta g/f$ the (0,5) mode is seriously perturbed by a shell resonance. Since the deviation from the mean is negative this implies that the shell resonance is at a higher frequency than the acoustic mode.

a)

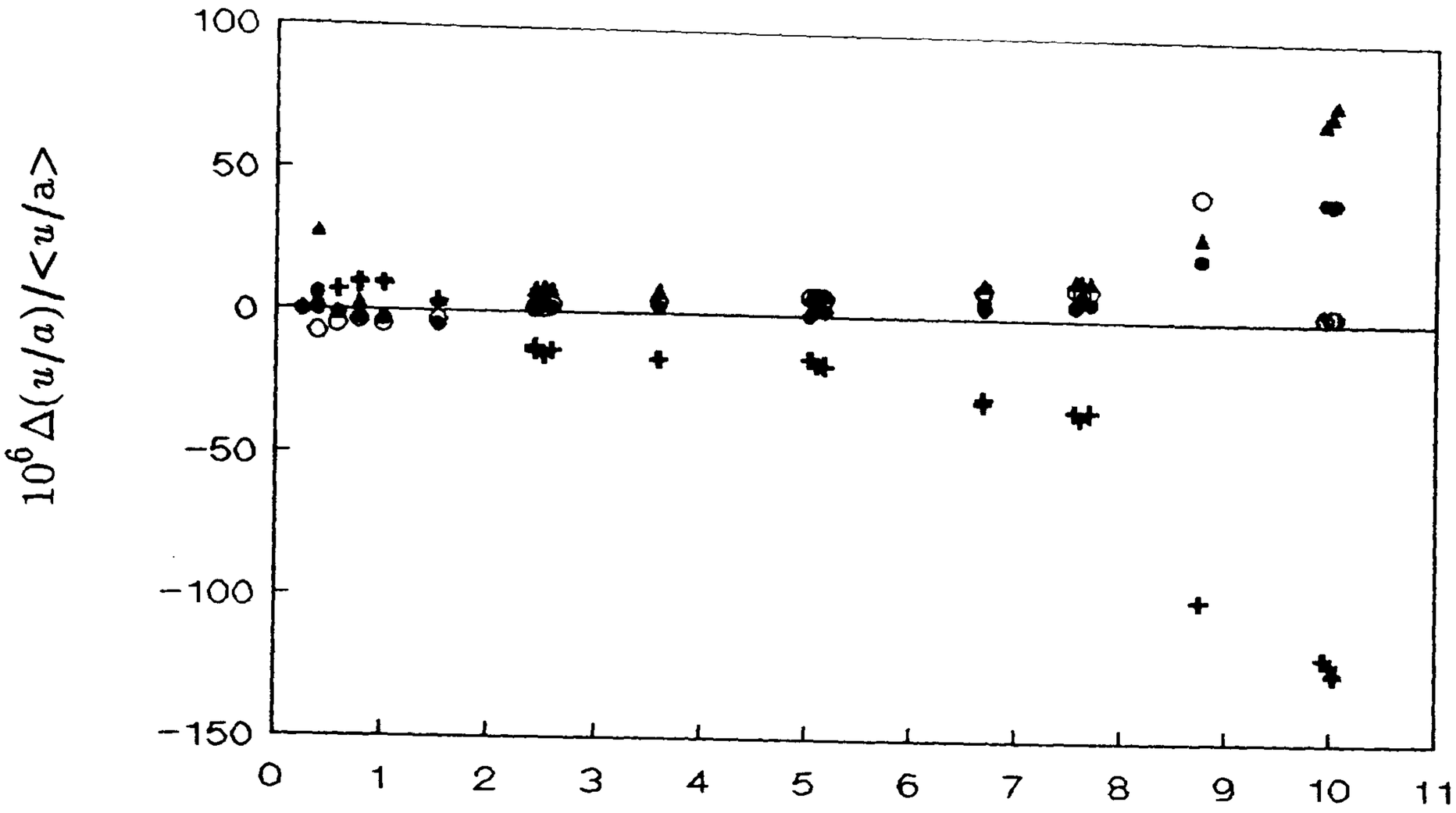

b)

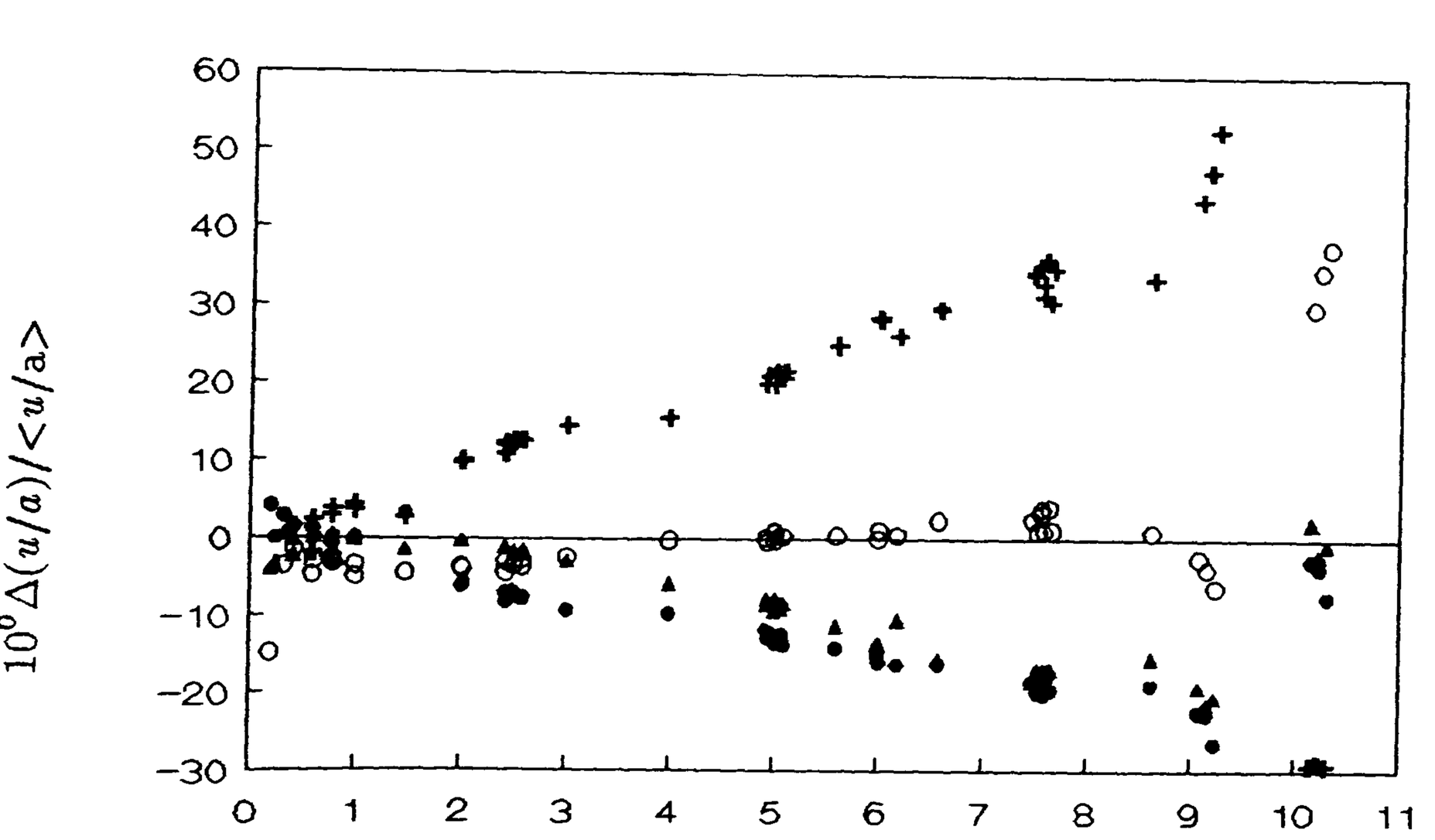

p/MPa

Figure 5.47: Fractional deviations of (u/a) for individual modes in methane from $<u/a>$ of the modes finally selected. a) 250 K, b) 275 and 275.1 K.

• , (0,2); ▲ , (0,3); ∘ , (0,4); + , (0,5).

a)

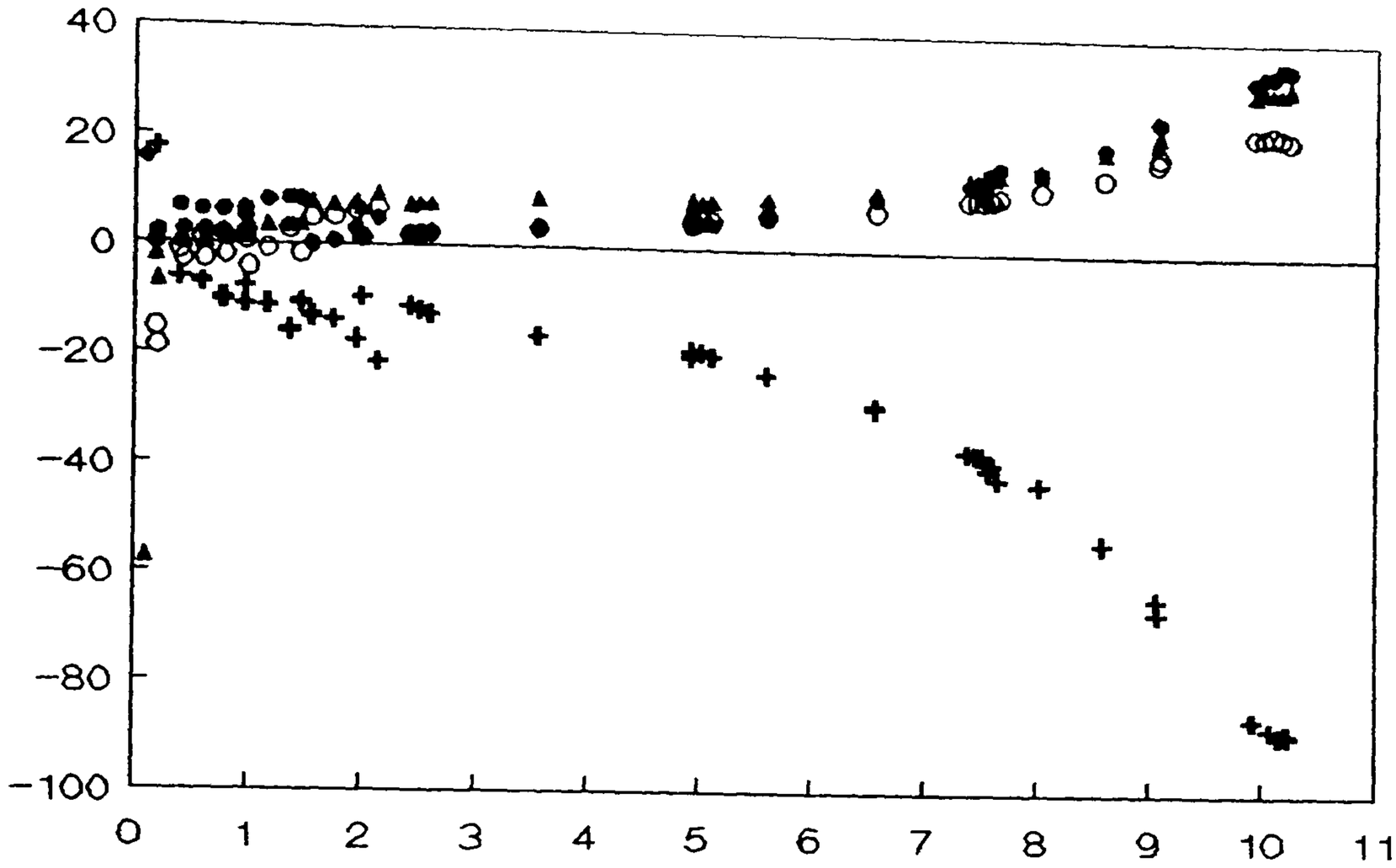

b)

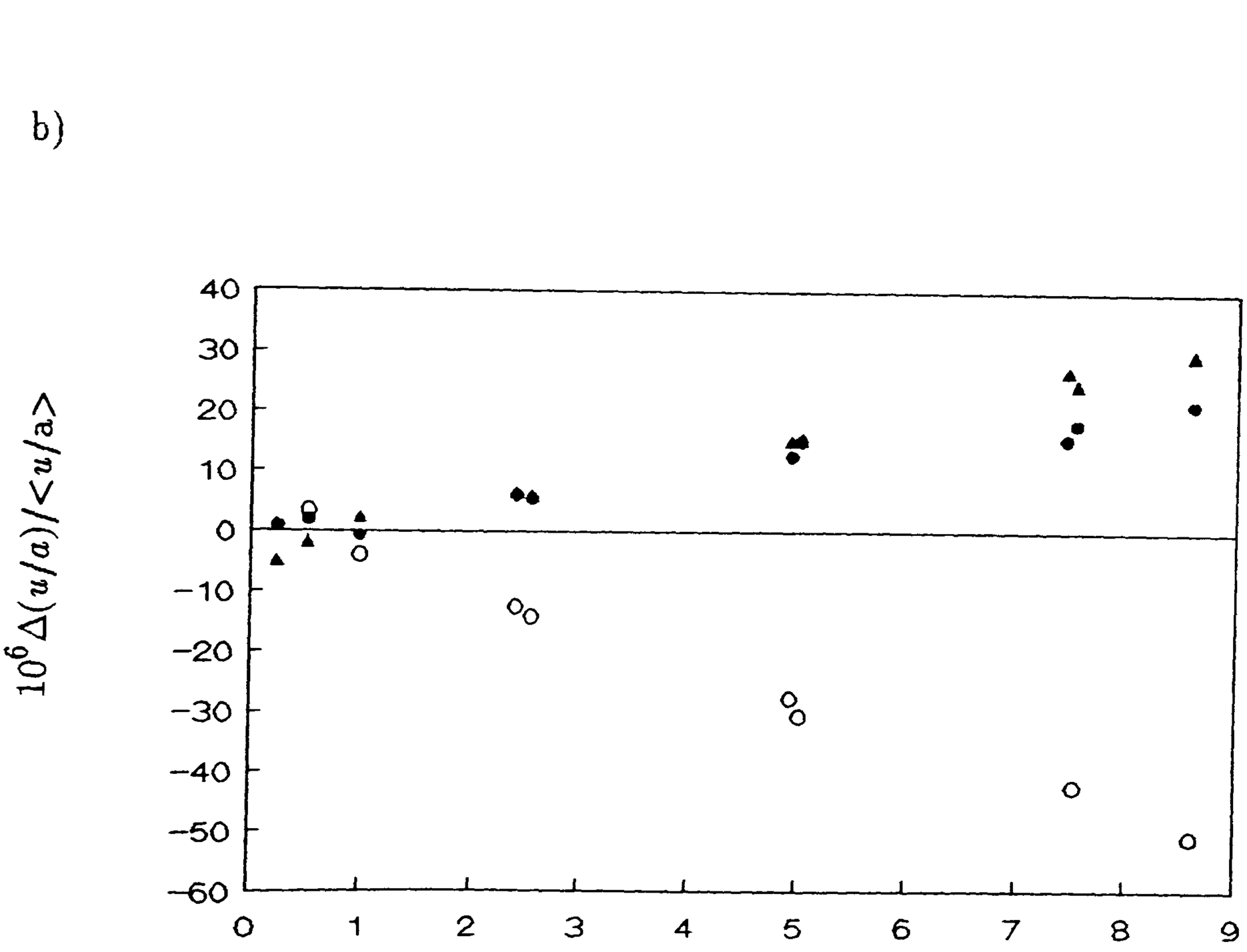

Figure 5.48: Fractional deviations of (u/a) for individual modes in methane from $<u/a>$ of the modes finally selected. a) 299 and 300 K, and b) 349 K.

• , (0,2); ▲ , (0,3); ∘ , (0,4); + , (0,5).

The perturbation is a maximum at the highest pressure where the deviation reaches about 125 ppm. The perturbation tends to zero as the pressure is reduced, as expected. The remaining modes agree to better than 50 ppm across the whole range. At pressures below 9 MPa the agreement is better than 20 ppm and is usually better than 10 ppm.

The deviations of the individual (u/a) from the mean for the two isotherms at 275 K are considered together and shown in figure 5.47. Again the (0,5) mode is seriously perturbed by shell motion but, since the sign of the perturbation is reversed, the shell resonance is at lower frequency than the acoustic mode. The maximum deviation from the mean is about 55 ppm. Exclusion of this mode brings the agreement to about 30 ppm at the highest pressures and at pressures below 8 MPa to better than 20 ppm. It is pleasing to note that the two isotherms show almost coincidental behaviour for the acoustic modes in terms of ordering and magnitude of deviations from the mean at a given state.

At temperatures near 300 K the isotherms are considered together and the deviations of the (u/a) from the mean are shown in figure 5.48. The (0,5) mode is perturbed by a shell resonance at higher frequency than the acoustic resonance. The deviation has a maximum of about 90 ppm at the highest pressure. The remaining modes agree to better than 20 ppm across the whole range and usually better than 10 ppm.

At 350 K deviations of the (u/a) are shown in figure 5.48. The (0,4) mode appears to be perturbed by a shell resonance. The maximum deviation reaches –50 ppm at 8.6 MPa. The remaining modes agree to better than about 10 ppm across the whole range.

In figure 5.49 we show the speed of sound in methane as a function of temperature and pressure. As can be seen, a minimum occurs in each isotherm reflecting the fact that p extends to sufficiently high pressures that the compression factor, Z, becomes greater than unity. The (u/a) finally selected for analysis were accommodated by up to six terms in the infinite series (5.2.3). All coefficients were significant at a probability of 0.999. The (A_i/a^2) determined in this analysis are given in table 5.17 along with the

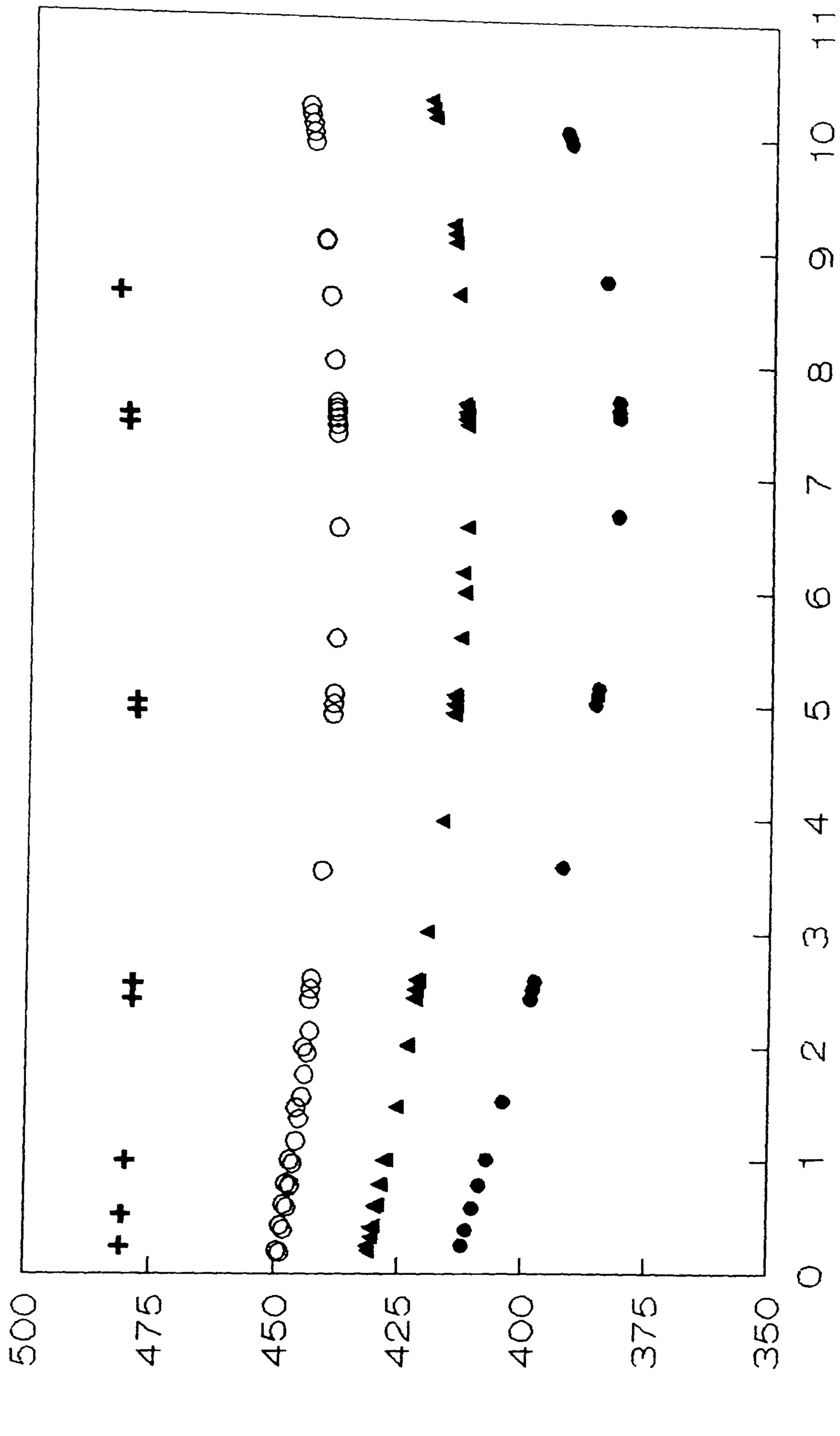

$_{1}$-s · m/n

Figure 5.49: Speed of sound, u, as a function of pressure, p, in methane at various temperatures.

• , 250 K; ▲ , 275 K; ∘ , 300 K; + , 349 K.

Table 5.16: Coefficients of equation (5.2.3) required to represent measurements of (u/a) in methane with standard deviation σ at temperatures T.

T/K	i	$\{A_i/a^2\}$/s^{-2}·Pa^{-i}	T/K	i	$\{A_i/a^2\}$/s^{-2}·Pa^{-i}
249.977		$10^6\sigma(u^2)/u^2 = 11.3$	274.974		$10^6\sigma(u^2)/u^2 = 8.4$
	0	$(84.6525 \pm 0.0010)\cdot 10^6$		0	$(92.43804 \pm 0.00053)\cdot 10^6$
	1	-0.2678 ± 0.0022		1	-1.96177 ± 0.00083
	2	$(0.644 \pm 0.014)\cdot 10^{-7}$		2	$(0.6846 \pm 0.0035)\cdot 10^{-7}$
	3	$(0.291 \pm 0.036)\cdot 10^{-14}$		3	$(0.4464 \pm 0.0052)\cdot 10^{-14}$
	4	$(0.610 \pm 0.040)\cdot 10^{-21}$		4	$(0.2726 \pm 0.0025)\cdot 10^{-21}$
	5	$(0.287 \pm 0.016)\cdot 10^{-28}$			
275.098		$10^6\sigma(u^2)/u^2 = 6.3$	298.885		$10^6\sigma(u^2)/u^2 = 5.8$
	0	$(92.21866 \pm 0.00029)\cdot 10^6$		0	$(99.74893 \pm 0.00063)\cdot 10^6$
	1	-1.95013 ± 0.00049		1	-1.4314 ± 0.0020
	2	$(0.70700 \pm 0.0038)\cdot 10^{-7}$		2	$(0.680 \pm 0.019)\cdot 10^{-7}$
	3	$(0.4015 \pm 0.0038)\cdot 10^{-14}$		3	$(0.508 \pm 0.055)\cdot 10^{-14}$
	4	$(0.2924 \pm 0.0021)\cdot 10^{-21}$			
300.000		$10^6\sigma(u^2)/u^2 = 7.4$	348.762		$10^6\sigma(u^2)/u^2 = 12.8$
	0	$(100.07154 \pm 0.00043)\cdot 10^6$		0	$(114.2111 \pm 0.0011)\cdot 10^6$
	1	-1.41384 ± 0.00059		1	-0.6346 ± 0.0012
	2	$(0.7183 \pm 0.0023)\cdot 10^{-7}$		2	$(0.6984 \pm 0.0033)\cdot 10^{-7}$
	3	$(0.3875 \pm 0.0033)\cdot 10^{-14}$		3	$(0.1784 \pm 0.0025)\cdot 10^{-14}$
	4	$(0.653 \pm 0.015)\cdot 10^{-22}$			

number of modes, N, in the final regression and the fractional standard deviation for the isotherm. The deviations of $<u/a>$, for the selected modes, from the finally adopted smoothing equations are shown in figures 5.50 and 5.51. A typical standard deviation for an isotherm is less than 10 ppm with the majority of state points being within 7 ppm of the smoothing equation.

The perfect–gas heat capacities determined from A_0/a^2 are given in table 5.16. Values of a^2 were calculated using $a(T,\ p\to 0)$ determined from the measurements in

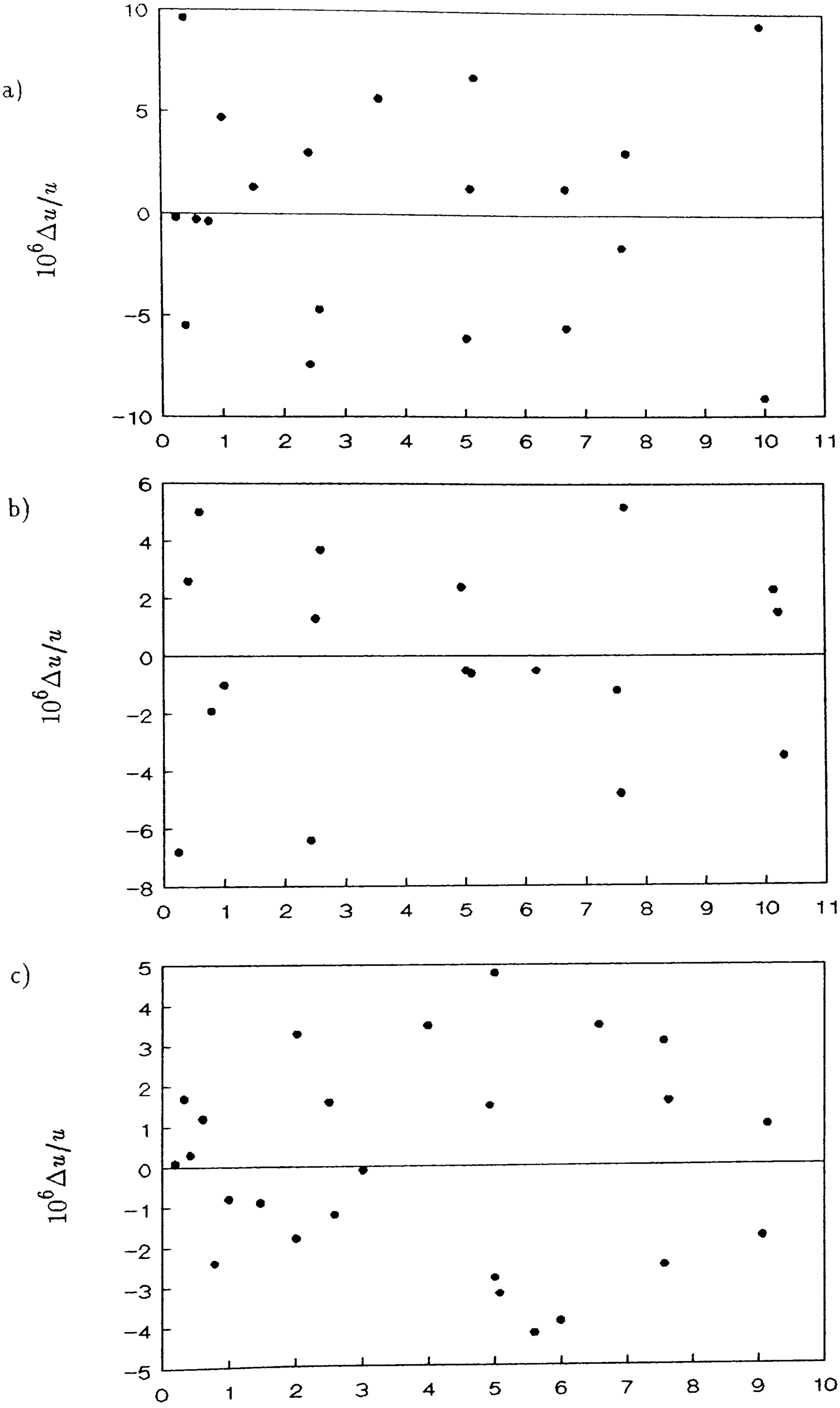

Figure 5.50: Fractional deviations of $<u/a>$ for the selected modes ffrom the adopted smoothing equation; a) 250 K, b) 275 K and c) 275.1 K.

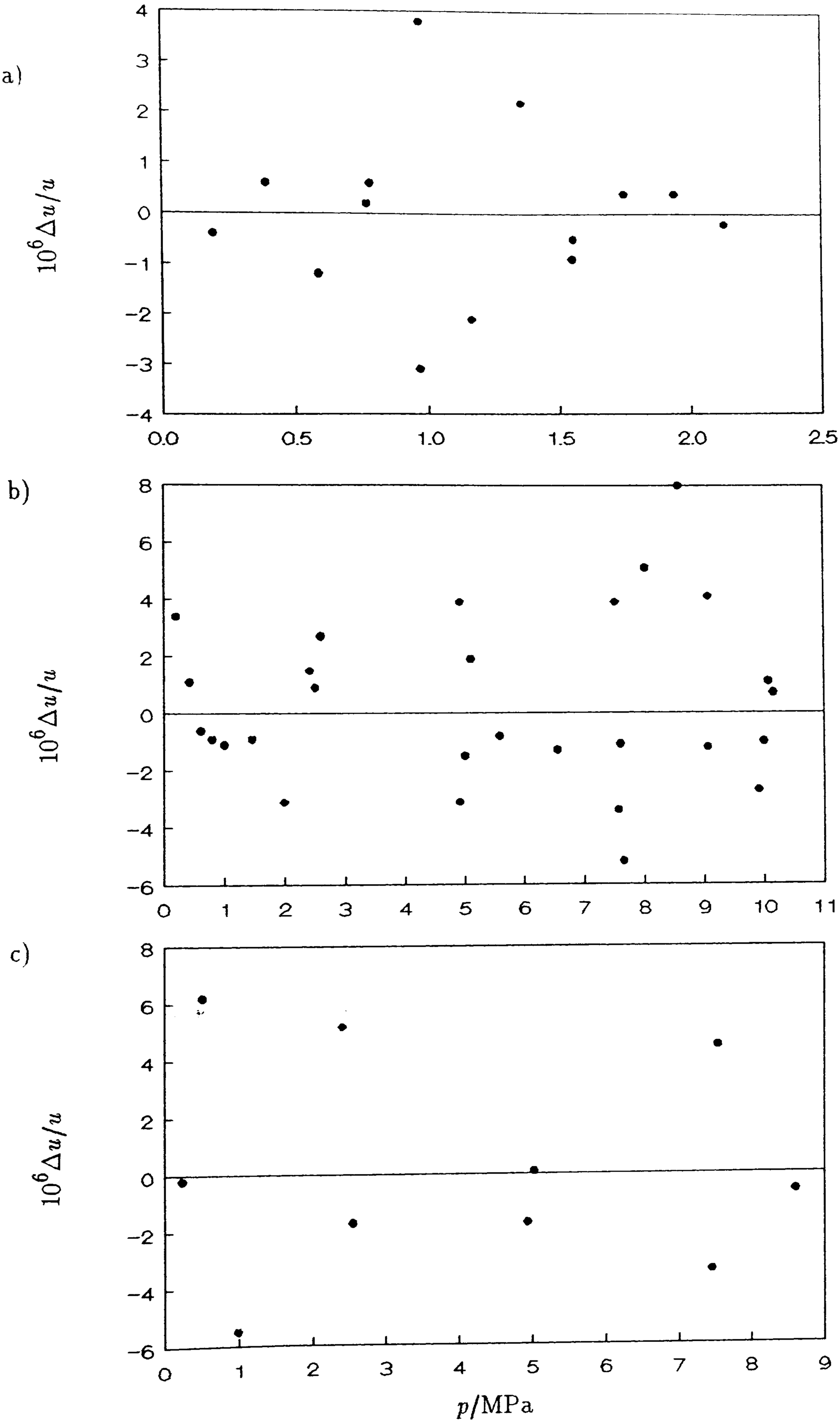

Figure 5.51: Fractional deviations of $<u/a>$ for the selected modes ffrom the adopted smoothing equation; a) 299 K, b) 300 K and c) 349 K.

Table 5.17: Perfect–gas heat capacities and second acoustic virial coefficients for methane at temperatures T. Second virial coefficients represented by equation (5.4.9).

T/K	$C^{pg}_{p,m}/R$	β_a/cm^3·mol^{-1}	B/cm^3·mol^{-1}
249.977	4.12039 ± 0.00030	–65.740 ± 0.053	–65.68
274.974	4.20052 ± 0.00016	–48.499 ± 0.020	–52.25
275.098	4.24491 ± 0.00009	–48.369 ± 0.012	–52.19
298.885	4.29654 ± 0.00018	–35.597 ± 0.050	–41.66
300.000	4.30291 ± 0.00012	–35.241 ± 0.015	–42.09
348.762	4.55815 ± 0.00033	–16.113 ± 0.032	–26.43

argon. The values so determined are compared with the results of Ewing and Goodwin[5] and the calculated values of 82. The calculated values rely entirely on spectroscopic information and include the effects of anharmonicity, vibration–rotation coupling and centrifugal distortion. The spectroscopic values were fit to a function determined using the adaptive regression algorithm and comparison of the calculated and experimental values are based on deviations from this equation. Deviations are shown in figure 5.52. As can be seen the calculated values show a systematic undulation from this equation indicating that the functional form is not entirely suitable; for purposes of comparison with the experimental determinations this is inconsequential. The results determined in this work show excellent agreement if the value at 275.098 K, which is adversely affected by sample purity, is neglected. In particular, the result at 300 K differs from the calculated value by only 0.00009 R (or 21 ppm) which is within experimental error. The low temperature results of Ewing and Goodwin are in good agreement but the higher temperature results deviate considerably. Since the samples are likely to be of similar purity the difference is ascribed to imperfect knowledge of the resonator radius in the high temperature measurements of Ewing and Goodwin.

The acoustic virial coefficients determined from A_1/a^2 are given in table 5.16. Comparison with previous determinations, and extraction of (p, V_m, T) virial coefficients from the acoustic coefficients, is by means of regression analysis using the

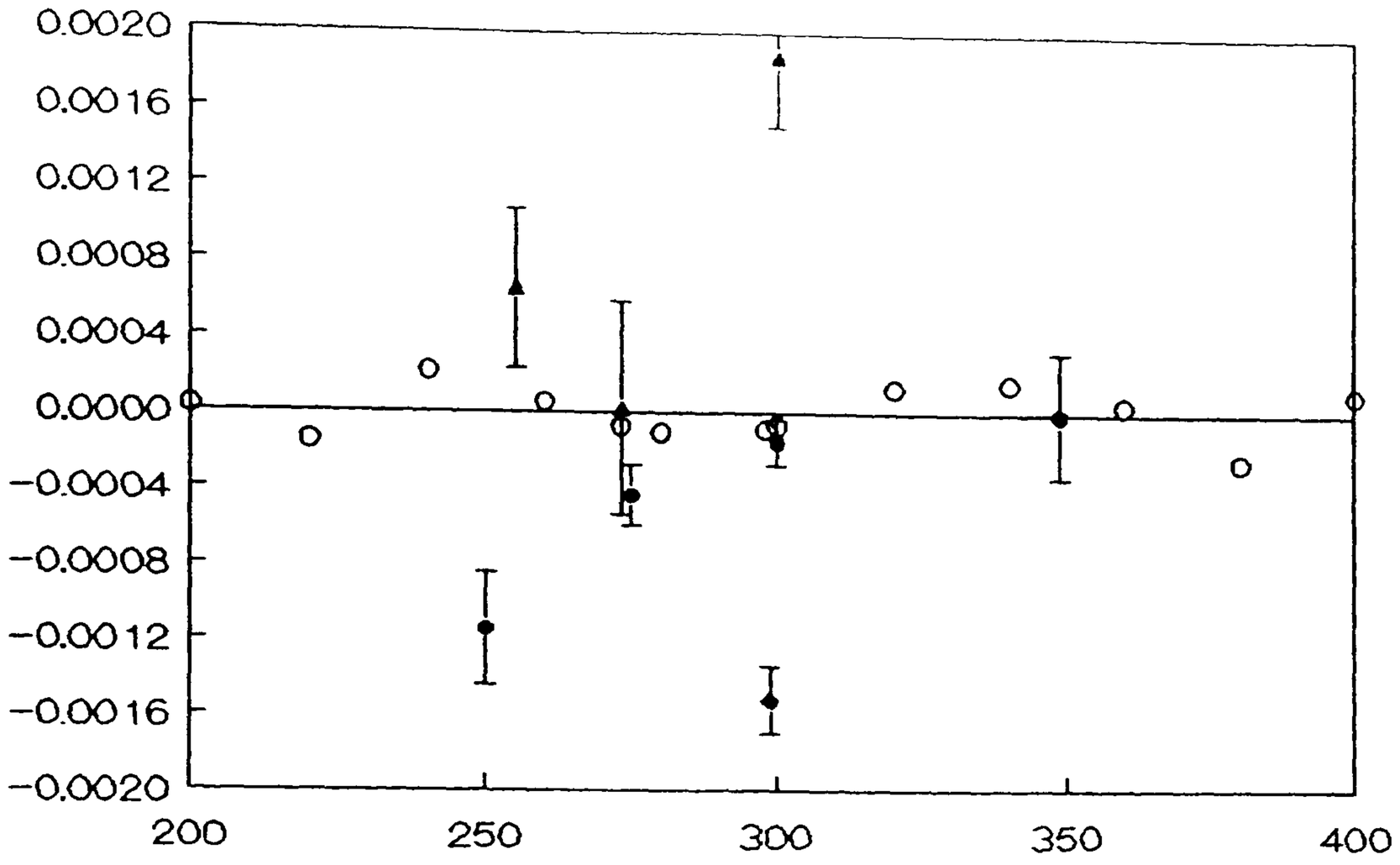

Figure 5.52: Deviatioons $\Delta C_{p,\mathrm{m}}^{\mathrm{pg}} = \{C_{p,\mathrm{m}}^{\mathrm{pg}}(\mathrm{exp.}) - C_{p,\mathrm{m}}^{\mathrm{pg}}(\mathrm{calc.})\}$ of experimental perfect–gas heat capacities at constant pressure from a smoothing equation determined from the calculated values of reference 82. • , this work; o , reference 82; ▲ , reference 5.

---

square–well and power series in T solutions to equation (3.2.15). The experimental determinations of $C_{p,\mathrm{m}}^{\mathrm{pg}}$ were used in conjunction with the acoustic virial coefficients. Weighted non–linear analysis of the experimental β_{a} with γ^{pg} and the square–well function yielded

$$B/(\mathrm{cm}^3\cdot\mathrm{mol}^{-1}) = 158.34 - 113.486\,\exp(170\ \mathrm{K}/T) \qquad (5.4.8)$$

which fit the results with a weighted standard deviation of 0.12 $\mathrm{cm}^3\cdot\mathrm{mol}^{-1}$ (about 0.2 % at 273 K).

The alternative polynomial solution was given by

$$B/(\mathrm{cm}^3\cdot\mathrm{mol}^{-1}) = 39.909 - 0.1446 \times 10^5(\mathrm{K}/T) - 0.3044 \times 10^7(\mathrm{K}/T)^2 \qquad (5.4.9)$$

which also fit the results with a weighted standard deviation of 0.12 $\mathrm{cm}^3\cdot\mathrm{mol}^{-1}$.

In figure 5.53 the experimental β_{a} are shown as deviations from equation (5.4.8) and (3.2.15). With the exclusion of the datum at 350 K, the previous acoustic determinations of Ewing and Goodwin[5] agree extremely well with these

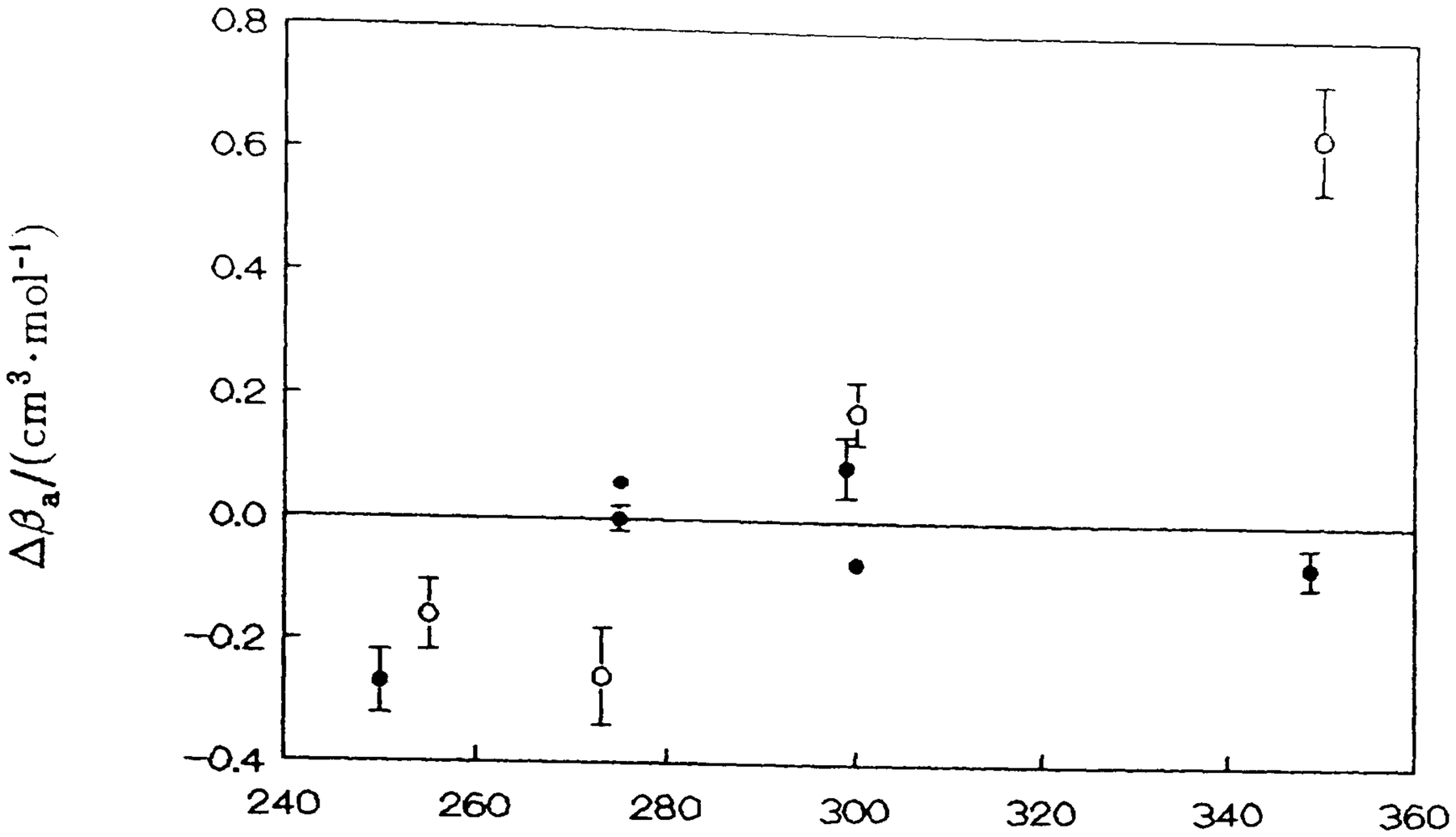

Figure 5.53: Deviations $\Delta\beta_a = \{\beta_a(\text{exp.}) - \beta_a(\text{calc.})\}$ of the experimental β_a from equation (5.4.8) and (3.2.15). • , this work; ∘ , reference 5.

---

results. The maximum difference is just 0.25 $cm^3 \cdot mol^{-1}$ (about 2.5 combined standard deviations) and at temperatures near 300 K the results agree to within experimental error. The value quoted by Goodwin at 350 K is suspected to be in error since the radius of the resonator was not determined at this temperature and problems with transducer stability compromised the results.

Deviations of the polynomial representation for B from equation (5.4.8) are shown in figure 5.54. The agreement between the two solutions is good with the worst deviation being about 1 $cm^3 \cdot mol^{-1}$ at the lowest temperature. At higher temperatures the two solutions converge initially, to give essentially the same answer, and then diverge to a difference of about 0.5 $cm^3 \cdot mol^{-1}$ at 650 K. On average, the difference between the two solutions to (3.2.15) is about 0.5 $cm^3 \cdot mol^{-1}$. Also shown in figure 5.54 are the second virial coefficients reported by other workers plotted as deviations from equation (5.4.8). It is immediately apparent that the agreement with the present results is excellent. In particular, the precise determinations of Douslin *et al*[84] differ from (5.4.8) by only 0.5 $cm^3 \cdot mol^{-1}$ over a temperature range of 400 K. The two sets of results reported by Wagner *et al*[65,83] also deviate by just 0.5 $cm^3 \cdot mol^{-1}$ from (5.4.8).

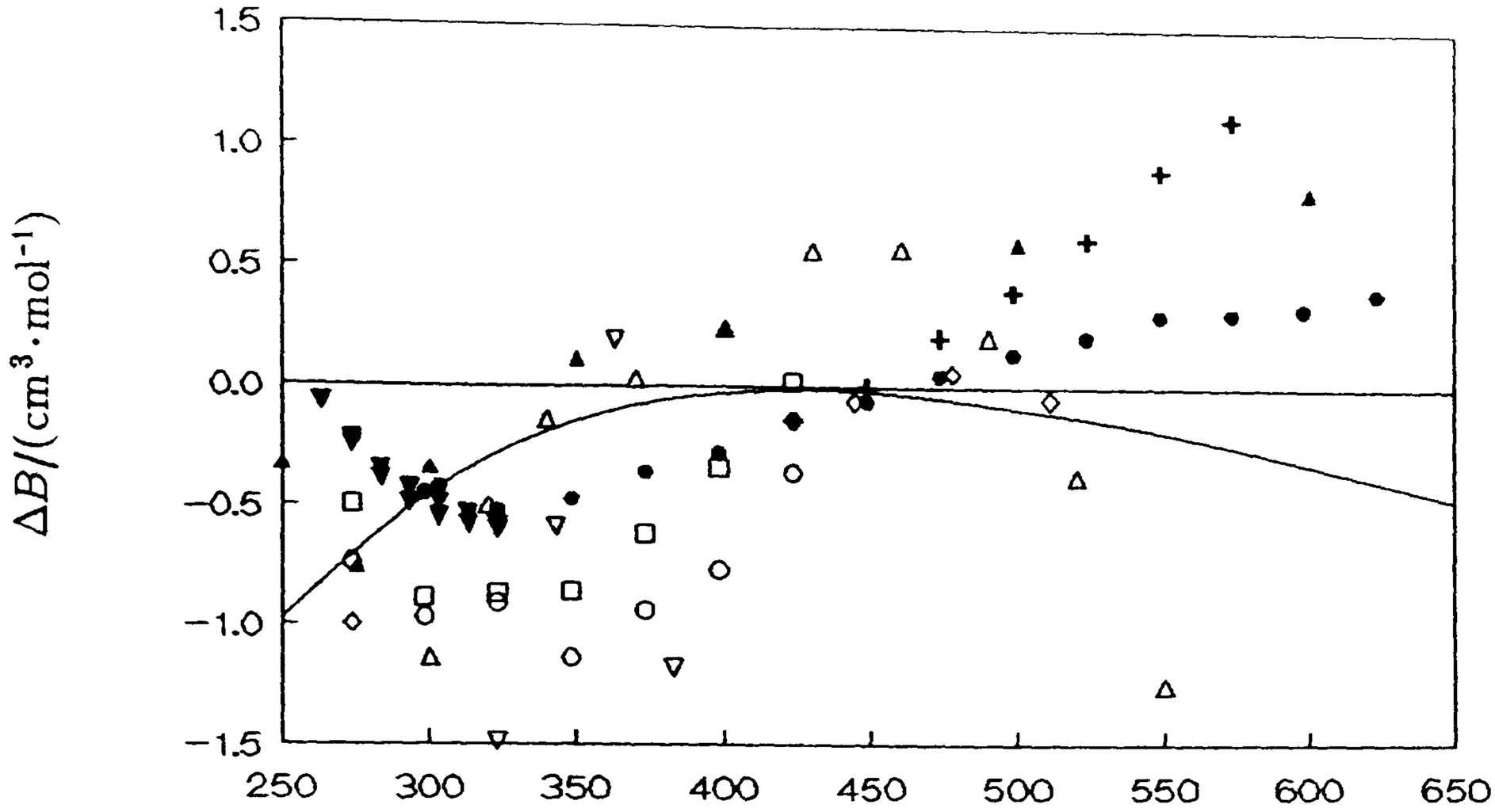

Figure 5.54: Deviations $\Delta B = \{B(\text{exp.}) - B(\text{calc.})\}$ of experimental second virial coefficients from equation (5.4.8). ————, polynomial in T (5.4.9); ▲ , reference 22; ▼ , reference 65 and 83; ● , reference 84; ○ , reference 85; + , reference 86; ▽ , reference 87; □ , reference 88; ◇ , reference 89; △ , reference 90.

If the average difference between the alternative solutions, about 0.5 $cm^3 \cdot mol^{-1}$, is regarded as an estimate of the likely systematic error associated with the imposition of a functional form for B, then (5.4.8) and the results of Wagner *et al* and Douslin *et al* are seen to be in agreement. The values recommended by Dymond and Smith[22] deviate by as much as 30 $cm^3 \cdot mol^{-1}$ below 250 K but, at temperatures above 250 K, agree with (5.4.8) to within the given error estimates. With the exclusion of the result at 273 K the values determined by Gunn[89] agree with (5.4.8) to better than 0.1 $cm^3 \cdot mol^{-1}$. The results of Michels *et al*[85] and Schamp *et al*[88] are initially too negative, by about 1 $cm^3 \cdot mol^{-1}$, but converge with (5.4.8) at higher temperatures. By contrast, the results of Beattie *et al*[86] diverge linearly from (5.4.8), the maximum deviation being about 1.2 $cm^3 \cdot mol^{-1}$ at 573 K. The results of Hamann *et al*[87] show significant scatter and the maximum difference reaches about 3 $cm^3 \cdot mol^{-1}$. The results

of Schramm and co–workers[90] agree with (5.4.8) to about 1 $cm^3 \cdot mol^{-1}$ but appear to contain a systematic error. In summary, the agreement of previous determinations with (5.4.8) are extremely good and again this illustrates the extraordinary precision with which virial coefficients may be estimated using acoustic techniques.

5.4.8: $\{(1-x)CH_4 + xC_2H_6\}$; $x = 0.15$.

The methane–ethane mixture has been studied at four temperatures between 250 and 350 K at pressures below 10 MPa. Experimentally determined frequencies were corrected as outlined in Chapter 2. The required transport properties were estimated from a package developed at NIST. Virial coefficients required in the various correction terms were estimated from a preliminary analysis of the results. In table 5.18 we list the mean quantity (u/a) determined from the N modes together with u and the standard deviation of the mean, σ. Also quoted are the deviations, δ, of the mean from the finally adopted smoothing equation. Small corrections have been applied to reduce all values of (u/a) to the stated temperature of each isotherm.

As with the previous measurements made at pressures up to 10 MPa the dominant correction at pressures greater than 1.5 MPa was that due to shell motion. This correction varied from 170 ppm for the (0,4) mode at 350 K and 10 MPa to 20 ppm for the (0,2) mode at 250 K and 1.1 MPa. Below 1.1 MPa the corrections were dominated by the thermal boundary layer.

Analysis of the excess half–widths in terms of the vibrational relaxation time and its density dependence yielded values of $\tau\rho$ and $\partial(\tau\rho)/\partial\rho$ as given in table 5.19. These values were then used to correct the frequencies for the small amount of dispersion which occurs at audio–frequencies. If we compare the values of $\tau\rho$ determined for the mixture with those determined for pure methane, we see that ethane is an efficient catalyst for the equilibration of energy throughout the available degrees of freedom. The time constant for the process is decreased by a factor of 300 at 350 K and 1000 at 250 K. No significance is attached to the value of $\tau\rho$ so determined. The excess half–widths, after allowance for vibrational relaxation, are shown in figures 5.55 and

Table 5.18: Mean values of (u/a) and u with standard deviations σ determined from N modes, with deviations δ from equation (5.2.3) at temperatures T and pressures p. The coefficients of equation (5.2.3) are given in table 5.20.

$\frac{T}{\mathrm{K}}$	$\frac{p}{\mathrm{kPa}}$	N	$\frac{u}{a}\cdot\mathrm{s}$	$\frac{u}{\mathrm{m}\cdot\mathrm{s}^{-1}}$	$\frac{10^6\sigma(u)}{u}$	$\frac{10^6\delta(u)}{u}$
249.806	9644.31	2	7874.2656	353.9852	3.9	–0.2
	9568.68	2	7844.1163	352.6298	5.0	(a)
	8696.52	2	7574.7882	340.5223	4.6	(a)
	7588.96	2	7427.8509	333.9167	5.3	–9.8
	7585.44	2	7427.8509	333.9167	5.3	11.6
	7489.38	2	7424.0625	333.7464	0.0	2.3
	7420.28	2	7424.0636	333.7465	0.1	(a)
	6030.69	2	7486.8072	336.5671	0.5	–15.6
	6021.25	2	7489.4370	336.6853	3.2	(a)
	5103.90	2	7606.3326	341.9403	0.4	(a)
	5011.89	2	7619.8975	342.5501	1.1	22.1
	3529.58	2	7873.7684	353.9628	1.3	–13.9
	2563.30	2	8057.3836	362.2172	1.3	–8.8
	2471.43	3	8075.3455	363.0247	4.6	6.8
	1115.94	3	8342.1867	375.0204	2.5	5.9
	781.43	3	8408.2935	377.9922	2.0	12.6
	598.63	3	8443.9694	379.5960	5.5	–18.3
	406.29	3	8481.4038	381.2789	1.9	(a)
	186.00	3	8524.3735	383.2106	1.5	–11.7
	98.40	3	8541.4537	383.9784	1.0	13.5
274.756	9955.17	2	8357.0841	375.8376	7.2	–12.1
	9883.86	2	8346.8759	375.3785	6.5	13.1
	9790.20	2	8334.1133	374.8045	6.0	(a)
	8613.33	2	8222.5813	369.7887	1.6	(a)
	7688.67	2	8193.3292	368.4731	2.1	–7.0
	7607.22	2	8193.0215	368.4593	0.9	2.0
	7424.64	2	8193.3239	368.4729	0.3	4.1
	6022.29	2	8241.4844	370.6388	3.7	–1.2
	5099.20	2	8310.3482	373.7358	0.4	(a)
	4974.85	2	8319.8796	374.1644	2.9	2.2
	3553.28	3	8467.0339	380.7823	3.3	(a)
	3552.28	3	8466.4836	380.7575	3.6	–0.3
	2588.17	3	8584.2514	386.0538	3.5	0.7
	2486.72	3	8597.2687	386.6392	3.7	–1.4
	1115.66	3	8782.2143	394.9567	4.0	–0.9
	787.92	3	8828.2865	397.0287	3.0	2.5
	599.19	3	8854.9590	398.2282	2.3	–4.6
	405.57	3	8882.6249	399.4724	1.6	6.5
	179.99	3	8914.8087	400.9198	1.7	–3.2
	99.38	3	8926.1081	401.4279	1.2	(a)
	99.35	2	8926.1134	401.4282	1.0	(a)

$\frac{T}{\mathrm{K}}$	$\frac{p}{\mathrm{kPa}}$	N	$\frac{u}{a}\cdot\mathrm{s}$	$\frac{u}{\mathrm{m}\cdot\mathrm{s}^{-1}}$	$\frac{10^6\sigma(u)}{u}$	$\frac{10^6\delta(u)}{u}$
299.750	10168.07	2	8921.0294	401.3584	2.5	–4.5
	10085.13	2	8913.9914	401.0418	2.1	1.9
	9987.85	2	8905.9842	400.6816	1.1	1.3
	8640.05	2	8828.8657	397.2120	1.4	7.3
	7642.12	2	8808.6148	396.3009	0.6	–0.4
	7555.82	2	8808.1487	396.2799	0.6	–6.6
	7475.33	2	8808.0028	396.2734	0.4	–0.2
	6057.90	2	8830.9826	397.3072	0.9	–4.4
	5118.74	2	8870.6748	399.0930	0.1	–1.2
	5111.56	2	8871.1116	399.1126	1.9	6.5
	5028.60	2	8875.3918	399.3052	1.8	1.2
	4951.21	2	8879.5282	399.4913	1.6	–0.1
	3555.87	3	8971.1677	403.6142	2.5	(a)
	3553.06	3	8971.4819	403.6283	1.9	(a)
	2585.56	3	9050.5976	407.1877	1.4	(a)
	2488.66	3	9058.9382	407.5630	1.4	1.1
	2403.02	3	9066.5361	407.9048	1.7	–0.8
	1036.71	3	9197.0391	413.7762	3.1	(a)
	790.84	3	9222.2509	414.9104	0.8	–8.5
	610.42	3	9241.0570	415.7565	1.9	4.5
	430.76	3	9259.8708	416.6030	1.3	4.1
	207.16	3	9283.5633	417.6689	4.1	3.9
	113.34	3	9293.4895	418.1155	3.6	–7.1
349.424	9140.79	3	9811.6015	441.7919	7.6	0.8
	9039.37	3	9807.5972	441.6116	6.3	0.5
	7573.47	3	9765.9038	439.7343	6.4	(a)
	7492.15	2	9764.6142	439.6762	4.7	–4.8
	5056.26	3	9760.4774	439.4900	6.8	–1.5
	2532.64	3	9825.4824	442.4170	3.5	3.5
	2448.96	3	9828.6371	442.5590	1.0	0.5
	1154.88	3	9885.1232	445.1024	1.3	–0.5
	669.59	3	9909.4317	446.1970	1.6	–12.2
	182.95	3	9935.7284	447.3811	0.8	9.0

5.56. As expected the $\Delta g/f$ are similar to those observed previously. With the exception of the isotherm at 250 K the $\Delta g/f$ never exceed 30 ppm and on average are always less than 10 ppm across the whole range. The isotherm at 250 K is significantly different from the others since at pressures greater than 5 MPa (where the partial pressure of ethane is 0.6 of the vapour pressure 250 K) the average $\Delta g/f$ increases steadily from about 5 ppm to a maximum, at approximately 8.7 MPa (where the partial pressure of ethane corresponds to the vapour pressure at 250 K), of about 30 ppm. This observation is consistent with precondensation occurring at pressures

a)

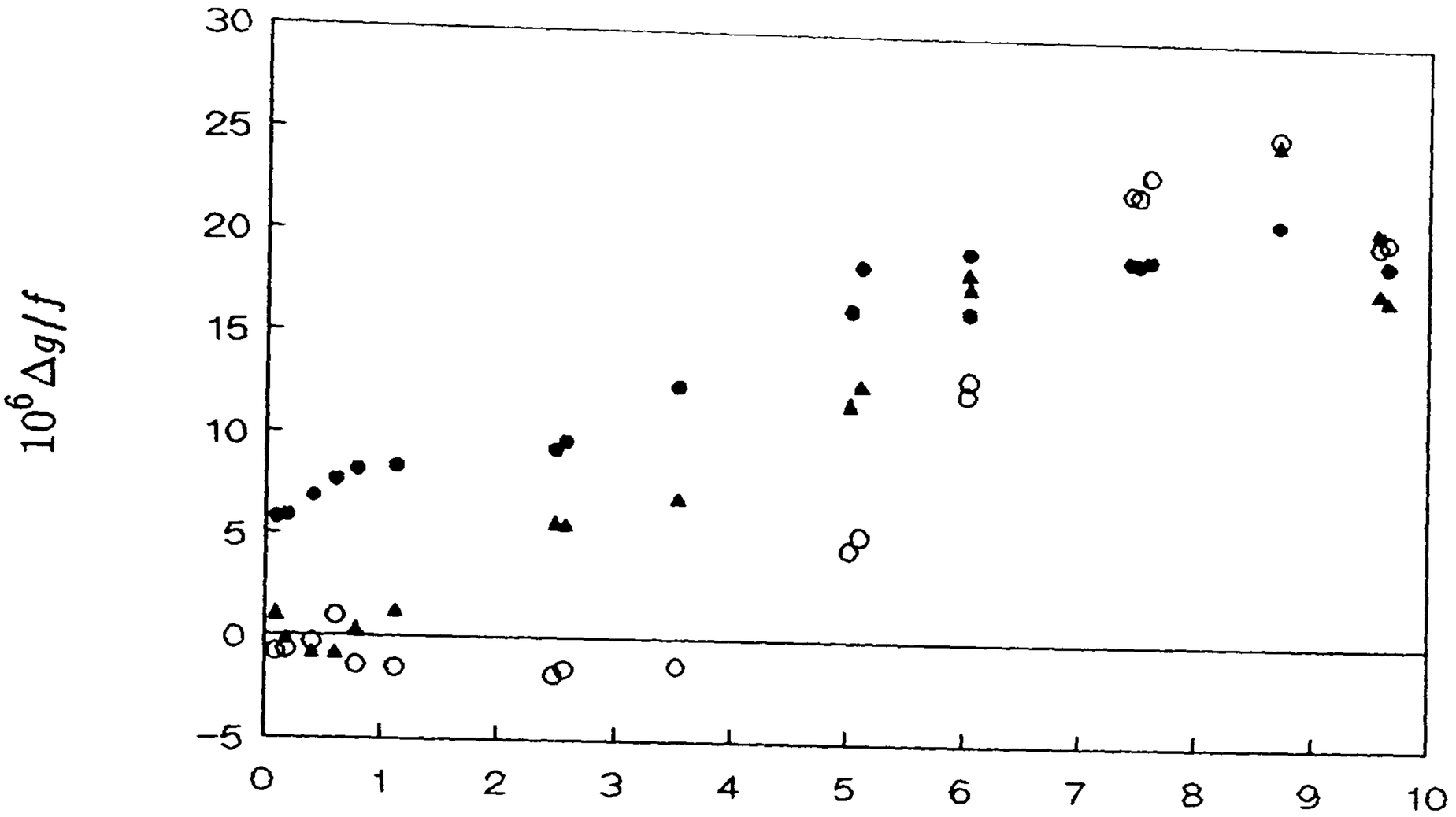

b)

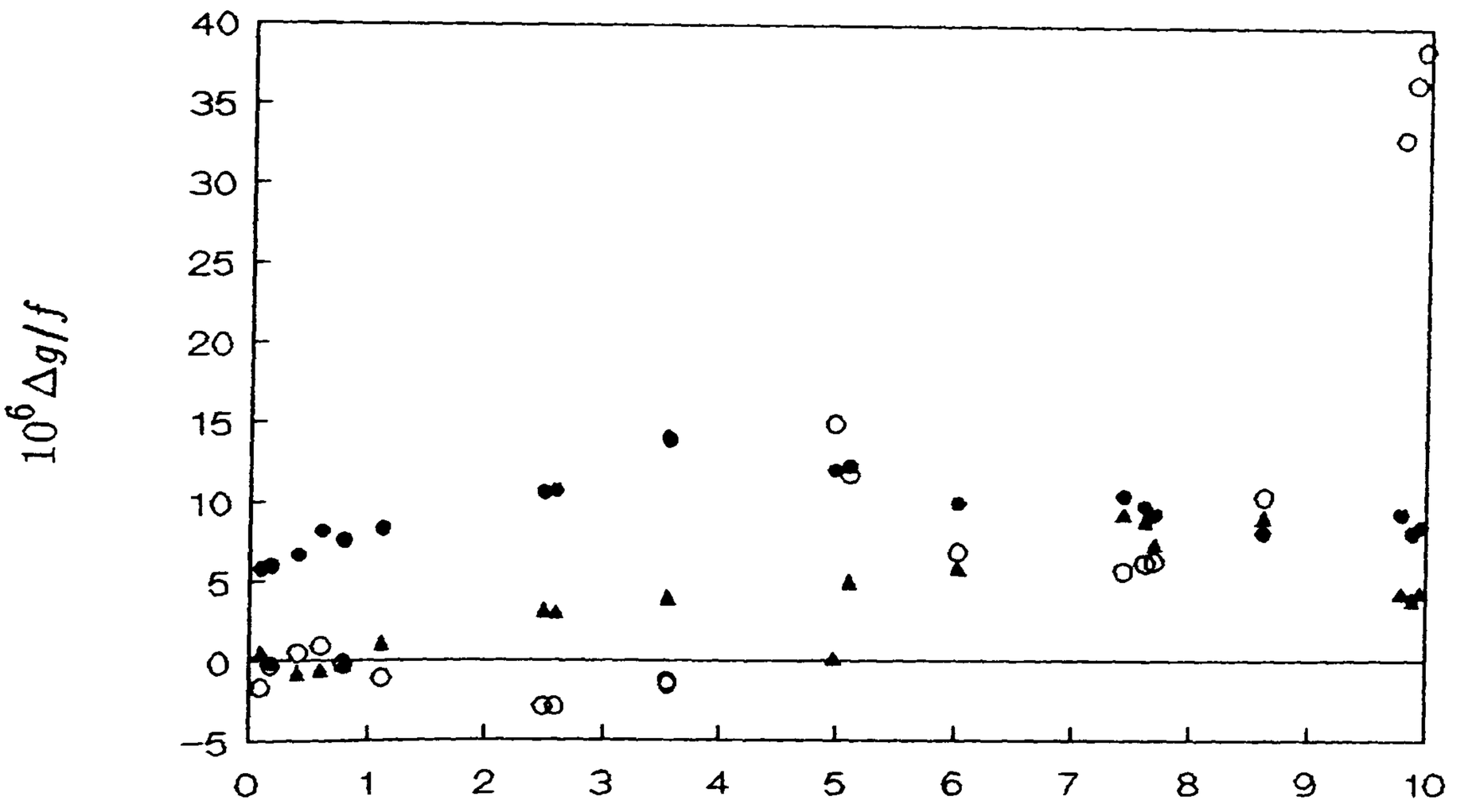

Figure 5.55: $\Delta g/f$, after allowance for vibrational relaxation, for the methane–ethane mixture at a) 250 and b) 275 K.

• , (0,2); ▲ , (0,3); ∘ , (0,4).

a)

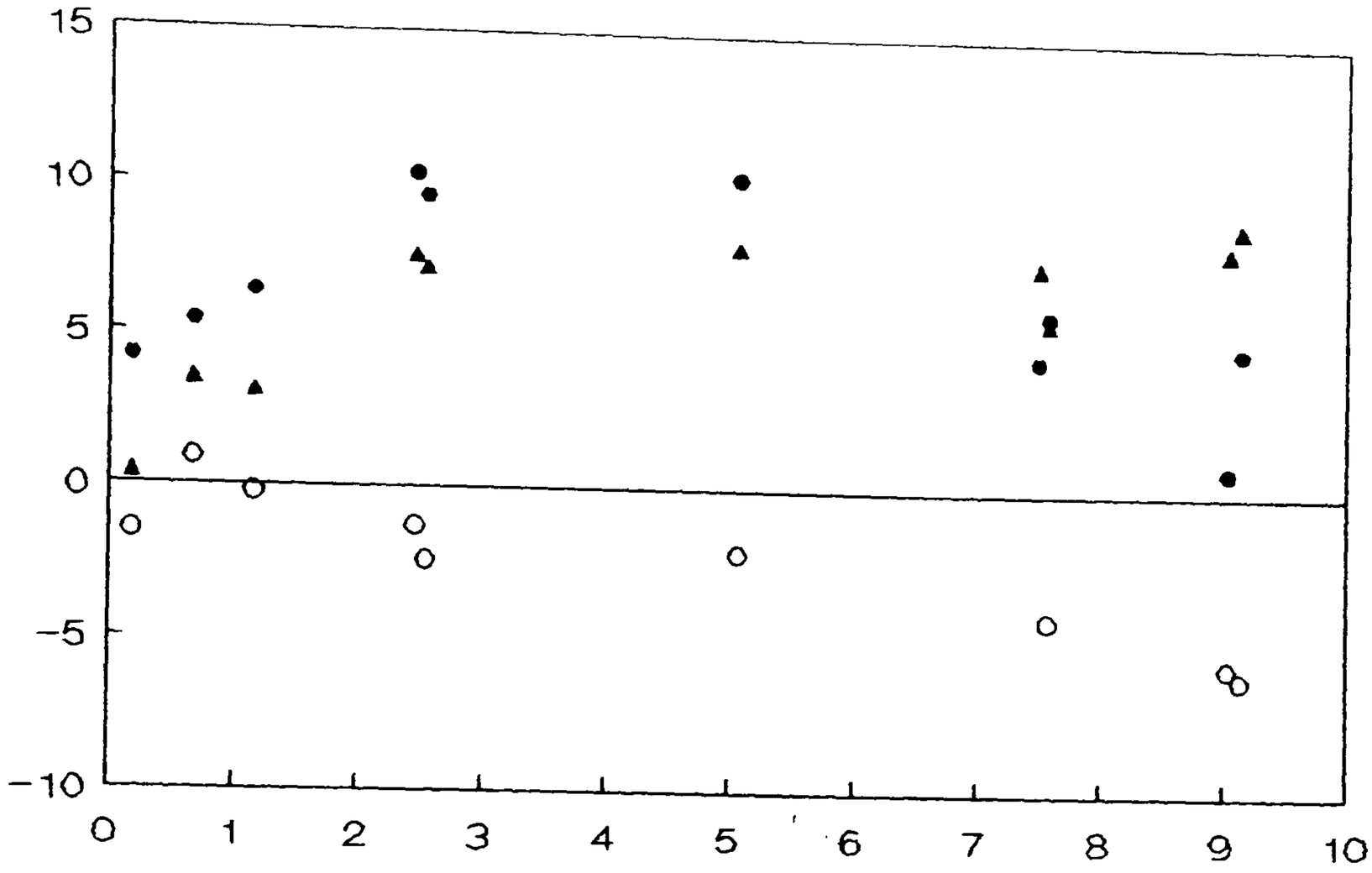

b)

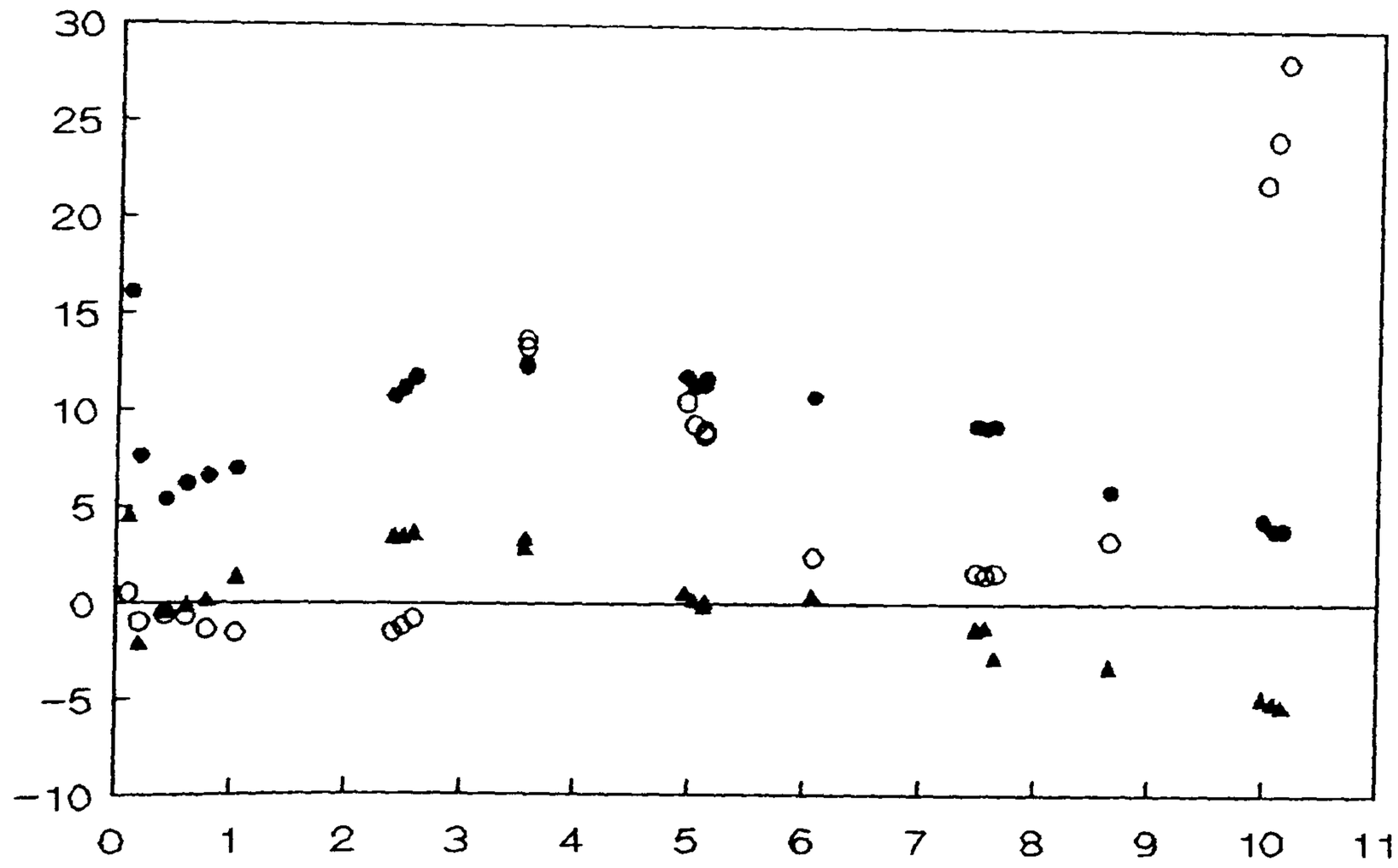

Figure 5.56: $\Delta g/f$, after allowance for vibrational relaxation, for the methane–ethane mixture at a) 300 and b) 350 K.

• , (0,2); ▲ , (0,3); ∘ , (0,4).

Table 5.19: Vibrational relaxation times, τ, for the methane–ethane mixture at a density of 1 $kg \cdot m^{-3}$ and density dependence of the product $\tau\rho$ at temperatures T.

T/K	$\tau\rho/(ns \cdot kg \cdot m^{-3})$	$\{\partial(\tau\rho)/\partial\rho\}_T$/ns
249.806	23.49 ± 1.75	13.25 ± 0.80
274.756	27.26 ± 1.11	10.07 ± 0.61
299.750	29.11 ± 1.17	7.92 ± 0.49
349.424	30.43 ± 1.63	4.18 ± 0.45

greater than 5 MPa (see below).

The deviations of the individual (u/a) from the mean at 250 K are shown in figure 5.57. The first three radial modes agree to better than 30 ppm across the whole range; at pressures below 5 MPa the agreement is generally better than 10 ppm. Exclusion of the (0,4) mode, which appears to be perturbed by a shell resonance, brings the agreement to better than 10 ppm across the whole range. As indicated above, precondensation is apparent at pressures greater than 5 MPa. This phenomenon affects the frequency measurements (and hence $\{u/a\}$), as well as the $\Delta g/f$, and manifests itself as a frequency dependent dispersion of the modes. This is not observed experimentally but, since the number of modes recorded is small, the frequency range of the measurements may too small to observe the effect when compared with other perturbations at the highest pressures. Therefore, it is proposed that the effect of precondensation on the frequency measurements is masked by other processes.

At 275 K deviations of the individual speeds of sound from the mean are shown in figure 5.57. Over the whole pressure range the agreement of the first three radial modes is better than 40 ppm. Again at pressures below 5 MPa the agreement is better than 10 ppm. The (0,4) mode is again perturbed by a shell resonance and removal of this mode brings the agreement to better than 10 ppm across the whole range.

At 300 K the deviations of the individual (u/a) from the mean are shown in figure 5.58. The first three radial modes agree to better than 40 ppm with the (0,4) mode again being perturbed by a shell resonance. Exclusion of this brings the agreement to

a)

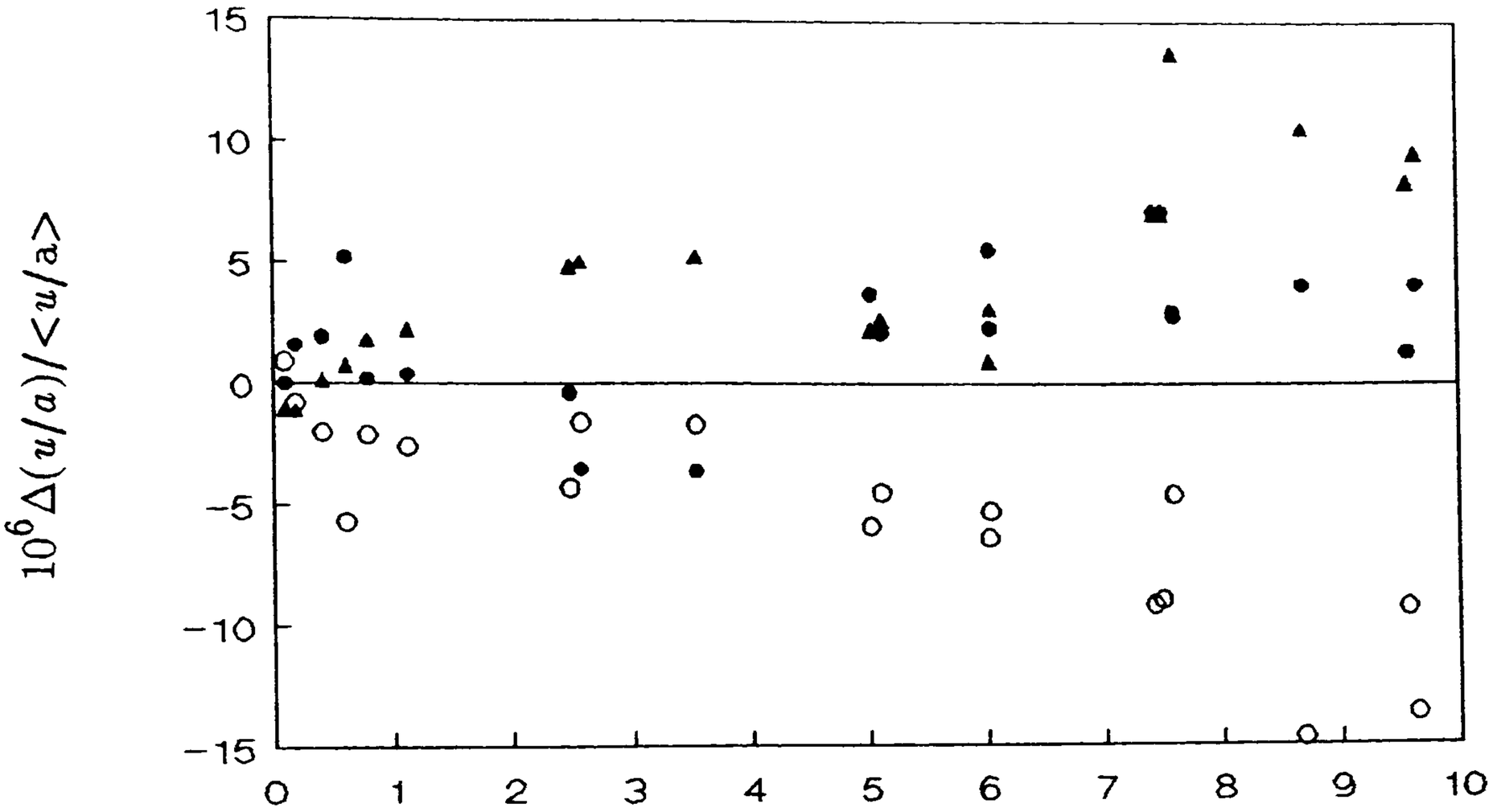

b)

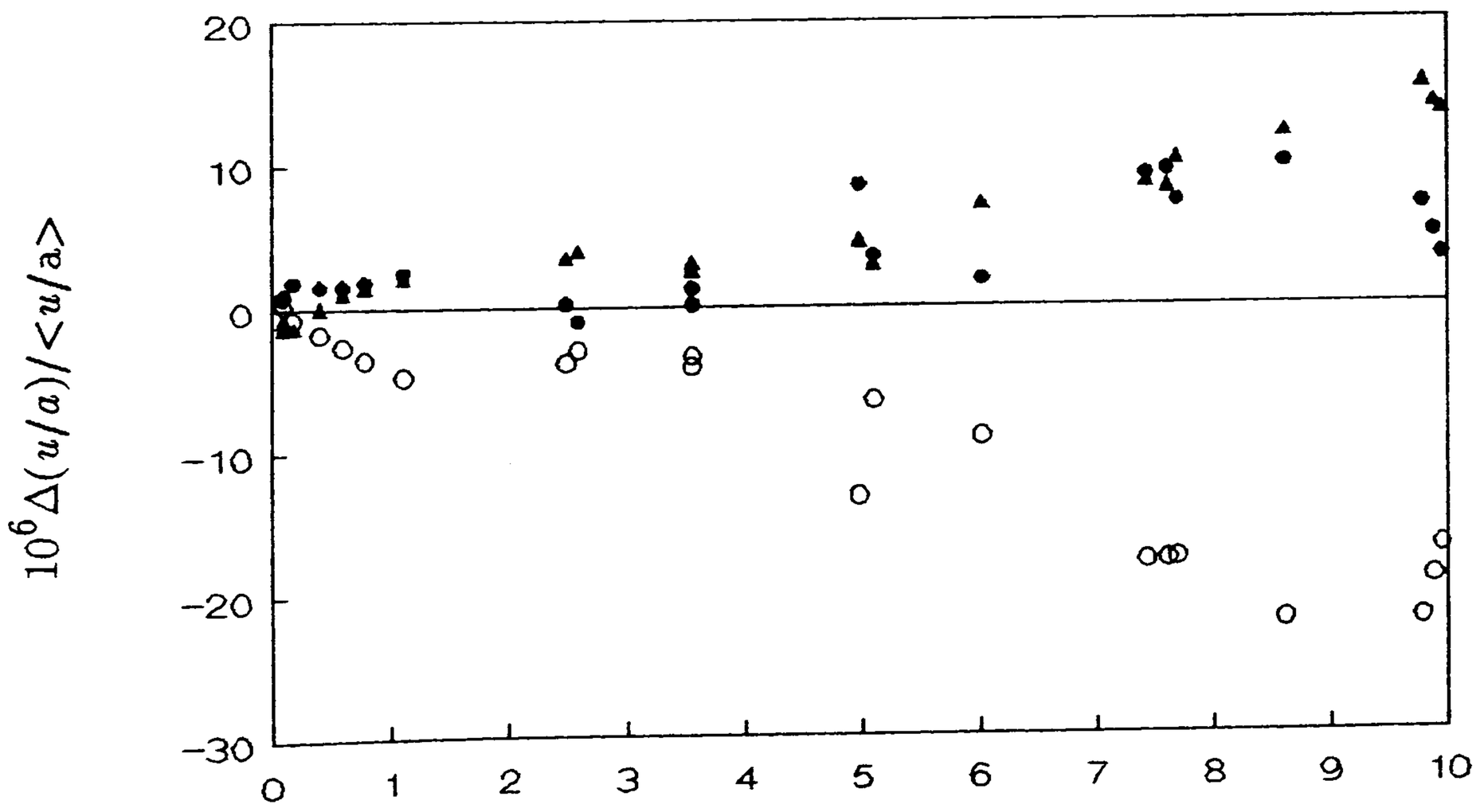

Figure 5.57: Fractional deviations of (u/a) for individual modes in the methane–ethane mixture from $<u/a>$ of the modes finally selected; a) 250 K, and b) 275 K.

• , (0,2); ▲ , (0,3); ∘ , (0,4).

a)

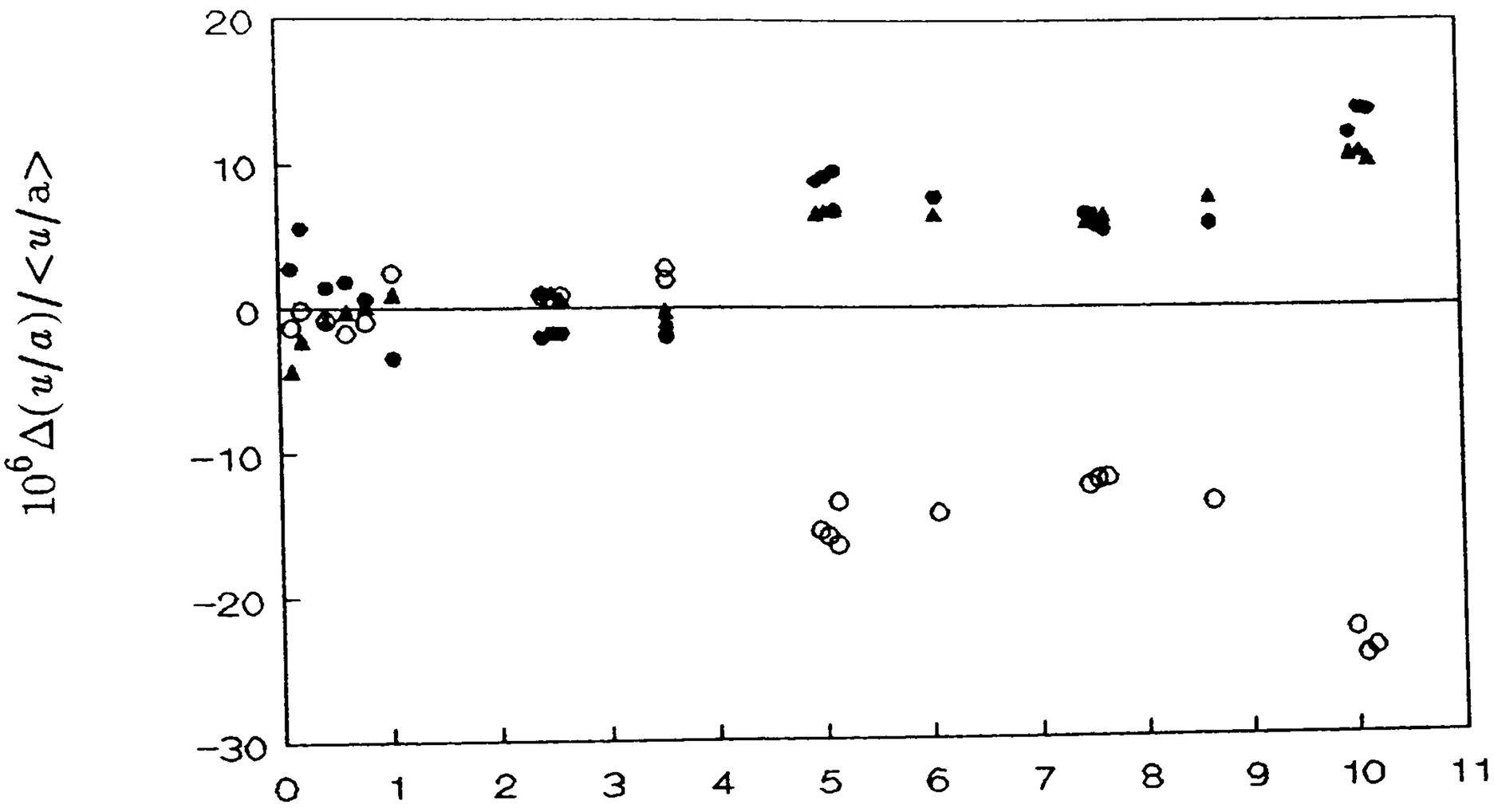

b)

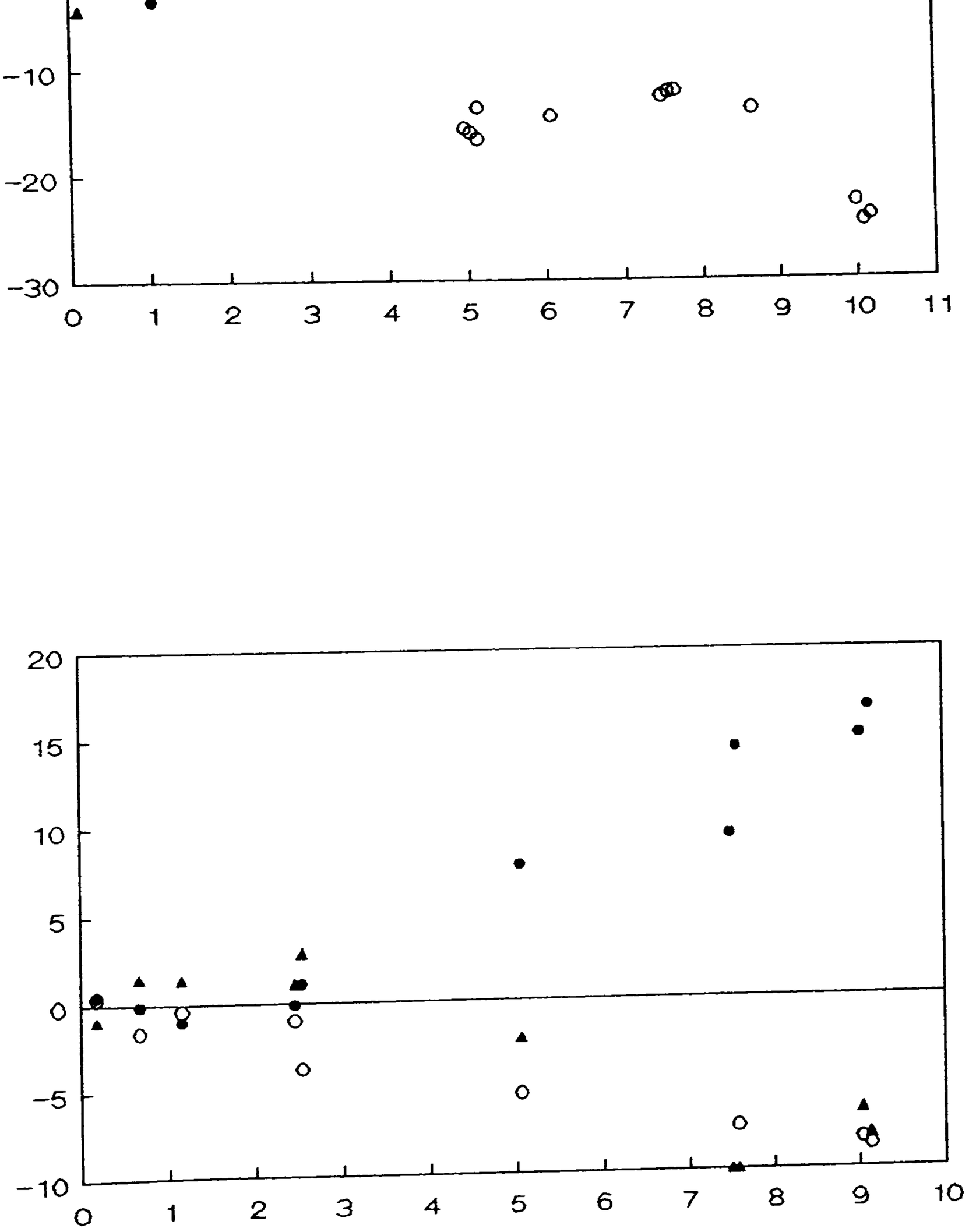

Figure 5.58: Fractional deviations of (u/a) for individual modes in the methane–ethane mixture from $<u/a>$ of the modes finally selected; a) 300 K, and b) 350 K.

• , (0,2); ▲ , (0,3); ∘ , (0,4).

Table 5.20: Coefficients of equation (5.2.3) required to represent the measurements of (u/a) in the binary mixture of methane and ethane with standard deviation σ at temperatures T.

T/K	i	$\{A_i/a^2\}$/s$^{-2}\cdot$Pa^{-i}	T/K	i	$\{A_i/a^2\}$/s$^{-2}\cdot$Pa^{-i}
249.806		$10^6\sigma(u^2)/u^2 = 25.4$	274.756		$10^6\sigma(u^2)/u^2 = 11.5$
	0	$(73.2767 \pm 0.0012)\cdot10^{6}$		0	$(79.93574 \pm 0.00070)\cdot10^{6}$
	1	-3.2679 ± 0.0048		1	-2.5708 ± 0.0018
	2	$(-0.720 \pm 0.058)\cdot10^{-7}$		2	$(0.385 \pm 0.012)\cdot10^{-7}$
	3	$(0.444 \pm 0.029)\cdot10^{-13}$		3	$(0.866 \pm 0.034)\cdot10^{-14}$
	4	$(-0.787 \pm 0.064)\cdot10^{-20}$		4	$(-0.144 \pm 0.040)\cdot10^{-21}$
	5	$(0.825 \pm 0.064)\cdot10^{-27}$		5	$(0.465 \pm 0.016)\cdot10^{-28}$
	6	$(-0.170 \pm 0.024)\cdot10^{-34}$			
299.750		$10^6\sigma(u^2)/u^2 = 9.0$	349.424		$10^6\sigma(u^2)/u^2 = 14.1$
	0	$(86.59674 \pm 0.00039)\cdot10^{6}$		0	$(98.91964 \pm 0.00077)\cdot10^{6}$
	1	-2.00605 ± 0.00071		1	-1.11972 ± 0.00088
	2	$(0.62174 \pm 0.0030)\cdot10^{-7}$		2	$(0.6532 \pm 0.0024)\cdot10^{-7}$
	3	$(0.4277 \pm 0.0044)\cdot10^{-14}$		3	$(0.2984 \pm 0.0017)\cdot10^{-14}$
	4	$(0.2303 \pm 0.0021)\cdot10^{-21}$			

better than 10 ppm.

The deviations of the individual (u/a) from the mean at 350 K are shown in figure 5.58. All modes measured agree to better than 15 ppm across the whole range; at pressures below 5 MPa the modes agree to better than 10 ppm.

The (u/a) finally selected for inclusion in the analysis can be represented by up to seven terms in the infinite series (5.2.3) the number of terms required in the infinite series increases from four at 350 K to seven at 250 K. The increase in the number of terms required in the series, as the temperature is reduced, is not unreasonable since the curvature of an isotherm increases with decreasing temperature; however, the number of terms is rather surprising, particularly at the lowest temperatures, and excessive, to

a)

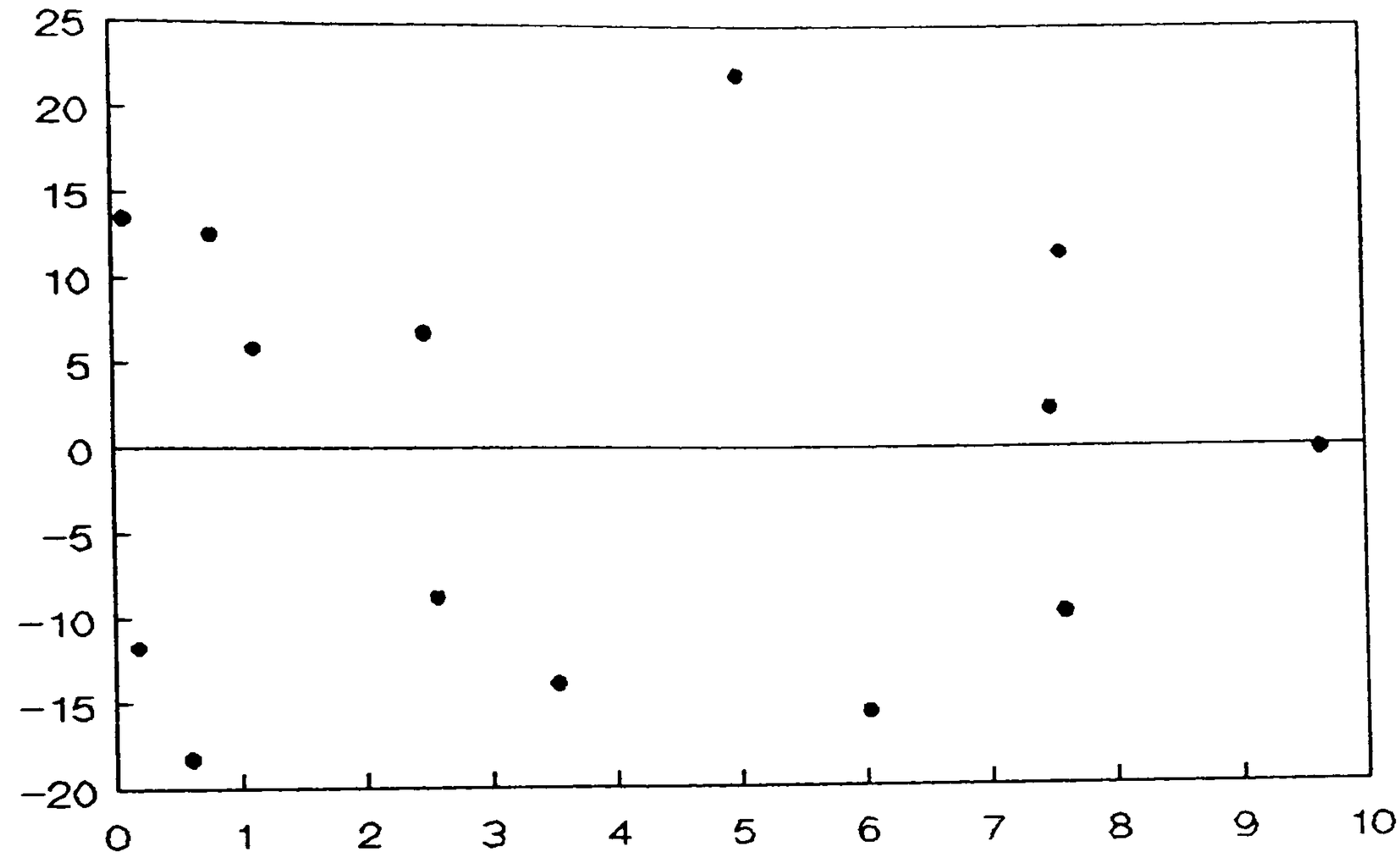

b)

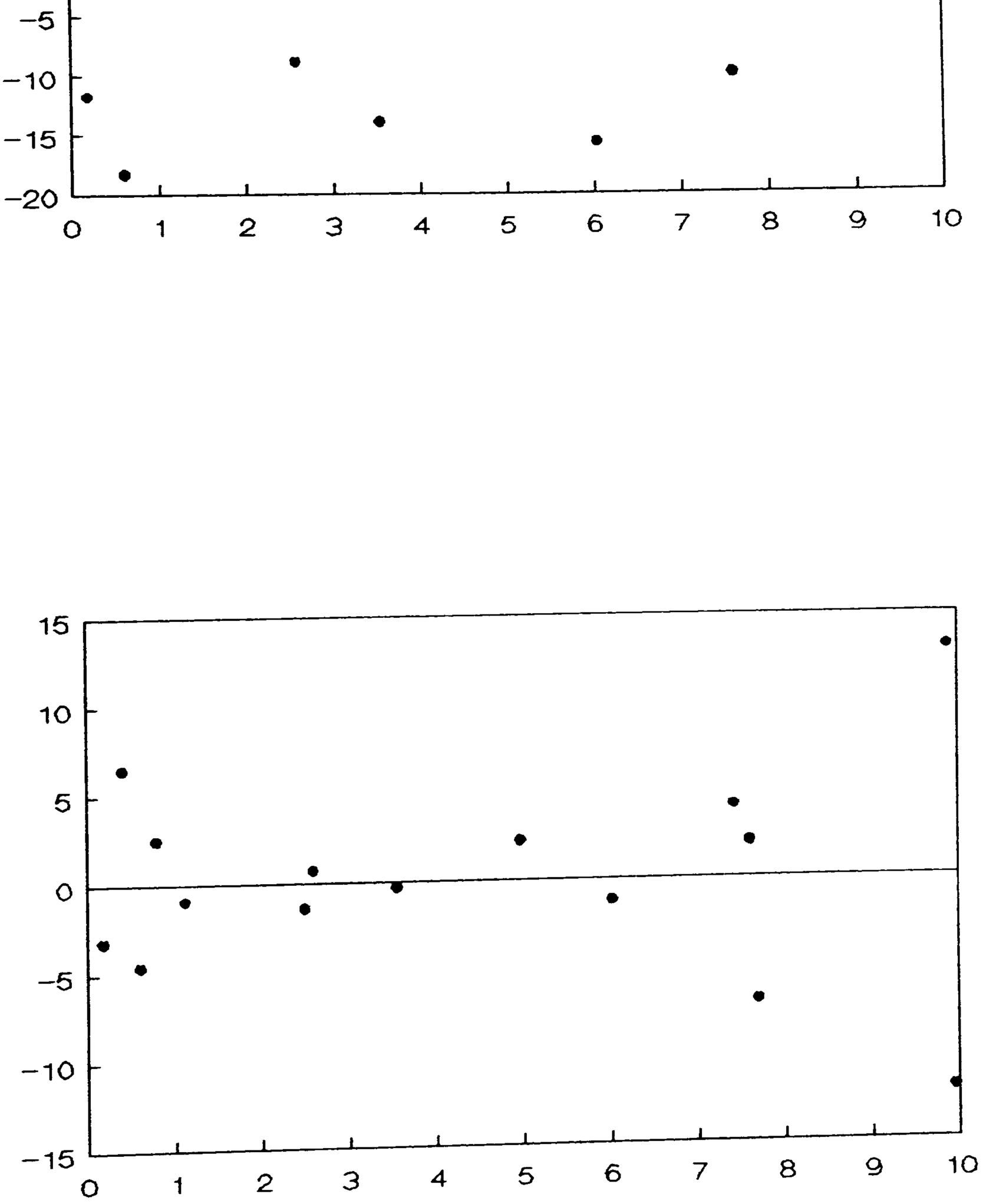

Figure 5.59: Fractional deviations of $<u/a>$ for the selected modes from the adopted smoothing equation; a) 250 K and b) 275 K.

a)

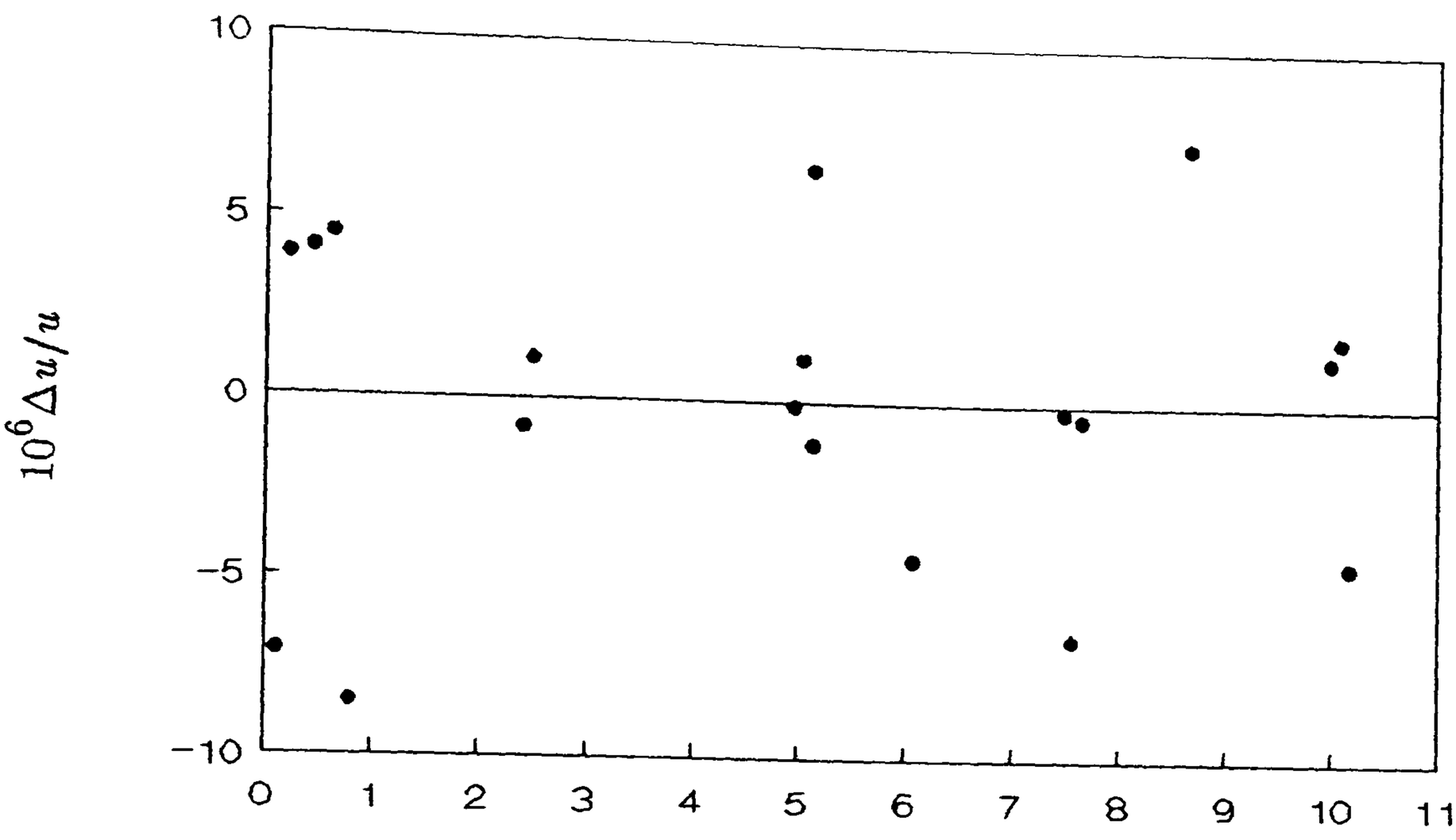

b)

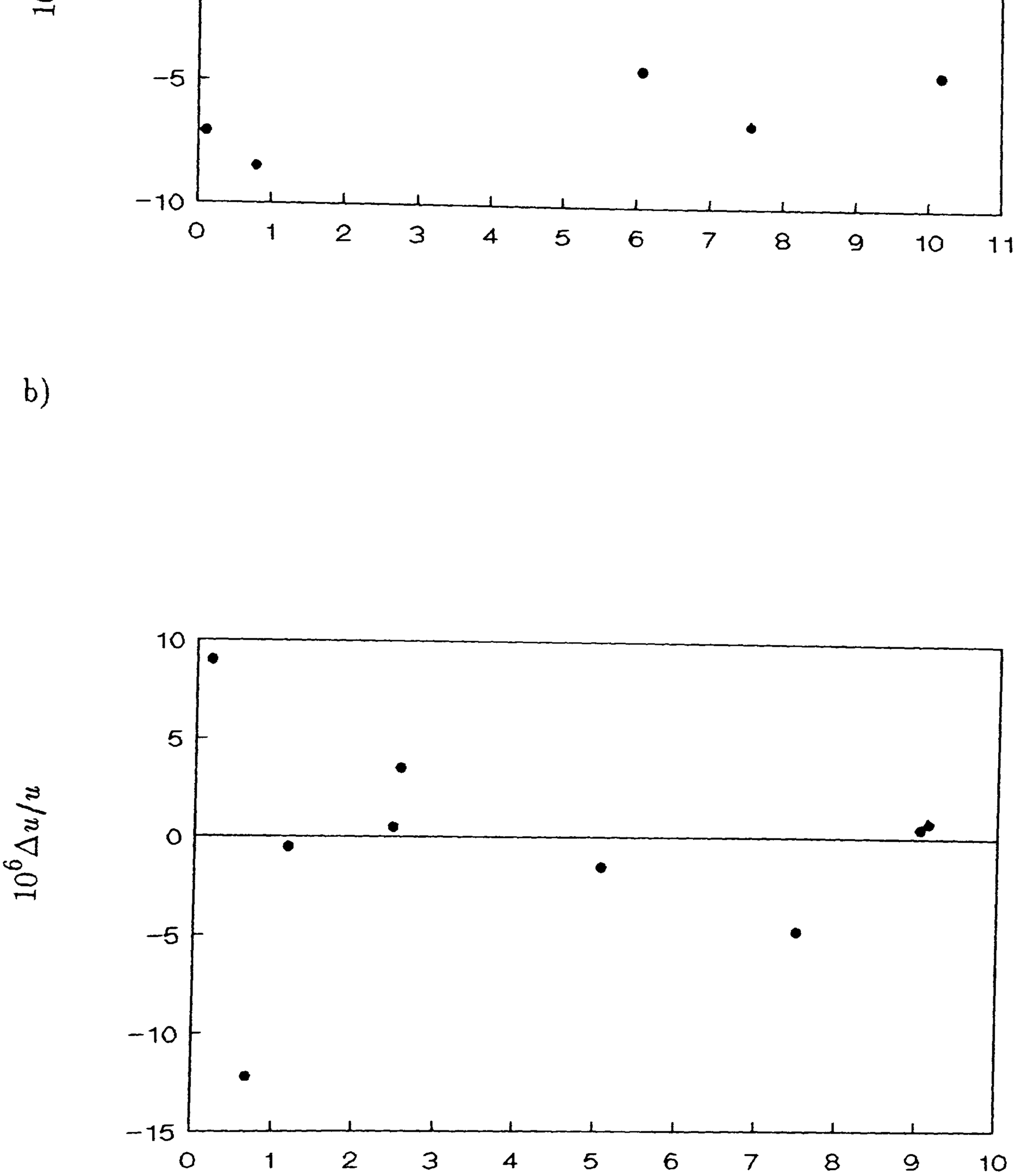

Figure 5.60: Fractional deviations of $<u/a>$ for the selected modes from the adopted smoothing equation; a) 300 K and b) 350 K.

Table 5.21: Perfect–gas heat capacities and second acoustic virial coefficients of the methane–ethane mixture at temperatures T. Mole fraction of ethane, x, determined from (A_0/a^2) in equation (5.2.3).

T/K	$C_{p,\mathrm{m}}^{\mathrm{pg}}/R$	x	$\beta_{\mathrm{a}}/(\mathrm{cm}^3\cdot\mathrm{mol}^{-1})$
349.424	4.94368 ± 0.00030	0.15092	–32.886 ± 0.026
299.750	4.60850 ± 0.00015	0.15084	–57.735 ± 0.020
274.756	4.47611 ± 0.00027	0.15361	–73.471 ± 0.052
249.806	4.35655 ± 0.00046	0.15402	–92.628 ± 0.135

say the least. However, the vapour pressure of ethane at 250 K is approximately 1.301 MPa and this is exceeded by the partial pressure of ethane in the mixture at 250 K and 10 MPa. At 275 K the partial pressure of ethane in the mixture at 10 MPa is very close to 0.6 of the calculated vapour pressure. Consequently, precondensation, or even condensation, will be occurring, at least at the highest pressures, and this will seriously distort the measurements. Removal of these points, and hence truncating the pressure range, brings the number of required coefficients for each isotherm down to the more acceptable level of five.

Perfect–gas heat capacities for the mixture were determined from (A_0/a^2) and are presented in table 5.21 along with the second acoustic virial coefficient for the mixture, determined from (A_1/a^2).

The mole fraction of ethane in the mixture was certified to be 0.1500 by the manufacturers[91]. However, during the course of an experiment, fractionation of the mixture was expected to occur when the pressure was changed. This effect can be monitored since it is possible to estimate the mole fraction from the zero–pressure limit of the speed of sound. Values of x determined for the four isotherms are given in table 5.21 and these were also determined from (A_0/a^2) assuming that

$$\gamma_{\mathrm{mix}}^{\mathrm{pg}} = \{(1-x)C_{p,\mathrm{m}}^{\mathrm{pg}}(\mathrm{CH_4}) + xC_{p,\mathrm{m}}^{\mathrm{pg}}(\mathrm{C_2H_6})\}/\{(1-x)C_{V,\mathrm{m}}^{\mathrm{pg}}(\mathrm{CH_4}) + xC_{V,\mathrm{m}}^{\mathrm{pg}}(\mathrm{C_2H_6})\}, \tag{5.4.10}$$

and

$$M_{\text{mix}} = (1 - x)M_{\text{CH}_4} + xM_{\text{C}_2\text{H}_6}. \tag{5.4.11}$$

The perfect–gas heat capacities of the pure components were taken from equation (5.3.4) for ethane and from reference 82 for methane. The average composition of the mixture determined from the four isotherms is 0.1523 ± 0.0029; this determination includes the value quoted by the manufacturer, within the estimated error. However, we note that the values differ systematically from the value quoted by the manufacturers. This is particularly apparent at the lowest temperatures. At the two highest temperatures the average mole fraction of ethane is 0.15088. This is an acceptable level of agreement with the manufacturers quoted value. However, at the lowest temperatures, as indicated above, precondensation occured. This will result in a liquid film of ethane on the inner surface of the resonator and so when the pressure is reduced the methane content in the mixture will be reduced preferentially. As the pressure is reduced further the film will evaporate and increase the ethane content of the mixture further still. Thus, one would expect to determine values of x that disagree by significant amounts from the manufacturers estimate.

Analysis of the acoustic virial coefficients is, in this instance, not straightforward. Since the measurements were performed isothermally, and not isochoricly, the overriding problem was that of sample uniformity. The quantities of interest depend on x and any variation in sample uniformity will lead to inconsistencies in the data set thus hampering analysis. The problem is particularly acute for the acoustic virial coefficient if fractionation of the mixture occurs along an isotherm. This will result in additional curvature and lead to systematic errors in the coefficients so determined. Accounting for this will be difficult, if not impossible. When the whole set of data was analysed in an attempt to extract $B(T, x)$ from β_{a}, it was impossible to arrive at a satisfactory solution. Therefore, having discussed the problems of sample uniformity and its influence on β_{a}, and since from table 5.21 it is known that x shows considerable variation, it was deemed necessary to assess the data prior to analysis in an attempt to reveal any irregularities. A convenient and sensitive test is to allow $\beta_{\text{mix}}(T, x)$ to be

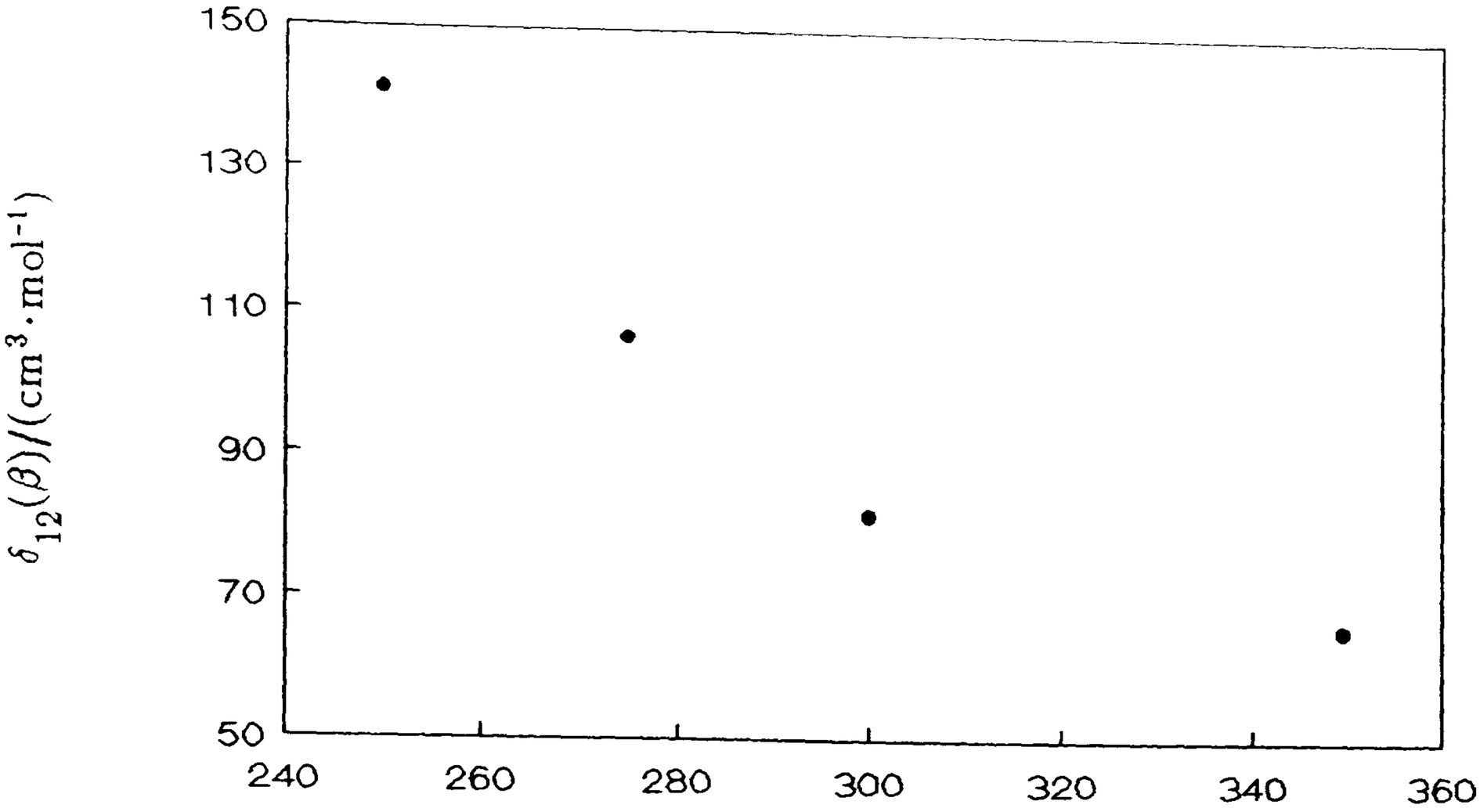

Figure 5.61: $\delta_{12}(\beta)$ calculated from (5.4.12) as a function of temperature for the mixture.

---

represented by

$$\beta_{\mathrm{mix}}(T, x) = (1-x)\beta_{11} + x(1-x)\delta_{12} + x\beta_{22} \qquad (5.4.12)$$

in which

$$\delta_{12}(\beta) = 2\beta_{12} - (\beta_{11} + \beta_{22}). \qquad (5.4.13)$$

Here β_{11} and β_{22} are the acoustic virial coefficients of pure 1 and 2 respectively, and β_{12} is the coefficient that takes acount of the pairwise molecular interactions of 1 and 2. This is, of course, an incorrect description for a mixture of gases in which $\gamma_1^{\mathrm{pg}} \neq \gamma_2^{\mathrm{pg}(92)}$. However, solely as a method of assessing the data, any inconsistencies will be patently manifest, since δ_{12} is an extremely sensitive quantity to departures from non–ideality. The quantity δ_{12} was determined from equation (5.4.12), using values of β_{11} and β_{22} calculated from equations (5.4.8) and (5.3.5) with (3.2.15) respectively, and is shown in figure 5.61. From this it is immediately apparent that the datum at 350 K departs significantly from the overall trend. The remaing values are seen to be consistent. In the resulting analysis of β_{a} only square–well function was used. This was, in the first instance, an attempt to reduce the likely systematic errors introduced when imposing a

Table 5.22: Second virial coefficients B for the binary mixture of methane and ethane at temperatures T represented by equation (5.4.17) and deviations δ of the acoustic virial coefficients from (5.4.17) and (3.2.15). Cross virial coefficients, B_{12}, and interaction coefficients, $\delta_{12}(B)$, for methane–ethane.

T/K	B/cm^3·mol^{-1}	δ	B_{12}/cm^3·mol^{-1}	$\delta_{12}(B)$/cm^3·mol^{-1}
349.423	–37.53	0.26	–60.91	35.60
299.750	–56.73	–0.31	–87.69	48.97
274.756	–69.91	0.65	–104.77	61.75
249.806	–86.69	2.59	–127.73	76.68

functional form for B; it is necessary to calculate values of B_{11} and B_{22} (from equations (5.4.8) and (5.3.5), respectively) to extract B_{12} and any inconsistencies in functional form can only compound the systematic error introduced. The second reason was due to the lack of usable data. The square–well function has three parameters and, with only three data points, this leaves no degrees of freedom. It is therefore necessary to constrain one of the parameters leaving one degree of freedom, and this is possible when using the square–well function. Within the Principle of Corresponding States[93,95] various properties of mixtures are calculated from the properties of the the pure components using combination rules. These are usually by means of the geometric and arithmetic means. Within this Principle the well–depth for a mixture is represented as

$$\epsilon_{\text{mix}} = (1-x)\epsilon_{11} + 2x(1-x)\epsilon_{12} + x\epsilon_{22} \tag{5.4.14}$$

in which

$$\epsilon_{12} = (\epsilon_{11}\epsilon_{22})^{1/2}. \tag{5.4.15}$$

However, these rules are known to fail for some substances and the geometric mean rule is modified by the introduction of the parameter ξ:

$$\epsilon_{12} = \xi(\epsilon_{11}\epsilon_{22})^{1/2}. \tag{5.4.16}$$

Using these we have a means of constraing the well–depth for the mixture, by using the values determined for the pure components.

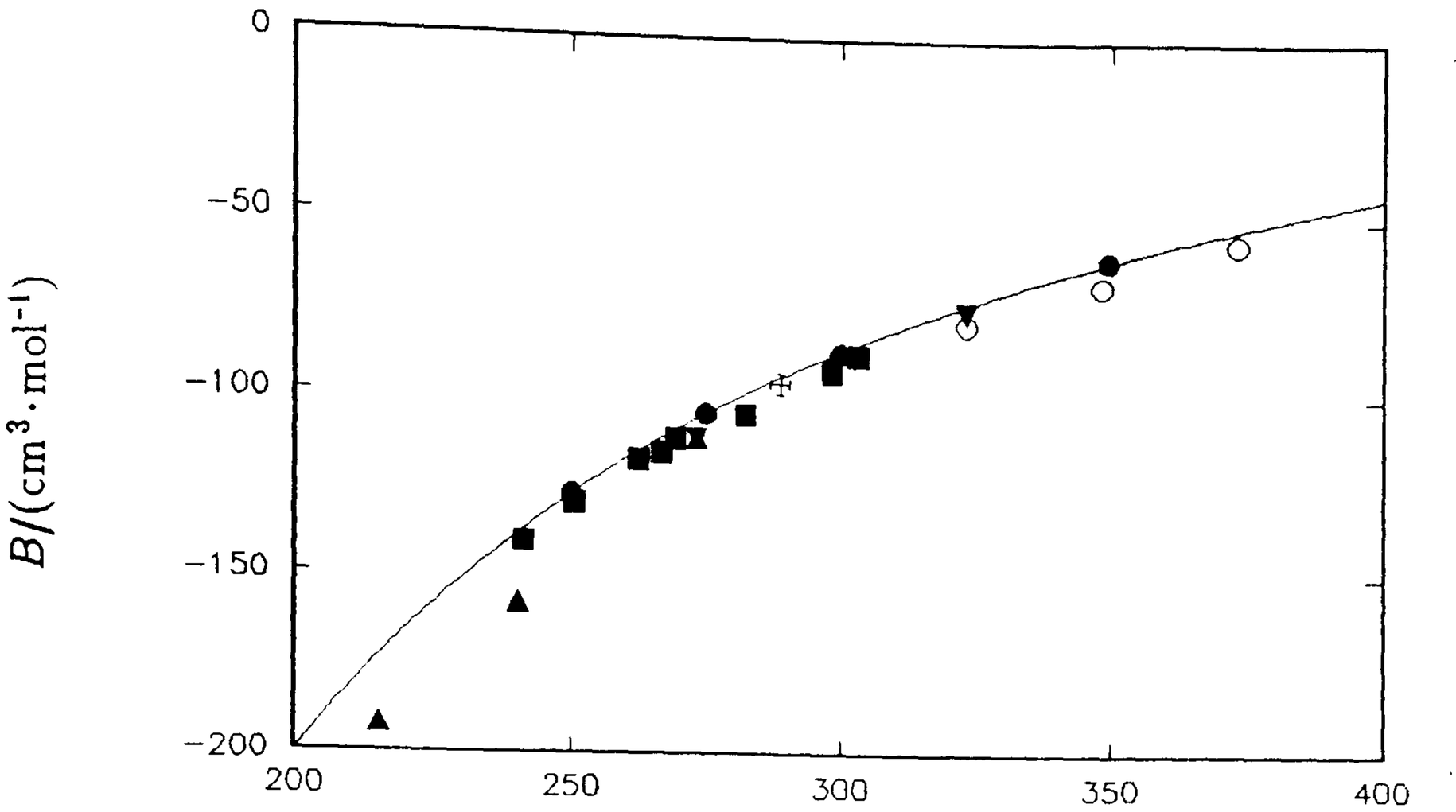

Figure 5.62: Cross virial coefficient, B_{12}, as a function of temperature for methane–ethane. ———— , equation (5.4.18); • , this work; + , reference 96; ▲ , reference 97; ○ , reference 98; ■ , reference 99; ▼ , reference 100.

The first solution obtained had $\xi = 1$ and the resulting expression was

$$B/\mathrm{cm}^3\cdot\mathrm{mol}^{-1} = 175.42 - 126.492\exp(182\ \mathrm{K}/T) \qquad (5.4.17)$$

which fit β_a with a weighted standard deviation of 0.13 $\mathrm{cm}^3\cdot\mathrm{mol}^{-1}$. The alternative solution, in which $\xi = 0.98$[94], made only trivial differences to the resulting values of B over the temperature range of study. Indeed, even when the expression quoted by McGlashan[95], in which the well–depth is given by $0.7002T^{c}_{mix}$, is used the resulting values of B differ by only 0.2 $\mathrm{cm}^3\cdot\mathrm{mol}^{-1}$ at 250 K. This is regarded as evidence that a satisfactory solution has been obtained.

Having achieved a satisfactory analysis, using equation (3.2.7) and a knowledge of the virial coefficients for the pure components (either (5.3.5) or (5.4.8)), estimates of B_{12} and $\delta_{12}(B)$ were determined for the mixture. These are given in table 5.22. Using the cross virial coefficients, B_{12}, so determined allows comparison with previous determinations. This is shown in figure 5.62, where B_{12} is shown as a function of temperature. As can be seen the level of agreement is rather poor, especially at low temperatures where the results differ by more than 15 $\mathrm{cm}^3\cdot\mathrm{mol}^{-1}$, although at higher

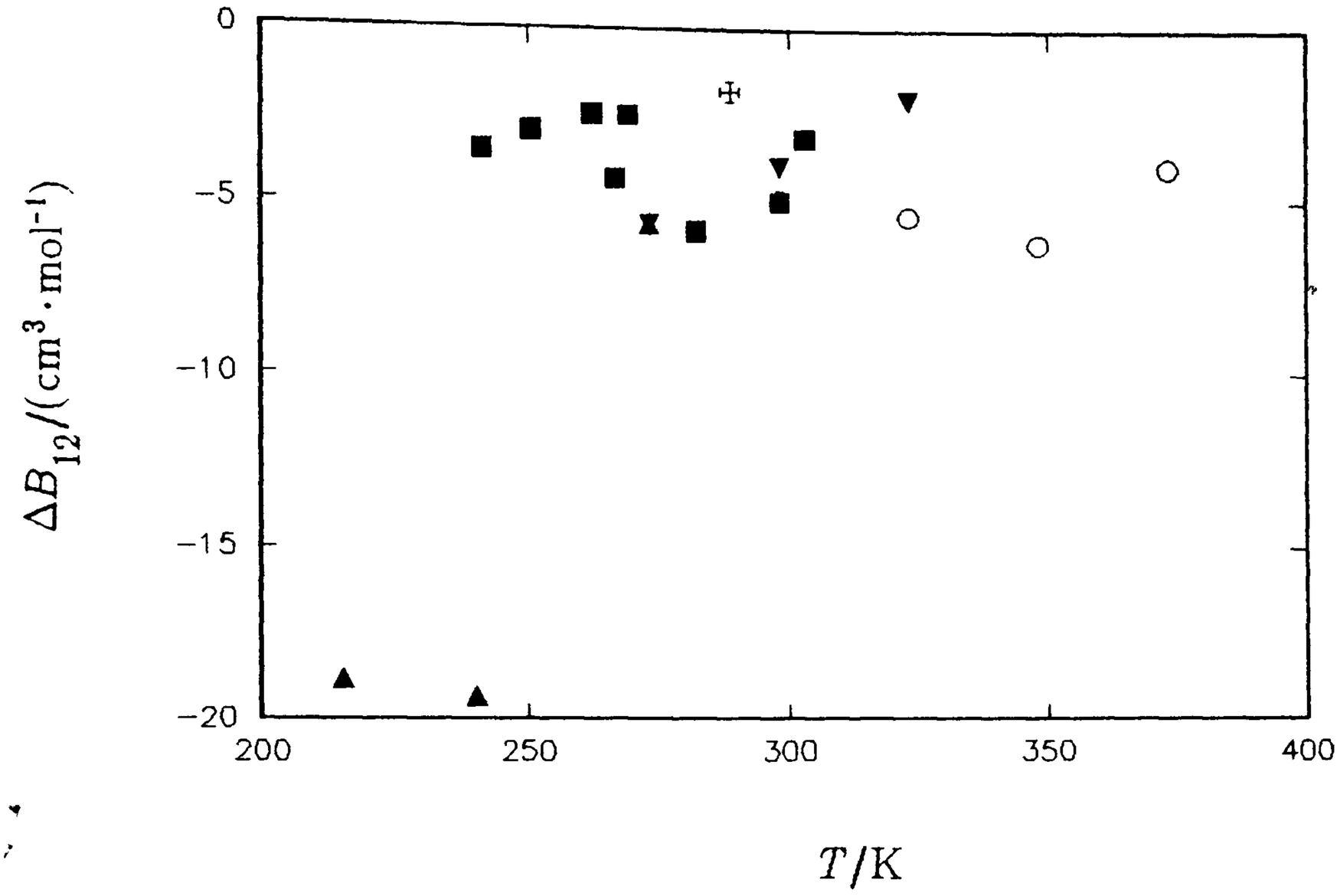

Figure 5.63: Deviations $\Delta B_{12} = \{B_{12}(\text{exp.}) - B_{12}(\text{calc.})\}$ of experimental cross virial coefficients from (5.4.18). + , reference 96; ▲ , reference 97; ∘ , reference 98; ■ , reference 99; ▼ , reference 100.

---

temperatures the results appear to be converging. To facilitate a more detailed comparison, the values of B_{12} determined in this work have been analysed using a square–well function. Although the values of B_{12} determined in this work are rather uncertain and likely to be subject to systematic error, the analysis in terms of the square–well can be considered as generating a smoothing equation to be used solely as a method of comparison. The number of data points is small and so the number of parameters in the model was reduced to two by using equation (5.4.15) to calculate the well depth, ϵ_{12}, from the values for the two pure components. Unweighted analysis of the results yielded

$$B/\text{cm}^3\cdot\text{mol}^{-1} = 186.08 - 135.997\exp(209\ \text{K}/T) \qquad (5.4.18)$$

with a standard deviation of 0.48 cm^3·mol^{-1}. Equation (5.4.18) is indicated by the solid line in figure 5.62. In figure 5.63 the virial coefficients of previous determinations are

shown as deviations from (5.4.18). As can be seen the agreement is really rather poor, especially at low temperatures. Apart from the two low temperature results of Hoover, Nagata, Leland and Kobayashi[97], which deviate by more than á 0 $cm^3 \cdot mol^{-1}$, the previous determinations[96–100] are quite consistent internally, showing scatter of about ± 5 $cm^3 \cdot mol^{-1}$, but deviate systematically from (5.4.18) by

5 $cm^3 \cdot mol^{-1}$; evidence from the slope of the deviation suggests that the results are converging with (5.4.18) with increasing temperature. The low temperature acoustic results may be in error since precondensation occurred, which complicated the uniformity of the mixture and hence the analysis of the results, although the disagreement may be due to adsorption complicating the (p, V, T) measurements. Since the high temperature results appear to be converging with (5.4.18) this adds weight to the argument that the differences are attributable to adsorption; from previous work this is the observed trend. Another possible explanation lies in the method of calculation of B_{12} from mixture data. A satisfactory analysis of mixture data, to determine B_{12}, requires knowledge of the virial coefficients for the pure components. Since it is likely that different authors use different values of B_{11} and B_{22} this will result in systematic differences in the cross virial coefficients calculated. If a rigorous comparison between mixture properties, calculated in this way, is to be performed, it is crucial that the individual data sets be assessed for any variations of this kind. If necessary, the previous determinations can be re–analysed using the appropriate values for B_{11} and B_{22}. Insufficient time was available to reassess the data in this fashion. Given the difficulties associated with sample uniformity and the complications arising from precondensation, the level of agreement is not too disastrous. However, it should be noted that the results obtained here should be treated with caution.

5.4.9: Concluding Remarks.

Measurements in the 45 mm stainless steel resonator have shown that it is possible to measure the speed of sound in a gas, over the temperature range 250 to 350

K, at pressures up to 10 MPa with a precision of better than 20 ppm in u^2. Over the whole range of pressures and temperatures at least two, and generally three, radial modes were used to determine $<u/a>$ at a given state point and the level of agreement between the modes was generally better than 20 ppm. At pressures below about 5 MPa more modes were used in the determination of $<u/a>$. The limited number of higher frequency modes retained at the highest pressures was due to the influence of shell motion. This is by far the most serious perturbation and, due to inadequacies in the theory under extreme conditions, difficult to model. Consequently, in most instances, measurements of the (0,5) and (0,6) modes were not performed since these modes are those which are most seriously affected by shell motion; or, if recorded, were omitted from the final analysis accept at the lowest pressures. For methane, and particularly, the methane–ethane mixture, where A_1 is comparatively large (compared with the values in argon or nitrogen), the limited precision of the pressure measurements appears to compromise the precision of the speed of sound measurements. Additionally, for the measurements in the binary mixture complications arising from precondensation and variation in the composition cause further loss of precision. The measurements in argon and nitrogen are considerably better and this may be attributable to the fact that they are well understood and the requirements on the pressure measurements less stringent. The fractional excess half–widths, $\Delta g/f$, recorded are in general better than 30 ppm, and often better than 20 ppm, across the whole range. Individual modes were adversely affected in some instances by shell motion and/or precondensation but, on average the excess half–widths were satisfyingly small.

These measurements have severely tested the current acoustic model and have shown that it is possible to measure the speed of sound in gases up to 10 MPa with a precision of better than 20 ppm. Theory and experiment are seen to agree to better than 20 ppm, across the whole range, by means of a comparison between calcuated and experimental g's; at pressures below 1 MPa the agreement is better than 10 ppm and in argon is about 5 ppm. The precision could be improved if a more perfect sphere was available since, as noted in Chapter 2, the geometry may be pressure dependent and

this will complicate things in a way which is difficult, if not impossible, to model. Further improvements could be achieved by using different materials for construction of the sphere; if the material has suitable elastic properties then the correction due to shell motion could be reduced. This would improve the agreement between modes.

5.5: References.

1. Bruch, L. W. *Phys. Rev.* **1969**, 178, 303.

2. Bruch, L. W. *Phys. Rev. A* **1970**, 2, 2164.

3. Mehl, J. B.; Moldover, M. R. *Proc. Eighth Symp. on Thermophysical Prop.* Sengers, J. V.: Editor. *Am. Soc. Mech Eng.*: New York. **1982**, p. 134.

4. Boyd, M. E.; Mountain, R. D. *Phys. Rev. A* **1970**, 2, 2164.

5. Goodwin, A. R. H. Ph.D Thesis, University of London, **1987**?.

6. Ewing, M. B.; Goodwin, A. R. H.; McGlashan, M. L.; Trusler, J. P. M. *J. Chem. Thermodynamics*, **1987**, 19, 721.

7. Ewing, M. B.; Owusu, A. A.; Trusler, J. P. M. *Physica A* **1989**, 156, 899.

8. Ewing, M. B.; Trusler, J. P. M. *J. Chem. Phys* **1989**, 90(2), 1106.

9. Mehl, J. B.; Moldover, M. R. *J. Chem. Phys* **1982**, 77(1), 455.

10. Ledbetter, H. M. *Cryogenics*, **1982**, 22, 653

11. Holmes, R.; Jones, G. R.; Pusat, N. *J. Chem. Phys.* **1964**, 41(8), 2512.

12. Lambert, J. D.; Salter, R. *Proc. Roy. Soc. (London)* **1959**, A253, 277.

13. Valley, L. M.; Legvold, S. *J. Chem. Phys.* **1962**, 36, 481.

14. Ernst, G.; Hochberg, U. E. *J. Chem. Thermodynamics* **1989**, 21, 407.

15. TRC Thermodynamic Tables–Hydrocarbons, Table 23–2–(1.101) Normal Alkanes , C_1 to C_{20}.

16. Bier, K.; Kunze, J.; Maurer, G. *J. Chem. Thermodynamics* **1976**, 8, 857.

17. Michels, A.; Van Straaten, W.; Dawson, J. *Physica* **1954**, 20, 17.

18. Ewing, M. B. unpublished work, **1989**.

19. Douslin, D. R.; Harrison, R. H. *J. Chem. Thermodynamics* **1973**, 5, 491.

20. Gammon, B. E.; Hall, K. R.; Holste, J. C.; Hou, H.; Marsh, K. N. *11th IUPAC International Conference on Chemical Thermodynamics*, Poster, **1990**.

21. Strein, K.; Lichtenthaler, R. N.; Schramm, B. Schäfer, K. *Ber. Bunsenges. Phys. Chem.* **1971**, 75, 1308.

22. Dymond J. H.; Smith, E. B. *The Virial Coefficients of Pure Gases and Mixtures.* Clarendon Press: Oxford. **1980**.

23. Pope. G. A.; Chappelear, P. S.; Kobayashi, R. *J. Chem. Phys.* **1973**, 59, 423.

24. Hoover, A. E.; Leland, T. W.; Kobayashi, R. *J. Chem. Phys.* **1966**, 45, 399.

25. Hamann, S. D.; McManamey, W. J. *Trans. Faraday Soc.* **1953**, 49, 149.

26. Eucken, A.; Parts, A. *Z. Phys. Chem.* **1933**, B20, 184.

27. Lichtenthaler, R. N.; Schäfer, K. *Ber. Bunsenges. Phys. Chem.* **1969**, 73, 42.

28. Measurements by Reamer, H. H.; Olds, R. H.; Sage, B. H.; Lacey, W. N. *Ind. Engng. Chem. ind Edn.* **1944**, 36, 956. Values of C calculated by David, H. G.; Hamann, S. D.; Prince R. G. H. *J. Chem. Phys.* **1953**, 49, 149.

29. Mansoorian, H.; Hall, K. R.; Eubank, P. T. *Proc. Seventh Symp. Thermophys. Props., Am. Soc. Mech. Eng.*, New York, **1977**, 456.

30. Michels, A.; Nederbragt, G. W. *Physica*, **1939**, 6, 656.

31. Boyes, S. J.; Ewing, M. B.; Trusler, J. P. M. *Proceedings of the Meeting of Commission B1 of the International Institute of Refrigeration*, Tel Aviv, Israel, **1990**.

32. Byers, J. W. *J. Chem. Phys.* **1943**, 11, 348.

33. Corran, P. G.; Lambert, J. D.; Salter, R.; Warburton, B. *Proc. Roy. Soc. London* **1958**, A244, 212.

34. Since a satisfactory analysis was extremely difficult to obtain, the analyses were conducted independently by S. J. Boyes, M. B. Ewing and A. R. H. Goodwin. A consensus was then reached the results of which are reported here.

35. Craven, P. M.; Lambert, J. D. *Proc. Roy. Soc.* **1951**, A205, 439.

36. Renner, T. A.; Kucera, G. H.; Blander, M. *J. Chem. Phys.* **1977**, 66, 177.

37. Ener, C.; Busala, A.; Hubbard, J. C. *J. Chem. Phys.* **1955**, 23(1), 155.

38. Tucker, E. E.; Farnham, S. B.; Christian, S. D. *J. Chem. Phys.* **1969**, 73, 3820.

39. Cheam, V.; Farnham, S. B.; Christian, S. D. *J. Chem. Phys.* **1970**, 74, 4157.

40. Craven, R. J. B.; de Reuck, K. M. *Int. J. Thermophysics* **1986**, 7, 541.

41. Bich, E.; Pietsch, R.; Opel, G. *Z. Phys. Chem.* **1984**, 265, 396.

42. Stockmayer, W. H. *J. Chem. Phys.* **1941**, 9, 398.

43. Pople, J. A. *Proc. Roy. Soc.* **1953**, A221, 498.

44. Pople, J. A. *Proc. Roy. Soc.* **1953**, A221, 508.

45. Lambert, J. D.; Roberts, G. A. H.; Rowlinson, J. S. *Proc. Roy. Soc.* **1949**, A196, 113.

46. Kretschmer, C. B.; Wiebe, R. *J. Am. Chem. Soc.* **1954**, 76, 2579.

47. Fox, O. R.; Morcillo, J.; Mendez, A. *An. R. Soc. Esp. Fis. Quim.* **1954**, 23, 17B.

48. Bottomley, G. A.; Spurling, T. H. *Aust. J. Chem.* **1967**, 20, 1789.

49. Knoebel, D. H.; Edmister, W. C. *J. Chem. Eng. Data.* **1968**, 13, 312.

50. Kell, G. S.; McLaurin, G. E. *J. Chem. Phys.* **1969**, 51, 4345.

51. Kudchadker, A. P.; Eubank, P. T. *J. Chem. Eng. Data.* **1970**, 15, 7.

52. Ewing, M. B.; Mehl, J. B.; Moldover, M. R.; Trusler, J. P. M. *Metrologia* **1988**, 25, 211.

53. Boyes, S. J.; Ewing, M. B.; Trusler, J. P. M. unpublished report **1989**.

54. Trusler, J. P. M. Ph.D Thesis, University of London, **1984**.

55. Maitland, G. C.; Rigby, M.; Smith, E. B.; Wakeham, W. A. *Intermolecular Forces.* Clarendon Press: Oxford **1981**.

56. Kestin, J.; Ro, S. T.; Wakeham, W. A. *J. Chem. Phys.* **1972**, 56, 4119.

57. Kestin, J.; Leidenfrost, W. *Physica*, **1959**, 25, 1033.

58. Kestin, J.; Paul, R.; Cliffird, A. A.; Wakeham, W. A. *Physica* **1980**, 100A, 349.

59. Kaye, G. W. C.; Laby, T. H. *Tables of Physical and Chemical Constants* Thirteenth Edition, Longmans **1966**.

60. Moldover, M. R.; Trusler, J. P. M.; Edwards, T. J.; Mehl, J. B.; Davis, R. S. *J. Res. Nat. Bur. Standards* **1988**, 93, 85.

61. Moldover, M. R.; Trusler, J. P. M. *Metrologia* **1988**, 25, 165.

62. Ewing, M. B.; Trusler, J. P. M. unpublished results **1988**.

63. Clifford, A. A.; Kestin, J.; Wakeham, W. A. *Physica* **1979**, 97A, 287.

64. Ewing, M. B.; Trusler, J. P. M. *11*th *IUPAC International Conference on Chemical Thermodynamics*, Oral Communication, **1990**.

65. Pieperbeck, N.; Kleinrahm, R.; Wagner, W.; Jaeschke, M. *J. Chem. Thermodynamics* **1991**, 23, 175.

66. Roe, D. R.; Saville, G. unpublished results **1972**.

67. Michels, A.; Lunbeck, R. J.; Wolkers, G. J.; *Physica*, 1951, 17, 801.

68. Holborn, L.; Otto, J. *Z. Phys.* 1925, 33, 1.

69. Gunn, R. D. Thesis, University of California, 1958.

70. Witonsky, R.J.; Miller, J. G. *J. Am. Chem. Soc.* 1963, 85, 282.

71. Hoover, A.. E.; Canfield, F. B.; Kobayashi, R.; Leland, T. W. *J. Chem. Eng. Data* 1964, 9, 568.

72. Crain, R. W.; Sonntag, R. E. *Adv. Cryogen. Engng.* 1966, 11, 379.

73. Pocock, G.; Wormald, C. J. *J. C. S. Faraday* I 1975, 71, 705.

74. Ewing, M. B.; Trusler, J. P. M. unpublished results 1991.

75. van Itterbeek, A.; Lambert, H.; Forres, G. *Appl. Scient. Res.* 1956, 6A, 15.

76. Kestin, J.; Ro, S. T.; Wakeham, W. A. *Trans. Faraday Soc.* 1971, 67, 2308.

77. Kestin, J.; Yata, J. *J. Chem. Phys.* 1968, 49, 4780.

78. Shimanouchi, T. NSRDS–NBS 1972.

79. Cottrell, T. L.; Matheson, A. J. *Trans. Faraday Soc.* 1962, 58, 2336.

80. Edmonds, P. D.; Lamb, J. *Proc. Phys. Soc. London* 1958, 72, 940.

81. Cottrell, T. L.; Martin, P. E. *Trans. Faraday Soc.* 1957, 53, 1157.

82. McDowell, R. S.; Kruse, F. H. *J. Chem. Eng. Data* 1963, 8, 547.

83. Kleinrahm, R.; Duschek, W.; Wagner, W.; Jaeschke, M. *J. Chem. Thermodynamics* 1988, 20(5), 621.

84. Douslin, D. R.; Harrison, R. H.; Moore, R. T.; McCullough, J. P. *J. Chem. Eng. Data* 1964, 9, 358.

85. Michels, A.; Nederbragt, G. W. *Physica*, 1936, 3, 569.

86. Beattie, J. W.; Stockmayer, W. H. *J. Chem. Phys.* 1942, 10, 473.

87. Hamann, S. D.; Lambert, J. A.; Thomas, R. B. *Aust. J. Chem.* 1955, 8, 149.

88. Schamp, H. W.; Mason, E. A.; Richardson, A. C. B.; Altman, A. *Physics Fluids* 1958, 1, 329.

89. Gunn, R. D. Thesis, University of California, 1958.

90. Bellm, J.; Reineke, K.; Schäfer, K.; Schramm, B. *Ber. (dtsch.) Bunseges. Phys. Chem.* 1974, 78, 282.

91. Certificate of Composition 504208 1991.

92. Van Dael, W. *Experimental Thermodynamics Volume II*, Butterworths: London, 1968.

93. Specialist Periodical Reports: Chemical Thermodynamics, Volume 2 The Chemical Society, John Wright and Sons, 1978.

94. Value obtained from British Gas plc.

95. McGlashan, M. L. *Chemical Thermodynamics*, Academic Press, 1979.

96. Mason, D.; Eakin, B. E. *J. Chem. Eng. Data* 1961, 6, 499.

97. Hoover, A. E.; Nagata, I; Leland, T. W.; Kobayashi, R. *J. Chem. Phys.* 1968, 48, 2633.

98. Dantzler, E. M.; Knobler, C. M.; Windsor, M. L. *J. Phys. Chem.* 1968, 72, 676.

99. Wormald, C. J.; Lewis, E. J.; Hutchings, D. J. *J. Chem. Thermodynamics* 1979, 11, 1.

100. Gunn, R. D. Thesis, University of California, 1958.

CHAPTER 6: COMPARISON WITH EQUATIONS OF STATE.

6.1: Introduction.

The quantity u determined from the experimental results, and tabulated in Chapter 5, is compared with values calculated from a number of equations of state. Some of the equations of state are discussed in Chapter 3. The calculations were performed using a computer package developed by British Gas plc[1]. Comparisons were performed for the industrially important gases methane, and its binary mixture with ethane with composition $\{0.85\ CH_4 + 0.15\ C_2H_6\}$.

6.2: Comparison of Experimental Results with Calculated Results.

The speed of sound, u, for both pure methane and the binary mixture, has been calculated using a number of equations of state[1]. The equations were discussed in Chapter 3 and calculations were performed using a package developed by British Gas. The equations used were: 1) the Gibbons and Laughton (GL) equation[2]; 2) the GERG equation[3] which is applicable in the temperature range 265.15 to 335.15 K; 3) the GRI (AGA–8) equation[4]; 4) the McCarty modified BWR equation for CH_4 applied within the Leach–Leland Corresponding States Principle (MCSP)[5,6]; 5) the Benedict, Webb, Rubin and Starling (BWRS) equation[7]; 6) the Peng–Robinson (PR) equation[8]; and 7) the Redlich–Kwong–Soave (RKS) equation[9]. Additionally, for pure methane, an equation developed by Wagner *et al*[10] was used in the comparison. This equation was determined from experimental (p, ρ, T) measurements and is valid up to 12 MPa in the temperature range 273.15 to 323.15 K. Using an adaptive

regression algorithm to select the most significant terms from a bank based on

$$Z = pV_m/RT = 1 + \sum_{n=1}^{20} \delta^n \sum_{m=1}^{20} \tau^{\frac{m}{4}}, \qquad (6.1)$$

where $\delta = \rho/\rho_0$, $\rho_0 = 1$ kg·mol^{-1}, $\tau = T_0/T$ and $T_0 = 273.15$ K, the Wagner equation has the following form

$$Z = 1 + \delta(N_1\tau^{0.75} + N_2\tau) + \delta^2(N_3 + N_4\tau^{2.75}) + \delta^4(N_5 + N_6\tau). \qquad (6.2)$$

The values of the coefficients $N_1, \cdots N_6$, can be found in the literature[9]. This is essentially a truncated virial equation, with the omission of the δ^3 term, with the virial coefficients being represented by power series expansions in τ. The estimated uncertainty in the equation for representing the (p, ρ, T) surface of methane is 0.02 %.

6.2.1: Methane.

Figures 6.1 and 6.2 show the speed of sound obtained from the selected equations of state as deviations from the smoothing equations determined in methane at 250, 275, 300 and 348 K. All equations of state produce zero–pressure values of u at all temperatures which agree to within about 0.1 % of those determined from experiment. The GRI equation provides values of u which differ from the experimental results by less than 0.4 %. If the isotherm at 250 K is excluded then the agreement is better than 0.1 % at all the remaining tempperatures; indeed, at 300 and 348 K the agreement is better than 0.05 %. The MCSP equation provides estimates which agree to better than 1 % with the experimental results over the whole range. With the exclusion of the isotherm at 350 K the agreement is better than 0.5 %. The GERG equation produces values at 300 K which agree to better than 0.4 % and at 275 K the agreement is about 2 %; at the other temperatures, which are outside its range of validity, the deviation reaches about 6 % at 10 MPa. The Wagner equation produces results which agree to better than 1 % except at 250 K, which is outside its validity limits, where the deviation reaches about 4 % at 10 MPa. The BWRS equation is very poor and the deviation is generally worse than 4 % at pressures greater than about 3 MPa. The other equations show varying degrees of success at predicting the speed of sound. With

a)

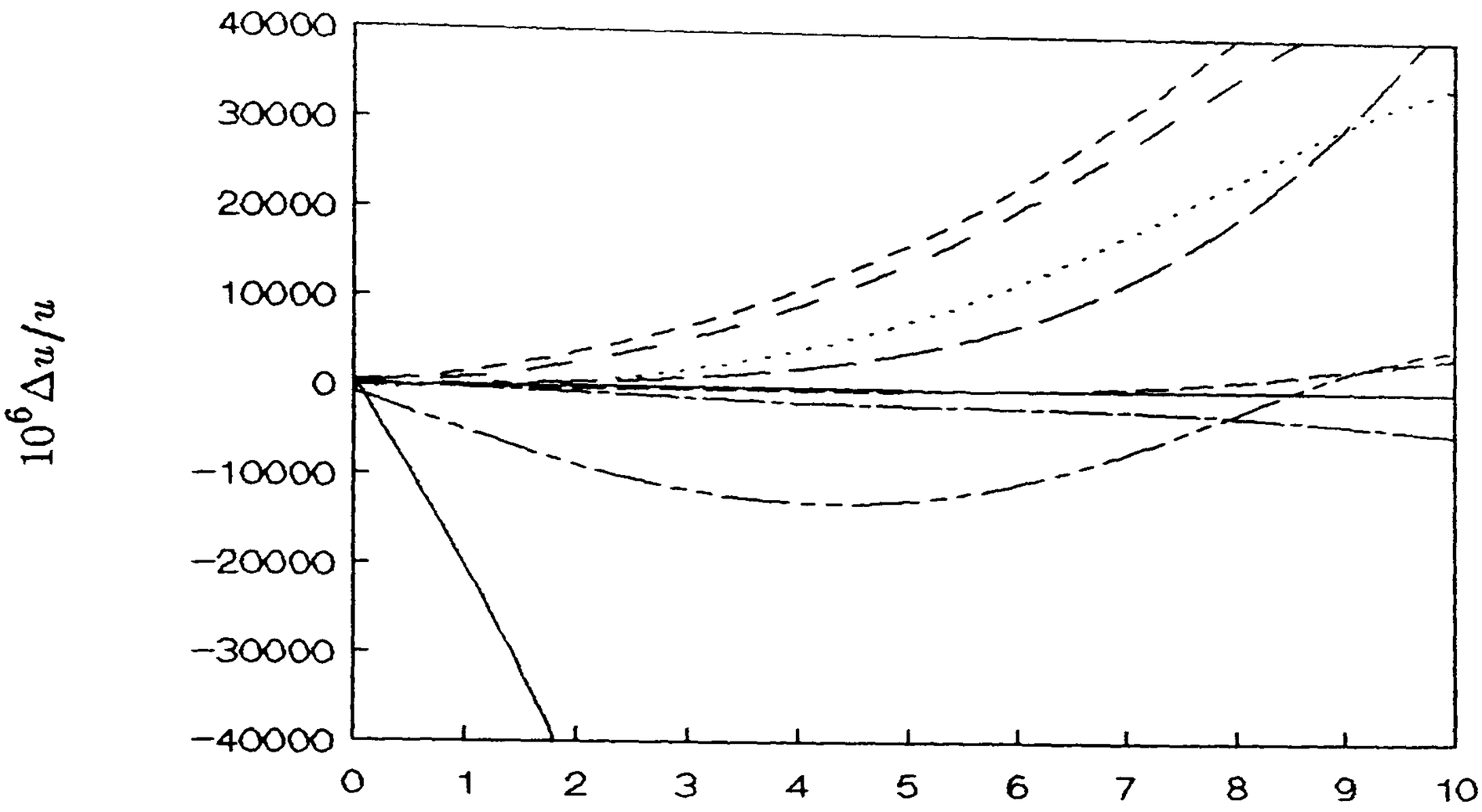

b)

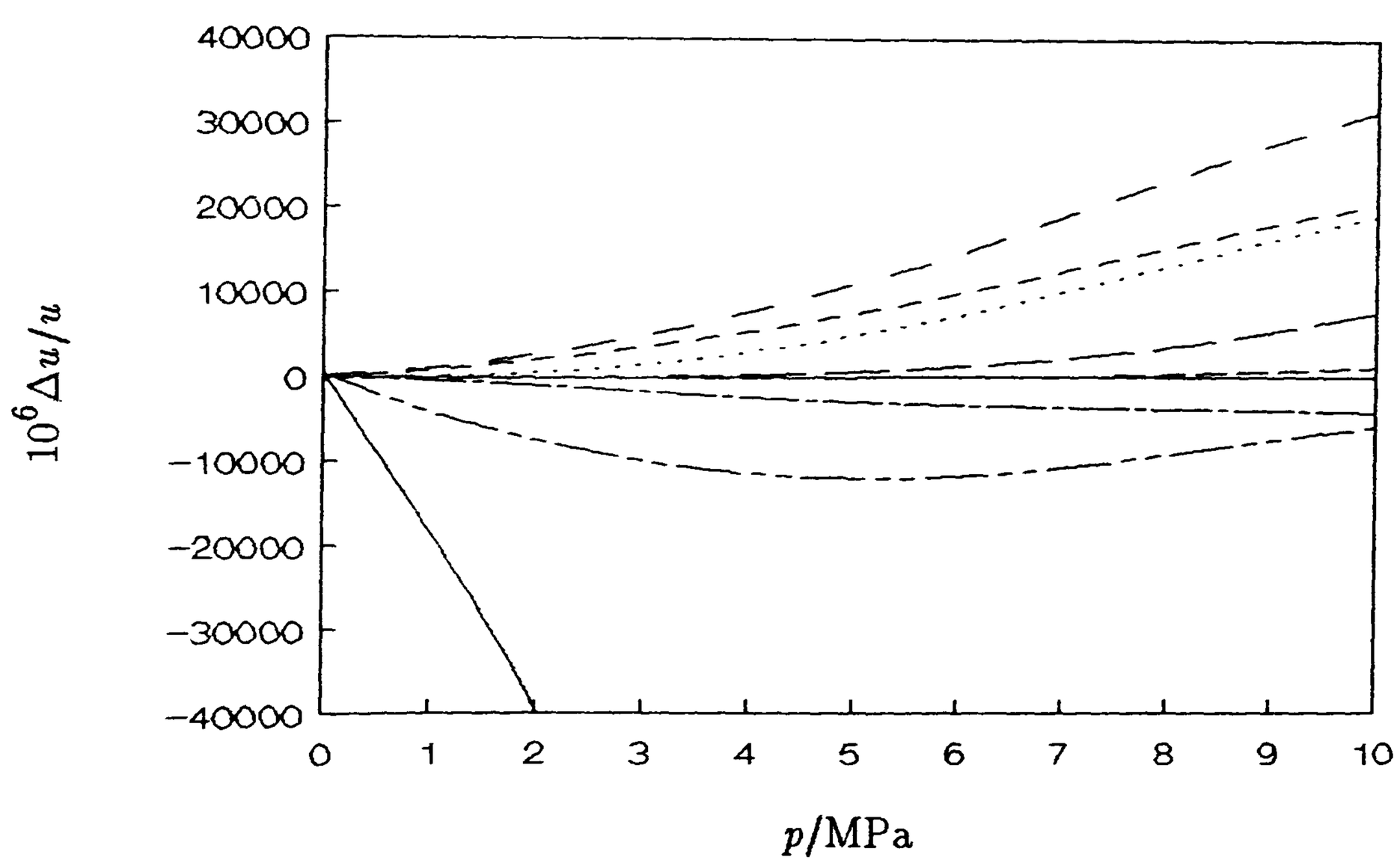

Figure 6.1: Fractional deviations $\Delta u/u = \{u(\text{e.o.s.}) - u\}/u$ for equation of state estimates of the speed of sound u(e.o.s.) for methane at a) 250 K and b) 275 K from u provided by equation (5.2.3) with coefficients from table 5.17. ····· , GL; – – – – , GERG; — — — , GRI; — – — , MCSP; ———— , BWRS; — – – — , PR; — — , RKS; ———— , Wagner *et al.*

a)

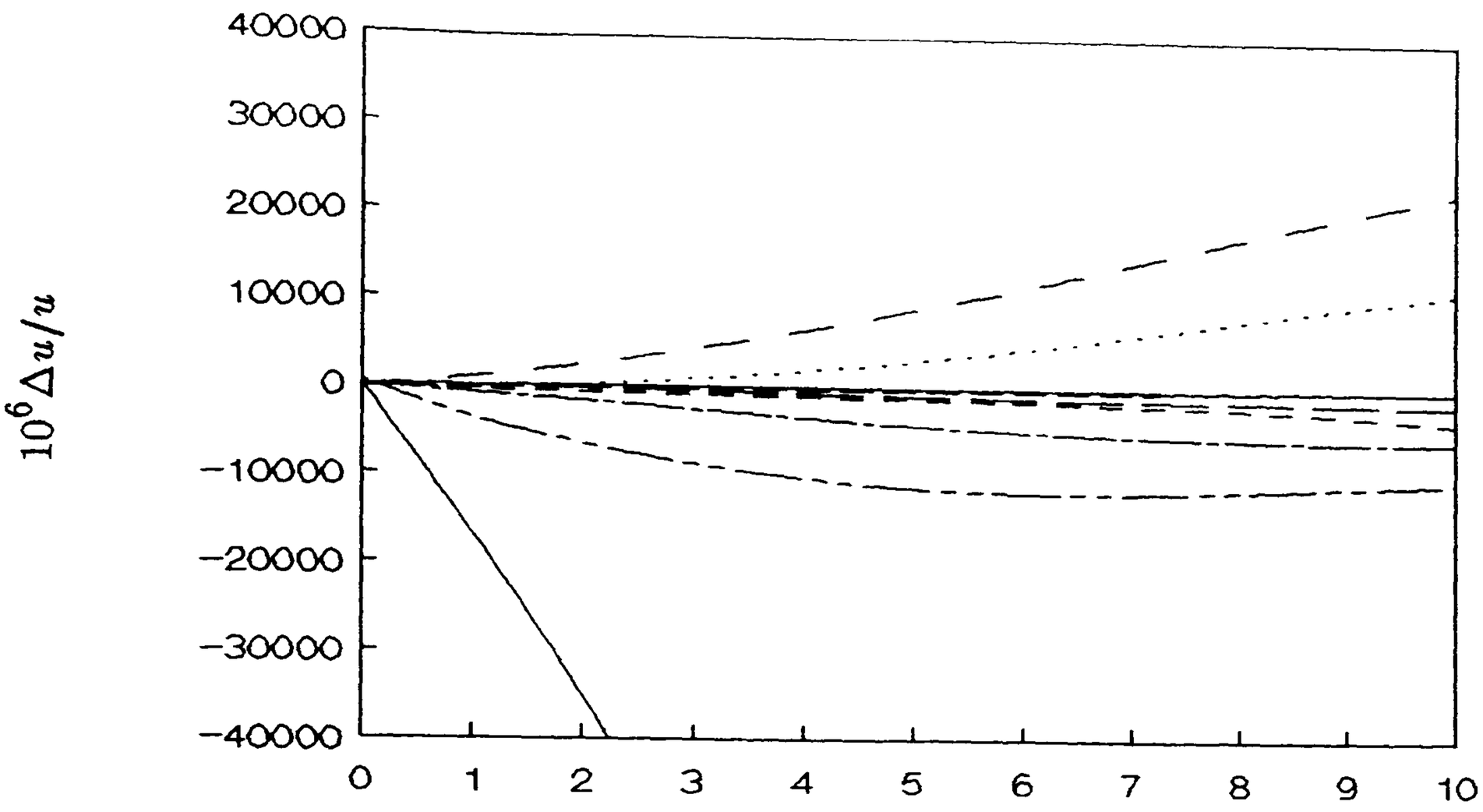

b)

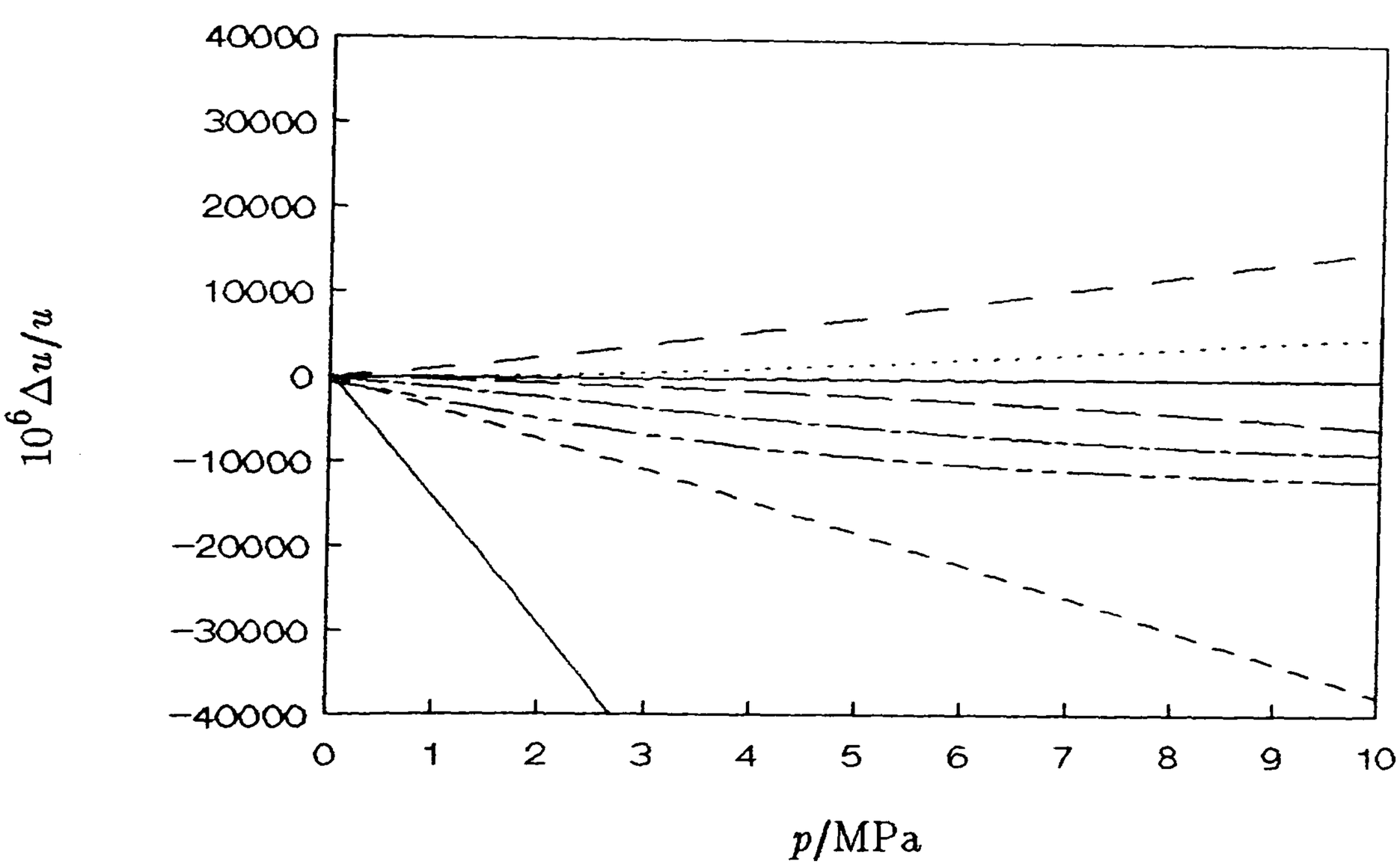

Figure 6.2: Fractional deviations $\Delta u/u = \{u(\text{e.o.s.}) - u\}/u$ for equation of state estimates of the speed of sound u(e.o.s.) for methane at a) 300 K and b) 350 K from u provided by equation (5.2.3) with coefficients from table 5.17. ····· , GL; – – – – , GERG; — — — , GRI; — – — , MCSP; ———— , BWRS; — – – – — , PR; — — , RKS; — — — — , Wagner *et al.*

the exclusion of the BWRS equation, the GERG equation is, on average, the poorest and all other equations produce values of u which agree to better than 5 %. Indeed, at some temperatures the agreement from the other equations approaches 1 %.

6.2.2: $\{(1-x)CH_4 + xC_2H_6\}$; $x \approx 0.15$.

Figures 6.3 and 6.4 show values of u obtained from the various equations of state as deviations from the smooting equations determined in the methane–ethane binary mixture at 250, 275, 300 and 350 K. The comparison of calculated and experimental results at 250 K will be considered separately since the partial pressure of ethane in the mixture exceeded the vapour pressure and condensation occurred. The zero–pressure values are seen to disagree by about 1 % and all equations show large deviations from the experimental equation. The GRI equation generally agrees to better than 1 % as does the MCSP equation. All other equations show deviations which exceed 2 %.† At 275, 300 and 350 K the deviations are similar to those observed in methane. The GRI equation produces values which agree to better than 0.15 % at all temperatures and pressures and the MCSP equation produces values which agree to better than 0.7 %. At best the GERG equation produces values which agree to about 0.4 % but at worst the deviations approach 4 % at 10 MPa. The BWRS equation again shows the worst deviation where it approaches 4 % at pressures greater than about 3 MPa. All other equations show varying degrees of success and these are similar to those observed in methane.

6.3: Discussion.

The GRI equation provides the best estimates of u for methane and the methane–ethane mixture. At worst the deviation is about 1 % but this was at 250 K in the mixture where condensation in the acoustic measurements occurred. At all other temperatures and pressures and in both the pure gas and the mixture the agreement is on the order of 0.1 %; indeed at most temperatures and pressures the deviations are less than 0.05 %. The MCSP equation also provides estimates which are extremely good.

† Since the equations themselves are inconsistent at a level of 1 % there may be some error in the perfect–gas heat capacities used in the correlating equations (see 6.3 a).

a)

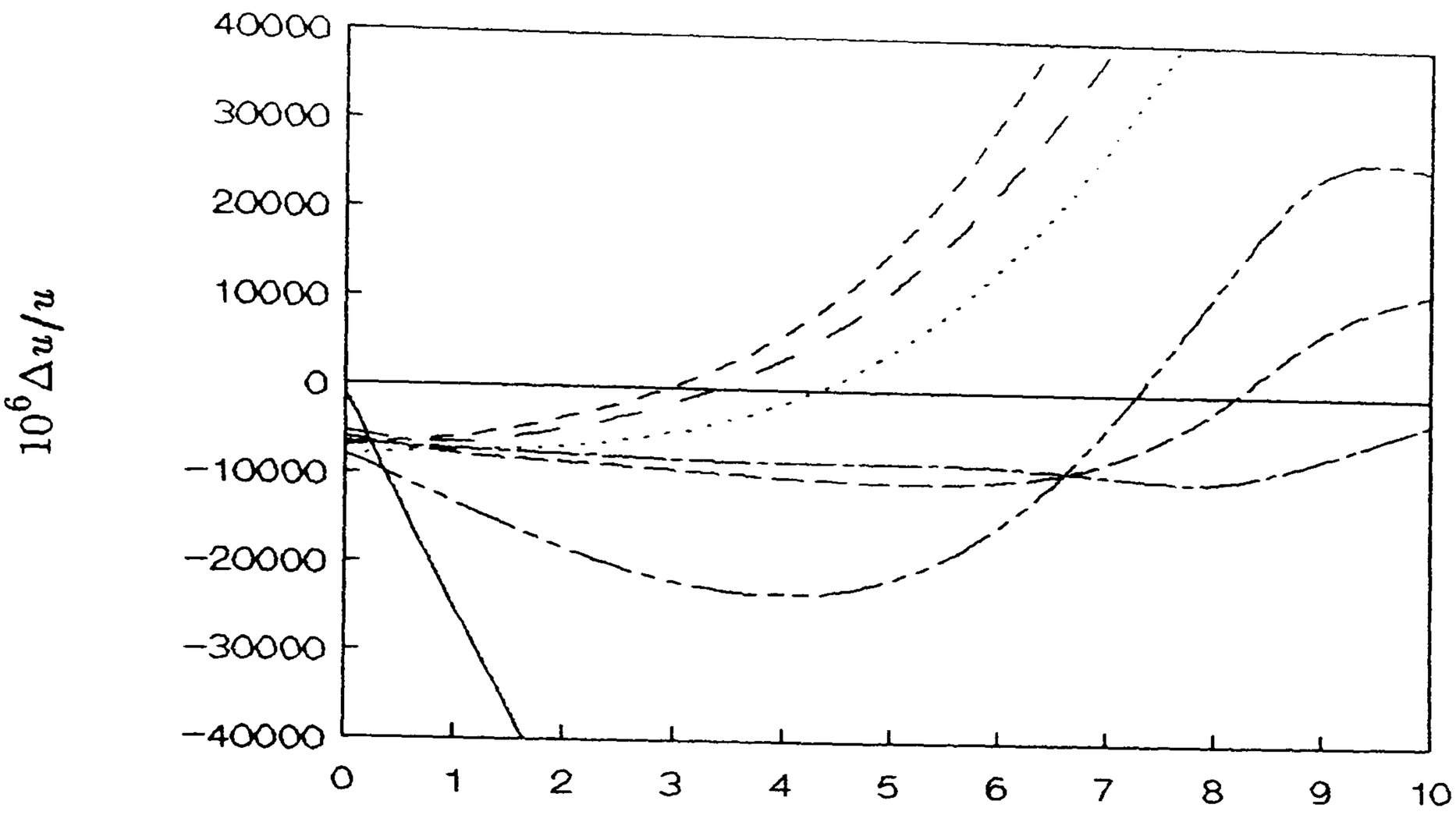

b)

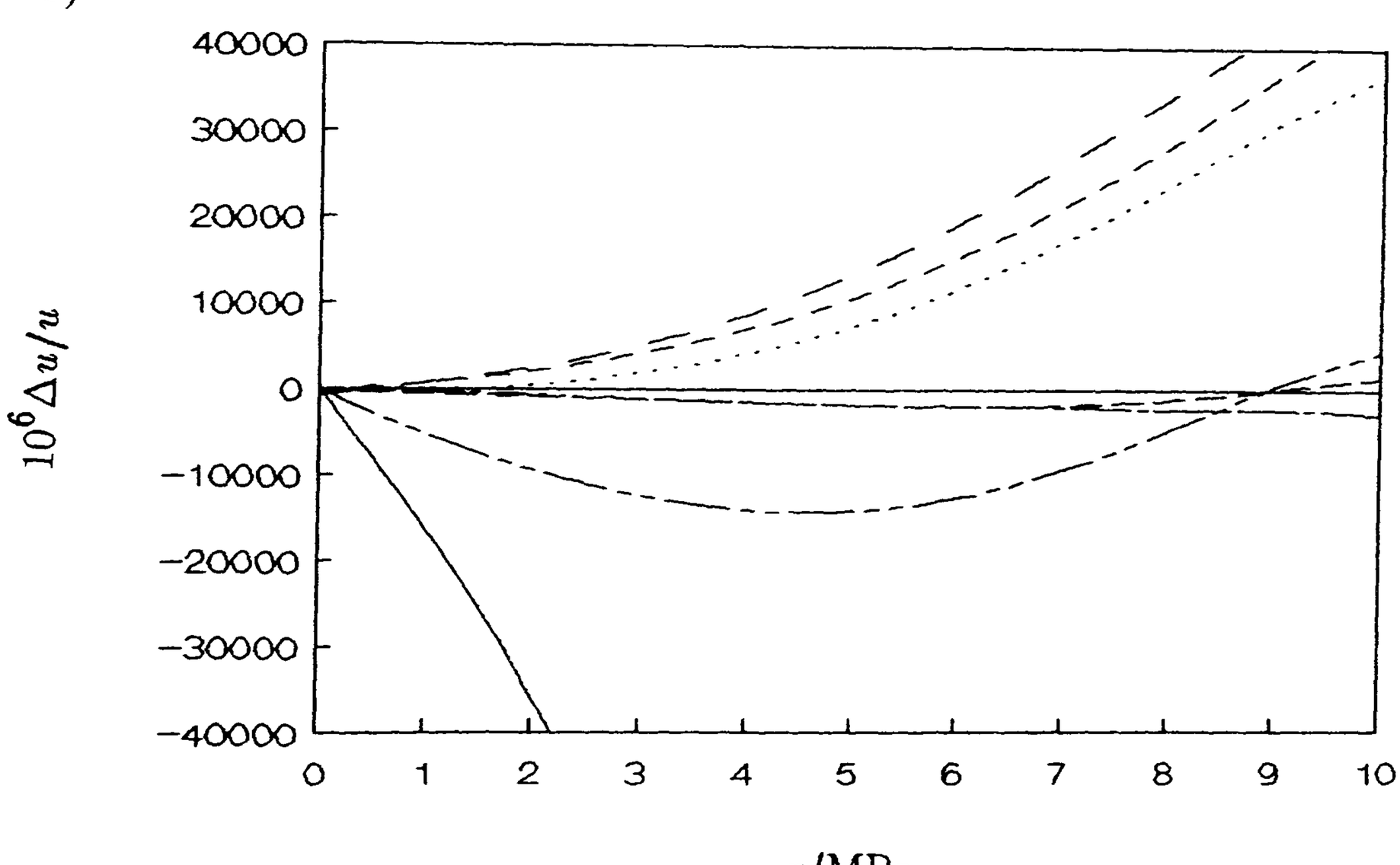

Figure 6.3: Fractional deviations $\Delta u/u = \{u(\text{e.o.s.}) - u\}/u$ for equation of state estimates of the speed of sound u(e.o.s.) for the mixture at a) 250 K and b) 275 K from u provided by equation (5.2.3) with coefficients from table 5.20. ·····, GL; – – –, GERG; — — —, GRI; — – —, MCSP; ————, BWRS; — – – —, PR; — —, RKS.

a)

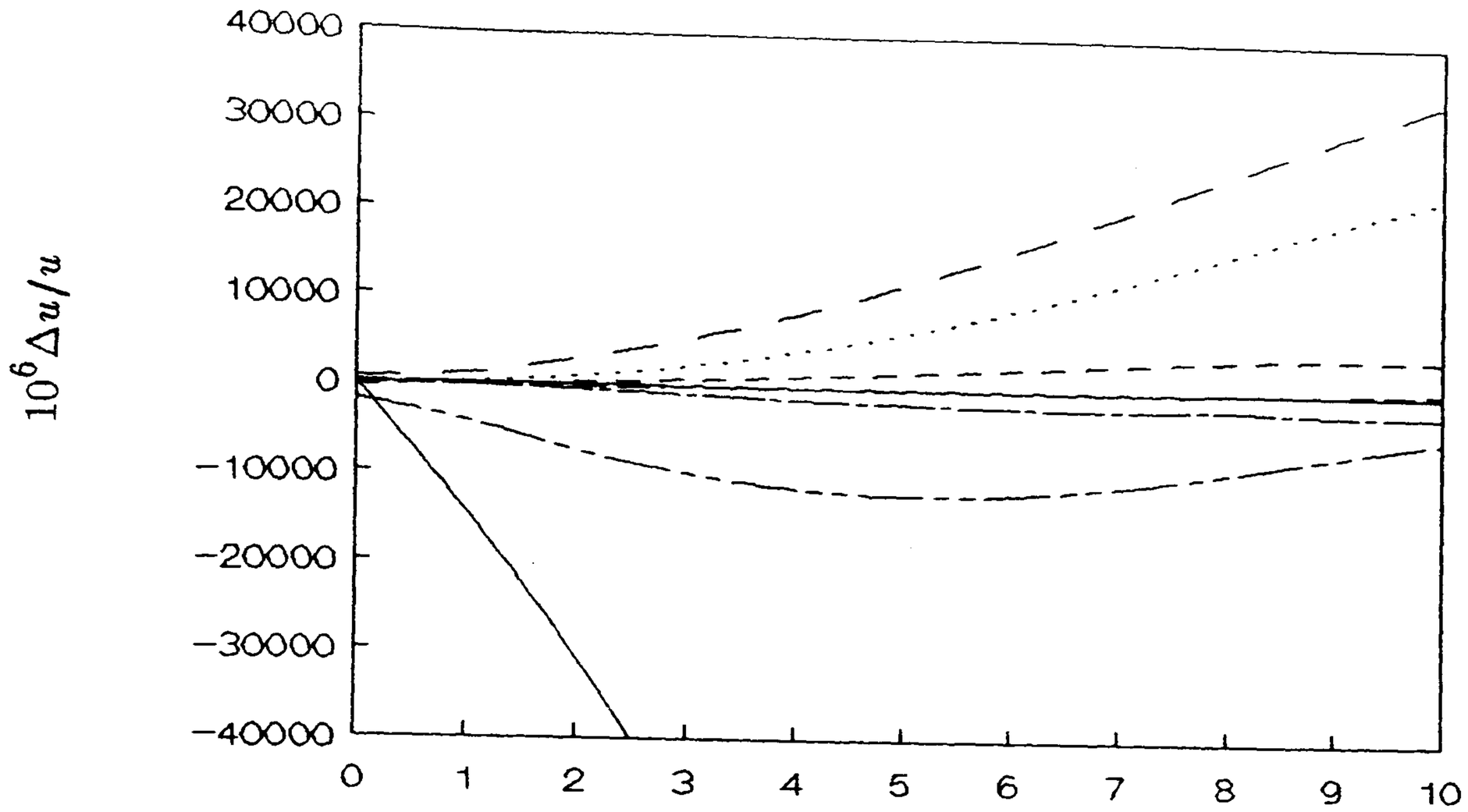

b)

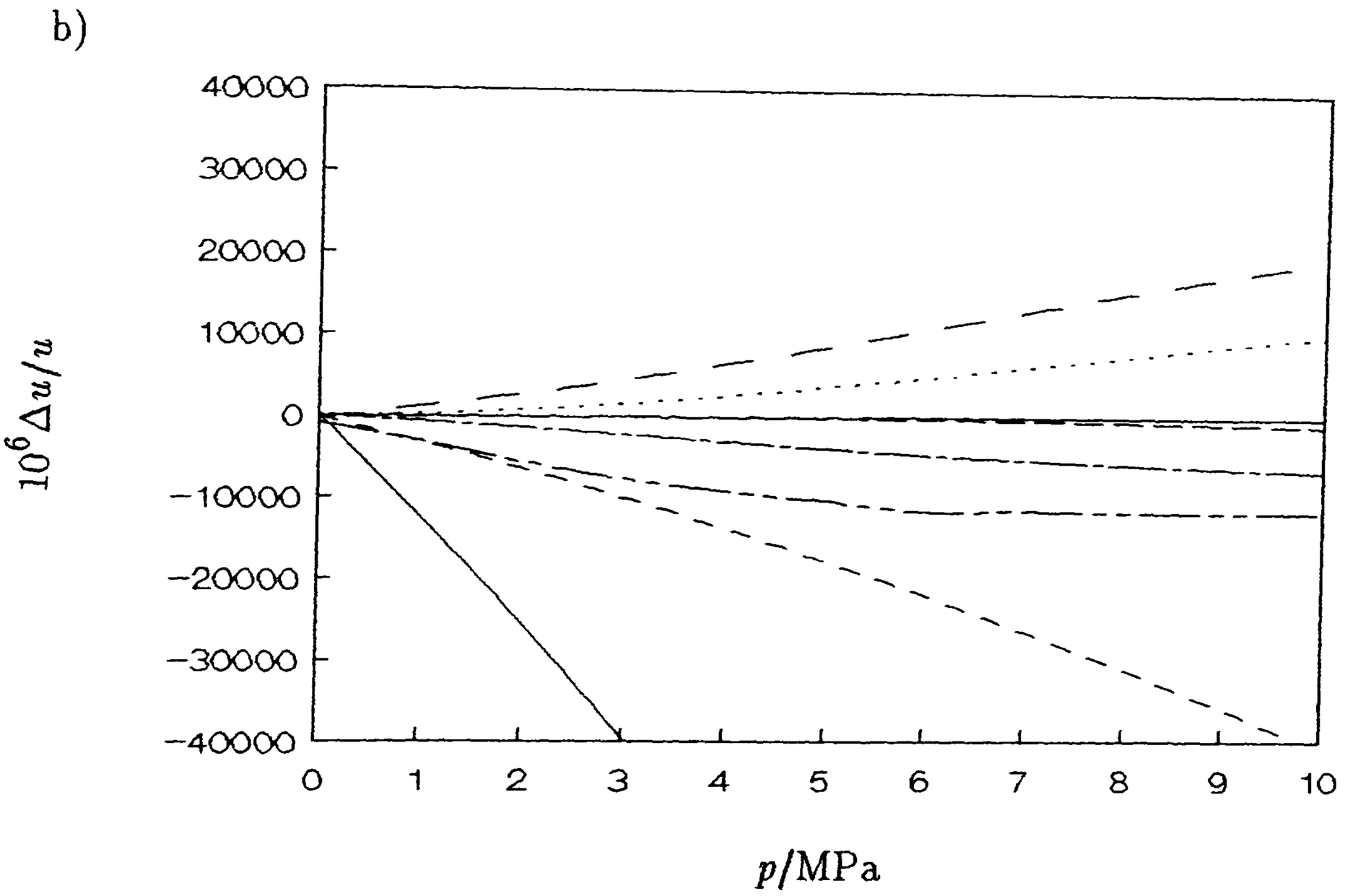

Figure 6.4: Fractional deviations $\Delta u/u = \{u(\text{e.o.s.}) - u\}/u$ for equation of state estimates of the speed of sound u(e.o.s.) for the mixture at a) 300 K and b) 350 K from u provided by equation (5.2.3) with coefficients from table 5.20. ·····, GL; – – –, GERG; — — —, GRI; — – —, MCSP; ————, BWRS; — – – —, PR; — —, RKS.

The deviations are less than 1 % at all temperatures and pressures and are generally better than 0.5 %. The GERG equation only provides good estimates of u at 300 K in both the pure gas and the mixture. To be fair some of the temperatures are outside its validity range but, at 275 K which is in the correct range, the estimates are really rather poor. All other equations provide estimates which deviate considerably from the experimentally determined values except sporadically and in limited instances.

In summary the GRI equation provides the best estimates of u with an alternative equation being the MCSP equation. Consequently for flow–metering applications the GRI equation should be the most applicable.

6.4: References.

1. A computer package called GASVLE was used; Copyright held by British Gas plc.

2. Gibbons, R. M.; Laughton, A. P. *J. Chem. Soc. Faraday Trans. 2* **1984**, 80, 1019.

3. Jaeschke, M.; Audibert, S.; van Canegham, P.; Humphreys, A. E.; Janssen–van Rosmalen, R.; Pellei, Q.; Michels, . P. J.; Schouten, J. A.; ten Seldam, C. A., GERG, Technical Monograph 2, VDI–Verlag: Düsseldorf. **1988**.

4. Starling, K. E.; Klein, M.; Little, F. G. *Proc. Congress Gas Quality – Specification and Measurement of Physical and Chemical Properties of Natural Gas.* van Rossum, G. J.: Editor. Elsevier: Oxford **1986**.

5. McCarty, R. D. *Cryogenics* **1974**, 14, 276.

6. Leach, J. W.; Chappelear, P. S.; Leland, T. W. *A. I. Ch. E. J.* **1968**, 14, 568.

7. Benedict, M.; Webb, G. B.; Rubin, L. C. *J. Chem. Phys.* **1940**, 8, 334.

8. Peng, D. Y.; Robinson, D. B. *IInd. Eng. Chem. Fundam.* **1976**, 15, 59.

9. Soave, G. *Chem. Eng. Sci.* **1972**, 27, 1197.

10. Pieperbeck, N.; Kleinrahm, R.; Wagner, W.; Jaeschke, M. *J. Chem. Thermodynamics* 1991, 23(2), 175.

THERMODYNAMIC PROPERTIES OF CF_4 BETWEEN 175 AND 375 K AT PRESSURES UP TO 1 MPa DETERMINED FROM THE SPEED OF SOUND.

S.J. Boyes and M.B. Ewing
Department of Chemistry, University College London, 20 Gordon Street, London WC1H OAJ (U.K.)
J.P.M. Trusler
Department of Chemical Engineering and Chemical Technology, Imperial College, Prince Consort Road, London SW7 2BY (U.K.)

1. INTRODUCTION

The speed of sound u in a non-relaxing gas is given in terms of the pressure p, amount-of-substance density ρ, and molar mass M by

$$u^2 = M(\partial p/\partial \rho)_S. \tag{1}$$

When combined with the virial equation of state,

$$p/\rho RT = 1 + B\rho + C\rho^2 + \cdots \tag{2}$$

where B, C, $\cdots$ are the second, third, $\cdots$ virial coefficients, Eq. (1) gives

$$u^2 = (RT\gamma_0/M)\{1 + \beta_a\rho + \gamma_a\rho^2 + \cdots\}. \tag{3}$$

Here R is the gas constant, T is the thermodynamic temperature, and γ_0 is the ratio of the perfect-gas heat capacities. The quantities β_a, γ_a, $\cdots$ are the second, third, $\cdots$ acoustic virial coefficients and are related to the coefficients of the virial equation of state by second-order differential equations; in particular, β_a is related to B and its first two temperature derivatives by

$$\tfrac{1}{2}\beta_a = B + (\gamma_0-1)T(dB/dT) + \{(\gamma_0-1)^2/2\gamma_0\}T^2(d^2B/dT^2). \tag{4}$$

Thus, B may be obtained from measurements of β_a over a range of temperatures by integration of Eq. (4); similar procedures can be applied to obtain the third and higher virial coefficients from the corresponding acoustic virial coefficients. In each case two boundary or initial values of the virial coefficient and/or its temperature derivatives are required before a numerical integration of the differential equation may be performed. Conditions of numerical stability strongly favour the use of initial conditions (*e.g.* B and dB/dT in Eq. 4) at the lowest temperature. Unfortunately, accurate virial coefficients are not usually available at low temperatures and the requirement for them defeats the aim of exploiting acoustic measurements independently of other experimental methods. If, however, one imposes some functional form upon the temperature dependence of the virial coefficients then the boundary value problem is eliminated at the expense of possible systematic error arising from imperfections in the chosen functional form. Such a functional form need not be explicit. For example, since B is related to the intermolecular pair potential energy function $u(r)$ by the integral equation

$$B(T) = 2\pi L\int_0^\infty [1 - \exp\{-u(r)/kT\}]\, r^2 dr, \tag{5}$$

where r is intermolecular separation, the assumption of a functional form for $u(r)$ implicitly imposes a functional form on B and provides a route to the solution of Eq. (4). Thus if one fits

the parameters of a model pair potential to experimental values of β_a using Eqs (4) and (5) then a self-consistent solution may be obtained. This is the method that we prefer. In its support we note that virial coefficients (especially B) are not very sensitive to the detailed shape of the intermolecular pair potential and that many simple three-parameter model potentials are able to represent them with high accuracy over a considerable temperature range. This assertion is subjected to test during the analysis in two ways. First, the model is required to fit the data; and second, we employ at least two different model potentials and compare the results that we obtain. Usually, two-parameter model potentials fail on the basis of the first criterion. In previous work we have always found that three-parameter model potentials that fit β_a within experimental uncertainties yield values of B that agree with each other to high accuracy within the temperature range of the measurements. As a bonus, this method allows extrapolation of the results to temperatures outside the experimental range and we find that the good level of agreement between the different models decays remarkably slowly as the extrapolations are extended to higher temperatures. Since the virial coefficients diverge to $-\infty$ as $T \to 0$, downward extrapolation is probably less reliable.

Although this is an indirect method of obtaining equation-of-state information it has several advantages over conventional methods. The speed of sound can be measured with very high precision and the method is less susceptible to many of the systematic errors that make volumetric measurements so difficult (especially at low temperatures). Typically, we are able to determine β_a with a precision of at least 0.1 cm^3/mol or 0.1% from measurements performed at low pressures. In addition the constant-pressure perfect-gas heat capacity C_{p0} is obtained with high precision from the zero-density limit of u^2:

$$C_{p0}/R = \gamma_0/(\gamma_0-1) = [1/\{1-(RT/Mu^2)\}]_{p\to 0}. \quad (6)$$

The precision here is usually much greater than the absolute accuracy because both γ_0 and the molar mass are sensitive to the presence of impurities in the gas. Nevertheless typical results are accurate to around 0.1% – an achievement comparable to the best results from flow calorimetry /1/.

Much of the recent success with acoustic measurements on gases is due to the use of the spherical acoustic resonator /2,3/. In this method, the speed of sound is obtained from measurements of the resonance frequencies of a gas-filled spherical cavity. Under certain simplifying assumptions, the relation between a resonance frequency f_n and the sound speed is

$$f_n = \nu_{1n}(u/2\pi a). \quad (7)$$

Here, ν_{1n} is an eigenvalue that is known exactly and a is the internal radius of the sphere. The subscripts on f and ν denote the symmetry and order of the resonance under consideration. We shall deal exclusively with modes of radial symmetry; for these modes $l = 0$. The lowest frequency radial mode of interest is usually denoted by f_{02} (the 0,1 mode being at zero frequency). In this work the mode (0,2) to (0,6) were studied. Two transducers are used in the measurements; one generates sound while the other is used to detect the response. The resonance frequencies are determined from measurements of the amplitude and phase of the detected signal as the frequency of the source is varied near to resonance. The method is extremely precise because the line widths in the spherical resonator are very small. Typically, the resonance frequencies of the first few radial resonance can each be determined to better than 1 ppm (parts per million).

Eq. (7) requires some correction for real resonators containing real fluids /2,3/. The simple theory neglects the effects of temperature fluctuations that exist in the fluid in the presence of sound. Inclusion of these effects leads to a fractional correction to the resonance frequencies that has the frequency and density dependence of $1/\sqrt{(\rho f)}$. This correction can be calculated from knowledge of the thermal conductivity of the gas and in the present case never exceeded 58 ppm. The simple theory also assumes that the walls of the cavity are perfectly rigid whereas in practical resonators they yield slightly to the acoustic pressure. Allowance for the mechanical compliance of the wall leads to a fractional correction that increases in proportion to the density. It can be calculated from knowledge of the elastic constants of the wall material and in the present case did not exceed 36 ppm. Several other smaller corrections are also included in the theory. Once these corrections are included the values of (u/a) obtained from the first four or five radial modes typically agree to better than 5 ppm. In the present case the lower five radial modes gave results at each state point that typically ranged over just

3 ppm. In order to obtain absolute values of the speed of sound it is necessary to know the radius of the sphere. In the present case, a was determined from measurements with argon for which the zero-density limit of the sound speed is known to high accuracy.

2. APPARATUS

The apparatus used in the present work is the same as that described previously /4/. It consists of an aluminium spherical resonator of internal radius 40 mm and wall thickness 10 mm housed inside a thermostat for operation in the range 77 to 400 K. The sphere was made in two hemispheres and joined at the equator by an electron beam weld /5/. A small (1 mm × 40 mm) tube embedded in the wall is used to admit the gas from a larger bore (6 mm) tube that enters the thermostat from the external gas supply.

The two transducers were mounted in small housings that screwed into ports in the wall of the sphere. Both were small capacitance type transducers using polymer-film diaphragms of diameter 3 mm.

The sphere was thermally anchored to a massive copper block where the temperature was controlled by a PID controller. The temperature of the shield that surrounded the resonator was also controlled but, since the thermostat was operated in vacuum, the sphere was fairly insensitive to fluctuations of the shield temperature.

The temperature was measured using capsule type platinum resistance thermometers mounted in blocks attached to the sphere. For the measurements below 300 K only a single thermometer was employed while in the later measurements at and above 300 K two thermometers mounted opposite to each other on the sphere were used. Temperature stability was excellent: typically constant to a few tenths of 1 mK during the 10 min required to obtain data at one state point. When both thermometers were in use they gave temperatures that agreed to within 1 mK.

The pressure of the gas was measured using a capacitance manometer (MKS type 310CD) mounted in the external pipe work. When calibrated against an air-lubricated pressure balance, the gauge was found to be linear and reproducible to about 0.02% of reading.

3. MEASUREMENTS

The tetrafluromethane was electronics grade material with a specified minimum purity of 99.99 moles per cent. Information provided by the manufacturer indicated that air and water were the main impurities. Before use, a sample was transferred under vacuum to a small stainless-steel cylinder where it was degassed by repeated cycles of freezing, evacuation, and melting. The apparatus was then filled by allowing the sample to warm slowly from 77 K until the required pressure was reached. No further purification was attempted.

The measurements reported here were performed along nine isotherms between 175 and 375 K. Five of these isotherms have been reported in an earlier publication /4/ in which many more details of the method are given. The maximum pressure used at 175 K (where the vapour pressure is 0.58 MPa) was 0.4 MPa, chosen to avoid the known effects of precondensation, but along the other isotherms the measurements extend up to 1 MPa. Ten equally spaced pressures were used on each isotherm. The frequencies used in this work range from 2.5 kHz for the 0,2 mode at 175 K to 13.6 kHz For the 0,6 mode at 375 K. CF_4 has a comparatively long vibrational relaxation time and, at low pressures, relaxation absorption leads to increased line widths even at the low frequencies of the experiment. These in turn cause some erosion of the otherwise high precision with which the resonance frequencies could be determined, particularly for the higher frequency modes. Consequently, whereas in previous work /1/ very low pressures have been included, the lowest pressure used in the present case was 0.08 MPa at 175 K and 0.1 MPa at the other temperatures. In addition the (0,5) and (0,6) modes were not used at the lower pressures. Maximum uncertainties were then limited to around 5 ppm for the (0,2) mode.

4. RESULTS

The results consist of speeds of sound determined from each of the modes studied at a total of 90 state points between 175 and 375 K and 0.08 and 1.0 MPa. Each measurement is associated with a statistical weight equal to the lesser of $2 \times 10^{-6}(\delta f/f)$ and unity, where δf is the estimated uncertainty of the resonance frequency from which u was determined. Thus the majority of the measurements ($\delta f < 2$ ppm) receive equal weight while the few at low pressures for which the uncertainties exceed 2 ppm have reduced weight. The results reported previously have been reanalyzed. together with the new measurements, using improved estimates of the thermal conductivity /6/ for calculation of the boundary layer correction; this leads to slight differences in the derived properties of the gas.

Heat capacities and acoustic virial coefficients were determined by regression analysis

with equation (3). The results obtained from the different resonance modes at each state point were not averaged prior to the analysis so that each pressure is represented by up to five points. Use of the density-explicit expansion u^2 leads to more rapid convergence than with a pressure-explicit series (which typically requires one more coefficient to fit the data); however, an iterative procedure is required. First, we estimated the densities assuming perfect-gas behavior and analyzed to obtain β_a and the other coefficients required to fit the data. Then the second virial coefficient B was calculated from β_a, by the method described below, and used to obtain improved estimates of the density. Two iterations were required to obtain internal consistency. Elementary considerations imply that β_a will be independent of the value of B used and that γ_a will be independent of the value of the third virial coefficient C, provided that sufficiently low densities are employed. Here we have neglected C and higher virial coefficients in calculating the density.

At the higher temperatures only three terms were required to fit the data (coefficients of ρ^0, ρ^1, and ρ^2), while at the three lower temperatures four were required. Two state points were rejected from the analysis. These are the maximum pressures on the isotherms at 200 and 225 K which could only be accommodated within the very small experimental error if a five term fit was employed.

Table 1 gives the values of C_{p0}, β_a, and γ_a that we recommend together with their standard deviations and the fractional standard deviation of u^2 for each isotherm. The standard deviations were obtained from the variance-covariance matrix generated in the regression analysis.

Table 1. Heat capacities and acoustic virial coefficients of CF_4

T/K	C_{p0}/R	$\beta_a/(cm^3 \cdot mol^{-1})$	$\gamma_a/(dm^6 \cdot mol^{-2})$	$10^6\sigma(u^2)/u^2$
375.02	8.4227 ± 0.0006	−48.21 ± 0.05	0.0140 ± 0.0001	6
350.09	8.0958 ± 0.0004	−66.43 ± 0.04	0.0147 ± 0.0001	5
325.00	7.7408 ± 0.0004	−88.01 ± 0.04	0.0157 ± 0.0001	6
300.00	7.3756 ± 0.0004	−113.87 ± 0.04	0.0172 ± 0.0001	6
275.00	6.9813 ± 0.0005	−144.84 ± 0.05	0.0183 ± 0.0001	8
249.30	6.5580 ± 0.0003	−184.91 ± 0.03	0.0205 ± 0.0001	6
224.45	6.1349 ± 0.0005	−234.42 ± 0.11	0.0241 ± 0.0005	8
199.96	5.6956 ± 0.0005	−299.68 ± 0.09	0.0296 ± 0.0003	6
174.78	5.2459 ± 0.0013	−394.04 ± 0.47	0.0390 ± 0.0025	6

In Fig. 1, we show deviations of the perfect gas heat capacity from an independent calculation. The standard deviation of the experimental values is less than 0.01%, except at the lowest temperature where it reaches 0.03%. The calculated heat capacity is $4R$ plus the sum of four Planck-Einstein functions, one for each of the vibrational modes of the CF_4 molecule. These were calculated using the vibrational frequencies recommended by Shimanouchi /7/. The estimated uncertainty in the spectroscopic data propagates into an uncertainty in C_{p0} that increases from $0.007R$ at 175 K to 0.014 R at 375 K. Thus our results are consistent with the those calculated from totally independent data. However, we note that the experimental results are not as smooth a function of temperature as one might expect on the basis of the standard deviation at each temperature. We attribute this to variations in the sample purity.

Fig. 2 shows deviations of β_a from our correlation of the results using the Kihara spherical core model pair potential. The three adjustable parameters in that model were determined in weighted non-linear analysis of the results using Eqs (4) and (5) together with the experimentally determined values of γ_0. The uncertainty that we ascribe to each value of β_a is the sum (in quadrature) of the standard deviation reported in the Table 1 and the estimated systematic uncertainty of 0.1 cm^3/mol. This total uncertainty was used as the basis of the weighting scheme in preference to one based only on random errors. The Kihara spherical core model is defined by

$$\begin{aligned} u(r) &= \infty && r < d \\ u(r) &= 4\epsilon[\{(\sigma-d)/(r-d)\}^{12} - \{(\sigma-d)/(r-d)\}^{6}] && r \geq d \end{aligned} \qquad (8)$$

where d is the core diameter, σ is the separation at which $u(r) = 0$, and ϵ is the depth of the potential-energy well. The standard deviation of the fit was 0.15 cm^3/mol and the parameters obtained are given by

$$b_0 = 2\pi L\sigma^3/3 = 96.977 \text{ cm}^3/\text{mol}$$
$$\epsilon/k = 308.5 \text{ K}$$
$$d/\sigma = 0.361.$$

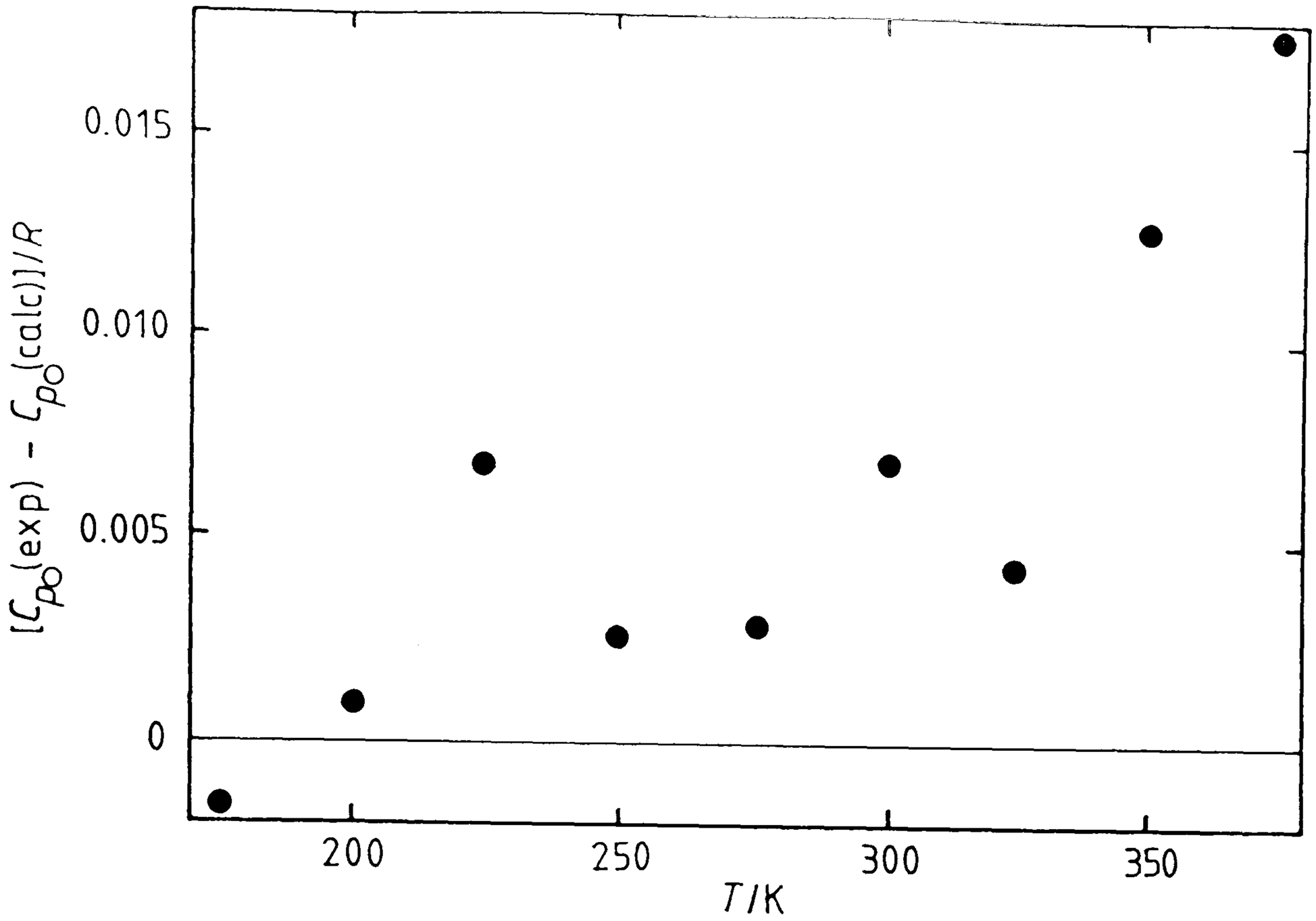

Figure 1. Deviations of experimental heat capacities $C_{p0}(exp)$ from spectroscopic values $C_{p0}(calc)$.

As can be seen in fig. 2, the model fits the results essentially to within the experimental uncertainties. Consequently, this was the model used to calculate the density in the analysis of the speed of sound described above. In Table 2 we list values of B calculated from the correlation.

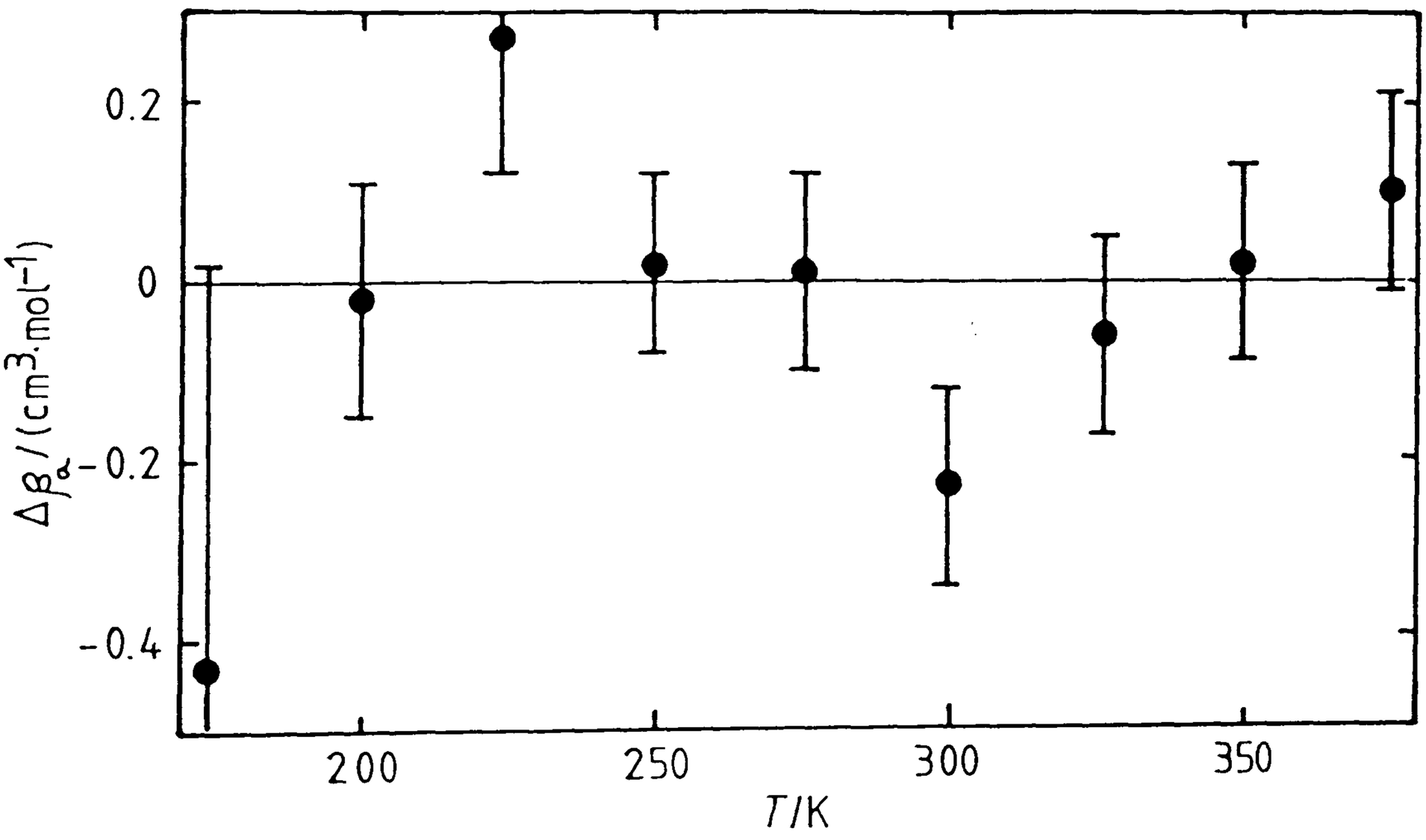

Figure 2. Deviations $\Delta\beta_a$ of experimental β_a's from the correlation using the Kihara pair potential.

Table 2. Second virial coefficients of CF_4.

T/K	175	200	225	250	275	300	325	350	375
$-B$/cm^3·mol^{-1}	304.3	227.4	175.1	137.5	109.1	87.1	69.4	55.0	43.0

We have also investigated the square-well potential as an alternative model. This potential fits the data with a standard deviation of 0.20 cm^3/mol and gives the following simple analytic expression for B:

$$B/(cm^3 \cdot mol^{-1}) = 256.32 - 172.80 \cdot \exp(206.0\ K/T) \quad (9)$$

Values of B calculated from Eq. (9) differ from those obtained from the Kihara correlation by an amount that varies from a maximum of 0.37 cm^3/mol at 195 K (about 0.15 %) to just 0.01 cm^3/mol at 375 K; even when extrapolated to 675 K, the two model differ by only 0.03 cm^3/mol.

There are four previous sets of measurements of B at temperatures above 240 K reported in the literature with which we may compare the values we obtain from our correlation of β_a using the Kihara model. All of the previous data, with the possible exception of the highly precise results of Douslin *et al* /8/, are consistent with ours to within their estimated precision. The data of Douslin *et al* ($T \geq 273.16$ K) have a precision of ±0.05 cm^3/mol and deviate from the present results by an amount that varies from less than 0.05 cm^3/mol at 275 K to about 0.3 cm^3/mol at 375 K. Douslin's results are subject to systematic uncertainty estimated at between 0.1 and 0.7 cm^3/mol; thus, these data too are consistent with our own. There are only two experimental results reported in the literature for temperatures below 240 K. These are the results of Lange and Stein /9/ which both lie above ours: by 1.3 cm^3/mol at 223.15 K and by 2.9 cm^3/mol at 203.15 K. We regard this as fair agreement for low temperature (p,ρ,T) results.

5. ACKNOWLEDGEMENTS

The authors gratefully acknowledge the contributions of Dr. Anthony Goodwin, who made a major contribution to the design of the resonator used in this work, and of Mr David Morfett, who expertly fabricated the apparatus. We thank Mr Albert Owusu for his assistance with some of the early measurements. Finally we also warmly acknowledge our many useful and stimulating discussions with Dr. Michael Moldover and with Prof. Jim Mehl.

REFERENCES

1. M.B. EWING, A.R.H. GOODWIN, M.L. McGLASHAN and J.P.M. TRUSLER, J. Chem. Thermodyn. vol. 19 (1987) 721–739.
2. J.B. MEHL and M.R. MOLDOVER, J. Chem. Phys. vol. 74 (1981) 4062–76.
3. M.R. MOLDOVER, J.B. MEHL, and M. GREENSPAN, J. Acoust. Soc. Am. vol. 79 (1986) 253–72.
4. M.B. EWING and J.P.M. TRUSLER, J. Chem. Phys. vol. 90 (1989) 1106–15.
5. A.R.H. GOODWIN, PhD Thesis, University of London (1984).
6. M.J. ASSAEL, J. MILLAT, V. VESOVIC, and W.A. WAKEHAM, J. Phys. Chem. Ref. Data, to be published.
7. T. SHIMANOUCHI, 'Tables of Molecular Vibrational Frequencies Part 1', Natl. Stand. Ref. Data Ser. 6 (US GPO Washington DC, 1967) p.11.
8. D.R. DOUSLIN, R.H. HARRISON, R.T. MOORE, and J.P. McCULLOUGH, J. Chem. Phys. vol. 35 (1961) 1357–66.
9. H.B. LANGE Jr. and F.P. STEIN, J. Chem. Eng. Data vol. 15 (1970) 56.
10. K.E. MacCORMACK and W.G. SCHNEIDER, J. Chem. Phys. vol. 19 (1951) 845.
11. P.M. SIGMUND, I.H. SILBERBERG, and J.J. McKETTA, J. Chem. Eng. Data vol. 17 (1972) 168.

PROPRIETES THERMODYNAMIQUES DE CF4 ENTRE 175 ET 375 K ET JUSQU'A LA PRESSION DE 1 MPa, DETERMINEES A PARTIR DE LA VITESSE DU SON

RESUME : La vitesse du son dans le gaz CF4 a été mesurée entre 175 et 375 K et entre 0.08 à 1 MPa. Ces mesures ont été faites avec un résonateur acoustique sphérique dont la précision est meilleure que 0.001 %. Les résultats ont été utilisés pour estimer les capacités calorifiques des gaz parfaits et les deuxième et troisième coefficients acoustiques du viriel de CF4. Les coefficients du viriel en volume, calculés à partir des mesures acoustiques, sont en bon accord avec ceux de la littérature.